THE ENCOUNTER BAY GRANITES, SOUTH AUSTRALIA, AND THEIR ENVIRONMENT

by

ANTHONY RICHARD MILNES

B.Sc.(Hons) Adelaide

Submitted for Ph.D.

in the

Department of Geology and Mineralogy

at

The University of Adelaide,

South Australia

April, 1973

This thesis contains no material which has been accepted for the award of any other degree or diploma in any University and, to the best of my knowledge and belief, it contains no material previously written or published by another person except where due reference is made in the text.

Signed:

A.R. Milnes

CONTENTS PAGE

CONTENTS (Cont'd) PAGE

CONTENTS (Cont'd) PAGE

CONTENTS (Cont'd) PAGE

SUMMARY

The Encounter Bay Granites are essentially pre-tectonic biotite granites that have intruded Kanmantoo Group metasedimentary rocks in the Encounter Bay area of Fleurieu Peninsula and at Cape Willoughby on Kangaroo Island. The granites are broadly concordant with bedding in the metasedimentary rocks, but in detail the contact between the granites and the metasedimentary rocks is sharp.

The type section of the Kanmantoo Group occurs along the southern coastline of Fleurieu Peninsula and extends into the Encounter Bay area. In the western part of the type section, the Kanmantoo Group, which includes metasandstones and metasiltstones, phyllites and carbonate-rich metasediments, conformably overlies fossiliferous Lower Cambrian metasediments and is therefore regarded as Cambrian in age. East of this boundary, the Kanmantoo Group stratigraphic sequence extends without unconformity into the Encounter Bay area and is relatively straight-forward, despite the andalusite-grade metamorphism and the occurrence of folds.

Two phases of folding are recognised in Kanmantoo Group metasedimentary rocks in the type section. First generation folds are of regional significance and have axial planes defined by a penetrative mica schistosity. Second generation folds are well developed only in the eastern part of the type section and have axial planes defined by a crenulation cleavage. The marginal phase of the Encounter Bay Granites in the Encounter Bay area was deformed during the first phase of folding and contains a well developed S_1 schistosity. Low pressure-intermediate type metamorphism commenced at about the time of emplacement of the Encounter Bay Granites.

The major variety of the Encounter Bay Granites is a medium to coarse grained megacrystic granite which can be subdivided into a border facies and an inner facies on the basis of texture and xenolith population. Other granite types are subordinate in areal extent, and include uncontaminated medium grained granites, leucogranites and aplites, and hybrid granites which are regarded as partly assimilated metasedimentary rock xenoliths. All granite varieties contain a distinctive opalescent blue quartz.

Fe/(Fe+Mg) ratios for biotites in the granites are sensitive to compositional changes due to contamination with metasedimentary rock.

The preservation of orthoclase in the cores of potash feldspar megacrysts in the border facies megacrystic granite, and the enrichment of Ba in the cores relative to the margins, is taken in conjunction with field and petrographic observations as evidence for the early crystallisation of the megacrysts. The compositions of coexisting potash feldspar and plagioclase megacrysts in the megacrystic granites are generally consistent with equilibrium crystallisation.

Chemical analyses of the Encounter Bay Granites define a conspicuous contamination trend of the type described by many authors as the result of differentiation. Normative An, Ab and Or ratios for the granites suggest that potash feldspar was the first phase to crystallise in a liquid of the composition assumed for the parental magma. Subsequent contamination with metasedimentary rock displaced the composition of the parental magma into either the plagioclase field or the quartz field of the Q-An-Ab-Or-H_2O system so that quartz and two feldspars were crystallising at the time of emplacement of the megacrystic granites.

On the basis of Rb-Sr isotope dilution data, the Encounter Bay Granites were emplaced between 523m.y. and 531m.y. ago at the onset of metamorphism in the Kanmantoo Group metasedimentary rocks. Both Rb-Sr and K-Ar data suggest that the metamorphic conditions did not wane until about 470m.y. ago.

Contamination of the border facies megacrystic granite is evident from initial Sr^{87}/Sr^{86} ratios. On the other hand, the uncontaminated granites have a high initial Sr^{87}/Sr^{86} ratio (0.711) which is used as a basis for discussion of the origin of the Encounter Bay Granites.

PREFACE

"Encounter Bay Granites" is the formal collective name herein given to the Lower Palaeozoic granites that crop out in the Encounter Bay area on the southern coast of Fleurieu Peninsula, approximately 80km south of Adelaide, and at Cape Willoughby on the eastern end of Kangaroo Island, South Australia (Figures 1 and 2). Although the two areas are more than 50km apart, the granites belong to the same suite, and may form part of the same intrusive mass. The granites have intruded a sequence of metasedimentary rocks which can be demonstrated to be of Cambrian age, and is known as the Kanmantoo Group.

This thesis is concerned with the nature and field relationships of the several granite types that make up the Encounter Bay Granites, and with the stratigraphic, structural and metamorphic environment of the intrusion as a whole. Parts of the thesis have been based on the results of a preliminary study of the petrology of the granites completed in 1967[1]. The field work and the petrological and geochemical aspects of the present project were completed in the Department of Geology and Mineralogy at the University of Adelaide under the supervision of Dr. A.W. Kleeman and Dr. J.B. Jones. Most of the data concerned with the study of the environment of the granites were collected during joint investigations with Dr. B. Daily on the geology of the Kanmantoo Group[2]. Electron probe microanalytical data were obtained using the C.S.I.R.O. Division of Soils microanalyser under the supervision of Dr. K. Norrish and Dr. T.R. Sweatman. Preliminary Rb-Sr isotope data were obtained initially during a joint research project with Dr. E.J. Dasch (a visiting Research Fellow in the Department of Geophysics and Geochemistry at the Australian National University) and Dr. R.W. Nesbitt[3]. However, the majority of the Rb-Sr data were collected under the supervision of Dr. W. Compston during a four month visit to the Department of Geophysics and Geochemistry at the Australian National University.

---

[1]Milnes, A.R. (1967). A petrological study of the Encounter Bay Granites. B.Sc.(Hons) thesis, University of Adelaide (unpublished).

[2]Daily, B. and Milnes, A.R. (1971a, 1971b, 1972a, 1972b, 1973). See Appendix A.

[3]Dasch, E.J., Milnes, A.R. and Nesbitt, R.W. (1971). See Appendix A.

ACKNOWLEDGMENTS

Many persons gave freely of their time in assisting me during my research. I wish to thank Dr. A.W. Kleeman for his advice and discussion on all aspects of the thesis, and especially for his criticism of the final draft. Dr. J.B. Jones contributed many hours of valued discussion and supervision, especially in relation to the feldspar studies. I wish to record my special thanks to Dr. B. Daily, with whom I spent many weeks in the field, and who contributed a great deal to my knowledge of geology through discussions and patient instruction in the ways of stratigraphy.

Many other members of the Department of Geology and Mineralogy at the University of Adelaide provided valuable assistance and opportunity for discussions. Notable among these are Dr. R.L. Oliver, Dr. R.W. Nesbitt, Dr. J.A. Cooper (who was formerly in the Department of Geophysics and Geochemistry at A.N.U., and who discussed with me many aspects of the Rb-Sr data), and Dr. M.A. Etheridge.

I am also grateful to Dr. P.D. Fleming (Department of Geology, University of Toronto), Dr. E.J. Dasch (Department of Geology, Oregon State University), Dr. A.C. Moore (Department of Geology, University of Capetown), and Mr. R.G. Wiltshire (Department of Applied Geology, South Australian Institute of Technology) for discussions on various aspects of the thesis.

I am indebted to Dr. K. Norrish for the opportunity to use the C.S.I.R.O. Division of Soils electron probe microanalyser, and for his patient supervision and instruction in the techniques involved. I am thankful to Dr. T.R. Sweatman and Mr. H. Rosser for their guidance in microanalyser techniques.

I am also indebted to Dr. W. Compston for the opportunity to visit his laboratory in the Department of Geophysics and Geochemistry at A.N.U. to receive his instruction in Rb-Sr geochronology. Mr. M.J. Vernon, Mr. D.J. Millar, Dr. C.M. Gray, Mr. J.C. Roddick, and Dr. P.A. Arriens contributed valued assistance in the techniques of sample preparation and mass spectrometry.

The preparation of thin sections examined during the research was ably carried out by Mr. R. Flossman and Mr. R. Mottershead.

The research for this thesis was carried out during the tenure of a Commonwealth Post-graduate Award.

The Chief of C.S.I.R.O. Division of Soils, Dr. E.G. Hallsworth, kindly allowed me to use C.S.I.R.O. facilities during the preparation of the thesis.

I am grateful to Miss S.P. Veitch for typing the final manuscript, and to Mr. D.A. Wright of the C.S.I.R.O. Drafting Office for preparation of the maps and assistance with the diagrams.

Finally, I wish to formally acknowledge the patience, understanding and encouragement of my wife and daughter during the research and preparation of my thesis.

SECTION 1

INTRODUCTION

1.1 *DISTRIBUTION OF PALAEOZOIC GRANITES IN SOUTH-EASTERN SOUTH AUSTRALIA*

The Encounter Bay Granites crop out in one of two intersecting zones of foliated and non-foliated granitic rocks in south-eastern South Australia and south-western Victoria. Discontinuous outcrops of granitic rocks along the eastern flank of the Mount Lofty Ranges from the south-western tip of Kangaroo Island to the Anabama area define the western zone, whilst similar outcrops through the Murray Basin area and extending to Dergholm in south-western Victoria define the eastern zone (Figure 2). The two zones intersect in an area of high grade metamorphism centred around Palmer, approximately 50km east of Adelaide (Figures 2 and 3).

A Lower Palaeozoic age for many of these granites has been established in recent years as the result of radiometric age dating techniques (Fander, 1961; Evernden and Richards, 1962; Compston, Crawford and Bofinger, 1966; White, Compston and Kleeman, 1967; Thomson, 1970; Dasch, Milnes and Nesbitt, 1971).

1.2 *REGIONAL GEOLOGICAL ENVIRONMENT OF THE GRANITES*

The arcuate Mount Lofty Ranges metamorphic belt, which contains many of the granites, extends from the western end of Kangaroo Island to Eudunda, approximately 100km north-east of Adelaide (Figure 2). It consists of Precambrian and Cambrian rocks, and exhibits a well defined arrangement of metamorphic zones (Offler and Fleming, 1968; Figure 3 of this thesis). On Fleurieu Peninsula, the metamorphic rocks on both the western and eastern flanks of the Ranges are overlapped by Permian and Cainozoic sediments. The Ranges are a Tertiary to Quaternary topographic feature that was uplifted relative to the adjacent areas along steeply dipping, north-easterly trending normal and reverse faults (Thomson and Horwitz, 1962; Stuart and von Sanden, 1972).

East of the Ranges, discontinuous granite outcrops extending from Murray Bridge to Kingston define a subsurface structure known as the Padthaway Ridge (O'Driscoll, 1960; Ludbrook, 1961), of which there is little geological knowledge. These granites are overlapped by Cainozoic sediments. Although there are rare outcrops of metamorphic rocks, as for example near Tailem Bend and in one locality south-west of Keith, they have not been described in any detail, and thus their

relationships with the granitic rocks are unknown. However, the granite at Dergholm in south-western Victoria occurs within metamorphic rocks of the Glenelg River Complex of possible Early Palaeozoic age (Wells, 1956).

1.2.1 *Older Proterozoic basement*

Older Proterozoic basement rocks occur as isolated inliers forming the core of the Mount Lofty Ranges metamorphic belt, and are unconformably overlain by Late Proterozoic rocks of the Adelaide Supergroup (Campana, 1958; Thomson, 1969). The inliers are actually the cores of regional anticlinal structures, in which the western limbs are overturned and are commonly dislocated along thrust zones. They consist of metasedimentary rocks and metamorphosed igneous rocks that record the effects of retrograde metamorphism from the amphibolite facies to the lower greenschist facies (Forbes, 1957; Talbot, 1963). According to Talbot (1963), at least one period of greenschist facies metamorphism occurred prior to the deposition of the Adelaide Supergroup sediments.

As seen in Figure 1, basement rocks (referred to as "Archaean") occur sporadically throughout South Australia. In the past, they have been grouped as Archaean because they underlie the oldest sedimentary rocks yet recognised, and exhibit broad petrologic similarities. However, there is presently no basis for either lithological or stratigraphic correlation within this rock group from one area to another, and there is insufficient radiometric data on which to base a chronology of events.

An Archaean age for the basement rocks was first proposed by Howchin (1906), and they have been referred to as such on maps published by the South Australian Geological Survey as recently as 1962. However, radiometric age determinations on samples collected from the Myponga area (Figure 2) indicated K-Ar ages of 390 and 650 m.y. for two biotites, and a U-Pb age of 520 m.y. for uraninite (Greenhalgh and Jeffrey, 1959). Furthermore, Compston, Crawford and Bofinger (1966) obtained ages between 1500 and approximately 1700 m.y. for basement rocks collected from Yorke Peninsula and to the north of the Anabama area (Figure 1) on the basis of Rb-Sr data, but also obtained ages of about 850 and 1345 m.y. for two suites of volcanic rocks that unconformably overlie basement in other parts of South Australia. Cooper and Compston (1971) suggested an age of 867 m.y. for the amphibolite facies metamorphism of a suite of basement rocks from the inlier to the north-east of

Adelaide on the basis of further Rb-Sr data. Thus it would appear that the Older Precambrian basement in these areas is comprised of rocks of a wide range of ages and/or geological histories. None of the ages obtained is older than Middle Proterozoic, but several, at least at face value, record events extending into the Late Palaeozoic.

1.2.2 *Adelaide Supergroup*

The Adelaide Supergroup consists of a thick succession of metamorphosed non-fossiliferous sandstones, shales, quartzites, limestones and glacigene sediments that unconformably overlie the Older Proterozoic basement rocks. In the type area, near Adelaide, the succession attains a thickness of approximately 8000m (Mawson and Sprigg, 1950). The sediments were deposited in an elongate zone known as the "Adelaide Geosyncline" that extended from Kangaroo Island to the northern border of South Australia, and was active during Late Proterozoic and Early Cambrian time (Sprigg, 1952).

Adelaide Supergroup metasediments are disconformably overlain by the earliest Cambrian metasediments in the Sellick Hill and Delamere areas on the western side of the Older Proterozoic basement inliers (Daily, 1963, 1969; Figure 2 of this thesis). To the east of the inliers, Horwitz, Thomson and Webb (1959) mapped an unconformable boundary between the Adelaide Supergroup metasediments and overlying metasediments of presumed Cambrian age, including those of the Kanmantoo Group. However, recent investigations have shown that this boundary is a fault contact in several localities in the eastern Mount Lofty Ranges. (Daily and Milnes, 1971a, 1971b, 1972a) and corresponds to the Nairne Fault originally mapped by Sprigg, Whittle and Campana (1951), Campana (1953) and Sprigg and Wilson (1954).

On the basis of the disconformable boundary between the Adelaide Supergroup and Lower Cambrian rocks in the Sellick Hill and Delamere areas, the Adelaide Supergroup is generally considered to be of Upper Proterozoic age. Rb-Sr radiometric age data for volcanic rocks near the base of the sequence in the northern Flinders Ranges indicate an age of about 850 m.y., whilst the age of petrologically similar volcanic rocks in north-eastern Eyre Peninsula, also associated with rocks of Adelaide Supergroup type, is about 1345 m.y. (Compston, Crawford and Bofinger, 1966; Thomson, 1966). The relationship between the volcanics in each of these regions is not known with certainty, and therefore the base of the Adelaide Supergroup there may be as old as 1345 m.y. or as

young as 850 m.y. However, the 867 m.y. age for the high grade metamorphism affecting basement rocks east of Adelaide, prior to the deposition of the Adelaide Supergroup (Cooper and Compston, 1971), does seem to support an uppermost Proterozoic age for its base.

1.2.3 *Cambrian Succession*

On the western side of the basement inliers in the Sellick Hill area (Figure 2) Adelaide Supergroup rocks are disconformably overlain by a sequence of arkoses, mottled argillaceous limestones, massive clean limestones and phosphatic shales of low metamorphic grade containing an abundant Lower Cambrian fauna that includes Hyolithes (Daily, 1956, 1969; Abele and McGowran, 1959). At Carrickalinga Head the uppermost formation of the Sellick Hill sequence, namely the Heatherdale Shale, is conformably overlain by non-fossiliferous alternating shales and thin impure sandstones of the Carrickalinga Head Formation, which marks the base of the Kanmantoo Group (Campana, Wilson and Whittle, 1954; Daily, 1963, 1969; Daily and Milnes, 1971a).

Further south in the Delamere area (Figure 2), the rocks have been metamorphosed to biotite grade (Offler and Fleming, 1968). However, the fossiliferous Lower Cambrian succession is almost identical to that at Sellick Hill (Daily, 1963, 1969).

On the south coast of Fleurieu Peninsula at Madigan Inlet (Figure 2), the more highly metamorphosed equivalents of the two uppermost formations of the fossiliferous Lower Cambrian succession, namely the Forktree Limestone and the Heatherdale Shale, are exposed in the core of an overturned regional anticline (Daily and Milnes, 1971a). They are conformably overlain on the normal eastern limb of this structure by an almost continuous sequence of Kanmantoo Group metasedimentary rocks that are exposed perfectly in the coastal cliffs. The cliffs extend eastwards for nearly 45km to the Encounter Bay area, and form the type section of the Kanmantoo Group (Sprigg and Campana, 1953; Daily and Milnes, 1971a, 1973). This sequence of Kanmantoo Group metasedimentary rocks is also present, despite some complications, along the northern coastline of Dudley Peninsula, Kangaroo Island (Daily and Milnes, 1971b, 1972a, and unpublished observations)[4].

Isolated outcrops of metasedimentary rocks, similar in

---

[4]The geology of the Kanmantoo Group in these areas forms part of the subject of this thesis, and is described in more detail in later sections

appearance to those of the Kanmantoo Group, occur in the western portion of the Murray Basin (Offler and Fleming, 1968). In addition, lithologically similar rocks of equivalent metamorphic grade make up the Glenelg River Complex of south-western Victoria (Wells, 1956). However, in both cases, their relationship to Kanmantoo Group metasedimentary rocks is not known.

Fossiliferous Cambrian sediments crop out along much of the northern coast of Kangaroo Island between Middle River and Point Marsden (Figure 2). They consist of a sequence of sandstones, conglomerates and shales, the latter containing a trilobite-rich Lower Cambrian fauna (Daily, 1956). Daily (1969) and Stuart and von Sanden (1972) have correlated them with the Kanmantoo Group succession. However, as fossils (with the exception of worm casts) have yet to be discovered within the Kanmantoo Group, this lithological correlation must remain tentative.

The relationships of a thick sequence of fossiliferous Lower and Middle Cambrian sediments in stratigraphic bores on Yorke Peninsula have similarly been described by Daily (1956, 1969) and Stuart and von Sanden (1972). In their correlation charts, the Kanmantoo Group and the Kangaroo Island fossiliferous Lower Cambrian sediments are shown to be absent, as the result of erosion, from the Yorke Peninsula succession (Figure 4).

1.2.4 *Palaeozoic tectonics and metamorphism*

The basement rocks, and Upper Proterozoic and Lower Cambrian sediments of the Mount Lofty Ranges were metamorphosed and deformed as the result of an Upper Cambrian to Ordovician orogeny (Thomson, 1969; Stuart and von Sanden, 1972). The orogenesis, for which an age of 465 m.y. has been suggested by Compston, Crawford and Bofinger (1966), resulted in a complex fold belt with a series of metamorphic zones ranging from a chlorite zone on the western side, to a migmatite zone on the eastern side (Offler and Fleming, 1968; Figure 3 of this thesis). Andalusite, staurolite, kyanite and sillimanite schists, migmatites, granitic gneisses and granites occur within the high grade metamorphic zones. It is of note that, in contrast with many other metamorphic belts, the high grade metamorphism indicated by the crystallisation of andalusite commenced prior to the first phase of folding (Fleming and Offler, 1968).

According to Offler and Fleming (1968), at least three generations of folding occurred during the orogeny, and in some cases a fourth generation can be recognised. First generation folds tend to be inclined and asymmetric, with east limbs of antiforms longer than west limbs, and easterly dipping axial planes. The axial traces of first generation folds follow the regional trends of the metamorphic belt. Second and third generation folds are distinguished from first generation folds by their more open style, and by their refolding of first generation structures. Macroscopic third generation folds apparently dominate the structure in the eastern part of the metamorphic belt, and have NNW - SSE axial trends.

Stuart and von Sanden (1972) delineated the broad scale pattern of faults within the Mount Lofty Ranges and adjacent areas from geophysical data and surface reconnaissance. Moreover, they noted the occurrence of several reverse and thrust faults that are associated with the overturned regional anticlinal structures containing Older Proterozoic basement cores. As shown by Daily and Milnes (1971b, 1972a), the recognition of thrust faults of this type is vital to an understanding of the geology of the metamorphic belt as a whole.

1.2.5 *Late Palaeozoic glacigene sediments*

Unconsolidated Late Palaeozoic glacigene sediments obscure large areas of Proterozoic and Cambrian metasedimentary rocks on Fleurieu Peninsula, and are also present on Yorke Peninsula and in many localities on Kangaroo Island (Figure 2). In addition, they have been intersected in bores in many parts of the Murray Basin (O'Driscoll, 1960; Ludbrook, 1961). On Fleurieu Peninsula and Kangaroo Island, the glacigene sediments rest unconformably on smoothed and striated surfaces of basement, Adelaide Supergroup and Kanmantoo Group metasedimentary rocks.

The glacigene sediments consist of boulder sands and silts, associated with rythmically bedded thin sands and clays containing dropstones. Erratics, most of which are granitic, occur within the sediments and are randomly strewn over the present land surface. Many of them have been locally derived from outcrops of Encounter Bay Granites, although several exotic types can be recognised.

The age of the glacigene sediments has only recently been established as Lower Permian (Balme, 1957; Ludbrook, 1956, 1967; Harris and McGowran, 1972), although a Permian or Permo-Carboniferous

age had been favoured by earlier workers (Howchin, 1898, 1899, 1900, 1910, 1926; Campana and Wilson, 1955). Ludbrook (1956, 1967) described Lower Permian marine foraminifera in glacigene sediments from Cape Jervis, localities on Yorke Peninsula, and in bore cores from the Murray Basin, and suggested that the sediments were at least in part deposited in a marine environment. Crowell and Frakes (1971) suggested that sedimentation occurred in a discontinuous marine and lagoonal epeiric sea.

The direction of movement of Late Palaeozoic ice across Fleurieu Peninsula, as documented by the striations, grooves and other features on glaciated surfaces, was approximately from east to west (Milnes and Bourman, 1972)[5]. The multi-glaciation hypothesis of Crowell and Frakes (1971), which includes an initial south to north movement of ice across Fleurieu Peninsula, followed by a second phase development of separate ice tongues in an irregular system of original stream valleys is not consistent with the evidence presently available.

1.2.6 *Post-Palaeozoic sediments*

Tertiary sediments of the St. Vincent and Murray Basins overlap the flanks of the Mount Lofty Ranges metamorphic belt, and are also found as isolated outliers within the ranges at heights of up to 240m above present sea level. They range in age from Eocene to Pliocene (Glaessner and Wade, 1958; Stuart, 1970; Ludbrook, 1961, 1969).

The oldest post-Palaeozoic sediments yet known in the vicinity of the Mount Lofty Ranges are of Eocene age. However, Dr. P. Wellman (private communication, 1971) has obtained a Jurassic age for the basaltic rocks of tholeiitic affinities that occur on Kangaroo Island on the basis of K-Ar data. Previous interpretations had classified the Kangaroo Island basalts as a suite of extrusive rocks of similar age but different origin to the Tertiary and Quaternary basaltic rocks of the Mount Gambier region of the far south-east of South Australia. The present inclination (Dr. P. Wellman, private communication, 1971) is to relate the Kangaroo Island basalts to the tholeiitic suite of Jurassic dolerites in Tasmania.

Quaternary and Recent deposits in the region effectively mask a large proportion of the older sediments and rocks. They include beach-dune sandstones that are spectacularly developed in the Murray Basin area

---

[5]See Appendix A

(Hossfeld, 1950; Sprigg, 1952; Blackburn, Bond and Clark, 1965) and in coastal areas of southern Kangaroo Island and Yorke Peninsula. Younger deposits, including the aeolian sands of the Murray Basin, as well as outwash from the Mount Lofty Ranges and coastal beach and dune sands, are all part of the modern landscape.

1.3 *NATURE AND FIELD RELATIONSHIPS OF THE GRANITES*

The Palaeozoic granites[6] of south-eastern South Australia can be conveniently divided into schistose[7] and non-schistose granites on the basis of field observations. They may be further classified into pre-tectonic or syn-tectonic, depending on the degree of development and orientation of the schistosity in relation to the penetrative structural elements in the contiguous rocks, or post-tectonic. In addition to this classification, the granites can be grouped into suites on the basis of the presently available field, petrographic and chemical data, including that obtained during this investigation. It remains to be seen however, in the light of detailed structural studies of the margins of the granites and important Rb-Sr and K-Ar data now being gathered by the South Australian Geological Survey, whether or not such a scheme is tenable.

Granites of the Cape Willoughby and Encounter Bay areas that constitute a large portion of the western granite belt are grouped as the non-schistose Encounter Bay Granites, on the basis of the above scheme. The granites of similar type that crop out at Cape Kersaint and east of Cape du Couedic, along the southern coast of Kangaroo Island (Figure 2), are also assigned to this suite. The Encounter Bay Granites, which are to be described in greater detail in the following sections, are grey coloured biotite granites containing distinctive opalescent blue quartz. The major variety is a coarse grained megacrystic granite that contains abundant large, ovoid crystals of potash feldspar, and fragments of metasedimentary rocks. Where exposed, the contacts between the granites and the contiguous Kanmantoo Group metasedimentary rocks are sharp.

---

[6]The term "granites" is used here in its broadest sense

[7]Schistose granites are those that contain an obvious penetrative preferred orientation of one or more minerals, usually micas. Granite schistosity of this type is distinguished from the non-penetrative preferred orientation of minerals such as micas and feldspars commonly referred to as flow layering or flow foliation

The major part of the eastern granite belt is comprised of the suite of granites that are exposed at Long Ridge, Mannum, Murray Bridge, Swanport, west of Coonalpyn and Tintinara, south of Keith, and at Dergholm in south-western Victoria (Figure 2). This granite suite, herein referred to as the Murray Bridge Granites, includes extrusive varieties (Mawson and Dallwitz, 1944; Mawson and Segnit, 1945a; Henstridge, 1970). The intrusive members of the suite are non-schistose, generally coarse grained, red coloured granites that contain smoky quartz. Contacts with metasedimentary rocks are not exposed, although rare fragments of metasedimentary rocks occur within the granites. At Long Ridge, Mannum and Murray Bridge, the granites may be intrusive into Kanmantoo Group rocks. Further east however, the nature of the intruded rocks is quite unknown. The extrusive granite varieties, which crop out to the south of Keith in association with intrusive granites of the same suite, include feldspar - quartz porphyries, feldspar porphyries, and flow-banded rhyolites (Henstridge, 1970). A distinctive feature of this granite suite is the ubiquitous occurrence of accessory fluorite.

Other granitic rocks of the eastern granite belt include the non-schistose Meningie granite (Mawson and Parkin, 1943; Mawson and Dallwitz, 1944) and the Taratap granite (Mawson and Parkin, 1943), as shown in Figure 2. The Meningie granite is similar in texture to the coarse grained varieties of the Encounter Bay Granites, but is so poorly exposed and in such a highly weathered condition that positive identification of any distinctive features is not possible. The Taratap granite is also similar in texture to the coarse grained varieties of the Encounter Bay Granites. It contains large euhedral feldspar megacrysts that are characteristically aligned as the result of flow, and abundant biotite-rich hornfels xenoliths. The presence of smoky quartz instead of the distinctive opalescent blue quartz suggests that it may not belong to the Encounter Bay Granites. On the other hand, its grey colour and absence of accessory fluorite distinguish it from the Murray Bridge Granites. Thus the relationships of both the Meningie granite and the Taratap granite are unknown.

A number of apparently unrelated schistose granites occur within Kanmantoo Group metasedimentary rocks in the zone of intersection of the two granite belts in the region of Palmer. These include the Rathjen

Gneiss (White, 1966), the Palmer Granite (White, Compston and Kleeman, 1967), the Reedy Creek granite (Sando, 1957), the Monarto Granite (Johns and Kruger, 1949), and the Tanunda Creek Gneiss (Hossfeld, 1925; Chinner, 1955; Offler, 1966). All are considered to be pre- or syn-tectonic, and contrast with the non-schistose Encounter Bay Granites and Murray Bridge Granites. The Mount Crawford granite gneiss (Mills, 1963), which occurs within Adelaide Supergroup metasedimentary rocks, is also placed in this category.

The Anabama Granite (Mirams, 1961) occurs a significant distance to the north of the zone of intersection of the granite belts and within Adelaide Supergroup metasedimentary rocks. Compston, Crawford and Bofinger (1966) have shown it to be of Lower Palaeozoic age, but at present its relationships with the granites further south are not known.

It is within this framework of the regional geology of the Mount Lofty Ranges metamorphic belt and the nature and field relationships of the adjacent rocks that the geology of the Encounter Bay Granites and their immediate environment will be discussed.

SECTION 2

THE ENVIRONMENT OF THE ENCOUNTER BAY GRANITES

2.1 *GENERAL DESCRIPTION*

The Encounter Bay Granites crop out in the Encounter Bay area as discontinuous masses along the coastline at Rosetta Head and Port Elliot, and on the adjacent small islands (Figure 7; Plate 1). The contact of the granites with the surrounding Kanmantoo Group metasedimentary rocks is exposed in only two localities, namely Rosetta Head and Wright Island. In all other localities the contact is obscured either by post-Palaeozoic to modern sediments or by the sea, and so its position can only be inferred. However, the outcrops are interpreted as remnants of the north-western wall of a large pluton of Encounter Bay Granites that may have extended for a considerable distance south and east of the present coastline of Encounter Bay.

Late Palaeozoic to Recent sediments blanket much of the land surface in the Encounter Bay area, and overlie the Kanmantoo Group metasediments with marked unconformity (Figure 7). Late Palaeozoic glacigene sediments, which include boulder sands and silts and varve-like deposits containing drop-stones, occupy ice-eroded depressions in the Kanmantoo Group bedrock (Bourman, 1969; Crowell and Frakes, 1971). A Tertiary (Eocene) sandy limestone has been intersected in a bore approximately 5km west of Rosetta Head (Bourman and Lindsay, 1973), but outcrops of Tertiary sediments have not been recognised. Younger sediments include beach and dune sandstones (probably of Pleistocene age) which crop out up to 70m above present sea level in coastal areas. Outwash, alluvium and present-day beach and dune sands make up the modern sediments.

The occurrence of a glaciated granite surface at Port Elliot, together with the abundance of erratics of Encounter Bay Granites in areas of glacigene sediments throughout Fleurieu Peninsula, demonstrates that the granites were exposed during the Late Palaeozoic glaciation, and at the same level within the intrusion as presently exposed. In fact, the present broad distribution of the granite outcrops is interpreted as the result of the dissection of an originally extensive pluton of Encounter Bay Granites by a westerly or north-westerly moving ice-sheet (Milnes and Bourman, 1972). Thus the long-held opinion that many of the landforms in the Encounter Bay area are principally the result

of ice action (Howchin, 1910, 1926; Campana and Wilson, 1955; Bourman, 1969) is probably correct. However, there has been significant subsequent erosional modification of some of the granite landforms, as indicated by the occurrence of features characteristic of inselberg structures, for example sheeting, flared slopes and gnammas. In addition, there is a marked development of tafoni, micropediments and corestones (Bourman, 1969; Milnes and Bourman, 1972).

Cape Willoughby is a prominent outcrop of Encounter Bay Granites forming the easternmost extension of Dudley Peninsula, Kangaroo Island (Figures 2 and 8). As in the Encounter Bay area, the granites are very well exposed in the coastal cliffs, but poorly exposed inland from the coast where a significant proportion of the land surface is covered by thick vegetation. Furthermore, a calcrete crust, overlying Pliocene to Pleistocene carbonate-rich sediments, covers much of the central portion of the headland and considerable areas of the rest of Dudley Peninsula.

The contact between the granites and the Kanmantoo Group metasedimentary rocks is exposed on the coast to the north-east and the south-west of the headland, as seen in Figure 8. Thus the outcrop is interpreted as a part of the north-western wall of a more extensive granite body which may be continuous with that in the Encounter Bay area, over 50km to the north-east. The occurrence of Late Palaeozoic glacigene deposits with abundant erratics of Encounter Bay Granites immediately west of Cape Willoughby, and along the north coast of Kangaroo Island, indicates that the granites here were also exposed during the glaciation.

2.2 *THE KANMANTOO GROUP*

The Kanmantoo Group is a thick repetitious sequence of metasedimentary rocks, and is shown on South Australian Geological Survey map sheets (Thomson and Horwitz, 1962; Sprigg, 1954) as forming the major part of the Mount Lofty Ranges metamorphic belt to the east of the Older Proterozoic basement inliers and on the southern parts of Fleurieu Peninsula and Kangaroo Island. The Encounter Bay Granites and other granite masses such as the Palmer Granite, the Monarto Granite, the Reedy Creek granite, the Rathjen Gneiss and the Tanunda Creek Gneiss (Figure 2) occur within Kanmantoo Group metasedimentary rocks, as noted in an earlier section. However, the age of the Kanmantoo Group and its relationships with rocks of known Lower Cambrian and Proterozoic age have long been a source of controversy amongst geologists working in the Mount Lofty Ranges.

2.2.1 *Previous investigations*

Howchin (1906, 1910) assigned a Cambrian age to all post-basement metamorphic rocks on Fleurieu Peninsula, including the Kanmantoo Group metasediments in the Encounter Bay area. However, Tilley (1919b) alluded to a possible Proterozoic age for the Kanmantoo Group on the basis of a suggested correlation with Proterozoic sediments that underlie the fossiliferous Lower Cambrian sequence at Sellick Hill.

Madigan (1925) discovered a flaggy limestone on the south coast of Fleurieu Peninsula, during a traverse along the coastline from Sellick Hill to Victor Harbour, and equated it with the Delamere marble, which he believed to be of Cambrian age. On this basis, he argued that the rocks exposed to the east of the marble were also likely to be of Cambrian age because they appeared to be stratigraphically overlying the marble. Thus the earlier suggestion of Howchin regarding the age of the Kanmantoo Group in the Encounter Bay area received considerable support from Madigan's interpretation. However, in 1926, Howchin relegated the Kanmantoo Group to the Proterozoic on the basis of his investigations in the River Inman valley near Grey Spur (Figure 2), where he suggested that Kanmantoo Group metasedimentary rocks unconformably overlie rocks of the basement inlier. He concluded that the Encounter Bay Granites had intruded "a sedimentary series which, as superior to the Basal Grits, can be no other than the Adelaide Series" (Adelaide Supergroup using the presently accepted terminology).

Sprigg and Campana (1953) collated data accumulated by the South Australian Geological Survey during regional mapping of the Kanmantoo Group, and proposed that the type section of the Kanmantoo Group should be the section "observable along the south coast of Fleurieu Peninsula, between Campbell Creek and Rosetta Head, Victor Harbour, where the formations are well exposed and very characteristic". They described the Kanmantoo Group in this section as consisting mainly of quartzites and micaceous quartzites, siltstones, quartz schists and phyllites stratigraphically overlying mottled limestones and "(?) coprolitic phyllite slates". Moreover, they supported a Cambrian age for the rocks as proposed by Madigan, but suggested that they might extend into the Ordovician.

Campana, Wilson and Whittle (1954) and Daily (1963, 1969) suggested that the alternating shales and sandstones of the Carrickalinga

Head Formation, which conformably overlie the Heatherdale Shale at Carrickalinga Head, mark the base of the Kanmantoo Group. However, the relationships of the Carrickalinga Head Formation to Kanmantoo Group rocks in the type section and elsewhere was not known.

Forbes (1957) described and subdivided the sequence of metasedimentary rocks between Grey Spur and Port Elliot (Figures 2 and 9), but was not certain of the stratigraphic relationships of any but the youngest formation, which he correlated with the Kanmantoo Group. However, subsequent workers such as Crawford and Thomson (1959), Horwitz and Thomson (1960), Thomson and Horwitz (1962) and Thomson (1969, 1970) applied his scheme, with only minor modification, directly to the Kanmantoo Group. Consequently, a dilemma regarding the base of the Kanmantoo Group arose. Thomson and his co-workers recognised the Strangway Hill Formation (Strangway Hill Beds of Forbes) as the basal formation on the eastern side of the basement inliers, and suggested that it was transgressive over rocks of age ranging from the Older Proterozoic to the Lower Cambrian. On the other hand, Campana, Wilson and Whittle (1954) and Daily (1963, 1969) recognised the Carrickalinga Head Formation, conformably overlying Lower Cambrian fossiliferous rocks on the western side of the basement inliers, as the basal formation.

2.2.2 *The Kanmantoo Group in its type section, and on Dudley Peninsula*

Daily and Milnes (1971a, 1973) have described the stratigraphic sequence of metasedimentary rocks constituting the type section of the Kanmantoo Group. The sequence was confirmed by subsequent investigations of Kanmantoo Group metasedimentary rocks exposed along the north coast of Dudley Peninsula (Daily and Milnes, 1971b, 1972a, and unpublished observations), and along the Mount Barker Creek, over 100km north of the type section. On the basis of these investigations, and of an examination of several intervening areas, it has been possible to demonstrate that the Kanmantoo Group conformably overlies Lower Cambrian fossiliferous rocks and is therefore probably Cambrian in age, and to completely revise the pre-existing stratigraphic nomenclature for the Kanmantoo Group (Daily and Milnes, 1972b). The implications of the new stratigraphic scheme, with regard to the interpretation of the stratigraphy and structure of the eastern part of the Mount Lofty Ranges, are considerable.

The geology of the type section is shown in Figures 5, 6 and 7, and the corresponding stratigraphic sequence is summarised in Figure 10. Except for a section of approximately 1km in length west of Campbell Creek

(Figure 5), the stratigraphic succession occurs on the normal easterly dipping limb of an overturned regional anticline and is relatively simple, despite the amphibolite facies metamorphism and the occurrence of small- to large-scale parasitic folds. The Kanmantoo Group conformably overlies Lower Cambrian fossiliferous metasediments, including the upper member of the Forktree Limestone and the Heatherdale Shale which form the core of the regional fold, and can be traced almost continuously eastwards into contact with the Encounter Bay Granites at Rosetta Head.

The metasandstones, metasiltstones and phyllites of the Carrickalinga Head Formation, the Tapanappa Formation, the Balquhidder Formation, the Petrel Cove Formation and the Middleton Sandstone are generally similar and to a large degree repetitious. They will not be described here. However, certain of the formations contain unique lithologies or lithologic intervals, which can and have been used successfully as marker beds (Daily and Milnes, 1972b). For example, the Backstairs Passage Formation is composed of well-laminated, light coloured metasandstones with prominent cross-bedding and small to large scale slumps. The Talisker Calc-siltstone is a formation of banded calcareous phyllites, which contain abundant pyrrhotite in some localities. The base of the Tunkalilla Formation is marked by a distinctive blue-black coloured carbonaceous phyllite intervals that also contain significant amounts of pyrrhotite. Similar phyllites mark the top of the formation, and occur sporadically throughout the overlying Balquhidder Formation as well. In fact, rocks of this type are confined to the Brown Hill Subgroup.

The stratigraphic sequence in the type section is duplicated, with some complications, along the northern coastline of Dudley Peninsula (Daily and Milnes, 1971b, 1972a, and unpublished observations; Figure 8 of this thesis). The geology here is dominated by an overturned regional anticline (the counterpart of that in the type section) which forms the core of a large scale thrusted block composed of Adelaide Supergroup metasediments. However, a succession of Kanmantoo Group metasediments occurs on the normal easterly dipping limb of the regional fold. The lowermost Madigan Inlet Member of the Carrickalinga Head Formation is absent due to faulting, but the middle member of the formation is in faulted contact with a sequence of basal Cambrian metasediments, namely the Mount Terrible Formation and overlying Wangkonda Limestone, which occur within a complex fault zone marking the eastern edge of the thrusted block (Daily and Milnes, 1972a). Unfortunately, the uppermost

part of the Tapanappa Formation, all of the Brown Hill Subgroup (Tunkalilla Formation and Balquhidder Formation), some of the Petrel Cove Formation, and some of the Middleton Sandstone are missing due to lack of outcrop in Antechamber Bay (Figures 8 and 10). However, from Cape St. Albans southwards to the contact with the Encounter Bay Granites at Cape Willoughby, it is possible to traverse a significantly thicker and better exposed interval of Middleton Sandstone than is present in the Encounter Bay area. The formation here consists of well-laminated, light coloured, relatively pure metasandstones in beds generally less than 1m thick. Cross-bedding is very common, and cut-and-fill structures, slumped beds and shale-chip conglomerates are present.

Two groups of basic dykes occur within the Kanmantoo Group in the areas examined during this investigation. Along the south coast of Dudley Peninsula west of Cape Hart (Figure 8), a number of extensively contaminated metadolerites have intruded the Middleton Sandstone along fractures trending at approximately 120°. The dykes are up to 50m wide, and have a complex and variable mineralogy and texture. Many of them contain megacrysts of quartz and feldspar, in addition to xenoliths of metasandstone and carbonate-rich metasediment. Several contain streams of quartz and carbonate xenocrysts. Others contain epidote-filled miarolitic cavities. The dykes occur within tensional fractures in the metasandstones, and are parallel to a conspicuous joint set that has controlled albitisation in the Encounter Bay Granites at Cape Willoughby. The fractures and joints are approximately normal to the contact between the granites and the Middleton Sandstone, but the relationships between the granites and the dykes are not exposed.

Two similar extensively contaminated basic dykes crop out along the south coast of Fleurieu Peninsula in the vicinity of Tunk Head (Figure 6). Madigan (1925) recorded the dyke that crops out in the wave-cut platform to the east of Tunk Head.

The second group of intrusive basic dykes consists of fine to medium grained metadolerites that occur both within the Encounter Bay Granites at Rosetta Head and Port Elliot, and within the Kanmantoo Group metasediments in many places along the south coast of Fleurieu Peninsula. These will be discussed in relation to the structural and metamorphic environment of the Encounter Bay Granites in subsequent sections.

2.3 *THE NATURE OF THE CONTACT BETWEEN THE GRANITES AND THE KANMANTOO GROUP*

2.3.1 *Encounter Bay area*

The contact between the Encounter Bay Granites and the Kanmantoo Group is exposed along the landward sides of Rosetta Head and Wright Island, where a coarse grained megacrystic granite containing large crystals of potash feldspar, plagioclase, and opalescent blue quartz is in extremely sharp contact with well-laminated metasiltstones and phyllites, and porphyroblastic andalusite-cordierite schists of the Petrel Cove Formation (Figures 7, 11 and 12). The granite is concordant with bedding in the metasediments on a broad scale, but in detail may transgress bedding. The contact plane has an approximate dip of 45 to 60° towards the east, as recorded by Browne (1920) and Bowes (1954). Thus the Encounter Bay Granites actually overlie the Kanmantoo Group. Because of the limited exposure however, it is impossible to determine whether this is a minor irregularity in the contact, or its true nature.

The contact is not exposed elsewhere in the Encounter Bay area. However, if the trend of the granite outcrops (as seen in Figure 7) is taken to approximate the trend of the contact, then the granites must transgress the stratigraphic boundary between the Petrel Cove Formation and the overlying Middleton Sandstone. The latter formation crops out immediately adjacent to the granites at Port Elliot.

Within the Petrel Cove Formation on Wright Island (Figure 11), there are several markedly concordant granite sheets, most of which are less than 1m wide (Plate 2: 1, 2 and 3). Although they are not connected to the main granite mass at the present level of exposure, they are evidently offshoots from it, and have been intruded along bedding planes in the metasediments. The wider sheets are generally composed of coarse grained megacrystic granite of a similar type to the main granite mass. However, thinner sheets consist of fine to medium grained granite. Transgressive vein offshoots from the granite sheets have also been noted (Plate 3: 1, 2 and 3). At Rosetta Head, granite sheets occur within the metasediments near the contact, but are poorly exposed (Figure 12).

The contact between the main mass of megacrystic granite and the metasediments is very sharp, but extremely irregular due to the growth of feldspar and quartz crystals from the granite across the contact

(Plate 3: 4). There is little variation in the grain size of either the granite or the metasediments near the contact, although a thin (1 to 2mm wide) biotite-rich zone occurs within the metasediments along the serrated boundary.

The main mass of megacrystic granite near the contact contains abundant angular well-laminated metasiltstone xenoliths that become progressively disoriented with respect to bedding in the adjacent metasediments with distance away from the contact (Plate 4: 1). The xenoliths and the host granite in such instances rarely show evidence of deformation. However, well developed penetrative deformation structures do occur in the adjacent metasediments, and in parts of the granite sheets.

In accordance with all of these observations, the contact between the Encounter Bay Granites and the Kanmantoo Group metasediments on Wright Island and Rosetta Head is interpreted as an intrusive contact.

In many places along the contact at Rosetta Head, the megacrystic granite and the metasediments have been extensively altered by late-stage, fracture-controlled albitisation. The rocks resulting from this alteration have been described by Browne (1920) and Bowes (1954). The alteration is a widespread and characteristic phenomenon within the Encounter Bay Granites.

2.3.2 *Cape Willoughby*

The Encounter Bay Granites here are intrusive into the Middleton Sandstone. The contact between the granites and the metasediments is not well exposed, but the broad scale relationships, as shown in Figure 8, indicate that the contact is probably roughly concordant with bedding. Discordant relationships between the granites and the metasediments are apparent in the two localities where the contact intersects the coastline (Figure 13). In these localities, the granites appear to overlie the metasediments as in the Encounter Bay area.

Tilley (1919b) briefly described the contact relationships exposed on the coastline to the north and south-west of the Cape. He referred to the transgressive nature of the granites, the presence of metasedimentary rock xenoliths in the marginal phase, the lack of any obvious contact metamorphic zone, and the occurrence of "small aplitic veins" that "proceed into the micaceous quartzites". Furthermore, he noted the present of tourmaline-filled "quartz geodes" in the granites near the contact.

The marginal granite variety is a medium grained megacrystic granite similar to that exposed in the Encounter Bay area. It contains disoriented xenoliths of Middleton Sandstone metasediments, particularly near the contact exposed on the coastline north of the Cape (Plate 4: 2 and 3). These have sharp boundaries with the granite, and as noted by Tilley, do not show any obvious contact metamorphic effects.

Fine grained, pink coloured aplite dykes have intruded both the megacrystic granite and the metasediments near the northern contact. There is also abundant evidence of late-stage, joint-controlled metasomatic alteration (albitisation and greisenisation) in the vicinity of this contact exposure, particularly within the granite. Near the contact on the coastline to the south-west of the Cape, abundant pegmatites containing smoky quartz occur within the metasediments.

2.4 *THE STRUCTURAL ENVIRONMENT OF THE GRANITES*

2.4.1 *Introduction*

The stratigraphy of the Kanmantoo Group in its type section and in the adjacent Brown Hill to Middleton area has been described by Daily and Milnes (1973) and is summarised in Figure 10. The Petrel Cove Formation is the highest stratigraphic interval exposed in the type section, whereas in the Brown Hill to Middleton area there is a continuous sequence through the upper part of the Balquhidder Formation, the Petrel Cove Formation, and part of the overlying Middleton Sandstone (Figure 7). The two areas are separated by a zone of no outcrop some 8km wide. Moreover, rocks in the Brown Hill to Middleton area do not contain metamorphic minerals such as andalusite and cordierite that are conspicuous in metasediments of equivalent stratigraphic position in the type section. This is the basis for the separate description of the two areas.

There have been few previous investigations of the structural geology of the Kanmantoo Group in its type section or in the Brown Hill to Middleton area. Hobbs and Talbot (1966) and Talbot and Hobbs (1968, 1969) described types of metamorphic layering in the Petrel Cove Formation metasediments near Rosetta Head, and presented an analysis of strain in the rocks, using the deformed shape of small-scale sedimentary structures as a basis for their calculations. Asthana (1958) studied the orientation of joints in the Encounter Bay Granites at Port Elliot and in the nearby Kanmantoo Group metasediments in the Port Elliot and Middleton quarries. R.G. Wiltshire (private communication, 1970) made

a brief study of the structural geology of the Kanmantoo Group in the type section.

2.4.2 *Type section of the Kanmantoo Group*

(i) Description of structural elements

An interpretation of observations and measurements of structural elements in the Kanmantoo Group metasediments exposed between Campbell Creek and Tunkalilla Beach has already been published (Daily and Milnes, 1971a). The present interpretation of these data can be summarised with reference to Figure 14 as follows:

a. poles to S_0 indicate a statistical fold axis plunging towards 047° at a low angle, although mesoscale F_1 folds plunge at variable angles both to the north-east and the south-west;

b. intersections of S_0 with S_1, long axes of phosphatic nodules (in the Heatherdale Shale), and the elongation of boudins resulting from the deformation of calc-silicate bands, are parallel to the axes of mesoscale F_1 folds;

c. mesoscale F_1 fold axes and the long axes of phosphate nodules and calc-silicate boudins define a great circle distribution which may be the result either of refolding or of inhomogeneous strain;

d. a lineation defined by the elongation of calcite and mica crystals on S_1 surfaces in calcareous and pelitic intervals respectively pitches at up to 20° from L_1, and is interpreted as a first generation structure (L_1') which developed parallel to the direction of maximum elongation; and,

e. a lineation defined by the preferred orientation of hornblende poikiloblasts and chlorite porphyroblasts on S_1 surfaces in calc-silicate boudins and pelitic intervals respectively is approximately parallel to L_1' and may represent a first generation structure.

The rocks occupying this interval of coastline consist of the fossiliferous Lower Cambrian Forktree Limestone and Heatherdale Shale, and the basal formations of the Kanmantoo Group from the Carrickalinga Head Formation up to and including the major part of the Tapanappa Formation (Figures 5 and 10). This complete sequence occurs to the east of Madigan Inlet on the normal eastern limb of a regional F_1 anticline which is overturned to the west. All mesoscale folds

observed are F_1 structures, and conform to the style of the regional structure, in that they are inclined and asymmetric, with east limbs of anticlines longer than west limbs. Moreover, they exhibit an axial plane schistosity that dips steeply towards the south-east. In many instances, dislocation of the overturned west limbs of anticlines and east limbs of synclines has taken place along fault zones that nearly parallel the axial plane schistosity (Plate 5: 1).

The metasediments between Tunkalilla Beach and Rosetta Head (Figures 6 and 7), constituting the Brown Hill Subgroup and part of the Petrel Cove Formation of the Wattaberri Subgroup (Figure 10), also occur on the normal eastern limb of the overturned regional anticline, but are at least 14km eastwards along the coastline from its closure. The mesoscale folds mapped in this interval of coastline as F_1 structures contrast with the style of the regional fold. Folds in metasandstone units are broad, open structures with both limbs normal and dipping at moderate angles away from the hinges. Folds in phyllite and metasiltstone units, particularly within the Petrel Cove Formation, are smaller scale structures that tend to be moderately tight and upright (Plate 5: 2, 3 and 4). At present, neither the nature of the transition from one fold style to the other, nor the precise location of the transition in the type section, is known. However, it is perhaps significant that the highly appressed and overturned F_1 folds occur in the lowermost formations of the stratigraphic sequence, whereas the more open upright folds occur in the progressively younger formations. A similar situation has been observed along the north coast of Dudley Peninsula, where highly appressed and overturned F_1 folds occur in the vicinity of the overturned regional anticline in Adelaide Supergroup and basal Kanmantoo Group metasediments, while large-scale open F_1 folds characterise the deformation in Tapanappa Formation metasediments at Cape Coutts (Figure 8), some 4.5km from the regional fold hinge.

The axial plane schistosity in F_1 folds is defined by the preferred orientation of micas, and is particularly well developed in pelitic units. In many metasiltstones and fine grained metasandstones, S_1 deforms sedimentary structures (Talbot and Hobbs, 1969; Plate 6: 1 and 2 of this thesis). In addition, it commonly enwraps small quartzo-feldspathic clots, and in some localities east of Newland Head (Figure 7), cordierite and andalusite porphyroblasts. When

present in sufficient abundance, the resulting augen define a unique augen layering parallel to S_1 (Plate 6: 3 and 4 of this thesis; Talbot and Hobbs, 1968). An elongation of the augen in S_1 is responsible for the distinct but often discontinuous lineation on S_1 surfaces (Plate 7: 1). This lineation is markedly different in orientation to the intersection of S_0 and S_1 surfaces and the direction of elongation of calc-silicate boudins, both of which are parallel to the axes of F_1 folds, and is interpreted as an L_1' lineation which developed parallel to the direction of maximum elongation.

A fine scale crenulation of S_1 is conspicuous in pelites in the Balquhidder Formation near Coolawang Creek (Figure 6), and becomes progressively more distinct eastwards. It provides evidence for the overprinting of first generation structures. In fact, this crenulation in the pelites of the Petrel Cove Formation is the expression of a penetrative strain-slip cleavage (S_2) which is axial plane to mesoscale F_2 folds. F_2 folds are especially well developed adjacent to pre-F_2 metamorphic pegmatites (Plate 7: 2, 3 and 4; Plate 8: 1). These folds refold small-scale F_1 folds, and are responsible for the local variation in the plunge of F_1 fold axes from north-easterly to south-westerly.

A distinctive striped layering (S_s) occurs at a low angle to S_1 in the metasediments of the Petrel Cove Formation, and is best developed in the coastal exposures just west of Petrel Cove. It is a penetrative planar structure on an outcrop scale, and has been described by Talbot and Hobbs (1968), who also reported the occurrence of similar layering in the Kanmantoo Mine area, some 60km north of Rosetta Head, in metasediments assigned by Daily and Milnes (1972b) to the Tapanappa Formation. The stripes are light coloured layers containing quartz and plagioclase, and are of variable width up to 3cm. They are bordered by thin biotite-rich zones, and commonly contain a median biotite- and/or quartz-filled fracture (Plate 8: 2). The striped layering exhibits features such as refraction across lithological boundaries and flaring (Plate 8: 3 and 4). Moreover, thin quartz-feldspar-mica pegmatites that parallel the striped layering often define planes of small-scale dislocation, especially in the hinge zones of mesoscale F_1 folds (Plate 9: 1 and 2). The stripes cut across S_1. However, a relict S_1 schistosity, outlined by the preferred orientation of muscovite and rare

biotite, rather than biotite as in the host metasediment, can still be observed within the stripes. It is of interest that the alteration of metasediments in fractured and brecciated zones that occur along the shorter limbs of mesoscale F_1 folds in several localities between King Head and Rosetta Head (Plate 10: 1 and 2) is superficially similar to that present in the stripes. Tourmaline-filled fractures were noted in these brecciated zones in the coastal exposures just east of King Beach. The albite and chlorite schists that crop out along the coastline west of Petrel Cove (Bowes, 1954) are considered to represent albitisation of Petrel Cove formation metasediments in similar fractured and brecciated zones.

Although the striped layering is not obviously related to any known folds, its relative age can be deduced from the structural relationships observed in the field. It clearly cuts across and therefore post-dates S_1. However, it has been folded on a small scale by S_2 in andalusite schist bands, and therefore pre-dates S_2 (Plate 10: 3).

(ii) Geometry of the structural elements

The structural geometry of the metasediments in the type section of the Kanmantoo Group between Campbell Creek and Tunkalilla Beach (Daily and Milnes, 1971a) has been summarised in the preceding section with reference to Figure 14. Measurements of structural elements in the metasediments between Tunkalilla Beach and Rosetta Head are presented in Figures 15a, 15b, 15c and 15d.

Poles to S_0 between Tunkalilla Beach and Rosetta Head show a great circle spread, and indicate a statistical[8] fold axis plunging at 25° towards 200° (Figure 15a). This is supported by the attitudes of L_1 lineations defined by the intersection of S_1 and S_0 surfaces, and the elongation of calc-silicate boudins (Figure 15b). However, axes of mesoscale F_1 folds are distributed around two point maxima, indicating plunges towards the north-east and the south-west at shallow angles (Figure 15c). This variation in plunge together with the significant spread of poles to S_1 (Figure 15c), may indicate refolding of first generation structures. L_2 lineations (the axes of crenulations in S_1) plot as a diffuse maximum plunging at 65° towards 165° (Figure 15d)[9],

[8]Statistical is not used here in its strict sense. Statistical fold orientations have been estimated from structural diagrams by eye

[9]Mesoscale F_2 folds are uncommon, but generally occur near the margins of pre-F_2 pegmatite dykes in the Petrel Cove Formation. No attempt was made to measure their orientation in such localities

which coincides with the distribution of lineations (L_1') defined by the elongation of augen in S_1.

2.4.3 *Brown Hill area*

(i) Description of structural elements

In the Brown Hill area (Figure 7), large scale north-easterly plunging F_1 folds in metasandstones and interbedded metasiltstones and phyllites of the Balquhidder Formation occupy a narrow north-easterly trending zone. The folds are upright, and have the broad open style typical of F_1 folds in metasandstone units in the eastern part of the type section. The axial plane schistosity is defined by the preferred orientation of micas. A lineation formed by the intersection of S_1 and S_o surfaces is parallel to F_1 fold axes. S_1 surfaces in pelites contain a mineral lineation defined by the preferred orientation of micas. The lineation has a steep south-easterly pitch in S_1, and is interpreted as a first generation structure (L_1'). It is best seen in the Lincoln Park quarry, south of Brown Hill.

(ii) Geometry of the structural elements

The few measurements of attitudes of structural elements taken in this area have been plotted in Figure 15e. Poles to S_o lie along a great circle, and indicate a statistical F_1 fold axis plunging at 35° towards 051°. This is supported by the attitudes of L_1 lineations. Two measured L_1' lineations plunge steeply towards the south.

2.4.4 *Middleton area*

(i) Description of structural elements

East of the Brown Hill area, F_1 folds in metasediments assigned to the Petrel Cove Formation and the Middleton Sandstone have been overprinted by large- and small-scale F_2 folds that plunge at shallow angles towards the south-east. The relationships between F_1 and F_2 structures, both of which exhibit varying degrees of development in the area, are best examined in the Middleton quarry about 1.6km north-west of Middleton (Figure 7).

South-easterly plunging F_2 folds are the dominant structures in the Middleton quarry, and are moderately appressed, inclined folds in which the northern limbs of anticlines are longer than the southern limbs, and tend to be overturned. The larger folds contain small-scale refolded F_1 folds in pelitic units (Plate 10: 4 and 5). An axial plane schistosity to F_2 folds is not well developed. However, a prominent set

of parallel fractures occurs in F_2 folds in metasandstones and is parallel to the inferred axial plane of the folds (Plate 11: 1). The intersections between bedding surfaces and the fractures defines a prominent ridge-and-furrow lineation which is parallel to the axes of F_2 folds, and is referred to here as L_2 (Plate 11: 2).

The fractures (which are hereafter termed S_2) are closely spaced in the hinge zones of F_2 folds, and to a large extent have controlled albitisation and the emplacement of thin pegmatites (Plate 11: 1, 3 and 4). They have also been planes of post-alteration movement, and are presently characterised by thin coatings of fibrous hornblende (see Appendix B). Thin brecciated zones may parallel the fractures.

A well developed axial plane schistosity in some mesoscale folds in fine grained metasandstones in the Middleton quarry can be seen in thin sections to crenulate a relict schistosity that is approximately parallel to bedding (Plate 12: 2). An examination of the axial plane schistosity surfaces shows a conspicuous mica-streaking lineation that is not parallel to the intersection between bedding and the axial plane schistosity (Plate 12: 1). Such folds have the style of F_1 folds in the Brown Hill area and in the eastern part of the type section, but the presence of two schistosities makes their identification difficult. In contrast with these folds, small-scale F_2 folds in the Middleton quarry are characterised by a poorly developed axial plane schistosity (S_2) that overprints a moderately well developed schistosity parallel to bedding. However, in these folds, it is the older schistosity that contains a prominent mica-streaking lineation. The mica-streaking lineation is similar in nature to the L_1' lineation recorded in metasediments in the type section and in the Brown Hill area, and has been tentatively designated L_1'. In the Middleton quarry, it is readily seen on the surfaces of large-scale F_2 folds where it is oriented at a significant angle to the intersection between bedding and S_2 (Plate 12: 3 and 4). In view of these observations, the mescoscale folds of uncertain affinities are best interpreted as first generation structures that formed in metasediments containing a pre-tectonic bedding plane schistosity. The prominent mica-streaking lineation that occurs on the axial plane schistosity to these folds is therefore L_1'.

F_2 folds were not observed in the rather poor exposures outside

the Middleton quarry, or in the small quarry exposures north-west of Port Elliot. In these localities, folds presently interpreted as first generation structures because of their orientation and style form the dominant elements. Such folds are best seen in the exposures to the north of the Middleton quarry. They are inclined, and plunge at steep angles towards the south-east. The axial plane schistosity is a pronounced mica preferred orientation which overprints a poorly preserved presumed pre-tectonic bedding plane schistosity in some specimens. The intersection of bedding with the axial plane schistosity is parallel to the axes of the folds. However, a prominent mica streaking lineation on schistosity surfaces pitches up to 20° from the intersection between bedding and the axial plane schistosity.

S_1 surfaces in phyllites of the Petrel Cove Formation equivalent exposed in the quarries north-west of Port Elliot and in the cuttings along the Crow's Nest road exhibit a fine-scale crenulation. The crenulation appears to have a similar orientation to the conspicuous mica streaking lineation (presumed L_1') on S_1 surfaces in metasandstones in the Middleton area, but is interpreted as a second generation structure.

The exposures of Middleton Sandstone along the coastline at Middleton are dominated by F_2 structural elements. Although F_2 folds are not common, the attitude of the prominent ridge-and-furrow lineation (L_2) indicates a shallow easterly plunge for such structures.

(ii) Geometry of the structural elements

Poles to S_0 measured in the Middleton quarry (Figure 15f) do not reflect the attitudes of first generation folds, but define a statistical F_2 fold axis plunging at 50° towards 118°. This agrees very well with the attitudes of measured F_2 fold axes and L_2 ridge-and-furrow lineations (Figure 16a). In addition, it is consistent with the distribution of poles to F_2 fractures in metasandstones.

The distribution of measured mica streaking lineations in the Middleton quarry indicates a statistical plunge towards 122° at 65°, whilst the attitude of the related schistosity indicates a steeply plunging inclined style for folds herein interpreted as first generation structures (Figure 16b).

The structural elements S_0 and L_2 measured in the exposures at Middleton Beach define an F_2 fold axis plunging at 28° towards 090°,

and this is supported by the attitude of one mesoscale F_2 fold axis (Figure 16c).

In all other parts of the Middleton area, first generation structures are dominant. Poles to S_o define a statistical F_1 fold axis plunging at 60° towards 142° (Figure 16d). The rather diffuse distribution of S_o poles on the western side of the diagram may reflect the influence of second generation folds. The attitude of the statistical F_1 fold axis is confirmed by the distribution of mica streaking lineations and the attitudes of poles to the axial plane schistosity (Figure 16e), and approximately coincides with the orientation of presumed first generation structures mapped in the Middleton quarry.

2.4.5 *The contact between the granites and the Kanmantoo Group*

The structural elements at the contact between the granites and the Kanmantoo Group have been studied in the Encounter Bay area only, and are best examined on Wright Island (Figure 11). The most obvious of these structural elements is a prominent schistosity, which occurs in both the marginal granite phases and in the Petrel Cove Formation metasediments.

The schistosity is spectacularly developed in thin granite sheets, near the margins and constricted portions of wider but strongly boudinaged sheets (Plate 13: 1 and 2), and in the main granite mass within a metre or so of the contact on the northern part of the island (Plate 13: 3). It should perhaps be more correctly termed a layered schistosity, since it is defined by an alternation of layers, less than 2mm wide, containing extensively recrystallised biotite and quartz. The layers enwrap large potash feldspar and plagioclase megacrysts (Plate 13: 4). Many of the feldspars have been rotated. However, most have retained their original structures and textures such as growth twinning, compositional zoning, and zonal arrangement of inclusions. Many have also retained their gross external morphology, but recrystallisation of their margins has occurred with the associated development of strain-shadow structures. In addition, myrmekitic intergrowths are common in the recrystallised margins of the potash feldspar megacrysts. Biotite-rich layers consist predominantly of fine grained biotite crystals, but may contain medium to coarse grained augen-shaped biotite crystals. Moreover, biotite has a strong preferred orientation in the plane of the layers. Quartz layers consist of a mosaic of unstressed, fine grained equigranular crystals. Microfolds in the layered

schistosity are relatively common in the strain shadows of large feldspar megacrysts, and have as axial plane schistosity the very biotite schistosity that partly defines the layered schistosity (Plate 14: 1 and 2). This seemingly ambiguous situation must reflect a monogenetic origin for both the microfolds and the layered schistosity. In some localities, metasedimentary rock xenoliths have been markedly deformed in the plane of the schistosity.

The schistose granite is best classified as a protomylonite (Higgins, 1971). The schistosity is interpreted as a post-consolidation feature imposed as the result of plastic deformation at sufficiently high temperatures to allow recrystallisation of the deformed quartz. Waters and Krauskopf (1941) and subsequently Higgins (1971) have applied the term "protoclastic" to the schistose margins of granite plutons, and have suggested that the schistosity is due to late intrusive movements of the plutons. In this area however, the schistosity is considered to have been imposed during regional deformation. The variable development of the schistosity in the granites along the contact, together with its complete absence from the internal parts of the pluton, is taken as evidence for the high yield strength of the granites at this time, and suggests that the pluton possessed rigid body properties during the regional deformation.

Mesoscopic folds occur in the metasediments immediately adjacent to the granite sheets, especially on the southern side of the island. Many of the folds are truncated by the granite sheets, and by thin granite veins which are offshoots from the sheets. These folds therefore pre-date the emplacement of the granites. However, other examples occur in which the granite sheets and their vein offshoots are folded with bedding in the metasediments. These folds were clearly developed after granite emplacement. Folds predating granite emplacement vary in orientation, and seem to have been disoriented during granite emplacement. On the other hand, folds post-dating granite emplacement have an orientation that is consistent with the attitude of the schistosity in the granite sheets and in the metasediments, and with the attitude of first generation folds in the metasediments near Rosetta Head. It would appear from these observations that the granites were emplaced after the initiation of folding in the metasediments, but had crystallised prior to the main phase of first generation folding and

associated S_1 schistosity development. The early folds are assumed to have developed during the initial stages of first generation deformation, since older tectonic structures have not been recognised in the region. Moreover, the presence of a poorly developed schistosity oriented at moderate angles to bedding in a few metasediments xenoliths within the granites is consistent with the incipient development of S_1 during folding prior to granite emplacement.

Younger structures also occur within the metasediments and granite sheets on Wright Island. Fine scale crenulations of the S_1 mica schistosity in the metasediments and of the schistosity in the granite sheets define an L_2 lineation, which plunges steeply towards the south-east. Thin sections of contacts between granite sheets and metasediments show that L_2 is the expression of a penetrative although poorly developed crenulation cleavage (Plate 14: 3).

Broad kink folding of bedding and thin granite sheets has also been noted (Plate 14: 4). The folds occur as isolated structures in narrow belts, and plunge at moderate angles towards the south-east. An irregular fracture set is approximately parallel to the axial planes of these folds. The folds are similar in orientation to F_2 folds mapped between King Beach and Rosetta Head, and in the Middleton area, but their relationships have not been studied.

A small zone of knotted andalusite schist occurs within the metasediments on the southern side of Wright Island, but is visible only at low tide. The andalusite porphyroblasts have crystallised in thin bands parallel to bedding, and along the margins of cross-cutting granitic veinlets, and post-date the development of the S_1 schistosity.

A 6-7m wide cataclastic zone crosses the contact on the southern side of Wright Island (Plate 15: 1). Cataclastic textures are conspicuous in the marginal parts of the megacrystic granite, in which the S_1 schistosity and many xenoliths are deformed, but are not so obvious in the adjacent metasediments. The cataclastic zone consists of a number of thin sub-zones of mylonitised granite that grade outwards into cataclastic granite, and follows a major joint set that has controlled albitisation in the granites in this locality. The cataclastic deformation however, is clearly post-albitisation since the albite megacrysts are strongly fractured and broken apart, and the rock possesses a moderately well developed fluxion structure (Plate 15: 2). The textures present are strikingly different from those of the

granite, and are interpreted as the result of low temperature brittle deformation. Minor post-albitisation deformation of similar joint sets has occurred in the granites in other localities.

The structural relationships between the Encounter Bay Granites and the metasediments of the Petrel Cove Formation are not as easily examined at Rosetta Head because of the relatively poor exposure of the contact. However, there are some interesting features in outcrops along the wave-cut platform near the southern tip of the headland. The megacrystic granite here has been completely albitised, and is littered with albitised metasedimentary rock xenoliths (Plate 15: 3). Moreover, it is completely devoid of any deformation textures. The adjacent metasediments contain several noteworthy structures, perhaps the most obvious of which are mesoscopic folds that are developed in bands parallel to bedding (Plate 15: 4; Plate 16: 1). The complicated style of these folds, and their occurrence in an interval of otherwise planar-laminated metasiltstones, suggests that they formed prior to consolidation of the original sediments. The peculiar structure illustrated in Plate 16: 2 probably has the same origin.

Small-scale deformation folds occur along narrow zones of dislocation that mark the extensions of granitic veinlets in this locality (Plate 16: 3 and 4). The folds plunge at shallow angles to the northeast, and are reminiscent both in style and orientation of F_1 folds elsewhere within the Petrel Cove Formation (e.g. Plate 10: 1).

One additional feature is the development of very small post-F_1 andalusite porphyroblasts, similar to those observed on the southern side of Wright Island, in thin bands parallel to bedding and immediately adjacent to thin cross-cutting granitic veinlets (Plate 17: 1 and 2).

2.4.6 *Discussion*

The observations and measurements of structural elements made during this investigation indicate the presence of two main phases of deformation in the Kanmantoo Group metasediments in the type section and in the Brown Hill to Middleton area. With the exception of parts of the Middleton area, first generation structures are dominant throughout the region. However, second generation structures are moderately well developed in the eastern part of the type section, and are dominant in the exposures at Middleton Beach and in the Middleton quarry.

There are several features of the structural environment of the Encounter Bay Granites that will only be adequately explained after the

completion of a more comprehensive investigation of the structural geology of the Kanmantoo Group than was attempted here. The variable development of structural elements in the areas described is one example. This, together with the imperfect outcrop in the Encounter Bay area, has prevented an unambiguous correlation of structural elements between the type section and the Brown Hill to Middleton area, and even within the latter area, on the basis of the present structural data. The variability in style and orientation of F_1 folds from overturned, highly appressed, north-easterly plunging structures in the vicinity of the regional anticline at Madigan Inlet, to relatively open, upright south-westerly plunging structures in progressively younger formations further eastwards in the type section, and moderately appressed, overturned folds plunging steeply to the east in the Middleton area, is also inexplicable on the basis of the present data but is nonetheless considered to be an important observation.

Notwithstanding, the present data provide an adequate basis for interpretation of the time of emplacement of the Encounter Bay Granites, at least in the Encounter Bay area, in relation to the structural deformations recorded in the contiguous Kanmantoo Group metasedimentary rocks. The following observations are considered most pertinent to this discussion:

a. some mesoscopic folds in Petrel Cove Formation metasediments adjacent to the granite sheets, and in metasediment xenoliths in granite sheets on Wright Island, pre-date the emplacement of the granites;

b. the prominent layered schistosity that occurs within some parts of the megacrystic granite at the contact between the granite and the metasediments, and is particularly well developed in boudinaged granite sheets within the metasediments on Wright Island, is parallel to the S_1 schistosity in the metasediments and is axial plane to mesoscopic folds which deform both the granites and the metasediments; and,

c. metasediment xenoliths within the granites do not contain porphyroblasts of metamorphic minerals such as andalusite or cordierite, which occur in abundance in parts of the contiguous Petrel Cove Formation, and many are also devoid of tectonically imposed mica preferred orientations.

It was not possible to measure the attitudes of granite boudins. They appear to plunge at moderate angles towards the south, and may be consistent with the attitude of either of the first generation lineations (L_1 or L_1'), or with the attitudes of L_2 lineations (Figures 15b and 15d). However, they appear to have formed simultaneously with the S_1 schistosity, since this structure is especially well developed in the margins and constricted portions of the boudins (Plate 13: 2). Thus the boudins are considered to be first generation structures. Unaltered metasedimentary rock xenoliths within the megacrystic granite are abundant, and consist of well-laminated fine grained metasandstones and metasiltstones of identical lithology to metasediments of the Petrel Cove Formation. Many exhibit such sedimentary structures as fine-scale cross-bedding, ripple marks and shale-chip conglomerates. Although it is possible that the absence of a mica schistosity in many of the xenoliths examined is the result of recrystallisation, the lack of evidence of alteration or recrystallisation of the xenoliths suggests that a preferred orientation of mica had never developed in them.

Thus the Encounter Bay Granites are considered to have been emplaced prior to the main phase of first generation deformation, and in this sense are regarded as essentially pre-tectonic. The texture of the schistose granites indicates that, at least near the margins of the pluton, the granites had almost completely crystallised prior to the imposition of the S_1 schistosity during the main deformation phase, which occurred at sufficiently high temperature to promote recrystallisation of the deformed quartz. Abundant myrmekitic intergrowths in the recrystallised margins of feldspar megacrysts apparently formed as the result of exsolution subsequent to the deformation (see for example Ashworth, 1972), although Shelley (1964) and Parslow (1971) regard myrmekite of this type as related to stress acting upon solid but still hot granite. The absence of deformation structures within the granites away from the contact suggests that the pluton behaved essentially as a rigid body during the deformation.

The remarkable concordance of the granite sheets with bedding in the country rock metasediments is worthy of comment. It indicates that the bedding planes were preferentially available as planes of weakness to the intruding granites, and may have controlled the emplacement of the pluton as a whole, since it is generally concordant with bedding in all localities where the contact is exposed. In fact, the ready

accessibility of bedding planes to igneous emplacement seems to have been a characteristic feature of several intervals within the Kanmantoo Group at about the time of granite emplacement. For example, concordance of the granites occurs both within the Petrel Cove Formation (in the Encounter Bay area) and the Middleton Sandstone (at Cape Willoughby). In addition, similarly concordant feldspar-quartz-muscovite-tourmaline-spessartite pegmatites, of approximately the same age as the granites (as described in a later section) occur within Tapanappa Formation metasediments east of Snapper Point on the north coast of Dudley Peninsula (Figure 8). This situation does not appear to have ensued in post-granite emplacement times however, since pegmatite and dolerite dykes of this age are clearly discordant.

Second generation structures have overprinted the S_1 schistosity in the granites and adjacent metasediments on Wright Island. However, the sporadic development of conspicuous second generation structural elements has prevented a reliable assessment of the broad scale effect of this deformation on the granites. On the other hand, these structures provide an important reference point in a discussion of the relative ages of pegmatite and metadolerite dykes in the type section of the Kanmantoo Group. For example, both pegmatites and metadolerites occur as transgressive dykes within the Petrel Cove Formation, and do not exhibit recognisable first generation structural elements. However, they have been strongly folded and boudinaged during the second phase of deformation. In fact, second generation structures including mesoscopic folds and an obvious crenulation cleavage are commonly best developed immediately adjacent to these dykes. Thus the pegmatites and the metadolerites appear to post-date the first generation of folding, and pre-date the second. Similar rock-types intruding metasediments further west in the type section are probably of the same age, although this can not be confirmed because of the poor development of second generation structures. There are however, thin quartz-rich pegmatites in the vicinity of Madigan Inlet that are folded about S_1 as axial plane cleavage, and clearly must pre-date the first phase of deformation.

The origin of the striped layering (S_s) within metasediments of the Petrel Cove Formation is not completely understood. The stripes are post-F_1, pre-F_2 structures that seem to have been formed as the result of the differential migration of mineral components in the immediate vicinity of a set of fracture planes, possibly of tensional

origin, that occur at a low angle to S_1. This suggestion is supported by an electron microprobe examination of the stripes (Appendix C). The marked concentration and/or depletion of post-F_1 andalusite porphyroblasts adjacent to stripes in andalusite schist bands (Plate 5: 2) provides evidence for the migration of Al within the environment of the stripes during the crystallisation of andalusite.

2.5 *THE METAMORPHIC ENVIRONMENT OF THE GRANITES*

2.5.1 *Introduction*

Previous investigations of the metamorphic petrology of the Kanmantoo Group in its type section and on Dudley Peninsula, Kangaroo Island, are few. Tilley (1919b) referred briefly to the Kanmantoo Group metasediments adjacent to the granites at Cape Willoughby. Browne (1920), in an investigation of the field relationships and petrology of the granites in the Encounter Bay area, discovered the minerals andalusite and cordierite in the metasediments exposed along the coastline near Rosetta Head. Bowes (1954) made a more comprehensive petrological and chemical examination of the metasediments in the Rosetta Head locality, and subdivided the rocks into three groups; namely quartz-biotite schists, andalusite and cordierite schists, and albite and chlorite schists. He considered that the metamorphic assemblages were a direct result of the emplacement of the granites. Offler and Fleming (1968) briefly described the occurrence of cordierite and andalusite in the metasediments near Rosetta Head, and suggested that the minerals were "produced during a deformation phase before the intrusion" of the Encounter Bay Granites.

In a publication describing the stratigraphy of the Kanmantoo Group in the western part of the type section between Campbell Creek and Tunkalilla Beach, Daily and Milnes (1971a) summarised the results of a brief examination of the metamorphic petrology of the rocks collected during that traverse, and suggested that the grade of metamorphism was between the almandine isograd and the staurolite isograd as defined by Winkler (1970). A stratigraphic investigation of the remainder of the type section, in addition to the Brown Hill to Middleton area, has now been completed (Daily and Milnes, 1973) together with petrographic studies of the rocks collected. The results of these investigations suggest that earlier interpretation of the metamorphism, although correct, was oversimplified to a large degree.

In order to present a more accurate interpretation of the nature

of the metamorphism, it was necessary to describe the various metamorphic minerals and mineral assemblages in relation to readily identifiable structural elements in the rocks, particularly the S_1 and S_2 cleavages. This technique of describing the time relations between crystal growth and deformation has been generally used to determine fluctuations in the grade of metamorphism with time (e.g. Zwart, 1962; Spry, 1963, 1969; Offler and Fleming, 1968). However, an attempt has been made here to assess the grade of metamorphism associated with recognisable structural events, and so elucidate the long-standing problem of the relationship of the metamorphism to the Encounter Bay Granites.

A comprehensive investigation of the metamorphic petrology of the Kanmantoo Group in this region was not within the scope of this thesis. The metamorphic petrology has therefore been discussed in relation to specific structural events, contrary to normal presentation.

2.5.2 *Metamorphic petrology*

(i) The type section of the Kanmantoo Group

The fabric of the metasedimentary rocks throughout the type section of the Kanmantoo Group is dominated by a well developed S_1 schistosity defined by the preferred orientation of groundmass micas. A second generation microfolding of S_1 becomes apparent as a penetrative structural element (S_2) east of Coolawang Creek (Figure 6), and more particularly, east of Newland Head (Figure 7). It should be emphasised however, that practically all of the metasediments except the phyllites retain aspects of their original detrital texture despite the deformation. Such textures include a marked variation in grain size of the quartzo-feldspathic constituents, their ubiquitous angular grain shape, and the occurrence of pebbles composed of quartz, quartz + feldspar and carbonate in several intervals.

With the exception of a calcareous phyllite sequence (Talisker Calc-siltstone), several sulphide-rich intervals within the Tapanappa Formation, and a number of carbonaceous and sulphide-rich phyllites confined to the Brown Hill Subgroup (Figure 10), the Kanmantoo Group is dominated by metasandstones, metasiltstones and phyllites. Conspicuous metamorphic mineral assemblages are uncommon, and are confined to thin calc-silicate bands and segregations distributed throughout the type section, and to some phyllite intervals, especially within the upper part

of the Balquhidder Formation and in the Petrel Cove Formation adjacent to the Encounter Bay Granites at Rosetta Head and on West Island (Figure 7). The following assemblages of major minerals seem to be representative of the various rock types:

1. metasandstones and metasiltstones -
   quartz + plagioclase + biotite + muscovite ± calcite ± chlorite ± garnet ± scapolite ± epidote;
2. phyllites -
   quartz + plagioclase + biotite + muscovite ± chlorite ± garnet ± andalusite ± cordierite;
3. carbonaceous and sulphide-rich phyllites -
   quartz + muscovite + pyrrhotite + carbonaceous material;
4. calc-silicates -
   quartz + plagioclase ± hornblende ± garnet ± chlorite ± calcite ± biotite ± muscovite ± pyrrhotite ± epidote.

A. Metamorphic crystallisation in relation to structural deformation

a. Pre- to syn-F_1 metamorphic crystallisation

Metamorphic elements attributed to pre- to syn-F_1 crystallisation include small quartz-rich aggregates, groundmass biotite and muscovite, biotite porphyroblasts, and cordierite, andalusite and chlorite poikiloblasts. Quartz-rich aggregates and biotite porphyroblasts occur with groundmass micas throughout the type section. However, cordierite and andalusite poikiloblasts are restricted to some phyllites in the upper part of the Balquhidder Formation and in the Petrel Cove Formation in the eastern part of the type section.

Metamorphic elements of pre-F_1 age are uncommon. Relict elements of sedimentary origin, such as quartzo-feldspathic groundmass minerals, are not included in this discussion. However, some small aggregates composed mainly of quartz, together with opaque minerals and micas, may represent pre-F_1 structures. The aggregates are enwrapped by the S_1 mica schistosity, but generally contain a random internal mica fabric (Plate 18: 1 and 2). Moreover, the grain size of the minerals within the aggregates is always finer than the grain size of the same minerals in the groundmass of the rock. The aggregates are unlikely to be remnant sedimentary quartz-rich laminae because of their uniform distribution through the host metasediments. Offler and Fleming (1968)

described similar aggregates that precede the first appearance of andalusite in parts of the northern Mount Lofty Ranges, and suggested that they were "pseudomorphs after andalusite produced during a peak of metamorphism when the andalusite stability field was just entered". Some poikiloblastic cordierite augen in metasediments in the Petrel Cove Formation exhibit a random inclusion fabric (Plate 18: 3 and 4), and may represent pre-F_1 crystallisation.

Metamorphic elements formed during the first phase of deformation include the micas that define the S_1 schistosity. These micas are generally fine grained, although biotite porphyroblasts (sometimes partly altered to chlorite) have been noted. S_1 is also commonly marked by a preferred orientation of opaque mineral laths that may have crystallised during the first phase of deformation.

Cordierite[10] poikiloblasts are generally enwrapped by the groundmass S_1 schistosity, and occur as augen with oriented internal inclusion fabrics in which the inclusions define either a planar fabric oriented at a significant angle to S_1 (Plate 19: 1 and 2), or an S- or Z-shaped fabric (Plate 19: 3 and 4). In both cases, the internal fabric is continuous with the external fabric. These textures[11] are interpreted as the result of crystallisation and rotation of the augen during the formation of S_1. As the cordierite augen are generally enwrapped by S_1, and the inclusions within the augen are invariably finer grained than the groundmass minerals, the cordierite is probably early-syn-F_1.

Andalusite commonly occurs as S-shaped poikiloblasts with S-shaped inclusion trails which are continuous with the external S_1 fabric of the host rock (Plate 20: 1). These poikiloblasts are thus considered

---

[10] In addition to cordierite poikiloblasts in these metasediments, there are inclusion-filled poikiloblasts composed of a microcrystalline, yellow-brown coloured, almost isotropic material, which has been identified by electron microprobe analysis and X-ray diffraction as kaolinite (Appendix D). The poikiloblasts are similar in texture to cordierite poikiloblasts. Moreover, cordierite poikiloblasts are commonly partly altered to a similar material. Thus the poikiloblasts are interpreted as altered cordierite poikiloblasts.

[11] As suggested by Powell and Treagus (1970) in relation to garnets, both planar and S-shaped fabrics may occur within the same augen but appear different because of the "cut effect".

to be the result of late-syn-F_1 crystallisation and rotation. However, the outer margins of some poikiloblasts transgress the groundmass S_1 schistosity and therefore represent post-F_1 crystallisation (Plate 20: 2 and 3).

Syn-F_1 andalusite and chlorite occur in poikiloblastic clots in some phyllites in the eastern part of the type section, and may coexist with late-syn-F_1 S-shaped andalusite poikiloblasts and early-syn-F_1 cordierite augen. Many of the clots also contain porphyroblastic quartz and muscovite. The andalusite and chlorite generally occur at the margins of the clots, where they have overgrown the groundmass S_1 schistosity but have been subsequently rotated prior to the ultimate crystallisation of the external S_1 fabric (Plate 20: 4; Plate 21: 1). Post-F_1 overgrowths of both andalusite and chlorite occur at the margins of the clots.

b. Post-F_1 metamorphic crystallisation

The major porphyroblast crystallisation in metasediments in the type section of the Kanmantoo Group occurred during the post-F_1, pre-F_2 static phase, when andalusite, chlorite, garnet, hornblende, muscovite, scapolite and epidote crystallised in rocks of appropriate lithology. These minerals have grown across the groundmass S_1 schistosity and contain relicts of it, but are deformed by the S_2 crenulation cleavage in rocks in which this structure is developed. The following minerals and mineral assemblages are characteristic of this metamorphic episode:

1. phyllites -
   chlorite ± andalusite ± muscovite ± scapolite ± garnet;
2. calc-silicates -
   hornblende ± plagioclase ± garnet ± chlorite ± epidote;
3. metasandstones and metasiltstones -
   muscovite ± garnet ± chlorite ± epidote.

In addition, there are several minor components such as tourmaline and some opaque minerals which appear to have crystallised across the groundmass S_1 schistosity, and are similarly attributed to this metamorphic episode.

Post-F_1 andalusite occurs both as overgrowths on syn-F_1 poikiloblasts, and as poikiloblasts that have grown across the groundmass S_1 schistosity in andalusite schists in the eastern part of the type section. The poikiloblasts retain relicts of the schistosity in

the form of oriented opaque mineral laths and quartz grains that are planar and continuous with the groundmass S_1 fabric of the rock (Plate 21: 2).

Post-F_1 chlorite also occurs in phyllites throughout the type section as subhedral and euhedral poikiloblasts that have grown across S_1, but contain undeflected relicts of S_1 in the form of opaque mineral laths and lenticular quartz grains (Plate 21: 3 and 4). Muscovite of similar habit occurs in phyllites, but is less common than chlorite. Scapolite occurs in phyllites about 1km east of Coolawang Creek in small porphyroblastic clots that appear to have grown across S_1 (Plate 22: 1).

Calc-silicates occur throughout the type section as deformed thin bands that parallel bedding, and as boudins that are elongate parallel to F_1 fold axes. On the basis of their mineralogy and composition (see Appendix E), the calc-silicates are considered to have been originally impure dolomitic siltstones. The S_1 schistosity in these rocks is a relict structure defined by the preferred orientation of lenticular or lath-like opaque mineral grains and in some cases, pale brown micas. This structure contrasts strongly with the well defined S_1 schistosity in the surrounding metasediments, and is taken as evidence that the present calc-silicate mineralogy is predominantly the result of post-F_1 crystallisation. This proposal is supported by textural changes near the contacts between many calc-silicates and the surrounding quartzo-feldspathic metasediments, including a significant increase in grain size of biotite in the quartzo-feldspathic metasediments as the contact is approached, together with a simultaneous decrease in degree of preferred orientation. Hornblende[12] (see Appendix E) occurs in many calc-silicates as medium to coarse grained poikiloblasts which generally exhibit a lack of preferred orientation, although in some speciments they may show a moderate degree of preferred orientation parallel to the relict S_1 schistosity. Hornblende poikiloblasts cutting across the relict S_1 schistosity contain undeflected opaque mineral inclusion trains that are continuous with the schistosity

---

[12]Hornblende in these calc-silicates was previously incorrectly identified as actinolite on the basis of its optical characteristics (Daily and Milnes, 1971a)

in the groundmass of the rock. Garnet (see Appendix E) occurs in calc-silicates as chemically zoned subhedral poikiloblasts that also cut across, but have inherited the groundmass schistosity.

Garnet[13] occurs in metasandstones and metasiltstones throughout the type section as porphyroblasts that cut across the groundmass S_1 schistosity (Plate 22: 2, 3 and 4). As in the case of the calc-silicate garnets, they are zoned from core to rim (see Appendix E). They commonly coexist with muscovite, chlorite, epidote and tourmaline which also appear to have grown across S_1.

In a locality about half way between King Beach and Rosetta Head (Figure 7), abundant round-shaped cordierite poikiloblasts occur in pelites within 1m of a metadolerite dyke. The pelites contain a relict S_1 schistosity defined by micas and opaque mineral laths, and the cordierite poikiloblasts appear to have grown across this (Plate 23: 1 and 2). Small andalusite poikiloblasts and euhedral muscovite and chlorite laths coexist with the cordierite and are similarly interpreted as post-F_1 minerals. As metadolerite dykes are post-F_1, pre-F_2 intrusions (page 35), the coarse grained post-F_1 cordierite appears to have crystallised as the result of a local increase in temperature along the margins of the dyke.

Post-F_1 metamorphic minerals that occur in phyllites in the eastern part of the type section, where the S_2 crenulation cleavage is best developed, are deformed by S_2. Textures such as the microfolding of chlorite and andalusite porphyroblasts, and the small scale dislocation of these poikiloblasts along zones commonly defined by trains of opaque mineral grains (Plate 23: 3 and 4), are especially evident in some phyllites in the Petrel Cove Formation in which S_2 assumes the characteristics of a strain slip cleavage.

---

[13]The occurrence of garnet in Kanmantoo Group metasediments throughout the type section, as well as in Adelaide Supergroup and Kanmantoo Group metasediments on Dudley Peninsula, has not been previously recorded. The widespread development of garnet-rich heavy mineral sands on beaches along the south coast of Fleurieu Peninsula has long been considered an anomaly, in view of the apparent absence of garnet in the metamorphic rocks of the region, but can now be readily explained either by direct coastal weathering and erosion of the metasediments, by reworking of Permian glacial sediments derived from the metasediments, or by a combination of these processes

c. Summary

A petrographic examination of Kanmantoo Group metasediments in the type section seems to indicate a relatively simple sequence of metamorphic crystallisation. This sequence began with the formation of quartz-rich aggregates and the crystallisation of cordierite during the pre- to early-syn-F_1 phase of deformation, was followed by the syn-F_1 crystallisation of andalusite and chlorite, and ended with the post-F_1 crystallisation of a wide variety of porphyroblastic minerals including andalusite, chlorite, garnet, hornblende, muscovite, and scapolite.

B. Metamorphic pegmatites and veins

Pegmatites occur in abundance throughout the type section of the Kanmantoo Group. Many are composed of the metamorphic minerals that characterise the post-F_1 assemblages of the host metasediments. For example, pegmatites in garnetiferous metasediments that occur in the lower member of the Carrickalinga Head Formation contain garnet as well as calcite, muscovite, quartz and chlorite. Veins in the Talisker Calc-siltstone are composed mainly of coarse grained calcite. Pyrrhotite-rich pegmatites occur in intervals containing abundant sulphides. Scapolite-rich pegmatites occur in Balquhidder Formation metasediments that contain abundant scapolite porphyroblasts. Andalusite-rich pegmatites that also contain muscovite and corundum, occur within the Petrel Cove Formation, which includes andalusite and cordierite schists. This marked association between the mineralogy of the pegmatites and the post-F_1 mineralogy of their host rocks supports a metamorphic/metasomatic origin for the pegmatites (see for example San Miguel, 1969). Rivalenti and Sighinolfi (1971) go so far as to propose that such pegmatites were formed in rocks in which there was a local low pressure gradient.

The mineralogy of these pegmatites suggests that they were formed during the post-F_1, pre-F_2 static phase, at which time the same minerals crystallised in the adjacent metasediments. An identical age for the pegmatites was deduced on the basis of structural observations along the coastal section between King Beach and Petrel Cove (page 35).

(ii) The Brown Hill to Middleton area

The sequence of metasedimentary rocks between Brown Hill and Middleton (Figure 7) includes part of the Balquhidder Formation, the Petrel Cove Formation and part of the overlying Middleton Sandstone, and is considered to correspond approximately to the section exposed along the coastline between Newland Head and Rosetta Head (Daily and Milnes,

1972c). However, the metamorphic petrology of the stratigraphically equivalent rocks in the two sections is quite different. Metasediments in the Brown Hill to Middleton area contain none of the distinctive minerals present in metasediments in the type section. However, the occurrence of plagioclase of oligiclase-andesine composition in metasediments in the former area suggests that the metamorphic grade is not significantly lower than in the type section.

In the Brown Hill area, an S_1 mica schistosity is the dominant structural element. Groundmass biotite and muscovite and rare porphyroblasts of biotite represent syn-F_1 metamorphic elements. Pre-F_1 metamorphic elements comparable with quartz-rich aggregates and cordierite augen in metasediments in the type section are not known. Post-F_1 metamorphic elements include biotite and/or chlorite poikiloblasts that have grown across S_1.

Further east towards Middleton, the geology is complicated by the variable development of first and second generation structural elements. The most conspicuous metamorphic assemblage in this area is epidote + quartz, which occurs in fine grained metasandstones in the Middleton Sandstone as bands and lenses that tend to mimic bedding, even to the point of outlining bottom sets in cross-bedded strata[14]. Epidote generally replaces pre-existing plagioclase in these rocks. However, the age of the assemblage in relation to the first and second phases of structural deformation is difficult to establish because of the poor development of overprinting relationships in the host rocks. Chlorite and hornblende occur within metasiltstone intervals in the Middleton Sandstone exposed along Middleton Beach (Figure 7), but are similarly of unknown age relative to the first and second generation deformation phases. Groundmass mica fabrics of three ages can be recognised in Middleton Sandstone metasediments in the Middleton quarry. These include

---

[14]The metasediments of the Middleton Sandstone have been described by Crawford and Thomson (1959) as "phyllites and greywacke with impure marbles". Thus they have alluded to the epidote-rich bands and lenses as originally carbonate-rich sedimentary bands. This interpretation is accepted here, especially in view of the capacity of the epidote-rich bands to mimic bedding. The epidote-rich bands and lenses are comparable with the calc-silicate bands and rods in the type section, and may have had a similar structural and metamorphic history

a relict pre-F_1 bedding plane schistosity, a well developed syn-F_1 schistosity axial plane to first generation folds, and a poorly developed syn-F_2 schistosity axial plane to second generation folds.

Pegmatites containing epidote and chlorite occur within the Middleton Sandstone, and are well exposed at Middleton Beach. These pegmatites are similar, in terms of the association between pegmatite and host-rock mineralogy, to the post-F_1, pre-F_2 metamorphic/metasomatic pegmatites that occur throughout the type section.

(iii) Dudley Peninsula, Kangaroo Island

The metamorphic petrology of the Kanmantoo Group and Adelaide Supergroup rocks collected on Dudley Peninsula during joint stratigraphic investigations with Dr. B. Daily has not been studied in detail at this stage. However, there are several preliminary observations of importance to this discussion.

The repetition of stratigraphic units, including such characteristic intervals as the Hallett Arkose equivalent and the Brighton Limestone of the Adelaide Supergroup and the Talisker Calc-siltstone of the Kanmantoo Group, on both sides of the regional anticline on the north coast of Dudley Peninsula (Daily and Milnes, 1971b), will enable changes in metamorphic grade to be closely documented. In fact, the preliminary evidence does indicate an increase in metamorphic grade from west to east as the Encounter Bay Granites at Cape Willoughby are approached. This is best revealed by the appearance of diopside in carbonate-rich metasediments on the eastern side of the thrusted block of Adelaide Supergroup metasediments (Daily and Milnes, 1971b, 1972a), in contrast with its absence in rocks of equivalent lithology and stratigraphic position further west. However, there is a magnificent development of syn- to post-F_1 metamorphic minerals such as andalusite, hornblende, scapolite and garnet in the Adelaide Supergroup metasediments, which crop out at least 12km from the granites at Cape Willoughby, compared with a conspicuous paucity of these minerals in Kanmantoo Group metasediments even closer to the granites. Thus, Kanmantoo Group metasedimentary rocks in this area appear, on the whole, to be of such composition (for example, deficient in carbonate and alumina) that they fail to contain mineral assemblages that are indicators of metamorphic grade.

2.5.3 *Relationship of the metamorphism to the emplacement of the Encounter Bay Granites*

The Encounter Bay Granites were emplaced prior to the main phase

of first generation deformation on the basis of the structural features exposed near the contact between the granites and the Kanmantoo Group at Rosetta Head and on Wright Island (pages 33 and 34). Metamorphism of the Kanmantoo Group in this area began with the pre- to early-syn-F_1 crystallisation of quartz-rich aggregates and cordierite in metasediments of appropriate composition, continued with the late-syn-S_1 crystallisation of andalusite and chlorite, and ended in the post-F_1 structurally static phase where the crystallisation of andalusite, chlorite, muscovite, garnet, hornblende and scapolite occurred in metasediments of appropriate composition.

Cordierite is restricted to some phyllites in the upper part of the Balquhidder Formation and in the Petrel Cove Formation in the eastern part of the type section, and its crystallisation records the highest grade of metamorphism attained in the region. Cordierite makes its first appearance as altered augen in phyllite bands that crop out on the coastline at the eastern end of the headland that separates Parsons Beach from Waitpinga Beach (Figure 7) - it has not been recognised in rocks in the type section to the west of this locality, nor in rocks in the Brown Hill to Middleton area. Moreover, the generally poor outcrop inland has so far prevented its discovery away from the coast. Andalusite occurs mainly in some pelites in the upper part of the Balquhidder Formation and in the Petrel Cove Formation east of Newland Head in association with cordierite. However, rare altered post-F_1 poikiloblasts that occur further west in the type section, for example in Tapanappa Formation metasediments near the western end of Tunkalilla Beach and at Tunk Head (Figure 6), are considered to be altered andalusite poikiloblasts. The poikiloblasts are composed mainly of very fine grained illite (see Appendix D). Many andalusite poikiloblasts in the eastern part of the type section are partly altered along cleavages to optically similar material. Minerals such as hornblende and garnet, which are characteristic of calc-silicate lithologies, occur throughout the type section. Scapolite however, is confined to certain phyllites that occur about 1km east of Coolawang Creek (Figure 6).

As remarked upon, the Kanmantoo Group metasediments on Dudley Peninsula, Kangaroo Island, are generally of inappropriate bulk chemical composition to contain mineral assemblages that are indicators of metamorphic grade. This may explain the lack of evidence for contact

metamorphism in the Kanmantoo Group metasediments in the vicinity of the Encounter Bay Granites at Cape Willoughby. On the other hand, the occurrence of syn- to post-F_1 metamorphic mineral assemblages of andalusite grade in Adelaide Supergroup metasediments more than 12km from the granites suggests that metamorphism occurred on a regional scale. Unfortunately however, a relationship between the metamorphism and the Encounter Bay Granites in this area can not be established on the basis of the data presently available.

The entire type section of the Kanmantoo Group, as well as Dudley Peninsula, occurs within the regional andalusite-staurolite zone of metamorphism (Offler and Fleming, 1968; Figure 3 of this thesis). Thus, the paucity of andalusite in all but the metasediments in the eastern part of the type section is best interpreted as the result of an absence of metasediments of appropriate bulk chemical composition. The absence of staurolite in metasediments throughout the type section may be the result of a lack of metasediments of appropriate bulk composition, or conditions of insufficiently high temperature and pressure during metamorphism. At present, there is no evidence in support of either possibility. The restricted occurrence of cordierite to some pelites in the eastern part of the type section may have been controlled solely by the presence of metasediments of appropriate bulk composition. However, the conspicuous local development of very large post-F_1 cordierite poikiloblasts near a post-F_1 metadolerite dyke intruding metasediments of the Petrel Cove Formation (page 42) suggests that proximity to a heat source, such as the Encounter Bay Granites, may have influenced the development of cordierite on a broader scale. The absence of cordierite and andalusite and other porphyroblastic minerals in Balquhidder Formation and Petrel Cove Formation metasediments in the Brown Hill to Middleton area, compared with their abundance in metasediments in the same stratigraphic position in the type section, is anomalous. It may be the result either of inappropriate bulk compositions of metasediments in the Brown Hill to Middleton area, perhaps due to facies changes along strike from the type section, or the effect of significantly lower conditions of metamorphic grade than existed in the type section. However, in view of the occurrence of plagioclase of oligoclase-andesine composition in the metasediments in this area, the former suggestion is favoured. Alternatively, the interpretation of the stratigraphy and structure of the Brown

Hill to Middleton area (Daily and Milnes, 1973; pages 26-29 of this thesis) may not be correct.

The relationships between structural deformation, metamorphism and the emplacement of the Encounter Bay Granites in the Encounter Bay area can be deduced from field and petrographic evidence, and are illustrated diagrammatically in Figure 17. The crystallisation of cordierite appears to have been approximately synchronous with the emplacement of the granites, and records the highest grade attained during metamorphism in the region. Andalusite and chlorite also began crystallising during the first phase of deformation. Additional andalusite and chlorite, together with muscovite crystallised after the first phase of deformation was complete and prior to the second phase of deformation, and significantly post-date the emplacement of the granites. The crystallisation of the calc-silicate mineral assemblages, and minerals such as scapolite and garnet, also occurred at this time.

Browne (1920) and Bowes (1954) interpreted the andalusite-cordierite assemblage in metasediments in the Petrel Cove locality (Figure 7) as having crystallised in the contact aureole of the Encounter Bay Granites. Offler and Fleming (1968) regarded both andalusite and cordierite porphyroblasts in the metasediments in this locality as syn-tectonic, but considered the Encounter Bay Granites to be post-tectonic. Thus, they suggested that the crystallisation of andalusite and cordierite could have been caused by the "rise of isothermal surfaces" preceding the emplacement of the granites. The present data indicate approximate contemporaneity between the peak of metamorphism, as indicated by the crystallisation of pre- to early-syn-F_1 cordierite, and the emplacement of the Encounter Bay Granites in the Encounter Bay area. These data therefore support the suggestion made earlier that the restricted occurrence of cordierite in some metasediments in the eastern part of the type section may be due to the presence of metasediments of appropriate composition in the thermal aureole of the Encounter Bay Granites. However, the emplacement of the granites does not appear to have been responsible for the syn- to post-F_1 crystallisation of andalusite and other minerals, in view of their much wider distribution. In fact, Offler and Fleming (1968) have recognised metamorphism of andalusite grade and higher, which occurred as early as pre-F_1, on a regional scale throughout the Mount Lofty Ranges.

2.5.4 *Conditions of metamorphism of the Kanmantoo Group in its type section*

A suggested model for the relationships between structural and metamorphic events in the Kanmantoo Group and the emplacement of the Encounter Bay Granites in the Encounter Bay area is depicted in Figure 17. The diagram illustrates the following sequence of events:

1. the initial development of first generation folds, and of an incipient S_1 schistosity in the Kanmantoo Group metasediments;
2. the emplacement and crystallisation of the granites prior to the main phase of first generation deformation;
3. the pre- to early-syn-F_1 crystallisation of quartz-rich aggregates and cordierite at about the time of granite emplacement, and at the highest metamorphic grade attained in the region;
4. the late-syn-F_1 to post-F_1 crystallisation of andalusite and chlorite; and
5. the post-F_1, pre-F_2 crystallisation of andalusite, chlorite, muscovite, hornblende, garnet and scapolite.

The metamorphic sequence seems to be one of progressively lower grades following the initial crystallisation of cordierite. Offler and Fleming (1968) regarded the metamorphic mineral assemblages throughout much of the Mount Lofty Ranges as characteristic of low pressure, intermediate-type metamorphism as defined by Miyashiro (1961). Moreover, they suggested that in the areas of highest grade, the metamorphism occurred at pressures ($P_{total} = P_{fluid}$) between 3 and 4kb, and at temperatures in the vicinity of 650°C[15]. The metamorphic minerals in the Kanmantoo Group metasediments in the Encounter Bay area are certainly consistent with conditions of low pressure, intermediate-type metamorphism, but are representative of lower temperatures and pressures than the assemblages upon which Offler and Fleming based their estimates. The coexistence of cordierite and andalusite fortunately provides a basis for assessment of these conditions.

Winkler (1967, 1970) defined the transition from the greenschist facies to the amphibolite facies of Abukumu-type metamorphism by the

---

[15]Using the alumino-silicate data of Newton (1966a, 1966b)

incoming of diopside, grossularite/andradite, Mg, Fe- amphibole, staurolite, and cordierite (only at relatively low to moderate pressures), and the disappearance of the assemblage quartz + chlorite. The crystallisation of cordierite at about the time of emplacement of the Encounter Bay Granites and the coexistence of cordierite with syn- to post-F_1 andalusite in some metasediments suggests that the conditions of metamorphism were consistent with the andalusite-cordierite-muscovite subfacies of the amphibolite facies. Winkler suggested the reaction

chlorite + muscovite + quartz = cordierite + biotite + alumino-silicate + water ...1,

which occurs at pressures between 2 and 4kb and over a temperature range from 515 to 540°C, for the paragenesis of cordierite under conditions of low pressure, intermediate-type metamorphism. At pressures higher than 4kb ($P_{total} = P_{fluid}$) however, almandine is reported to be present in lieu of or together with cordierite according to the following reactions:

chlorite + muscovite + quartz = almandine + biotite + alumino-silicate + water ...2, and

cordierite + $biotite_A$ = almandine + $biotite_B$ + alumino-silicate + quartz ...3,

of which 3 is highly pressure dependent. The absence of garnet of pre- to syn-F_1 age in Kanmantoo Group metasediments in the type section is significant, and indicates that if the cordierite crystallised according to reaction 1, the pressure was less than 4kb.

Hess (1969) suggested several reactions for the formation of cordierite in quartz-muscovite pelites, including

chlorite + muscovite + quartz = biotite + cordierite + garnet + water ...4,

which takes place at pressures below 2.7kb and over a temperature range from 510 to 550°C[16]. However, the ubiquitous occurrence of garnet with cordierite in the products of each of his reactions indicates that they did not apply to the paragenesis of cordierite in the type section of the Kanmantoo Group.

---

[16]The data given by Hess (1969) for reaction 4 is at variance with that given by Winkler (1970) for reaction 1. This is due to a difference in chlorite composition, since Hess used an Mg-Fe chlorite in his calculations, whereas Winkler's data (vide Hirschberg and Winkler, 1968) refers to chlorite compositions "that have not been extremely Fe-rich"

Seifert and Schreyer (1970) studied the stability limits of Mg-cordierite according to reactions involving the assemblages chlorite + alumino-silicate and chlorite + pyrophyllite. The results of their investigations indicate that

chlorite + andalusite + quartz = cordierite + vapour ...5

is the stable cordierite-forming reaction at pressures down to at least 1kb, whereas cordierite can be formed directly from pyrophyllite-bearing parageneses only at pressures well below 1kb.

It seems likely that cordierite formed in the metasediments in the type section of the Kanmantoo Group according to reactions such as 1 or 5. The occurrence of andalusite with cordierite in some metasediments, although these minerals did not form simultaneously, is consistent with metamorphic crystallisation at pressures below about 3kb and temperatures less than approximately 540°C, as defined by the intersection of the experimental equilibrium curves for these reactions with the andalusite/sillimanite phase boundary (Figure 18).

Syn- to post-F_1 metamorphic minerals in pelites containing cordierite include andalusite and chlorite, which may occur together with quartz and muscovite in conspicuous clots. This is perhaps consistent with reaction 5 having been the stable cordierite-forming reaction in the area, since Seifert and Schreyer (1970) made particular reference to the common occurrence of the assemblage andalusite + chlorite + quartz as a precursor of cordierite in the outer parts of thermal aureoles. In the Petrel Cove Formation metasediments, these clots may well be products of the retrogression of cordierite.

Post-F_1 metamorphic crystallisation produced further andalusite and chlorite, almandine garnets significantly rich in spessartite and grossularite components, hornblende, scapolite and muscovite in metasediments of appropriate composition. Although the pressure-temperature conditions of their formation are not precisely assessable from the available data, the minerals are expected to have crystallised within the stability field of chlorite + andalusite + quartz (Figure 18).

A crystallisation field for the metasediments in the type section of the Kanmantoo Group can only be based on an interpretation of the paragenesis of cordierite in the light of recent experimental data. Thus, a tentative crystallisation field is shown in Figure 18, and encompasses the crystallisation of cordierite and andalusite, and the post-F_1 crystallisation of andalusite, garnet, hornblende, scapolite, chlorite and muscovite.

SECTION 3

THE ENCOUNTER BAY GRANITES

3.1 INTRODUCTION

Possibly the earliest recorded geological investigation concerned with the Encounter Bay Granites is a brief petrological description of a "biotite granite" from Granite Island, in the Encounter Bay area (Moulden, 1895). Subsequently, Gartrell (1903) published the results of an investigation of the mineralogy and chemistry of the potash feldspar megacrysts, for which he recorded an anomalously high Ca content, in a megacrystic granite from Granite Island.

The first detailed descriptions of the Encounter Bay Granites and their field relationships were published by Tilley (1919a, 1919b), and concern the outcrops at Cape Willoughby, Kangaroo Island. Tilley recognised several granite varieties, including a major megacrystic granite and subordinate aplites and vein-like albitites. Furthermore, he assigned a Palaeozoic age to the granites on the basis of an inferred Proterozoic age for the country rock metasediments and a presumed Permo-Carboniferous age for the overlying glacigene sediments, and suggested that the granites were emplaced during the closing stages of a Late Cambrian or Ordovician orogenic episode.

Browne (1920) described the field relationships and petrology of the Encounter Bay Granites in the Encounter Bay area, where he too found that a megacrystic granite was the major granite variety. Browne and Tilley each recognised the relationship between the granites in the Encounter Bay area and at Cape Willoughby, and Tilley (1919b) described the granites as "chonolithic masses of limited surface extent, which are connected at depth to a single batholit(h)ic chamber". Based on the opinion of Howchin (1906, 1910) that the country rock metasediments in the Encounter Bay area were of Cambrian age, and also on the fact that the granites are overlain by glacigene sediments of presumed Permo-Carboniferous age, Browne supported Tilley's suggestion of a Palaeozoic age for the granites.

Mawson (1926) summarised the earlier work of Tilley (1919a, 1919b) and Browne (1920) in the context of a brief report on the field relationships and petrology of the igneous rocks of South Australia. At this time, there was considerable uncertainty about the age of the Kanmantoo Group metasediments, and consequently Mawson could only suggest

a "pre-Permo-Carboniferous" age for the Encounter Bay Granites.

Kleeman (1937) described in some detail the field relationships and petrology of a granite variety known as the "quartz mica diorite" (Browne, 1920), which occurs as inclusions within the megacrystic granite on Granite Island. He recognised several varieties of the "quartz mica diorite" and, contrary to the magmatic origin proposed by Browne, suggested that each of these varieties represented different stages in the assimilation of metasedimentary rock xenoliths.

Bowes (1954) investigated the field relationships, petrology and petrochemistry of the Encounter Bay Granites and the contiguous Kanmantoo Group metasediments at Rosetta Head, where the contact between the granites and the metasediments is exposed. He suggested that thermal metamorphism of the metasediments within the aureole of the granites resulted in the formation of "andalusite, cordierite, albite and chlorite schists", which are well developed in parts of the Petrel Cove Formation. In a subsequent paper, Bowes (1959) briefly described the field relationships of the Encounter Bay Granites exposed at Port Elliot.

Asthana (1958) studied the relationships of joints developed in the granites at Port Elliot and compared them with joints present in Kanmantoo Group metasediments in the nearby Port Elliot and Middleton quarries and at Middleton Beach (Figure 7). In addition, he described the occurrence of biotite and feldspar alignments in the granites at Port Elliot.

Fander (1960) examined several specimens of the Encounter Bay Granites in the Encounter Bay area as part of a study of the accessory minerals in South Australian granitic rocks.

Slade (1962) studied the chemistry and X-ray diffraction properties of potash feldspar megacrysts collected from a traverse across a contact between the megacrystic granite and the "quartz mica diorite" exposed on Granite Island. He suggested that the variation in chemistry and X-ray properties of the potash feldspar megacrysts were consistent with the origin proposed by Kleeman (1937) for the "quartz mica diorite".

Milnes (1967) described some aspects of the field relations and petrology of the Encounter Bay Granites in the Encounter Bay area in an Honours thesis presented to the Department of Geology and Mineralogy at the University of Adelaide. This was a preliminary study, and together with the earlier investigations summarised above, has formed the basis

for the present investigation of the Encounter Bay Granites and their environment.

3.2 *THE NATURE AND FIELD RELATIONSHIPS OF THE ENCOUNTER BAY GRANITES IN THE ENCOUNTER BAY AREA*

3.2.1 *The megacrystic granite*

(i) General description

The major granite variety[17] in the Encounter Bay area is a coarse grained[18] non-schistose megacrystic biotite granite. It contains large ovoid potash feldspar megacrysts, which invariably enclose fine grained randomly or zonally arranged inclusions of plagioclase, quartz and biotite. Many potash feldspar megacrysts are mantled by plagioclase as in "wiborgite" rapakivi granites (Wahl, 1925). A distinctive opalescent blue quartz occurs as coarse grained subhedral megacrysts as well as groundmass grains. Plagioclase occurs as medium to coarse subhedral megacrysts, and biotite is present as medium grained laths and clusters of finer crystals (Plate 24: 1, 2, 3 and 4). The megacrystic granite is greyish-blue in colour where seen in several small quarries and in the coastal spray zone, but is pink to buff coloured in weathered exposures.

The megacrystic granite contains a large variety of xenoliths. The most conspicuous and abundant of these are apparently unaltered fragments of metasedimentary rocks that are identical in lithology and texture to some of the contiguous Kanmantoo Group metasediments. These xenoliths are completely variable in size from small chips several millimetres in diameter to very large blocks tens of metres in length. The largest metasediment xenoliths may represent wall or roof pendants, as suggested by Bowes (1954, 1959). For example, the large metasediment inclusion immediately south of the jetty at Rosetta Head (Figure 12) appears to be still connected to the Petrel Cove Formation metasediments

---

[17] In general, varieties of the Encounter Bay Granites have been classified and named according to the scheme proposed by Streckeisen (1967).

[18] Coarse is the term used in this thesis to describe granites and their minerals with an average grain size greater than 1cm. Medium and fine are the terms used to describe granites and their minerals with average grain sizes of between 2mm and 1 cm, and 2mm or less respectively

forming the wall of the intrusion. Hornfelses, hybrid granites, fine grained granites and granophyric leucogranites also occur as inclusions within the megacrystic granite, and are generally less than 1m in diameter, although hybrid granite inclusions may attain large dimensions. With the exception of large xenoliths of metasedimentary rock and hybrid granite, xenoliths are not shown on the accompanying maps (Figures 11, 12, 19, 21 and 22).

The megacrystic granite can be subdivided into two types on the basis of the field distribution of unaltered Kanmantoo Group metasediment xenoliths, and texture. For example, the megacrystic granite exposed on West Island, Rosetta Head, Wright Island, Granite Island, Seal Island, and in the vicinity of Green Bay at Port Elliot (Figures 7 and 19) is littered with unaltered metasediment xenoliths (Type 1). On the other hand, the megacrystic granite exposed in the remainder of the Port Elliot area (Type 2) does not contain unaltered metasediment xenoliths, but does contain abundant segregations of tourmaline-rich pegmatites, and inclusions of fine grained granites and granophyric[19] leucogranites.

Type 1 megacrystic granite is also characterised by a bimodal grain size distribution, such that coarse feldspar, quartz and less commonly biotite crystals are set in a fine grained groundmass, which commonly exhibits granophyric textures (Plate 25: 1). This texture is particularly well developed in exposures in the vicinity of Green Bay at Port Elliot, where the type 1 megacrystic granite contains abundant diffuse schlieren of light coloured granite of extremely variable grain size (Plate 25: 2 and 3). The schlieren commonly surround unaltered metasediment xenoliths, and may also contain small tourmaline-rich pegmatite clots and pods.

Type 2 megacrystic granite is confined to the Port Elliot area, and is exposed everywhere but in the immediate vicinity of Green Bay (Figure 19). In contrast with type 1 megacrystic granite, type 2 does not possess an obvious fine grained groundmass (Plate 25: 4), or leucogranite schlieren.

The two varieties of megacrystic granite are separated by a north-west to south-east trending fault, along which there has been considerable alteration, approximately 40m east of Green Bay (Figures 19 and 20). The

---

[19]The term granophyric is used according to the definition proposed by Barker (1970)

fault plane dips steeply towards the south-west. It is bounded to the west by type 1 megacrystic granite, which contains a number of intersecting dykes of fine grained granite, and to the east by a fine grained pink coloured albitite which grades eastwards over a distance of 1 to 2m into partly albitised type 2 megacrystic granite. The fault is readily recognised, because it truncates many of the fine grained granite dykes that occur within the type 1 megacrystic granite (Plate 26: 1). The fine grained albitite on the eastern side of the fault is composed of medium to coarse grained albite and opalescent blue quartz megacrysts in a fine grained groundmass of quartz and albite, with some biotite clots (Plate 26: 2). It was interpreted by Browne (1920) as an intrusive dyke of "soda aplite". However, it seems more likely to have been a fine grained leucogranite that was contaminated by type 2 megacrystic granite during its emplacement along the fault, and was subsequently altered during late-stage albitisation that affected the Encounter Bay Granites.

Type 1 megacrystic granite is interpreted as a border facies, and is considered to have been emplaced in a mobile, yet crystal-rich condition while being simultaneously contaminated by stoped fragments of Kanmantoo Group metasediments. The fine grained groundmass that is characteristic of type 1 megacrystic granite may have resulted either from rapid cooling, or from a sudden loss of water vapour, or from a combination of the two processes. The leucogranite schlieren are also considered to represent products of the inhomogeneous crystallisation of the granite as a result of one or other of these conditions. It is of interest that Parslow (1968) described the "frequent development of patches of very variable granularity and limited extent" in the Cairnsmore of Fleet Granite near its contact with the country rock. He explained the patches as products of disequilibrium conditions resulting from the variation in water content during crystallisation.

Type 2 megacrystic granite is interpreted as a slowly cooled inner facies, which was not contaminated by Kanmantoo Group metasedimentary rock fragments. Although a normal contact between both megacrystic granite varieties is not exposed, it seems likely that the type 2 megacrystic granite was shielded from the country rock Kanmantoo Group metasediments by the type 1 megacrystic granite.

(ii) Inclusions within the megacrystic granite

Each of the two varieties of the megacrystic granite contains

abundant inclusions. Inclusions that occur within the border facies megacrystic granite are as follows.

1. Unaltered metasedimentary rocks.

Metasedimentary rock xenoliths exhibit well-defined layering with associated sedimentary features such as ripple-marks and small-scale cross-bedding, and are lithologically and texturally identical to some of the contiguous Kanmantoo Group metasedimentary rocks. However, xenoliths containing the minerals andalusite or cordierite, which occur in abundance in parts of the Petrel Cove Formation, have not been identified. Metasediment xenoliths are extremely variable in size. Some large metasediment fragments that occur within the granite immediately adjacent to the exposed wall of the intrusion are clearly wall pendants. Other large metasediment fragments that occur within the granite some distance from the wall of the intrusion are possibly roof pendants, and may indicate the close proximity of the present level of exposure to the original roof of the intrusion. All metasediment xenoliths have very sharp contacts with the megacrystic granite (Plate 4: 1; Plate 27: 1 and 2).

2. Hornfels.

Hornfels xenoliths are non-layered, and are composed of fine grained, equigranular quartz, potash feldspar, plagioclase and biotite. They occur as round inclusions from 1cm to 1m in diameter (Plate 27: 3), and have relatively sharp contacts with the megacrystic granite. The grain size of the smaller hornfels xenoliths is commonly coarser than that of the larger xenoliths, a fact that indicates significant recrystallisation of the smaller xenoliths.

3. Hybrid granites.

Two types of hybrid granite, which together constitute the "quartz mica diorite" of Browne (1920), occur as inclusions within the border facies megacrystic granite. Type A hybrid granite is a dark grey to black rock which contains some megacrysts of plagioclase, opalescent blue quartz and potash feldspar, and clots of biotite and/or hornblende, set in a very fine grained groundmass of the same minerals. Type B hybrid granite is similar in texture and mineralogy to type A, but contains abundant

megacrysts, a coarser grained groundmass, and is lighter in colour. Both type A and type B hybrid granites contain inclusions of hornfels-type fragments, many of which exhibit layering.

The hybrid granites are best exposed on Granite Island (Figure 21), where they occur together in a large irregular dyke-like body, and as smaller round inclusions within the megacrystic granite (Plate 27: 4 and 5). Type B hybrid granite commonly occurs both as an intermediate phase at the contact between type A hybrid granite and the megacrystic granite, and as discrete inclusions within the megacrystic granite. In comparison with metasediment xenoliths, hybrid granite xenoliths have diffuse contacts with the megacrystic granite.

4. Biotite-rich material.

Biotite-rich inclusions with round outlines and diffuse margins occur within the border facies megacrystic granite, although they are not common. These inclusions consist predominantly of biotite and plagioclase, and may represent extensively recrystallised fragments of pelitic metasediments.

5. Granophyric leucogranite.

Fine grained, pink to buff coloured granite patches composed of potash feldspar, quartz and plagioclase intergrown in granophyric texture have been mapped within the border facies megacrystic granite, but are not common. They are generally round, are rarely greater than 30cm in diameter, and have relatively sharp contacts with the megacrystic granite.

6. Fine to medium grained leucogranites.

Leucocratic granites of variable texture and grain size commonly occur as diffuse pink to buff coloured patches or schlieren in the border facies megacrystic granite, and are especially well exposed in the vicinity of Green Bay at Port Elliot (Figure 19; Plate 25: 2 and 3). Patches of this material are variable in shape, and usually have such diffuse contacts with the megacrystic granite that they are often difficult to delineate. In accordance with the explanation given by Parslow (1968) for similar patches in the Cairnsmore of Fleet granite, the leucogranite patches and schlieren are probably best interpreted as inhomogeneities in the border facies megacrystic granite rather

than inclusions.

Inclusions that occur within the inner facies megacrystic granite are as follows.

1. Granophyric leucogranite.

Round, pink to buff coloured patches of fine grained granophyric-textured granite composed of potash feldspar, quartz and plagioclase, are common in the inner facies megacrystic granite (Plate 28: 1). They are rarely greater than 30cm in diameter, and have relatively sharp contacts with the megacrystic granite. Similar inclusions occur within the border facies megacrystic granite.

2. Fine grained megacrystic granite.

Inclusions of fine grained pink to red coloured megacrystic granite within the inner facies megacrystic granite have round outlines and relatively sharp contacts with the megacrystic granite, and are rarely greater than 1m in diameter (Plate 28: 2). They are composed of fine grained quartz, feldspar and biotite, and contain medium and coarse grained megacrysts of plagioclase and opalescent blue quartz.

3. Hornfels and hybrid granites.

Round, dark coloured xenoliths of hornfels and hybrid granite occur within the inner facies megacrystic granite, but are not common, and are always smaller than about 30cm in diameter. In addition, rare layered hornfels xenoliths occur within the inner facies megacrystic granite (Plate 28: 3). Xenoliths of these types have relatively sharp contacts with the megacrystic granite.

4. Schist-like material.

Dark coloured inclusions of mica-rich schist-like material occur within the inner facies megacrystic granite immediately east of its fault contact with the border facies megacrystic granite near Green Bay, Port Elliot (Figure 20). The inclusions are irregular in shape, are up to 1m in length, and are commonly surrounded by massive opalescent blue quartz (Plate 28: 4). Small clots of schist-like material up to 10cm in diameter occur within the megacrystic granite exposed on the eastern side of the rocky cove, approximately 100m east of Green Bay (Figure 19; Plate 28: 5), and in thin pegmatite dykes in

the megacrystic granite along the coastline north-east of Commodore Point. The schist-like material, while variable in mineralogy and texture, is generally composed of fine grained megacrysts of apatite, quartz and chlorite, together with clots of fine grained brown biotite, set in a very fine grained groundmass of muscovite and green biotite. Molybdenite and its alteration product powellite have been identified in specimens of this material. The mineralogy of this rock-type and its association in part with pegmatite dykes suggests that it may be of hydrothermal origin.

The inner facies megacrystic granite is also characterised by the presence of abundant circular clot- or pod-like pegmatite bodies, which may be concentrated along north-east to south-west trending joints. Many pegmatites consist predominantly of tourmaline and quartz, and are zoned such that a tourmaline-rich core is surrounded by an intermediate quartz-rich zone, which is enwrapped by an outer margin of feldspathised megacrystic granite (Plate 29: 1 and 2). Some pegmatite pods are composed of quartz, feldspar, apatite and muscovite. All pegmatite pods have diffuse contacts with the megacrystic granite, partly as a result of feldspathisation of the granite in the immediate vicinity of the pods. The pods are variable in size, but rarely exceed 1m in maximum diameter.

The observations listed here indicate that several types of inclusions are restricted to one or other of the two varieties of megacrystic granite. In particular, unaltered metasedimentary rock xenoliths are restricted to the border facies megacrystic granite whereas pegmatite bodies occur only within the inner facies megacrystic granite. The different distribution of metasediment fragments and pegmatite bodies may therefore reflect different and independent syn- and post-emplacement processes or events in each of the host granites: for example a concentration of late stage components (particularly volatiles) and relatively slow cooling in the inner facies megacrystic granite, as distinct from contamination and relatively rapid crystallisation, possibly due to loss of volatiles, in the border facies megacrystic granite. Hornfels, hybrid granite and granophyric leucogranite inclusions occur within both varieties of the megacrystic granite. These inclusions may represent processes or events in a homogeneous parent granite magma prior to its emplacement into the Kanmantoo Group metasediments.

(iii) Accumulations of potash feldspar megacrysts

Zones of accumulation of very coarse grained potash feldspar megacrysts occur in many parts of the border facies megacrystic granite, particularly in association with groups of xenoliths, but have not been observed in the inner facies megacrystic granite. In general, the megacrysts have accumulated amongst groups of hornfels and hybrid granite xenoliths (Plate 29: 3 and 4). The megacrysts vary in shape from subhedral and euhedral to rounded, and are packed closely together to the virtual exclusion of other minerals.

The concentration of potash feldspar megacrysts is interpreted as resulting from the entrapment and accumulation of early-formed potash feldspar crystals during the movement of xenoliths through an essentially liquid magma. The absence of quartz and plagioclase megacrysts from these zones, and the large size of the potash feldspar megacrysts, suggests that potash feldspar was possibly the first felsic mineral to crystallise from the magma, and that it may have continued to crystallise for a significant length of time prior to the major crystallisation of other felsic minerals. However, the presence of inclusions of plagioclase, quartz and biotite within the potash feldspar megacrysts, and their zonal arrangement in some cases, indicates that these minerals had commenced crystallisation from the magma during the formation of the megacrysts. Nevertheless, the fact that the inclusions are significantly finer grained than the same minerals in the groundmass of the rock, supports the suggestion that the major crystallisation of these minerals post-dated the formation of the potash feldspar megacrysts. As the border facies megacrystic granite seems to have been emplaced in a mobile but crystal-rich condition, on the basis of textural evidence already described, the entrapment and accumulation of potash feldspar megacrysts must have occurred prior to the emplacement of the Encounter Bay Granites. The occurrence of similar potash feldspar megacrysts (as well as quartz, plagioclase and biotite megacrysts) in hybrid granite xenoliths within both varieties of the megacrystic granite is taken as evidence that these xenoliths were incorporated into the granite magma prior to its emplacement into the Kanmantoo Group metasediments, and during its early stages of crystallisation, and that the xenoliths attained a significant degree of chemical equilibrium with the magma.

The absence of zones of accumulation of potash feldspar megacrysts in the inner facies megacrystic granite may only be apparent, in

view of the comparatively small area of exposure of this granite variety. Alternatively, such concentrations may have been reworked or otherwise obliterated during the subsequent crystallisation of the inner facies megacrystic granite.

(iv) Layering within the megacrystic granite

Several types of layering have been mapped within the megacrystic granite. The most common type is composed of an alternation of biotite-rich layers with quartzo-feldspathic layers which may or may not be depleted in biotite. The zones of layering are always of limited extent, and the layers rarely exceed 3m in length. Planar biotite-rich layers in a layered zone within the inner facies megacrystic granite north-east of Commodore Point at Port Elliot (Figure 19) exhibit sharp bottom contacts, but gradational upper contacts with biotite-depleted medium grained quartzo-feldspathic layers (Plate 30: 1). The biotite crystals appear to have a preferred orientation in the plane of the biotite-rich layers, and two small tabular hornfels xenoliths within one biotite-rich layer have a similar orientation (Plate 30: 2).

Planar biotite-rich layers and associated irregular biotite-rich patches and schlieren occur in a layered zone within border facies megacrystic granite near the base of the steps on the eastern end of Granite Island (Figure 21). The biotite-rich layers alternate with biotite-depleted quartzo-feldspathic layers in which very coarse grained potash feldspar megacrysts may be concentrated (Plate 30: 3). Some potash feldspar megacrysts project into the overlying biotite-rich layers. As in the layered zone at Port Elliot, biotite crystals in the biotite-rich layers have a preferred orientation in the plane of the layers.

A spiral-shaped zone of biotite layering occurs within the border facies megacrystic granite on the Granite Island coastline just south of the previous locality (Figure 21). The zone consists of a series of concentric biotite-rich layers alternating with quartzo-feldspathic layers that may contain concentrations of potash feldspar megacrysts (Plate 30: 4). Several of the biotite-rich layers are split into two or more layers along their length.

Mineral layering has been described in many granites, and has been explained as the result of processes such as partial assimilation of country rock xenoliths (Pitcher and Read, 1958), variation in water vapour pressure and subsequent crystal accumulation governed by density contrast (Harry and Emeleus, 1960; Emeleus, 1963; Bateman et al, 1963;

Claxton, 1968; Coats and Wilson, 1971), and intense differential movement (Coats and Wilson, 1971) within a crystallising magma. The layered zone in the inner facies megacrystic granite at Port Elliot shows features that are consistent with gravity settling of early-formed biotite crystals in an essentially fluid magma. Biotite-rich layers in the planar layered zone within the border facies megacrystic granite on Granite Island may also have formed in this way. It is unlikely that the coarse grained potash feldspar megacrysts that are concentrated in some granite layers are magmatic cumulates because of their relatively low specific gravity. However, it is possible that the potash feldspar megacrysts were concentrated by magmatic currents, and forced to sink beneath blankets of sedimenting biotite crystals. The irregular biotite-rich patches and schlieren associated with the layered zone in this locality are possibly the result of reworking of the biotite-rich layers by magmatic currents. Similar biotite-rich patches and schlieren in some parts of the border facies megacrystic granite are associated with trains of biotite-rich xenoliths (Plate 31: 1), although biotite layering does not occur in these localities. The origin of the spiral-shaped layered zone within the border facies megacrystic granite on Granite Island is not known. The layering exhibits some features in common with that in the other two localities, but the spiral shape of the zone, and the splitting of single biotite layers along their length are difficult to explain.

The occurrence of biotite-rich layering of similar type in both varieties of the megacrystic granite suggests that the process or processes responsible for the layering were effective in a homogeneous granite magma prior to its emplacement. Moreover, the association of biotite with coarse grained potash feldspar crystals indicates that the development of the layering occurred during the early stages of crystallisation of the magma when biotite and potash feldspar seem to have been the only major crystalline phases.

A second type of layering occurs within the inner facies megacrystic granite immediately north of the small cove, north-east of Commodore Point at Port Elliot (Figure 19), and consists of zones in which thin bands of medium grained leucogranite alternate with megacrystic granite (Plate 31: 2). The leucogranite bands in each zone are 2 to 3cm wide, are irregularly spaced and often bifurcating, and are of limited extent. The layering in adjacent zones may intersect at a high angle. The origin of the layering is not clear. It occurs within the

megacrystic granite near a gradational contact between the megacrystic granite and a younger medium grained granite. It is possible that the leucogranite bands resulted from the introduction of material along irregular fractures or joints in the megacrystic granite during emplacement of the medium grained granite.

A poorly developed preferred orientation of biotite crystals, and in rare cases, feldspar crystals, occurs in both varieties of the megacrystic granite. These mineral alignments were first recorded by Asthana (1958) in the granites exposed at Port Elliot. They are difficult to detect in many outcrops, and no attempt was made to measure them. However, they appear to be quite variable in orientation, and are possibly due to flow alignment of biotite and feldspar in a mobile magma.

(v) Albitisation of the megacrystic granite

Late-stage albitisation of both varieties of the megacrystic granite was controlled by a prominent vertical joint set that strikes towards 300° and is approximately normal to the contact between the granites and the Kanmantoo Group metasediments. The joint set is composed of closely spaced joint planes, which appear to have provided access to the materials responsible for the alteration. The albitised zones are thus dyke-like in form (Figures 11, 12, 19, 21 and 22). Many joint planes within the albitised zones exhibit features such as polished surfaces and slickensides that indicate post-albitisation movement. Some albitised zones show evidence of post-alteration brecciation. Intense post-albitisation cataclastic deformation has occurred in a joint zone of this type in the border facies megacrystic granite on the southern side of Wright Island (Figure 11).

The albitised megacrystic granite is texturally identical to the normal megacrystic granite, but is composed of albite, quartz and biotite: all pre-existing potash feldspar has been replaced by albite. The albitised megacrystic granite can be readily distinguished from the unaltered megacrystic granite in the field because of the typical white or orange colour of the albite crystals, compared with the grey or pink colour of the feldspars in the unaltered granite. This colour difference is conspicuous near the margins of the albitised zones where many potash feldspar megacrysts have only been partly albitised (Plate 31: 3). The margins of many albitised zones are defined by one or more dark coloured bands, 2 to 3cm wide, containing very fine grained clay-like material (Plate 31: 4).

Parts of the border facies megacrystic granite on the western end of Granite Island, and in many places at Rosetta Head, exhibit a greater degree of albitisation than is evident in the albitised joint zones. The resulting rock type is a coarse grained megacrystic albite-chlorite rock, which is identical in texture to the border facies megacrystic granite. Browne (1920) suggested that the megacrystic albite-chlorite rock (which he termed "albite mica syenite") was the end product of magmatic differentiation of the Encounter Bay Granites. Bowes (1954) referred to the varieties of megacrystic albite-chlorite rock as "coarse albite chlorite rocks of igneous aspect", and suggested that they formed by "recrystallisation and partial mobilisation" of albite- and chlorite-rich metasediments during emplacement of the Encounter Bay Granites. The albite-chlorite rock at Rosetta Head crops out in a number of places along the contact between the granites and the Kanmantoo Group metasediments (Figure 12), and commonly contains albitised metasediment xenoliths. On the south-western tip of Rosetta Head, the albite-chlorite rock interfingers with border facies megacrystic granite along joints that have the same orientation as albitised joint zones elsewhere in the granites.

The contact between the border facies megacrystic granite and the albite-chlorite rock (Plate 32: 1) is gradational over about 5cm, and is marked by a significant decrease in quartz content and a change in colour of the quartz from opalescent blue to colourless as the albite-chlorite rock is approached. Albitisation of potash feldspar and plagioclase occurs to various degrees within the megacrystic granite up to 1m from the contact. In addition, the alteration of biotite to chlorite in the megacrystic granite is generally apparent several centimetres from the contact.

The nature and field relationships of the megacrystic albite-chlorite rock are not consistent with the origin proposed by Bowes (1954). The partial albitisation of both varieties of the megacrystic granite along joints of a particular orientation, together with the fact that the megacrystic albite-chlorite rock is identical in texture to the border facies megacrystic granite, suggest that the albite-chlorite rock has resulted from albitisation of border facies megacrystic granite in appropriately fractured and jointed zones. Albite-chlorite schists (Bowes, 1954) that occur within Petrel Cove Formation metasediments near Rosetta Head are similarly interpreted as the result of albitisation of

pre-existing metasediments.

3.2.2 *Fine and medium even-grained granites*

There are several outcrops of fine and medium even-grained granites in the Encounter Bay area, but all are of limited extent. The major exposures occur at Port Elliot (Figure 19).

(i) A pink to buff coloured medium even-grained granite composed mainly of potash feldspar and opalescent blue quartz, with plagioclase and minor biotite, crops out at Knights Beach and forms the western-most exposure of the Encounter Bay Granites at Port Elliot. In fact, the medium grained granite appears to envelop the border facies megacrystic granite exposed in this locality. Its contact with the border facies megacrystic granite is well exposed, and is gradational over nearly 1m (Plate 32: 2). The transition from medium grained granite to megacrystic granite is marked by an increase in average grain size due to an increase in the abundance of feldspar and opalescent blue quartz megacrysts. However, the groundmass of the megacrystic granite is finer grained than that of the medium grained granite.

The age relationships between the medium grained granite and the border facies megacrystic granite are not clear from the nature of their mutual contact. The megacrystic granite contains a number of unaltered metasedimentary rock xenoliths, and is therefore considered to be in close juxtaposition to the north-western wall or roof of the intrusion. As the medium grained granite does not contain metasedimentary rock xenoliths (or inclusions of any type), it is considered to be younger than the megacrystic granite. However, the gradational contact between the two may indicate that the medium grained granite was emplaced prior to complete solidification of the megacrystic granite, as suggested by Browne (1920) and Bowes (1959). The leucogranite patches and schlieren in the border facies megacrystic granite in this locality were identified by Browne (1920) and Bowes (1959) as contaminated medium grained granite. This led Bowes to suggest that the patches and schlieren represented "the tops of small cupola-type masses intruded into the porphyritic granite".

The contact between the medium grained granite and the megacrystic granite is cut by an aplite dyke approximately 40cm wide, with which pods of tourmaline-quartz pegmatite up to 1m in diameter are associated. Smaller aplite veins are associated with the main dyke, and also cross the contact.

(ii) A pink to grey coloured medium even-grained granite of similar type to that described above, but in contact with inner facies megacrystic granite, crops out along the coastline about 180m north of the small cove to the north-east of Commodore Point (Figure 19). The medium grained granite is composed of potash feldspar, opalescent blue quartz, plagioclase and biotite, and in some patches it contains abundant pyrrhotite. The contact zone between the medium grained granite and the megacrystic granite is about 30m wide, and the transition from medium grained granite to megacrystic granite is marked by an increase in average grain size due to an increase in the number of feldspar and quartz megacrysts.

The age relationships between the two rock types are not apparent from the nature of the contact. However, the absence of inclusions (except pegmatites) in the medium grained granite is taken as evidence that it is the younger of the two rock types. Moreover, the width of the contact between the medium grained granite and the megacrystic granite is an indication of the considerable intermixing that occurred during emplacement of the medium grained granite prior to consolidation of the megacrystic granite.

Several tourmaline-rich pegmatite pods, up to 40cm in diameter, occur within the medium grained granite. Pegmatites of this type are characteristic of the inner facies megacrystic granite and are throught to have resulted from the concentration of late-stage volatiles.

The medium grained granite has been albitised along sets of closely spaced vertical joint planes, resulting in the formation of a white albite-quartz-biotite rock identical in texture to the unaltered granite (Plate 32: 3). The joint set has the same orientation as that along which albitisation of both varieties of the megacrystic granite has occurred. As in the megacrystic granite, joint surfaces in albitised zones in the medium grained granite exhibit features such as polishing and slickensides that indicate post-albitisation movement (Plate 33: 1).

(iii) An oval, almost flat-lying sheet-like mass of buff-coloured medium even-grained granite crops out within the border facies megacrystic granite just east of Green Bay (Figures 19 and 20). The eastern margin of this mass is truncated by the fault which separates the inner facies megacrystic granite from the border facies megacrystic granite. The medium grained granite, which is similar in composition to the other medium grained granites described above, overlies the border facies

megacrystic granite. Its contact with the border facies megacrystic granite can be seen in a vertical joint plane on the seaward side of the mass, and is gradational over approximately 1m. Within this contact zone, there are two distinct but discontinuous layers of fine grained leucogranite, each about 6cm wide, separated by megacrystic granite.

The medium grained granite contains rare small xenoliths of laminated metasediment (Plate 33: 2) and fine grained leucogranite (Plate 33: 3), a feature that distinguishes it from the medium grained granites near Knights Beach and north-east of Commodore Point. In addition, the granite contains a large tourmaline-rich pegmatite pod rimmed by a fine grained feldspathised zone (Plate 33: 4).

(iv) A sheet-like body of fine grained grey coloured granite crops out within the border facies megacrystic granite approximately 30m seawards along the fault from the sheet-like mass of medium granite described above, and is similarly truncated by the fault (Figure 20). A series of irregular vein offshoots from the top of the fine grained granite sheet intrude the overlying megacrystic granite, and are also cut off by the fault (Plate 26: 2). A dyke-like body of medium grained granite appears to truncate the western end of the fine grained granite sheet.

The contact between the fine grained granite and the border facies megacrystic granite is sharp, a condition which indicates that the megacrystic granite was solid at the time of emplacement of the fine grained granite. On this basis, the fine grained granite must post-date the medium grained granites.

Discontinuous biotite-rich layers occur in the fine grained granite near its upper contact with the megacrystic granite. These biotite-rich layers may be the result of accumulation of early-formed biotite crystals near the cooler margins of the fine grained granite sheet during its emplacement. Near its lower contact with the megacrystic granite, the fine grained granite appears to be interlayered with megacrystic granite. This structure may have resulted from contamination of the fine grained granite during its emplacement.

3.2.3. *Red leucogranite*

A fine even-grained, brick-red coloured granite with a granophyric texture, herein termed the red leucogranite, crops out along the coastline immediately south of Fishermans Bay at Port Elliot (Figure 19). The red leucogranite, which was referred to as the "red aplite" by Browne

(1920), contains potash feldspar and opalescent blue quartz, with white plagioclase and minor biotite and muscovite. It is characterised by an abundance of granophyric quartz-feldspar intergrowths. The contact between the red leucogranite and the medium even-grained granite is gradational over 2 to 3m, and is marked by a decrease both in grain size and biotite content, and a significant increase in potash feldspar content, as the red leucogranite is approached.

The age relationships of the red leucogranite and the medium grained granite are difficult to determine from the limited exposure of their mutual contact. The same problem was experienced by Browne (1920), but he suggested that the red leucogranite was younger than the medium grained granite. Support for his suggestion is provided by the abundance of tourmaline-rich pegmatites within the red leucogranite, since pegmatites of this type are considered to represent concentrations of late-stage volatiles. Large, coarse grained quartz-muscovite-albite-tourmaline pegmatites also occur within the red leucogranite immediately north of its contact with the medium grained granite. Furthermore, there is evidence for late-stage greisenisation in parts of the red leucogranite, in the form of diffuse quartz- and muscovite-rich haloes around many tourmaline-rich pegmatites.

As in the case of the megacrystic granites, and the medium grained granite north east of Commodore Point, the red leucogranite has been albitised in jointed zones in which the joints are vertical and strike towards 300°. The rock-type formed as a result of albitisation in these zones consists predominantly of white albite and quartz, and is perhaps best termed an albite leucogranite, although it is identical in texture to the red leucogranite. The alternation of red leucogranite with zones of albitised red leucogranite has produced a striking red and white macroscopic banding in the field (Plate 34: 1).

Zones of albitised red leucogranite may be up to 7m wide. However, the contacts between the red leucogranite and its albitised equivalent are transitional over approximately 2cm. A number of conspicuous dark coloured bands or layers, each approximately 2cm wide, occur within the albitised zones and are parallel to the contacts with the red leucogranite (Plate 34: 2). The same bands occur around remnant red leucogranite lenses within the albitised zones (Plate 34: 3). In both situations, the dark bands become less distinct with distance away from the unaltered red leucogranite. The dark coloured bands contain

an abundance of very fine grained clay-like material. Although the origin of the dark bands is not clear they are thought to represent "still-stands" of the contact between the red leucogranite and its altered equivalent during albitisation. Thus, the recurrence of the bands with distance from the red leucogranite, together with the fact that they become less distinct with distance from the red leucogranite, suggests a number of separate stages of albitisation, rather than a continuous albitisation process.

3.2.4 *Fine grained miarolitic granophyre*

A fine grained granophyric-textured rock composed of potash feldspar, quartz, plagioclase and muscovite crops out in a small quarry inland from the red leucogranite, and also on the beach in Fishermans Bay (Figure 19), but its field relationships are obscured by modern beach and dune sands.

Browne (1920) referred to this rock as a "greisenised soda granophyre". However, it normally contains abundant potash feldspar. The striking feature of the rock is the occurrence of abundant miarolitic cavities, in which coarse grained muscovite and quartz are found together with tourmaline and albite, thus producing a spotted texture.

The granophyre is similar in texture to the red leucogranite, except for the miarolitic cavities. Therefore it is interpreted as a late-stage derivative of the Encounter Bay Granites. The granophyric leucogranite inclusions that occur in both varieties of the megacrystic granite are texturally very similar to the miarolitic granophyre.

3.2.5 *Hybrid granites*

Hybrid granites were first described in the Encounter Bay area by Browne (1920), who used the term "quartz mica diorite" to refer to them. Kleeman (1937) subdivided Browne's "quartz mica diorite" into two varieties; namely "hornblende diorite" and "quartz-mica diorite". In addition, Kleeman described another variety of the hybrid granites, the "adamellite porphyry", to which Browne had earlier alluded. Bowes (1954) recognised minor occurrences of the hybrid granites at Rosetta Head, but did not describe them in detail.

The hybrid granites are fine grained rocks which contain a groundmass rich in biotite and/or hornblende, together with coarse grained megacrysts of opalescent blue quartz, potash feldspar and plagioclase similar to those present in the surrounding megacrystic granite. According to the scheme proposed by Steckeisen (1967), the hybrid granites

could be termed fine grained megacrystic mela-granites. However, hybrid granites is considered to be the most useful term for the purpose of this discussion. Two types of hybrid granite are readily distinguished in the field: Type A hybrid granite is the term used to describe Browne's "quartz mica diorite", and Kleeman's "hornblende diorite" and "quartz-mica diorite"; and Type B hybrid granite is the term used to describe the "adamellite porphyry" of both Browne and Kleeman.

Rocks similar to the hybrid granites in both mineralogy and texture have been recorded and described in granites from many parts of the world by workers such as Grantham (1928), Wells and Wooldridge (1931), Thomas and Smith (1932), Bateman et al (1963) and Phillips (1968). In many cases, these rocks were interpreted as modified xenoliths of mafic country rock. However, Bateman et al (1963) suggested that they might also be either "clots of early formed crystals" or "refractory material that was not melted when the magma was formed".

The hybrid granites in the Encounter Bay area crop out mainly as a broad, irregular dyke-like body on Granite Island (Figure 21). The dyke-like body, which is approximately 150m wide, crops out on both the northern and the southern side of the island but is obscured beneath a cover of soil and calcrete in the central part of the island. Large, irregular-shaped bodies of hybrid granite up to 20m in diameter, and smaller subrounded bodies 10cm to 1m in diameter occur as inclusions within the border facies megacrystic granite on Granite Island, as well as other parts of the Encounter Bay area.

A large, heterogeneous collection of hornfels inclusions occurs within the hybrid granites. The inclusions are particularly difficult to see in type A hybrid granite, unless a careful field study is made, because of the very fine grained groundmass and dark colour of the rock. However, inclusions are obvious in type B hybrid granite. Earlier workers including Browne (1920) and Kleeman (1937) did not record these inclusions. The occurrence of the inclusions in the hybrid granites however, is responsible for an enigmatic xenolith-within-xenolith relationship.

(i) Type A hybrid granite

Hybrid granite$_A$ crops out on the northern side of Granite Island along the roadway to the screwpile jetty, and also on the southern side of the island in a locality known locally as "Nature's Eye". The outcrops in these localities represent the extremities of the broad dyke-like body.

In addition, hybrid granite$_A$ occurs as scattered xenoliths within the megacrystic granite.

Hybrid granite$_A$ is a dark grey coloured, very fine grained rock containing coarse grained megacrysts of opalescent blue quartz, plagioclase and less commonly potash feldspar, with some biotite and/or hornblende clots (Plate 35: 1). The potash feldspar megacrysts are commonly mantled by plagioclase. Inconspicuous dark coloured and fine grained hornfels inclusions which do not contain megacrysts of quartz and feldspar occur within hybrid granite$_A$ (Plate 35: 2). In addition, an indistinct layering, produced by differences in the grain size of groundmass minerals and megacryst abundance, has been observed in a specimen of hybrid granite$_A$ collected from Nature's Eye (Plate 35: 3).

An intertonguing contact between hybrid granite$_A$ and the border facies megacrystic granite is well exposed at Nature's Eye, and is sharp (Plate 36: 1). However, hybrid granite$_B$ is commonly present as an intermediate phase at the contact (Plate 36: 2), and may represent modification of hybrid granite$_A$. Biotite-rich schlieren that occur in the marginal parts of the megacrystic granite (Plate 36: 1) may also represent products of reaction between hybrid granite$_A$ and the megacrystic granite.

Large potash feldspar megacrysts, as well as quartz and plagioclase megacrysts, commonly straddle the contact between the hybrid granite and the megacrystic granite. These potash feldspar megacrysts are identical to potash feldspar megacrysts that are considered to have formed at a very early stage during the crystallisation of the megacrystic granite. On the other hand, potash feldspar megacrysts within the hybrid granite contain abundant groundmass mineral inclusions. Thus, potash feldspar seems to have grown as porphyroblasts in hybrid granite$_A$ while crystallising as phenocrysts within the megacrystic granite. A similar origin is envisaged for the quartz and plagioclase megacrysts within hybrid granite$_A$. A process such as this indicates conditions of chemical equilibrium or near chemical equilibrium between the hybrid granite and the megacrystic granite, and therefore the hybrid granite parent material is considered to have been incorporated into the megacrystic granite at a very early stage in its history, certainly prior to emplacement into its present position within the Kanmantoo Group metasedimentary rocks.

(ii) Type B hybrid granite

Hybrid granite$_B$ is a fine grained, light grey coloured rock which contains abundant coarse grained potash feldspar, opalescent blue quartz and plagioclase megacrysts, and is littered with disoriented megacryst-free hornfels inclusions, many of which are layered (Plate 37: 1 and 2). As described above, hybrid granite$_B$ commonly occurs as an intermediate phase at the contact between hybrid granite$_A$ and the megacrystic granite. However, it also occurs as discrete inclusions of variable size and shape within the megacrystic granite on Granite Island as well as in other localities.

The texture of hybrid granite$_B$ is variable, and in many cases, closely approaches the texture of the megacrystic granite. The contacts between hybrid granite$_B$ and the border facies megacrystic granite are generally intertonguing, and are gradational over 1 to 2cm, but are difficult to locate precisely in some outcrops because of the similarity in texture of the two rock types. Large potash feldspar megacrysts (and megacrysts of quartz and plagioclase) commonly straddle the contact between hybrid granite$_B$ and the megacrystic granite (Plate 37: 3).

On the basis of field evidence, hybrid granite$_B$ is interpreted as a modification of hybrid granite$_A$, brought about by recrystallisation and metasomatism during crystallisation of the megacrystic granite. This is consistent with the relationship between the hybrid granites proposed by Kleeman (1937).

The hybrid granites are interpreted as the result of variable degrees of assimilation of material that was incorporated into the megacrystic granite magma prior to the crystallisation of potash feldspar megacrysts, at an early stage in the history of the magma. A discussion of the nature of the hybrid granite parent material must be based on a consideration of the features of hybrid granite$_A$, since this is the less altered of the two hybrid granite varieties. As described above, hybrid granite$_A$ is a very fine grained rock containing inconspicuous hornfels inclusions, and scattered megacrysts of plagioclase, quartz and potash feldspar. The hornfels inclusions are generally finer grained than the groundmass of the hybrid granite, and are megacryst-free. They are interpreted as less altered fragments of the parent of the hybrid

granite[22]. It therefore seems likely that the hybrid granite parent rock was of sedimentary or metasedimentary origin.

3.2.6 *Minor granite varieties*

(i) Aplite dykes

Aplite dykes occur only at Port Elliot (Figure 19). They are pink to buff coloured, fine grained, granular-textured rocks that may contain medium grained feldspar and opalescent blue quartz megacrysts.

West of Green Bay, a fine grained pink coloured aplite dyke, approximately 30cm wide, crosses the contact between the border facies megacrystic granite and the medium even-grained granite. The dyke also appears in the cliff face marking the western side of Green Bay, in association with smaller aplite dykes (Plate 38: 1), and is probably the extension of a similar dyke that crops out at the edge of the pathway on the eastern side of the Bay (Figure 19). Tourmaline-rich pegmatite pods occur within the dyke, for example near the contact between the border facies megacrystic granite and the medium grained granite west of Green Bay. The probable extension of the dyke on the eastern side of Green Bay contains a pegmatitic core of opalescent blue quartz, with minor tourmaline.

Just south of Commodore Point (Figure 19), a 50cm wide aplite dyke within inner facies megacrystic granite strikes at 300°, parallel to the prominent joint set that has controlled albitisation in the granites in this area. Apparently as a result of its orientation, the dyke has been altered to a fine grained albite-quartz rock.

On the southern side of the small cove, north-east of Commodore Point (Figure 19), there is a limited exposure of an aplite dyke that is composed of feldspar and quartz intergrown in a distinct granophyric texture. The granophyric intergrowths are especially conspicuous as bulbous-shaped areas protruding from the contacts of the dyke with the inner facies megacrystic granite towards the centre of the dyke. These intergrowths may have resulted from rapid cooling and crystallisation of the aplite near its contacts with the megacrystic granite.

---

[22]Identical structures have been observed in pegmatitised migmatite at Vivonne Bay, on the south coast of Kangaroo Island, where irregular patches of extensively metasomatised and recrystallised migmatite contain disoriented "inclusions" of unaltered, well-laminated migmatite. In this situation, and perhaps in the case of the hybrid granites, particularly type B hybrid granite, some degree of mobility must have been present in the rock during alteration

(ii) Quartz veins

Quartz veins intruding both varieties of the megacrystic granite have been noted in many parts of the Encounter Bay area, including Port Elliot and Rosetta Head, but they also occur in association with the medium even-grained granite north-east of Commodore Point at Port Elliot. In all cases, the emplacement of quartz veins appears to have been controlled by joints.

At Port Elliot, quartz veins are post-albitisation features, and are commonly seen to cut across albitised joint zones, for example near the contact between the medium even-grained granite and the red leucogranite north-east of Commodore Point. In addition, many quartz veins within the megacrystic granite exhibit diagonal fractures, which suggest post-emplacement differential movement along the joints (Plate 38: 2). The diagonal fractures are consistent in orientation for the exposed length of the quartz veins, and are also consistent in orientation within different quartz veins in the same joint set in a particular locality.

3.2.7 *Metadolerite dykes*

Metadolerite dykes intruding the Encounter Bay Granites have been described by earlier workers including Chewings (1894), Moulden (1895), Browne (1920), and Bowes (1954, 1959).

At Port Elliot, a fine to medium grained metadolerite mass, presumed to be part of a dyke-like body, occurs amongst the boulders on the eastern side of the rocky cove east of Green Bay (Figure 19). The mass is only exposed at low tide, and therefore its field relationships are not known.

Several fine grained metadolerite dykes are exposed at Rosetta Head. Of these metadolerites, two have intruded the border facies megacrystic granite (Figure 12). The northernmost of these dykes can be traced almost continuously from the contact between the border facies megacrystic granite and the Kanmantoo Group metasediments south-eastwards to the coastline, where it is well exposed in a high cliff face at the head of a narrow gulch (Plate 38: 3). The southernmost metadolerite dyke can only be traced a short distance seawards from the contact between the border facies megacrystic granite and the Kanmantoo Group metasediments.

Contacts between the metadolerites and the megacrystic granite are well exposed only in the cliff section in which the northernmost

dyke intersects the coastline. Unfortunately, this locality is particularly difficult of access, and thus the contacts were not able to be readily examined. However, the contacts of the southernmost metadolerite dyke with the megacrystic granite are partly exposed, and significant alteration and recrystallisation of the megacrystic granite for up to 30cm away from the metadolerite can be seen. Moreover, the margins of the metadolerite dyke show evidence of rapid cooling, in the form of a significantly finer grained texture than is present away from the margins, as well as signs of contamination by the megacrystic granite in the form of quartz and altered feldspar xenocrysts.

The northernmost metadolerite dyke can not be traced from the megacrystic granite across the contact into the Kanmantoo Group metasedimentary rocks, and so the dyke is shown on Figure 12 extending only as far westwards as the contact. The southernmost metadolerite dyke can be traced for a short distance into the Kanmantoo Group metasediments from the megacrystic granite, and is seen to abruptly change direction (Figure 12). The probable extension of this dyke is exposed on the wave-cut platform in Petrel Cove and is strongly folded and boudinaged.

Metadolerite dykes within the Kanmantoo Group metasediments near Rosetta Head have been dated, on the basis of their structural and metamorphic relationships, as post-F_1, pre-F_2 intrusions and are thus significantly younger than the essentially pre-tectonic Encounter Bay Granites (Daily and Milnes, 1973). The fact that the metadolerite dykes within the megacrystic granite at Rosetta Head are not in any way deformed is taken as further evidence that the Encounter Bay Granites were essentially unaffected during the regional deformation episodes that post-date their emplacement.

3.2.8 *Jointing in the Encounter Bay Granites*

Asthana (1958) studied the jointing in the Encounter Bay Granites at Port Elliot, and compared the orientation of the joints with that of a poorly defined biotite and feldspar alignment, in an attempt to define the nature and origin of the joints according to the method outlined by Balk (1937). On this basis, Asthana recognised north-easterly trending primary "tension" joints, many of which were infilled with quartz and pegmatites; north-westerly trending primary "longitudinal" joints, which were parallel to the mineral alignment and which showed evidence of later movements; and north-north-westerly trending "shear" joints. A further study of the jointing in the Encounter Bay Granites was not

attempted during the present investigation. However, note was taken of the fact that the joint set controlling albitisation in the granites corresponds to the orientation of the north-westerly trending primary longitudinal joints of Asthana (1958).

3.3 *THE NATURE AND FIELD RELATIONSHIPS OF THE ENCOUNTER BAY GRANITES AT CAPE WILLOUGHBY, KANGAROO ISLAND*

The field relationships of the Encounter Bay Granites at Cape Willoughby are depicted in Figure 13.

3.3.1 *The megacrystic granite*

The major granite variety is a pink to buff coloured, fine to medium grained megacrystic biotite granite which is similar to but finer grained than the border facies megacrystic granite in the Encounter Bay area (Plate 39: 1). The affinity of the megacrystic granite (and other granite varieties at Cape Willoughby) to granites in the Encounter Bay area is initially apparent because of the ubiquitous occurrence of distinctive opalescent blue quartz. The presence of coarse grained potash feldspar megacrysts that contain abundant randomly or zonally arranged fine grained quartz, plagioclase and biotite inclusions, and are commonly mantled by plagioclase, further enhances the textural similarity of the megacrystic granites at Cape Willoughby and in the Encounter Bay area.

A variety of inclusions occurs within the megacrystic granite at Cape Willoughby, although they are not as abundant as in the border facies megacrystic granite in the Encounter Bay area. Metasediment xenoliths consist of dark coloured, well laminated biotite quartzites, which are texturally and lithologically identical to metasediments of the contiguous Middleton Sandstone. These metasediment xenoliths are rarely greater than 1m in diameter, and generally have sharp contacts with the megacrystic granite (Plate 4: 2 and 3; Plate 39: 2). However, the margins of some metasediment xenoliths have been considerably modified by metasomatism and recrystallisation to produce a rock-type similar in texture to hybrid granite$_B$ (Plate 39: 3). Non-layered hornfelses (Plate 39: 4), hybrid granites, fine grained granophyric leucogranites, and rare coarse grained quartz-feldspar pegmatites also occur as inclusions within the megacrystic granite.

Biotite layering occurs in parts of the megacrystic granite, and is composed of biotite-rich layers alternating with quartzo-feldspathic layers (Plate 40: 1 and 2). The layering is always of limited extent. Biotite crystals commonly have a preferred orientation parallel to the

plane of the layers, and some small tabular hornfels xenoliths that occur within the layered zones may have the same orientation. In one locality, the layering resembles sedimentary-type cross-stratification (Plate 40: 2).

3.3.2 *Red leucogranite*

A red leucogranite crops out as an inhomogeneous north-westerly dipping sheet-like body in a zone of complex geological relationships in the inlet immediately west of Cannon Hill (Figure 13; Plate 40: 3). In the westernmost part of the sheet-like body, the red leucogranite is a fine even-grained rock. Further eastwards however, it contains abundant medium grained feldspar and opalescent blue quartz megacrysts. Tilley (1919b) described the red leucogranite as "an aplite with development in part of a distinct granite porphyry facies". In addition, he recorded the occurrence of distinctive quartz-tourmaline segregations in the red leucogranite, and suggested that they resulted from the crystallisation of late-stage volatiles in miarolitic cavities (Tilley, 1919a).

The red leucogranite has been dissected along prominent near vertical north-westerly trending joints, and the moderately steep north-westerly dipping sheet-like form of the body is readily apparent from a study of these joint exposures. The upper contact of the sheet with the megacrystic granite is gradational over about 10cm (Plate 41: 1). At the lower contact, the red leucogranite appears to be interlayered with megacrystic granite (Plate 41: 2). However, the contacts between leucogranite and megacrystic granite are gradational over only 1 to 2cm. Just seawards of the sheet, there are several 3 to 4m diameter masses of red leucogranite, with associated irregular dyke offshoots, that are clearly intrusive into the megacrystic granite. Thus the red leucogranite sheet is considered to be intrusive into the megacrystic granite, and its gradational upper contact and layered bottom contact are possibly the result of contamination by megacrystic granite.

3.3.3 *Hybrid granites*

Hybrid granites, similar in texture to the hybrid granites in the Encounter Bay area, occur as a large dyke-like body westwards along the coast from Barn Bluff (Figure 13), and as xenoliths within the megacrystic granite, for example just south of Pink Bay. Hybrid granite$_B$ is the predominant type, and it is littered with layered and non-layered metasediment and hornfels inclusions, most of which are less than 10cm in diameter (Plate 41: 3 and 4). The contact between hybrid granite$_B$

and the megacrystic granite is gradational over 1 to 2cm (Plate 42: 1). Moreover, coarse grained potash feldspar megacrysts (as well as plagioclase and quartz megacrysts) straddle the contact between hybrid granite$_B$ and the megacrystic granite, as in the Encounter Bay area.

Hybrid granite$_A$ is comparatively rare at Cape Willoughby, but has been observed as round inclusions within the megacrystic granite (Plate 42: 2). However, it is of interest that hybrid granite$_B$, both in discrete inclusions and in the large dyke-like body, becomes distinctly finer grained with distance from its contacts with the megacrystic granite and tends to approach hybrid granite$_A$ in texture.

Tilley (1919b) did not record the exposures of hybrid granite along the coastline at Cape Willoughby. However, his "large elliptical (in cross section) mass of grey aplite" inland from the coastline at Barn Bluff appears to be an extension of the dyke-like body of hybrid granite exposed on the coastline west of Barn Bluff. The hybrid granite exposed on the coastline just south of Pink Bay (Figure 13) may represent the northernmost extension of this dyke-like body, although this can not be substantiated because of a lack of outcrop in the intervening area.

3.3.4 *Aplite dykes*

Thin red coloured aplite veins intrude both the red leucogranite and the megacrystic granite along the coastline just west of Cannon Hill (Figure 13). Small tourmaline-rich clots are commonly associated with these aplites, which have sharp contacts with the other rock types.

Red coloured aplite dykes occur in other parts of the Cape Willoughby area, and are intrusive into the megacrystic granite. All have sharp contacts with the megacrystic granite. Many contain conspicuous pyrrhotite.

3.3.5 *Late-stage joint-controlled alteration of the granites*

(i) Albitisation

In his study of the Encounter Bay Granites at Cape Willoughby, Tilley (1919b) described several varieties of "white pegmatite", some of which he mapped as veins, others of which he mapped as irregular masses within the megacrystic granite. He described the varieties of the "white pegmatite" as "albitite", "quartz-albitite" and "muscovite albitite". With regard to the origin of the albitites, Tilley suggested that they represented the "final differentiate or end product of the residual magma", having at first rejected the possibility that they may have either represented "an immiscible phase of the liquid residual magma", or

that they resulted from the "albitisation of original potassic rocks". However, a study of the occurrence of identical rock-types in identical situations in the granites in the Encounter Bay area has indicated that such rock-types are best interpreted as the result of albitisation of pre-existing potassic rocks.

As in the Encounter Bay area, albitisation of all granites (including the red coloured aplite dykes) has taken place in near vertical jointed zones in a prominent joint set striking towards 300°, approximately normal to the contact between the granites and the Kanmantoo Group metasediments. The albitites are distinguished from the unaltered megacrystic granite by their characteristic white colour, due to the predominance of white albite. The alteration is most intense immediately adjacent to joint planes in the altered joint zones, and becomes less pronounced away from these planes. Furthermore, the thickness of albitised megacrystic granite zones is completely variable from a few centimetres to several metres, depending on the intensity of jointing.

The unaltered megacrystic granite and its albitised equivalent are identical in texture. The contact between the megacrystic granite and its albitised equivalent is commonly sharp, and is marked by a significant decrease in quartz content as the albitised zone is approached, although albitisation of potash feldspar may occur within the megacrystic granite several centimetres from this contact. Such partly albitised zones of megacrystic granite, consisting of albite, opalescent blue quartz, and biotite, correspond to Tilley's "quartz albitite". However, the field relationships indicate a continuous gradation between megacrystic granite and albitite in the albitised joint zones, and subdivision of the altered rock types is not considered to be realistic. Of note is the considerable evidence of post-albitisation movement parallel to the joints in the albitised zones; for example, the occurrence of thin cataclastic zones.

On the eastern side of Barn Bluff, a prominent mass of jagged-weathering albite-muscovite rock occurs in a complexly fractured and jointed zone. The rock type was described by Tilley (1919b) as "muscovite albitite". The contact between the albite-muscovite rock and the megacrystic granite is gradational over approximately 30cm.

The albite-muscovite rock occurs at the intersection of two sets of joints: one set of joints is nearly vertical and strikes towards

300°, whereas the other joints dip at very shallow angles towards 115°. The vertical joint set has controlled the albitisation of the granites at Cape Willoughby. On the other hand, the shallow joint set has controlled late-stage greisenisation of the granites. Thus the field relationships of the albite-muscovite rock suggest that it may have developed as the result of mixing of the components of albitisation and greisenisation in this zone of joint intersection.

The albitisation post-dates the emplacement of aplite dykes at Cape Willoughby, as in the Encounter Bay area, since aplite dykes have been albitised along cross-cutting joints. Furthermore, displacement of one such dyke along these albitised joints indicates that the joints have acted as planes of post-albitisation movement.

(ii) Greisenisation

Tilley (1919b) described the effects of greisenisation only in relation to the red leucogranite. However, greisenisation has affected all rock types at Cape Willoughby, including the megacrystic granite, the hybrid granites, the red leucogranite, and the aplite dykes, along joints that dip at a very shallow angle towards 115° (Plate 43: 1). Such joints are commonly characterised by the presence of thin quartz veins. The alteration of megacrystic granite immediately adjacent to the quartz vein has resulted in the formation of an albite-quartz-muscovite-epidote rock, which is texturally identical to the megacrystic granite, but is markedly different in colour and composition. The zone of altered megacrystic granite varies in width from one joint to the next, but is commonly 5 to 10cm wide (Plate 43: 2), and is separated from the unaltered megacrystic granite by a thin altered zone of brick-red coloured megacrystic granite. This colour appears to be due to an intense clouding of the potash feldspar, presumably by very fine grained iron-rich particles.

In many localities, pronounced deformation of the megacrystic granite has occurred along these shallow dipping joints, resulting in the formation of a moderately well developed schistosity. The deformation probably occurred during alteration, since cataclastic textures are not evident.

The greisenised joint planes are easily recognised, especially along the coastline, by the dark greenish colour of the altered rock. In many places along the coastline, the lower portion of the altered joint is preserved as a distinct, sometimes strongly dissected capping

on joint blocks, due to the removal of the overlying joint block during coastal erosion.

(iii) The relative ages of joint-controlled alteration

The relative ages of albitisation and greisenisation are difficult to determine from their field relationships. There are localities in which both types of alteration occur in close juxtaposition. For example, at the head of the narrow inlet immediately south of the lighthouse, a zone of albitised megacrystic granite is cut by a series of shallow dipping joint planes along which greisenisation has occurred. The alteration resulting from greisenisation is conspicuous, and appears to persist through the albitised zone, thus indicating that greisenisation occurred later than albitisation. On the other hand, an extensive zone of altered megacrystic granite at the south-western tip of the Cape (Figure 13) shows evidence that suggests that albitisation occurred later than greisenisation. In this locality, zones of greisenised megacrystic granite, which are not restricted to the immediate environment of shallow dipping joints, have been albitised along near vertical joints striking towards 300°. Furthermore, the contacts between the greisenised megacrystic granite and the albitised zones are sharp. At Barn Bluff, the occurrence of an unusual albite-muscovite rock is perhaps consistent with the simultaneous alteration of the megacrystic granite by the components of albitisation and greisenisation in a zone of intersecting joints.

Thus, there is presently no unambiguous evidence on which to base an assessment of the relative ages of albitisation and greisenisation, and further field work is required in order to provide an answer to this problem.

3.4 *FURTHER OCCURRENCES OF POSSIBLE ENCOUNTER BAY GRANITES*

Sprigg (1954) mapped a number of discontinuous outcrops of "granite, pegmatitic granite and granodiorite" of presumed Lower Palaeozoic age in the south-western portion of Kangaroo Island. These granites are especially well exposed at intervals along the coastline between Vivonne Bay and Cape du Coedic (Figure 2), but are difficult of access.

At Cape Kersaint (Figure 2), a granite (hereafter referred to as the Cape Kersaint granite) is exposed along the base of the cliffs in four prominent headlands. The granite is a coarse grained, pink coloured, texturally inhomogeneous rock composed of pale opalescent blue quartz,

potash feldspar, plagioclase and biotite. Potash feldspar occurs as abundant coarse grained euhedral and ovoid megacrysts which are irregularly distributed throughout the granite (Plate 43: 3). The megacrysts commonly contain fine grained biotite inclusions, as well as quartz and plagioclase inclusions. Groundmass biotite crystals in the granite are arranged in a distinct but irregular schistosity, which enwraps the feldspar megacrysts. The schistosity is considered to be primary, rather than an imposed deformational feature. Abundant xenoliths of unaltered metasedimentary rocks litter the granite. Many exhibit well developed layering. In some cases, this layering outlines mesoscopic fold structures that may be of sedimentary origin (Plate 43: 4 and 5). The larger xenoliths appear to have a random orientation in the granite, but small hornfels xenoliths tend to be strung out parallel to the schistosity. Many hybrid granite xenoliths were observed. Pegmatites however, are rare.

The Cape Kersaint granite is similar in many respects to the megacrystic granite facies of the Encounter Bay Granites. However, the relationship of the granite either to the country rock, which consists mainly of migmatites as exposed at Vivonne Bay and along the banks of the Stun-Sail-Boom River, or to the Encounter Bay Granites, is unknown. Furthermore, the extent of the Cape Kersaint granite is not yet known. Texturally identical granites are exposed along the Stun-Sail-Boom River (Plate 43: 6), but the granites mapped by Sprigg (1954) westwards along the coast from Stun-Sail-Boom River (Figure 2) have yet to be investigated.

The granite about 6km east along the coast from Cape du Couedic forms spectacular outcrops, known locally as "Remarkable Rocks", extending from sea-level to the top of the 150 to 200m high cliffs. It is a coarse grained grey coloured granite composed of opalescent blue quartz, potash feldspar, plagioclase and biotite. Moreover, it is littered with xenoliths that include layered metasedimentary rocks, non-layered hornfelses, and hybrid granites. Further features include joint-controlled alteration which texturally resembles albitisation. Therefore, as in the case of the Cape Kersaint granite, the Remarkable Rocks granite has several characteristics that suggest an affinity with the Encounter Bay Granites. However, its field relationships are not exposed.

Granite outcrops inland from Cape du Couedic were also mapped by Sprigg, but were not studied in any detail during the present investigation.

3.5 *THE PETROLOGY OF THE ENCOUNTER BAY GRANITES*

3.5.1 *The megacrystic granite*

(i) The border facies megacrystic granite

The border facies megacrystic granite is a coarse grained biotite granite that contains abundant coarse grained megacrysts of potash feldspar, opalescent blue quartz and plagioclase in a fine to medium grained groundmass of quartz, feldspar and biotite. Macro-modal analyses[23] and total-rock chemical analyses[24] of several specimens of the border facies megacrystic granite are given in Appendices F (Table F1) and G (Table G1) respectively. The modes of the border facies megacrystic granite have been plotted on Figure 23.

Potash feldspar occurs in the border facies megacrystic granite as large euhedral to ovoid megacrysts, and also as fine to medium grained groundmass material. The groundmass material includes subhedral potash feldspar crystals and anhedral potash feldspar of interstitial habit. Some of the groundmass potash feldspar is intergrown with quartz in granophyric texture (Plate 44: 1 and 2). The occurrence of potash feldspar of such different habits is considered to reflect more than one generation of growth (von Eckermann, 1937; Turner and Verhoogen, 1962; Volborth, 1962; Hibbard, 1965; Dawes, 1966; Kerrick, 1969).

Potash feldspar megacrysts are most commonly ovoid in shape, and consist of an euhedral core sharply bounded by a granophyric quartz-feldspar zone (Plate 44: 3 and 4). The granophyric zone grades outwards into a potash feldspar rim which is continuous with interstitial groundmass potash feldspar. These structures are similar to the potash feldspar phenocrysts in some feldspar porphyries (Plate 44: 5 and 6), and were recognised by both Browne (1920) and Bowes (1954) in the border facies megacrystic granite. Similar structures have been described by Savolahti (1956), Shelley (1966) and Vorma (1971). In the case of the border facies megacrystic granite, the granophyric zones are considered to mark the change in conditions and rate of crystallisation consequent upon the emplacement of the granite into its present environment. Subsequent crystallisation resulted in the formation of the groundmass minerals and the outer zones of the megacrysts, and culminated in the crystallisation of interstitial potash feldspar.

---

[23] The technique used in macro-modal analysis is discussed in Appendix F

[24] All total-rock chemical analyses were carried out by X-ray fluorescence. The methods of sample preparation and analysis are discussed in Appendix G

The euhedral cores of many potash feldspar megacrysts exhibit concentric zones containing fine grained plagioclase and biotite inclusions, and also contain randomly disposed inclusions of plagioclase, biotite and quartz. The zonal arrangement of inclusions in euhedral potash feldspar megacrysts is usually interpreted as resulting from magmatic growth of the megacrysts (Schermerhorn, 1956; Hibbard, 1965; Kerrick, 1969). As the inclusions within the megacrysts in the border facies megacrystic granite are significantly finer grained than the same minerals in the groundmass of the granite, the major crystallisation of these minerals probably post-dated the crystallisation of the megacrysts.

Plagioclase inclusions in potash feldspar megacrysts are commonly aligned with their (010) faces parallel to crystal faces in the host megacryst. The plagioclase is generally saussuritised, and is surrounded by clear albitic borders which appear to be the result of late-stage alteration of the potash feldspar. Biotite inclusions in potash feldspar megacrysts are commonly rimmed by both quartz and muscovite. The shape of quartz inclusions in potash feldspar megacrysts is quite variable. Many authors have distinguished at least two generations of quartz inclusions on the basis of grain shape (see for example Savolahti, 1962; Terzaghi, 1940; Vorma, 1971), the most characteristic grain shapes being described as "aussenkonkave quartz" and "drop quartz". Both forms are present in potash feldspar megacrysts in the border facies megacrystic granite (Plate 44: 7 and 8). Quartz inclusions in potash feldspar megacrysts have been accorded a variety of origins from the products of eutectic crystallisation with potash feldspar to replacement veinlets, depending on their morphology. However, Voll (1960) attributed the shape of quartz and other inclusions in potash feldspar to the degree of misfit of the host and inclusion crystal lattices.

Mantling of potash feldspar megacrysts by plagioclase is a common feature in the border facies megacrystic granite, and can be likened to the texture of wiborgite rapakivi (Wahl, 1925; Savolahti, 1956, 1962; Volborth, 1962; Simonen and Vorma, 1969; Vorma, 1971). The plagioclase mantles may consist of several plagioclase subhedra or a single plagioclase crystal, and are of variable width (Plate 45: 1 and 2).

Potash feldspar megacrysts are typically perthitic, and exhibit one or more of the familiar film-, vein- or patch-perthite textures (Plate 45: 3, 4 and 5). Patch-perthite textures are particularly distinctive, and consist of comparatively large equidimensional areas of

lamellar-twinned albitic plagioclase separated by wisps of potash feldspar. In accordance with the suggestions of many authors, such textures are considered to be the result of exsolution, perhaps of original sodic anorthoclase.

Many potash feldspar megacrysts exhibit simple twinning. In some megacrysts however, apparent twin-individuals separated by a very irregular twin-plane are likely to be two crystals intergrown in synneusis relationship (Vance, 1969; Plate 45: 6 of this thesis). In the latter case, string-like quartz anhedra commonly occur along the "twin" planes. Potash feldspar megacrysts may also exhibit areas of cross-hatch twinning as well as areas in which twinning is absent. The cross-hatched areas are generally developed near the margins of the megacrysts. The groundmass potash feldspar is also cross-hatch twinned. Volborth (1962) described a similar distribution of cross-hatch twinning in potash feldspar megacrysts in rapakivi granites in Nevada, and suggested that the untwinned megacryst cores were early-formed orthoclase whereas the rims were composed of late-formed microcline. Evidence supporting this suggestion will be discussed in a subsequent section.

Plagioclase occurs both as megacrysts and as fine grained groundmass material, but in contrast to potash feldspar, the groundmass plagioclase does not possess an interstitial habit. Plagioclase megacrysts are commonly subhedral, and exhibit pronounced oscillatory zoning which is visible even in hand specimen. The cores of the megacrysts, which have a composition of about An_{40}, may be extensively saussuritised. Removal of the altered cores during weathering produces a pitted texture on exposed granite surfaces. Many oscillatorily zoned plagioclase crystals are untwinned, or exhibit only very fine lamellar twinning (Plate 45: 7 and 8). Several of the intermediate zones of oscillatorily zoned plagioclase grains contain bleb-like and vermicular quartz inclusions, forming myrmekitic intergrowths with the plagioclase (Plate 46: 1). Such textures have also been described by Shelley (1966), and may have developed simultaneously with the granophyric zones in potash feldspar megacrysts as the result of rapid simultaneous crystallisation of quartz and plagioclase. Typical bulbous myrmekitic intergrowths of plagioclase and quartz commonly occur at the boundaries between plagioclase and potash feldspar grains, and have also been noted at the boundaries between quartz and potash feldspar grains. However, these represent crystallisation at a much later stage than the zonal myrmekitic intergrowths in

plagioclase megacrysts.

Rare ovoid plagioclase megacrysts, consisting of an inner myrmekitic zone surrounded by a quartz-free outer zone, have been observed in specimens of the border facies megacrystic granite (Plate 46: 2). Their origin is not clear, but they may represent xenocrysts.

Many plagioclase crystals have clear albitic borders against potash feldspar, but not against other minerals (Plate 46: 3). Schermerhorn (1956), Ramberg (1962), and Peng (1970) have described similar textures, which they ascribe to late-stage replacement (that is albitisation) of the contiguous potash feldspar. Intergranular albite may also occur at the mutual boundaries between potash feldspar grains.

Quartz has a distinctive opalescent blue colour, and occurs as subhedral to euhedral megacrysts, and as fine to medium grained groundmass material. The interstitial spaces between quartz grains are occupied by fine grained potash feldspar (Plate 46: 4 and 5).

Quartz megacrysts display an unusual concentric zonal variation of the opalescent blue colour, a feature recorded by Browne (1920). This phenomenon is not obvious in the field, nor can it be seen in thin- or polished-sections. However, the colour zoning is clearly visible by eye in the cut and polished surfaces of hand specimens of the granite (Plate 46: 6). In view of the occurrence of zoned plagioclase, and potash feldspar megacrysts that contain concentric zones of fine grained inclusions, colour zoning in quartz megacrysts may also be a growth phenomenon. Preliminary electron microprobe analyses of quartz megacrysts indicate a significant but variable concentration of Al, which may be correlated with colour changes. Frondel (1962) also noted the possibility that zonation in quartz may be related to variations in the concentration of trace elements, including Al

Biotite (Z=Y=dark brown, dark brown-green, or dark brown-red: X=straw or buff) occurs in the border facies megacrystic granite both as randomly oriented medium grained crystals, and as aggregates of fine to medium grained crystals. Many biotite crystals contain fine grained muscovite aligned parallel to the biotite cleavage. Schermerhorn (1956) described muscovite of this habit as "early muscovite". Acicular ilmenite and haematite also occur along cleavage planes in biotite (Plate 46: 7). In addition, zircon is present as fine grained inclusions surrounded by pleochroic haloes (Plate 46: 8).

Biotite crystals may be partly altered to chlorite, probably as

the result of mild deuteric alteration. The appearance of fine rutile granules in biotite invariably accompanies the chloritisation. Schermerhorn (1956) reported both rutile and sphene granules along cleavage planes in altered biotites in the granites of Trancoso, Portugal. The appearance of these minerals must be related to the exclusion of Ti from the chlorite lattice.

Accessory minerals include zircon, apatite, opaque minerals, muscovite, chlorite and rutile. Muscovite, opaque minerals, zircon and apatite commonly occur as inclusions in biotite, whereas chlorite and rutile occur as alteration products of biotite.

The Cape Willoughby megacrystic granite, chemical analyses for which are given in Appendix G (Table G2), is generally finer grained than the border facies megacrystic granite in the Encounter Bay area, and is quite variable in texture, despite the statement by Tilley (1919b) to the contrary. Fine grained varieties of the Cape Willoughby megacrystic granite consist of scattered medium to coarse grained megacrysts of potash feldspar, quartz and plagioclase in a fine grained groundmass of these minerals and biotite. Conspicuous granophyric intergrowths form borders with sharp inner contacts around euhedral potash feldspar cores in both megacrysts and groundmass crystals. The coarse grained varieties of the Cape Willoughby megacrystic granite closely resemble the border facies megacrystic granite in the Encounter Bay area in texture. Tilley (1919b) described the petrography of the Cape Willoughby megacrystic granite in some detail. He recorded the zonal distribution of the opalescent blue colour in quartz megacrysts, and alluded to the origin of the zones as growth features. Moreover, he identified the granophyric intergrowths around euhedral potash feldspar (and rare quartz) crystals as products of "later crystallisation". As in the border facies megacrystic granite in the Encounter Bay area, these granophyric intergrowths are considered to mark the change in conditions and rate of crystallisation that occurred at the time of emplacement of the granite into its present environment. In keeping with this suggestion, the variation in texture of the Cape Willoughby megacrystic granite can be accounted for in terms of differences in the post-emplacement rate of crystallisation.

(ii) The inner facies megacrystic granite

On a textural basis, the inner facies megacrystic granite can be distinguished from the border facies megacrystic granite because of the absence of a fine grained granophyric-textured groundmass, and the

absence of granophyric border zones around potash feldspar megacrysts. Otherwise, the two varieties of megacrystic granite are similar in texture and mineralogy.

Macro-modal analyses of specimens of the inner facies megacrystic granite are given in Appendix F (Table F2), and have been plotted on Figure 23. Total-rock chemical analyses of specimens of the granite are given in Appendix G (Table G3). As indicated in Figure 23, the inner facies megacrystic granite is clearly different from the border facies megacrystic granite on the basis of proportions of major minerals.

Pyrrhotite and pyrite occur in abundance in parts of the inner facies megacrystic granite, and have been noted in the border facies megacrystic granite in one locality at Port Elliot. Pyrrhotite occurs as fine to medium grained subhedral crystals which are partly replaced by marcasite (Plate 47: 1). Medium grained pyrite euhedra are also common (Plate 47: 2).

(iii) Inclusions within the megacrystic granites

Total-rock chemical analyses of specimens representative of several types of inclusions within the megacrystic granites are given in Appendix G (Table G4). Metasedimentary rock xenoliths are fine grained and biotite-rich. They invariably exhibit well-defined bedding laminations, as well as small-scale sedimentary structures. Mica preferred orientations within the xenoliths are uncommon. If present however, mica preferred orientations are poorly developed in contrast to the conspicuous mica schistosities that occur in lithologically similar metasediments in the Kanmantoo Group country rock.

Granophyric leucogranite inclusions are generally fine grained, and are composed of cross-hatched microcline perthite, quartz, and lamellar-twinned plagioclase of oligoclase composition. Micas are subordinate constituents. Granophyric intergrowths of quartz and microcline are characteristic of these inclusions.

Fine grained megacrystic granite inclusions that occur within the inner facies megacrystic granite consist of opalescent blue quartz megacrysts, and less commonly potash feldspar and plagioclase megacrysts, in a fine grained groundmass of these minerals with minor muscovite and biotite. Opaque minerals are associated with biotite crystals, which may be partly altered to chlorite. The potash feldspar is a cross-hatched microcline perthite which is generally clouded by fine grained

alteration products. Plagioclase crystals are less altered, and exhibit compositional zoning from core to rim. Some inclusions of schist-like appearance have an unusual and highly variable texture and mineralogy, and are thought to be the products of late-stage hydrothermal crystallisation. The material is composed mainly of muscovite, which varies in size from extremely fine crystals to medium grained poikilitic laths. Chlorite, biotite, and apatite, with minor rutile, quartz, and molybdenite are the other constituents. Fine grained muscovite occurs in large patches and schlieren in which it shows a moderately well developed preferred orientation. Fine to medium grained poikilitic chlorite laths have grown across the muscovite schistosity, and clearly post-date its development. Biotite occurs in round aggregates of laths which may possess a preferred orientation. Rutile, molybdenite and fine to medium grained apatite subhedra are generally intergrown with biotite in these aggregates.

(iv) Albitised megacrystic granite

Albitisation of both varieties of the megacrystic granite along north-westerly trending vertical joints has resulted in the alteration of pre-existing potash feldspar to albite, and the decalcification of pre-existing plagioclase. Many specimens of the albitised megacrystic granites exhibit evidence of post-albitisation deformation in the form of peripheral granulation and brittle fracturing of quartz and albite, kinking of lamellar-twinned albite, and pronounced undulose extinction or deformation lamellae in quartz. In some specimens, thin cataclastic zones containing granulated quartz and albite were noted.

Pre-existing potash feldspar megacrysts, groundmass crystals and interstitial material can be recognised as distinctive fine-scale chess-board-twinned albite (Plate 47: 3 and 4). Original plagioclase occurs as lamellar-twinned albite, in which the twin lamellae are commonly spindle-shaped and kinked (Plate 47: 5). Pre-existing structures within potash feldspar megacrysts have been perfectly preserved despite the alteration of the potash feldspar to albite. For example, original simple twin boundaries, zonal arrangements of inclusions, granophyric border zones (in the border facies megacrystic granite), inclusion shapes, and perthite textures can still be recognised. Even original plagioclase inclusions and albitic perthite fabrics are preserved as lamellar-twinned albite in a chess-board-twinned host. Similar observations regarding the formation of chess-albite by albitisation of

pre-existing potash feldspar have been recorded by many authors (for example Starkey, 1959). Callegari and De Pieri (1967) suggested that chess-board twinning may result from the development of internal strain during replacement of potash feldspar on account of the marked difference between the cell volumes of potash feldspar and albite. Biotite occurs as aggregates of fine grained ragged laths, which are notably free of all but small rutile inclusions (Plate 47: 6), and as relict medium grained laths and plates which contain abundant rutile granules. The aggregates of fine grained laths appear to have developed at the expense of larger biotite crystals during the deformation.

With more extensive albitisation, the opalescent blue quartz becomes pale blue in colour, or colourless. Biotite is replaced by phlogopite, with associated rutile granules. Some of the phlogopite may be further altered to chlorite, which also contains abundant rutile granules (Plate 47: 7 and 8). Despite these mineralogical changes, the texture of the altered rock remains identical to that of the original megacrystic granite.

The features described above are also present in specimens of the albitised Cape Willoughby megacrystic granite. Tilley (1919b) referred to these rocks as quartz albitites.

(v) Megacrystic albite-chlorite rock

The megacrystic albite-chlorite rock is considered to be the result of more intensive albitisation of the border facies megacrystic granite than is observed along north-westerly trending vertical joints. This interpretation is supported by total-rock chemical analyses of specimens of both the albitised border facies megacrystic granite, and the megacrystic albite-chlorite rock given in Table G5. However, the texture of the megacrystic albite-chlorite has remained identical to that of the original megacrystic granite.

In general, the megacrystic albite-chlorite rock consists of albite with interstitial aggregates of fine grained chlorite. Albite occurs both as chess-board-twinned and lamellar-twinned megacrysts and groundmass crystals. Many of the crystals are fractured and partly granulated, and some contain kinked twin lamellae. Chlorite laths may also exhibit well defined kink bands. These structures are interpreted as the result of post-albitisation deformation. Fine grained zircon and apatite, as well as rutile, occur as inclusions in chlorite. Some specimens of the megacrystic albite-chlorite rock contain abundant muscovite,

which is closely associated with the interstitial chlorite aggregates. Relict biotite and/or phlogopite laths may be present, and are invariably littered with rutile granules. Colourless anhedral quartz occurs in most specimens of the megacrystic albite-chlorite rock, and exhibits pronounced undulose extinction. Many such quartz grains are partly replaced by albite (Plate 48: 1). Relict quartz megacrysts presently composed of albite can be recognised in specimens of the megacrystic albite-chlorite rock by their subhedral equidimensional shape.

There are variations in texture and in the relative proportions of albite and chlorite in the megacrystic albite-chlorite rock, as recorded by Bowes (1954). However, these variations reflect differences in the texture and mineralogy of the original megacrystic granite.

The dyke-like albitites that occur within the Cape Willoughby megacrystic granite are not primary intrusive rocks, as suggested by Tilley (1919b), but have resulted from joint-controlled albitisation of the megacrystic granite and appear to be the equivalents of the megacrystic albite-chlorite rock in the Encounter Bay area. As described by Tilley (1919b), the albitites are composed essentially of chess-board- and lamellar-twinned albite, with minor quartz and interstitial muscovite. Many specimens show evidence of post-albitisation deformation in the form of brittle fracturing and cataclasis. Despite the deformation, the albitites display textures that are identical to those present in the adjacent megacrystic granite.

(vi) Greisenised megacrystic granite

Greisenisation of the megacrystic granite and other granite varieties at Cape Willoughby was controlled by joints that dip at a shallow angle towards the south-east. Many such joints are quartz-filled. The greisenised megacrystic granite consists mainly of quartz and muscovite with minor feldspar. Quartz occurs as aggregates of sub-polygonal grains of varying size. Muscovite occurs in fine grained aggregates which appear to represent altered feldspar crystals, and in thin schlieren. In addition, thin quartz-muscovite veinlets commonly penetrate the altered granite. Further away from the joints, the megacrystic granite has been extensively sericitised, and is composed mainly of quartz, muscovite, potash feldspar and plagioclase: biotite and many feldspar crystals have been replaced by muscovite. Significant quantities of epidote and rutile appear to be by-products of the respective alteration of plagioclase and biotite. Anhedral opaque minerals

are also present, and are commonly associated with the muscovite. The overall texture of the altered rocks however, is practically identical to that of the original megacrystic granite.

The megacrystic granite adjacent to many greisenised joints exhibits a layered schistosity, which is defined by an alternate development of thin zones composed of fine grained quartz or micas. Micas in the mica-rich layers have a well developed preferred orientation parallel to the layering.

Tilley (1919b) recognised greisenisation of the red leucogranite only, and suggested that the alteration represented "pneumatolysis" along "fissures" developed prior to its consolidation. The layered schistosity developed in the megacrystic granite adjacent to the greisenised joints is similar to that present in parts of the megacrystic granite near its contact with the Petrel Cove Formation metasediments on Wright Island, and appears to have developed during deformation along the joints at elevated temperatures. In this regard, the schistosity contrasts with the post deformation brittle deformation experienced by the albitised zones.

3.5.2 *Fine and medium even-grained granites*

Macro-modal analyses and total-rock chemical analyses of fine and medium even-grained granites are given in Table F3 and in Table G6 respectively. Figure 23 shows the field of fine and medium even-grained granites partly overlapping that of the inner facies megacrystic granite, but displaced towards the potash feldspar apex of the triangular diagram. The medium even-grained granites that crop out near Knights Beach (4-59), adjacent to the fault east of Green Bay (4-75, 4-103) and north-east of Commodore Point (4-10, 4-15) at Port Elliot (Figure 19) are similar in texture, mineralogy and composition. They consist mainly of microcline and opalescent blue quartz, with plagioclase and minor biotite.

Microcline occurs as cross-hatched, simple-twinned anhedra that contain quartz inclusions and sericitised plagioclase inclusions with clear albitic borders. Perthite textures, including coarse-scale patch-perthite, are common (Plate 48: 2). Some microcline crystals are partly replaced by skeletal muscovite (Plate 48: 3). In the medium grained granite north-east of Commodore Point, post-crystallisation deformation is indicated by subgrain development along microcline boundaries, and by a marked subgrain development in quartz crystals (Plate 48: 4).

Plagioclase is present as anhedral and subhedral grains which are

zoned and contain extensively altered cores. Many plagioclase grains show oscillatory zoning. The average composition of the unaltered parts of several crystals was determined optically to be about An_{27}. Corrosion of plagioclase by microcline is a common feature, and probably represents late-stage replacement of plagioclase (Plate 48: 5). In addition, myrmekitic intergrowths of quartz and plagioclase commonly project into microcline from the mutual boundaries between plagioclase and microcline crystals, and between adjacent microcline crystals.

Quartz occurs as subhedral equant grains which trend towards a granular habit, especially in the medium grained granite at Knights Beach. Some quartz grains exhibit euhedral crystal outlines against microcline. Rare granophyric intergrowths of quartz with microcline have been noted in these granites.

Biotite (Z=Y=dark brown to dark reddish brown: X=straw to buff) is present as aggregates of crystals, or as individual crystals. Zircon, apatite and opaque minerals occur as inclusions in biotite crystals (Plate 48: 6). Muscovite is commonly intergrown with biotite. Some biotite crystals are in fact rimmed by fine grained muscovite.

The medium grained granite north-east of Commodore Point has been albitised along north-westerly trending vertical joints. The resulting rock consists of chess-board- and lamellar-twinned albite (Plate 48: 7), quartz and biotite. Chess-albite appears to pseudomorph microcline (Plate 48: 8). However, rare textures that indicate chess-albite replacing quartz have been noted (Plate 49: 1). Biotite occurs in the albitised medium grained granite as interstitial aggregates of crystals, or as individual crystals with associated muscovite and opaque minerals, and does not appear to have been altered. However, fractures in some albite crystals are filled with fine grained biotite and muscovite.

The fine grained sheet-like granite (4-52) with irregular vein offshoots intruding the border facies megacrystic granite adjacent to the fault east of Green Bay at Port Elliot (Figures 19 and 20), has a similar mineralogy and texture to the medium even-grained granites described above, but is significantly different to these granites in terms of chemical composition (Table G6). In this respect, the fine grained granite more closely resembles the border facies megacrystic granite. The medium grained granite (9-2) occurs as an inclusion in the border facies megacrystic granite on West Island and can be similarly classified.

3.5.3 *Red leucogranite*

The red leucogranite, for which total-rock chemical analyses are given in Table G7, is a fine grained granite composed mainly of microcline and opalescent blue quartz, with plagioclase and minor muscovite and biotite. It is characterised by an abundance of granophyric intergrowths. *Microcline* occurs as cross-hatched and perthitic anhedra, with very fine interstitial outgrowths, and is partly replaced by muscovite along cleavages and grain boundaries. The crystals are clouded by very fine grained opaque granules which appear to be responsible for the red colour of the feldspar in hand specimen. *Quartz* crystals are generally anhedral, and may exhibit sutured and granulated borders. *Plagioclase* anhedra are white in hand specimen, due to clouding by clay mineral alteration products. The composition of several plagioclase grains was determined optically to be about An_{27}. *Micas* include muscovite, which commonly replaces microcline, and biotite (Z=Y=dark brown: X=straw), which generally occurs as fine grained individual crystals.

The red leucogranite has been altered to a white albite leucogranite along north-westerly trending vertical joint zones. The albite leucogranite, for which a total-rock chemical analysis is given in Table G7, is composed almost entirely of chess-board- and lamellar-twinned albite and pale opalescent blue quartz. Relict granophyric intergrowths of quartz and microcline are presently represented by intergrowths of quartz and chess-albite. Both quartz and albite boundaries may be granulated, and quartz crystals commonly exhibit deformation lamellae. In addition, some specimens of the albite leucogranite contain thin cataclastic zones. These features are consistent with the evidence for post-albitisation deformation of the albitised joint zones observed in the field. Albite crystals in the albite leucogranite are commonly clouded by fine grained opaque mineral granules, and also contain abundant small biotite and muscovite laths. In addition, very fine grained interstitial aggregates of biotite and muscovite occur in some specimens. In fact, the dark coloured layers observed within the albite leucogranite near its contacts with the red leucogranite seem to be due to intensive clouding of albite crystals, together with the occurrence of abundant fine grained biotite and/or clay minerals as interstitial aggregates.

The inhomogeneous red leucogranite that crops out south of Cannon Hill at Cape Willoughby (Figure 13) as a sheet-like body with associated dykes is intrusive into the megacrystic granite, and varies from a fine

even-grained aplitic rock to a fine grained megacrystic granite. The megacrystic variety of the red leucogranite is characterised by abundant spectacular granophyric intergrowths which border euhedral quartz and feldspar megacrysts (Plate 49: 2 and 3), and which practically obliterate many groundmass microcline crystals (Plate 49: 4). Similar textures occur within the border facies megacrystic granite, as described on page 84. Apart from microcline, quartz and plagioclase, which are the dominant minerals in the leucogranite, biotite and muscovite are present in minor amounts. Biotite occurs mainly as interstitial aggregates of fine grained crystals. Muscovite may be associated with biotite, or is present as skeletal crystals replacing microcline.

The texture of the red leucogranite at Cape Willoughby suggests rapid crystallisation of a partly crystalline magma. Rapid crystallisation may have been achieved by rapid cooling due to emplacement of the leucogranite into a cold environment, or by sudden loss of volatiles, or by a combination of these conditions. As the contacts between the red leucogranite and the megacrystic granite are not sharp, it seems unlikely that the environment was sufficiently cold to account alone for rapid crystallisation. Consequently, rapid loss of volatiles may have been an important process in promoting rapid crystallisation. The occurrence within the red leucogranite of miarolitic cavities filled with tourmaline and quartz (Tilley, 1919a) is taken as evidence for the role played by volatiles during crystallisation. A similar argument can be advanced for the crystallisation history of the red leucogranite in the Encounter Bay area.

3.5.4 *Fine grained miarolitic granophyre*

The fine grained miarolitic granophyre is texturally similar to the red leucogranite, except for the presence of abundant miarolitic cavities filled with quartz, muscovite and minor albite. Tourmaline and opaque minerals also occur within the miaroles, but are less common. Total-rock chemical analyses of two specimens of the granophyre are given in Table G8.

Muscovite occurs in the granophyre as skeletal crystals replacing microcline, and as radiating aggregates within miarolitic cavities. In some specimens, muscovite has replaced microcline to such an extent that a granophyric quartz-muscovite intergrowth occurs in place of the original quartz-microcline intergrowth (Plate 49: 5). Cross-hatched *microcline* anhedra are invariably clouded with very fine grained opaque

mineral granules. Granophyric intergrowths of quartz and microcline are common, as in the red leucogranite. *Plagioclase* occurs as lamellar-twinned crystals that have a composition of about An_{29}. Many crystals have myrmekitic borders. *Quartz* is invariably anhedral, and commonly embays plagioclase and microcline crystals in typical replacement textures (Plate 49: 6). Such textures are particularly evident near the margins of the miarolitic cavities.

Browne (1920) suggested that the fine grained miarolitic granophyre resulted from late-stage greisenisation of an original granophyric leucogranite. Textures indicating replacement of feldspars by muscovite and quartz, and the occurrence of euhedral muscovite and quartz filling miarolitic cavities (which Browne did not comment upon) support this hypothesis. Granophyric textures in the fine grained miarolitic granophyre are similar to those present in the red leucogranites at Port Elliot and Cape Willoughby, and may have resulted from comparable conditions of crystallisation. The occurrence of miarolitic cavities in the granophyre and the red leucogranite at Cape Willoughby, and the association between tourmaline- and muscovite-rich pegmatites and these rocks, indicates that volatiles have played an important role during crystallisation. On the basis of the field association between the granophyre and the red leucogranite at Port Elliot, the granophyre might be interpreted as a variant of the leucogranite.

3.5.5 *Hybrid granites*

(i) Type A hybrid granite

Both the "hornblende diorite" and the "quartz-mica diorite" of Kleeman (1937) are herein grouped as Type A hybrid granite. The two varieties are identical in texture, and therefore can not be distinguished in the field or in hand specimen. However, they can be distinguished in thin section on the basis of the presence or absence of hornblende. In addition, they exhibit significant chemical differences, as seen in Table G9.

On the basis of field relationships, hybrid $granite_A$ is considered to be the less assimilated of the two hybrid granites (see page 72 This is supported by petrographic observations. For example, the proportion of megacrysts to groundmass in hybrid $granite_A$ is approximately 1:10, with plagioclase megacrysts being the most abundant.

Plagioclase megacrysts vary in shape from subhedral to anhedral, and exhibit both normal and oscillatory zoning (Plate 49: 7 and 8). The

cores of some plagioclase megacrysts have a composition of about An_{42}. Some megacrysts contain small rectangular potash feldspar inclusions, which may be arranged in concentric zones (Plate 50: 1). Other megacrysts contain randomly disposed inclusions of hornblende. Plagioclase also occurs as fine grained lath-shaped to equidimensional crystals which are compositionally zoned.

Potash feldspar is present as fine grained, generally untwinned groundmass anhedra, which may be concentrated in vague patches, and as the cores of large plagioclase-mantled megacrysts. The megacrysts may be extremely poikilitic (Plate 50: 2), and are composed of a patch-work pattern of equidimensional plagioclase and untwinned potash feldspar crystallites, which are rimmed by anhedral quartz, or in some cases sphene (Plate 50: 3). The quartz and sphene in these intergrowths exhibit optical continuity over relatively large areas, and have the form of graphic texture. Inclusions of hornblende, biotite, sphene, opaque minerals, epidote, calcite and apatite occur in abundance in the megacrysts, and tend to be of larger grain size than the same minerals in the groundmass. In some megacrysts, non-poikilitic perthitic potash feldspar cores are surrounded by an intermediate zone of patch-work texture (Plate 50: 4). Most potash feldspar megacrysts are bordered by plagioclase, which tends to form gradational contacts with the inner zones. It is of interest that similar textures in potash feldspar megacrysts in xenoliths have been alluded to by Schermerhorn (1956) and Phillips (1968). These textures are taken as evidence of the growth of potash feldspar megacrysts as porphyroblasts in hybrid $granite_A$.

Quartz occurs in hybrid $granite_A$ as fine grained groundmass anhedra, and as coarse grained subhedral megacrysts. The megacrysts are typically zoned with respect to their opalescent blue colour, as are the quartz megacrysts in both varieties of the megacrystic granite. The borders of the megacrysts are commonly serrated (Plate 50: 5), and may be surrounded by thin rims composed of fine grained potash feldspar. Parts of these rims protrude into the megacrysts (Plate 50: 6).

Groundmass minerals are fine grained and in addition to the minerals described above, include biotite, hornblende (in some varieties of hybrid $granite_A$) and sphene. Biotite and hornblende do not exhibit a preferred orientation. Biotite (Z=Y=dark brown green: X=straw) commonly contains opaque mineral, zircon and rutile inclusions. Hornblende (Z=green-blue: Y=dark green: X=yellow-green: Z>Y>X) may contain sphene

and zircon inclusions, and is generally less abundant than biotite in those rocks in which it occurs. It may also be present as rare skeletal and poikilitic megacrysts. Prismatic apatite crystals are abundant throughout the groundmass.

(ii) Type B hybrid granite

Type B hybrid granite is coarser grained than type A hybrid granite, and contains a greater proportion of megacrysts to groundmass (approximately 1:2). Potash feldspar accounts for the greatest number of megacrysts. The absence of hornblende and the paucity of sphene are also conspicuous features of hybrid granite$_B$.

Potash feldspar occurs both as megacrysts and groundmass crystals. The megacrysts are commonly ovoid in shape, and may be mantled by plagioclase. They are composed of orthoclase or microcline perthite, and invariably contain quartz inclusions. Some groups of quartz inclusions within anhedral groundmass potash feldspar crystals form granophyric intergrowths which partly outline euhedral crystal cores (Plate 50: 7). Biotite and plagioclase inclusions occur in most potash feldspar megacrysts.

Plagioclase megacrysts are generally subhedral, and exhibit both normal and oscillatory zoning. The cores of some megacrysts have a composition of about An_{45}. Many megacrysts contain abundant fine grained rectangular potash feldspar inclusions, which may be arranged in concentric zones. Groundmass plagioclase crystals tend to be lath-shaped, and may be extensively altered. They are commonly zoned in similar fashion to the megacrysts.

Biotite (Z=Y=dark brown to dark red brown: X=straw) is fine to medium grained, and occurs in random orientation. Opaque mineral and zircon inclusions are relatively common.

Accessory minerals include apatite, zircon and opaque minerals. Apatite occurs in abundance in the groundmass as fine grained euhedral prisms. Anhedral sphene and skeletal tourmaline have been observed, but are not common. In some specimens of hybrid granite$_B$, the assemblage chlorite + epidote occurs in association with biotite, and may represent the alteration of pre-existing hornblende.

3.5.6 *Aplites*

The aplites occur as dykes within the megacrystic granites at Port Elliot, and are fine grained rocks with a distinct granular texture. They are composed mainly of cross-hatched microcline, plagioclase (of

composition about An_{27}) and quartz. Biotite and muscovite are present as interstitial aggregates of fine laths. Granophyric intergrowths of microcline and quartz are rare, except in the dyke at the southern side of the small cove north-east of Commodore Point, Port Elliot (Figure 19). Many aplite dykes contain segregations of tourmaline and quartz. Total-rock chemical analyses of two aplites are given in Table G10.

3.6 *THE MINERALOGY OF THE ENCOUNTER BAY GRANITES*

3.6.1 *Micas, chlorite and hornblende*

The compositions of micas, chlorite and hornblende in different varieties of the Encounter Bay Granites were measured by X-ray fluorescence analysis of mineral separates[25] and by electron probe microanalysis of the minerals in polished-thin sections of the granites. The results are given in Appendix H.

(i) Megacrystic granites

Biotite in the border facies megacrystic granite (Table H1) exhibits a range in composition, and occupies a linear field on the triangular diagrams shown in Figures 24 and 25. Fe/(Fe+Mg) ratios for these biotites vary from 0.58 to 0.67. Electron microprobe analyses indicate that the biotite within single specimens of the border facies megacrystic granite is homogeneous in composition, whether it occurs as inclusions in potash feldspar megacrysts or as groundmass crystals (Table H1). This observation is consistent with the suggestion that biotite began crystallising during the formation of the potash feldspar megacrysts (see page 61). In specimens 4-63A and 7-52, biotite contained within hornfels xenoliths has the same composition as that in the groundmass of the host granite.

Biotite has been analysed in only two specimens of the inner facies megacrystic granite (Table H2). The composition of the biotite within each specimen is similar, and in both cases, lies within the range of composition of biotite in the border facies megacrystic granite, but near the Fe-rich extremity (Figures 24 and 25).

Analyses of biotite in xenoliths within the megacrystic granites are given in Table H3. Specimens 3-10 and 3-19 are metasedimentary rock xenoliths, and contain biotite of significantly different composition to that in the enclosing border facies megacrystic granite. However,

---

[25]The minerals were separated from crushed and sized fractions of the granites using standard electromagnetic and heavy liquid techniques

biotite separated from a xenolith of extensively recrystallised biotite-rich material (9-8) lies within the compositional range of biotites from the border facies megacrystic granite. The metasedimentary rock biotites, as plotted in Figures 24 and 25, fall beyond the extension of the linear field of border facies megacrystic granite biotites towards the total alkalis - MgO and the Al_2O_3 - MgO sides of the diagrams. Thus the linear field of biotites from specimens of the border facies megacrystic granite is interpreted as the result of variable contamination of a homogeneous parent magma by metasedimentary rock containing biotite of similar composition to that in the metasedimentary rock xenoliths 3-10 and 3-19, and in one specimen (V3) of Petrel Cove Formation metasediments (Table H3). As the biotite present in hornfels xenoliths in specimens 7-52 and 4-63A is not compositionally different from the biotite in the groundmass of the host granite, or to that in potash feldspar megacrysts, it seems likely that the contamination of the border facies megacrystic granite occurred either prior to or during biotite crystallisation. This suggestion is supported by field and petrographic evidence in relation to the hybrid granites.

Table H3 also lists electron microprobe analyses of micas and co-existing chlorite in a specimen of schist-like material (4-84) of possible hydrothermal origin that occurs within the inner facies megacrystic granite. These analyses indicate that biotite of lower Fe/(Fe+Mg) ratio than analysed in two specimens of the inner facies megacrystic granite coexists with muscovite and an Fe-rich chlorite (ripidolite according to the classification proposed by Deer, Howie and Zussman, 1962).

(ii) Albitised megacrystic granites and megacrystic albite-chlorite rock

Petrographic evidence indicates a change in the composition of the biotite during albitisation of the megacrystic granites. One of the first signs of alteration is the appearance of numbers of small rutile granules within biotite crystals. With more extensive albitisation of the host rock, the biotite is progressively altered to phlogopite and then chlorite, both of which are littered with small rutile granules. This alteration sequence is confirmed by X-ray fluorescence and electron microprobe analyses of the micas and chlorite in specimens of albitised megacrystic granite (Table H4) and in one specimen of megacrystic albite-chlorite rock (Table H5). The end-product of albitisation of the

megacrystic granite, as represented by the megacrystic albite-chlorite rock, contains a Mg-rich chlorite (sheridanite) and a subordinate Ti-poor phlogopite.

The alteration of biotite to phlogopite and chlorite as a result of albitisation of the host granite is illustrated in Figures 26 and 27. The total-rock compositions of specimens 7-53, 7-55 and 7-54 have been plotted on Figure 26. The linear relationship between the total-rock composition and the composition of muscovite and biotite (7-55), and phlogopite and chlorite (7-54) indicates that these minerals are part of equilibrium assemblages.

The loss of Ti from biotite as a result of its alteration during albitisation is an interesting phenomenon[26]. Ti-rich chlorites are apparently unknown, and so chloritisation of biotite containing significant TiO_2 is expected to result either in the loss of Ti from the system, or the formation of rutile inclusions in the chlorite. On the other hand, Ti-rich phlogopites are relatively common, and may contain up to 9% TiO_2 (Dr. K. Norrish, private communication). Thus the loss of Ti from biotite during its alteration to phlogopite is unlikely to be an effect of this composition change alone, but may be related in some way to the physical conditions under which the alteration occurred. It is possible that under certain conditions of pressure and temperature, Ti is incompatible with the available octahedral sites in the phlogopite structure.

(iii) Fine and medium even-grained granites

Biotites in five specimens of fine and medium even-grained granites (Table H6) are very similar in composition, and are significantly enriched in Fe relative to Mg compared with biotites in the megacrystic granites. As shown in Figures 24 and 25, biotites from the fine and medium grained granites plot at the Fe-rich extension of the field of biotites from the border facies megacrystic granite.

(iv) Fine grained miarolitic granophyre

Muscovite separated from two specimens of the fine grained miarolitic granophyre has been analysed (Table H7) and plotted on Figures 24 and 25. It falls within the range of composition of muscovite co-

---

[26]It should be noted that changes in TiO_2 concentration can only be measured by electron probe microanalysis, since X-ray fluorescence analysis of the mica and chlorite separates will be influenced by the presence of rutile inclusions

existing with biotite in specimens of the border facies megacrystic granite.

(v) Hybrid granites

Biotite in two specimens of hybrid granite$_A$ (Table H8) is similar in composition to biotite in the most contaminated specimens of the border facies megacrystic granite, and to biotite in metasedimentary rock xenoliths in the border facies megacrystic granite (Figures 24 and 25). This is consistent with the suggestion that the hybrid granites represent material of sedimentary or metasedimentary origin incorporated into the megacrystic granite at an early stage during its crystallisation history, and subsequently modified to varying degrees. Biotite in hybrid granite$_B$ (Table H9) is significantly more Fe-rich than that in hybrid granite$_A$ (Figures 24 and 25), as would be expected of sedimentary or metasedimentary rock more extensively assimilated by the megacrystic granite.

Hornblende is present in both specimens of hybrid granite$_A$ examined and its average composition from microprobe analyses is given in Table H8. The hornblende has a slightly higher Fe/(Fe+Mg) ratio than the coexisting biotite, and contains about 1.27 atoms of Al per formula unit in tetrahedral sites. However, several spot analyses within a single large hornblende crystal in specimen 3-29 indicate a significant range in composition from hornblende to actinolite (Table H8). In fact, colour changes within the crystal suggest that it may have a core of actinolite and a rim of hornblende. Compositional variability of this magnitude within a single amphibole crystal must indicate conditions of significant disequilibrium during its formation. Conditions of such disequilibrium may well have occurred as a result of thermal and metasomatic alteration of material incorporated into the granite at an early stage of its crystallisation history.

(vi) Discussion

Biotites within the inner facies megacrystic granite and the fine and medium even-grained granites are uniform in composition (Figures 24 and 25). However, biotites within the border facies megacrystic granite exhibit a significant range of composition, and are more Mg-rich. This is best explained as the result of varying degrees of contamination of granite having approximately the composition of the inner facies megacrystic granite, by metasedimentary rocks that contain comparatively Mg-rich biotite. As the composition of biotite within a given specimen

of the border facies megacrystic granite is uniform, the presence of xenocrysts of biotite derived directly from metasedimentary rocks during assimilation can be discounted. Therefore it seems likely that the crystallisation of comparatively Mg-rich biotite in the border facies megacrystic granite was effected by a compositional change consequent upon contamination. This may have been accompanied by an increase in oxygen fugacity which, according to the experimental data of Wones and Eugster (1965), also favours the crystallisation of Mg-rich biotites.

A comparison of the chemistry of hornblende in specimens of hybrid granite$_A$ (Table H8) with that of hornblende in calc-silicate bands and segregations in the country rock Kanmantoo Group (see Appendix E) is interesting. Hornblende in specimens of hybrid granite$_A$ contains about 1.27 atoms of tetrahedral Al per formula unit, and compares very well with the hornblende in granitic rocks of intermediate age in the Sierra Nevada Batholith (Dodge, Papike and Mays, 1968). On the other hand, hornblende in three specimens of calc-silicate rocks contains between 1.65 and 1.78 atoms of tetrahedral Al per formula unit. Harry (1952) and others have suggested that the amount of Al substituting for Si in amphiboles is a direct function of temperature of crystallisation. Dodge, Papike and Mays (1968) described a decrease in tetrahedral Al content in hornblende in progressively younger granitic rocks in the Sierra Nevada Batholith, and suggested that this trend recorded progressively lower temperatures of crystallisation of the granites. It is difficult to reconcile these suggestions with the comparative data for hornblende in rocks in the Encounter Bay area since the hybrid granite is considered to have recrystallised from sedimentary or metasedimentary rock material at magmatic temperatures, perhaps in excess of 700°C (Figure 18), whereas there is no evidence to suggest that the country rocks attained temperatures even approaching this value.

Cooper and Lovering (1970) suggested that the Ti content of amphiboles is an indicator of metamorphic grade, and a comparison of the Ti content of the calc-silicate hornblendes (0.05 atoms per formula unit) with the hybrid granite hornblende (about 0.13 atoms per formula unit) is at first consistent with the expected higher temperature of crystallisation of the latter. However, the single amphibole megacryst in specimen 3-29 contains a range of Ti concentration from 0.01 to 0.13 atoms per formula unit, which exceeds the variation between the hornblendes in the calc-silicates and the hybrid granites.

It thus appears that the composition of hornblende, and in particular the amount of Ti and tetrahedral Al, is dependent upon factors such as the environment and mode of crystallisation in addition to temperature.

3.6.2 *Potash feldspar megacrysts*

Petrographic studies of feldspars in granitic rocks have long been recognised as an important guide to the crystallisation history of these rocks. Within recent years however, feldspars have been studied in sufficient detail to provide a basis for routine determination and classification of unknown specimens using X-ray diffraction techniques. The work of Goldsmith and Laves (1954), Smith and MacKenzie (1955), Smith (1956), MacKenzie and Smith (1962), Orville (1967), Wright and Stewart (1968) and Wright (1968) is important in this regard. The interpretation of these X-ray data has been largely based on the results of accurate X-ray crystallographic structure analyses of several feldspars (Chao, Hargreaves and Taylor, 1940; Cole, Sørum and Kennard, 1949; Bailey and Taylor, 1955; Ferguson, Traill and Taylor, 1958; Jones and Taylor, 1961; Brown and Bailey, 1963; Finney and Bailey, 1964; Coleville and Ribbe, 1968; Bailey, 1969; and Ribbe, Megaw and Taylor, 1969). As a result, routine X-ray diffraction techniques are now commonly used to investigate the nature of granitic potash feldspars in order to assess aspects of the crystallisation history of the host rocks (for example Rao, 1960; Smithson, 1962; Dietrich, 1962; Marmo, Hytönen and Vorma, 1963; Nilssen and Smithson, 1965; Suwa, 1966; Wright, 1964, 1967; Steiger and Hart, 1967; Tilling, 1968; Fershtater, 1968; Ragland, 1970).

Potash feldspar megacrysts in both varieties of the megacrystic granite are considered, on the basis of field and petrographic evidence, to represent early-formed phenocrysts. Potash feldspar megacrysts in the border facies megacrystic granite are composed of euhedral cores sharply bounded by granophyric borders, which seem to be the product of rapid simultaneous crystallisation of potash feldspar and quartz consequent upon the emplacement of the granite. During the present investigation, potash feldspars from several specimens of megacrystic granite were examined for variations in structural state and chemistry that might be consistent with their suggested origin.

(i) X-ray diffraction properties

Samples were collected sequentially across selected potash feld-

spar megacrysts in both varieties of the megacrystic granite, and their X-ray diffraction properties were measured according to the techniques described in Appendix I. As also discussed in Appendix I, the $2\theta.\bar{2}04/060$ parameter is a unique and sensitive indicator of the degree of Al,Si order in alkali feldspars, and has been used to estimate the degree of order in the feldspars encountered during this investigation with reference to Figure 28. Anomalous alkali feldspars, as described by Wright and Stewart (1968) and Wright (1968), are readily distinguished using Wright's $2\theta.\bar{2}04$ - 060 graph. These feldspars are characterised by systematically low values of the c cell edge and systematically high 2θ values for the $\bar{2}04$ reflection as discussed in Appendix I, and they exhibit a different but parallel relationship between Al,Si order and the parameter $\bar{2}04/060$ to that observed for normal feldspars (Figure 28).

Potash feldspar fragments sampled from megacrysts in specimens of the border facies and the inner facies megacrystic granites (Tables I5 and I6 respectively) have been plotted on portion of the $2\theta.\bar{2}04$ - 060 graph of Wright (1968) in Figure 29. Potash feldspar in megacrysts in specimens of the border facies megacrystic granite exhibits a range of apparent structural states between the low albite III and maximum microcline alkali-exchange paths. On the other hand, potash feldspar in megacrysts in specimens of the inner facies megacrystic granite exhibits a range of apparent structural states between the Spencer B and maximum microcline alkali-exchange paths. Both varieties of the megacrystic granite yielded potash feldspars that are anomalous in terms of $\bar{2}04$ and 060.

Megacrysts in specimens of the border facies megacrystic granite contain both triclinic and monoclinic or near-monoclinic potash feldspar phases, as indicated by the structure of the diffraction patterns in the region of the 131 and $1\bar{3}1$ reflections. In fact, some fragments contain mixtures of monoclinic and triclinic phases, resulting in a smeared and often unintelligible patterns in the 131 - $1\bar{3}1$ region. Notwithstanding, several megacrysts exhibit a systematic variation in Al,Si order and $2\theta.1\bar{3}1$-131 from core to rim, indicating the presence of orthoclase in the core and phases of higher Al,Si order towards the rim (Figure 30). Other megacrysts contain an erratic and non-systematic variation in one or both of these parameters. The preservation of orthoclase with Spencer B ordering in several of these megacrysts is consistent with the suggested magmatic origin of the megacrysts, and also with the suggested origin of

the border facies megacrystic granite as a rapidly cooled crystal-rich magma. It is unlikely that the potash feldspar crystallised from the magma as orthoclase because the temperatures at this time are expected to have been well within the stability field of sanidine (MacKenzie and Smith, 1961). However, the orthoclase cores of the megacrysts are considered to represent the partly ordered equilibrium polymorph of potash feldspar that was stable at the time of emplacement of the megacrystic granite. As orthoclase is known to be the stable potash feldspar polymorph in nature at temperatures at least as low as 400°C (Steiger and Hart, 1967; Wright, 1967), its presence in the megacrysts places a lower limit on the temperature of emplacement of the megacrystic granite, consistent with the proposed upper limit (approximately 540°C) of the temperature of metamorphism in the contiguous Kanmantoo Group metasediments (see page 51 and Figure 18). Potash feldspar that crystallised with quartz in granophyric intergrowths in the groundmass of the megacrystic granite, and around the margins of the megacrysts, is generally more highly ordered than the material in the megacryst cores. This is consistent with the late-stage crystallisation of this material within the microcline stability field.

Potash feldspar megacrysts in specimens of the inner facies megacrystic granite contain only triclinic potash feldspar phases. However, the variation in Al,Si order and 20.$1\bar{3}1$-131 from core to rim in two of the megacrysts examined follows a similar pattern to that present in several megacrysts in the border facies megacrystic granite (Figure 30). On the basis of field and petrographic evidence, the inner facies megacrystic granite appears to have crystallised comparatively slowly, being shielded from the country rock metasediments by the border facies megacrystic granite. Conditions of slow cooling, and the presence of volatiles (for which there is abundant evidence in the form of tourmaline- and quartz-rich pegmatites) at least during the latter stages of crystallisation of the rocks, must have facilitated the diffusion of Al and Si in the feldspar lattice and thus promoted the inversion of original monoclinic potash feldspar to the more ordered triclinic phases now present. The occurrence of potash feldspar phases of lower Al,Si order in the cores of some megacrysts may indicate that the rate of crystallisation and cooling exceeded the rate of diffusion of Al and Si within the feldspar lattice.

Kerrick (1969) and Vorma (1971) are among the many authors who

have recorded significantly lower degrees of Al,Si order (as indicated by obliquity[27] measurements) in potash feldspar megacrysts than in the groundmass potash feldspar of granitic rocks. Kerrick compared obliquity measurements of potash feldspar megacrysts and groundmass material in the Cathedral Peak porphyritic quartz monzonite in California, and used them as indicators of the relative temperatures of formation of the two feldspar types. In conjunction with textural evidence, he suggested that lower obliquities in the megacrysts were the result of early magmatic growth. Vorma discussed the crystallisation of orthoclase and microcline polymorphs of potash feldspar in a suite of rapakivi granites from the Wiborgite massif in Finland, and suggested that the nature of the potash feldspar polymorph could be directly related to the volatile content and the temperature of crystallisation of the granite magma. These proposals are in harmony with the results obtained from the examination of potash feldspars in the Encounter Bay megacrystic granites.

Potash feldspar sampled from two megacrysts in a specimen of type B hybrid granite exhibits a range of apparent structural state between the Spencer B and Spencer U alkali-exchange paths (Table I7, Figure 29). One megacryst contains potash feldspar of orthoclase type. On the basis of field and petrographic evidence, these potash feldspar megacrysts are considered to have crystallised as porphyroblasts in an essentially solid medium at the same time, and in equilibrium with potash feldspars in the host megacrystic granite magma (see page 72). The preservation of orthoclase in one megacryst in the hybrid granite is consistent both with the early crystallisation of the megacryst, and with rapid cooling consequent upon emplacement of the border facies megacrystic granite in which this particular hybrid granite specimen occurs as an inclusion.

(ii) Chemistry of the potash feldspar megacrysts and of coexisting plagioclase

Electron probe microanalyses of potash feldspar were made at intervals in traverses across potash feldspar megacrysts in specimens of both the inner facies and the border facies megacrystic granites, and the results are given in Appendix J (Tables J1-J6). Microanalyses of exsolution bodies and plagioclase inclusions encountered in the traverses

---

[27]Obliquity or triclinicity was defined by Goldsmith and Laves (1954) as $12.5\times(20.1\bar{3}1-131)$

are also included in these Tables, in addition to microanalyses at intervals across plagioclase megacrysts in some specimens. The results can be summarised as follows:

a. Ba (expressed as molecular percentage of celsian) is enriched in the cores of the potash feldspar megacrysts relative to their margins (Figure 31). This trend is also reflected in a depletion in mol. percent orthoclase in the cores of the megacrysts relative to their margins since K and Ba are negatively correlated.

b. Groundmass potash feldspar in specimens 4-93 and 4-61 (Tables J2 and J4 respectively) contains Ba concentrations comparable with those in the margins of the potash feldspar megacrysts.

c. Exsolution lamellae in potash feldspar megacrysts are composed of albite which contains low percentages of Or and An consistent with subsolidus crystallisation (Elders, 1968; Seck, 1971).

d. Plagioclase inclusions within potash feldspar megacrysts are surrounded by albitic borders of secondary origin, but contain inner zones as calcic as about An_{39} (for example in specimen 4-61, Table J4).

e. Plagioclase megacrysts are compositionally zoned from calcic cores to sodic margins in an oscillatory fashion, and may contain inner zones as calcic as about An_{45} (for example in specimen 4-93, Table J2).

f. Plagioclase crystals within a small hornfels xenolith in a specimen of the border facies megacrystic granite (7-52) are zoned, and contain cores of composition about An_{29} and margins of composition about An_{24} (Table J5).

g. Plagioclase bordering one potash feldspar megacryst (specimen 3-26, Table J3) is of oligoclase-andesine composition, and is also zoned, with a calcic core (about An_{32}) and less calcic margins (about An_{20}).

The enrichment of Ba in the cores of the potash feldspar megacrysts relative to their margins and to the groundmass potash feldspar supports an early-formed origin for the megacrysts on the basis of crystallochemical considerations (see Taylor, 1965), and in this regard is consistent with the field, petrographic and X-ray diffraction data.

Many authors including Kerrick (1969) have described the enrichment of Ba in potash feldspar megacrysts relative to groundmass potash feldspar in granites and pegmatites, and have suggested an early-formed origin for the megacrysts. On the other hand, Emmermann (1969) has interpreted the potash feldspar megacrysts in the Abtal granite in Germany as the result of post-magmatic crystallisation, although they contain Ba concentrations approximately three times that of the groundmass potash feldspar in the same rocks, and exhibit many features that could as easily be interpreted as the result of magmatic crystallisation (see for example Hibbard, 1965; Elders, 1968).

The similar compositions of the inner parts of plagioclase megacrysts and plagioclase inclusions in potash feldspar megacrysts are consistent with the crystallisation of plagioclase during the formation of the potash feldspar megacrysts. However, the disparity in size between the plagioclase megacrysts and the plagioclase inclusions suggests that much of the crystallisation of plagioclase post-dates the formation of the potash feldspar megacrysts.

Coexisting potash feldspar and plagioclase megacrysts in two specimens of hybrid granite (3-29 and 3-27) were analysed by electron microprobe in the same manner as the megacrystic granite feldspars, and the results are given in Tables J7 and J8. The large potash feldspar megacryst in the specimen of hybrid granite$_A$ is in fact a "patch-work" intergrowth of potash feldspar and andesine (Table J7), and also contains abundant quartz, and inclusions of sphene, hornblende and biotite. As such, it is typical of many potash feldspar megacrysts in hybrid granite$_A$ (see page 98). It may have formed by simultaneous crystallisation of potash feldspar and plagioclase in an essentially solid medium, or alternatively by the replacement of one feldspar by another. The Ba content of the potash feldspar is moderately high, and compares with the Ba contents of the inner zones of potash feldspar megacrysts in the megacrystic granites. However, the plagioclase in these intergrowths is not zoned and is significantly more sodic than a nearby plagioclase megacryst, which is oscillatorily zoned from An_{42} in the core to about An_{31} at the margin. The composition of the plagioclase megacryst compares with that of plagioclase megacrysts in specimens of the megacrystic granites, although in contrast the latter possess distinct albitic margins. The potash feldspar megacryst in a specimen of hybrid granite$_B$ (3-27, Table J8) also contains moderately high Ba concentrations

consistent with those in the inner zones of potash feldspar megacrysts in the megacrystic granites. The compositions of two plagioclase megacrysts are consistent with that of the plagioclase megacryst in the specimen of hybrid granite$_A$.

Average compositions for potash feldspar megacrysts (excluding discrete plagioclase inclusions), groundmass potash feldspar, plagioclase inclusions in potash feldspar megacrysts, plagioclase megacrysts, and plagioclase crystals in a small hornfels inclusion in each specimen of megacrystic granite and hybrid granite examined were calculated from the electron microprobe analyses in Tables J1-J8. The results are given in Table J9 and have been plotted on a ternary An-Ab-Or diagram in Figure 32. Lines projected from the average composition of the potash feldspar megacrysts through points representing the bulk compositions of the host rocks (see Appendix G, Tables G1, G3 and G9) on to the An-Ab side of the diagram provide a means of estimating the composition of plagioclase in equilibrium with the potash feldspar (see Seck, 1971). It should be pointed out that an estimation of the average composition of perthitic potash feldspar megacrysts from routine microprobe spot analyses using a focussed electron beam is hazardous, and may result in an overestimation of the Or component. However, the alternative method of analysis, which involves separation of the feldspars from crushed rock specimens using heavy liquids, is also subject to large errors because of the occurrence in these rocks of more than one generation of potash feldspar, the presence of small plagioclase inclusions in the potash feldspar megacrysts, and the possibility of seriously depleting the perthite in albite component during separation. The most suitable method of analysing the potash feldspar phases would involve taking several spot analyses using a defocussed beam in the electron microprobe, but has yet to be attempted. Nevertheless, plagioclase compositions predicted from the tie-lines drawn on Figure 32 for specimens 4-93, 7-52 and 3-26 agree closely with the average compositions of plagioclase megacrysts (in the case of 7-52, plagioclase crystals in a small hornfels xenolith) calculated from the microprobe data, thus indicating equilibrium conditions of feldspar crystallisation. Moreover, the tie-lines are parallel to the experimental tie-lines determined at 650°C and 1kb P_{H_2O} by Seck (1971). In the case of specimen 4-93, the predicted composition of plagioclase in equilibrium with groundmass potash feldspar is approximately 10 mol. percent lower in An than that in equilibrium with the average potash

feldspar megacryst. The very low slope of this tie-line is consistent with the late-stage crystallisation of the groundmass potash feldspar at temperatures below 650°C at 1kb pressure, according to the experimental data of Seck. Plagioclase compositions predicted from the tie-lines for specimens 9-11 and 4-79 are similar to those obtained for 4-93, 7-52 and 3-26, although the compositions of plagioclase megacrysts in these specimens were not measured. In the case of 4-79, the predicted equilibrium plagioclase composition (about An_{20}) is close to the composition of a plagioclase inclusion in the potash feldspar megacryst (Table J9).

There seems to be marked disequilibrium between the average compositions of coexisting plagioclase and potash feldspar and the total-rock composition of the border facies megacrystic granite 4-61. Tie-lines projected from the composition of the average potash feldspar megacryst or the composition of the average groundmass potash feldspar through the composition of the total-rock to the An-Ab side of the diagram are consistent with tie-lines constructed from the experimental data at 650°C and 1kb, and predict an equilibrium plagioclase composition of about An_{13}. On the other hand, the average composition of a plagioclase inclusion in the potash feldspar megacryst is close to An_{32}. There are at least two possible explanations for this anomaly. The plagioclase inclusion may be a xenocryst, since it could not have crystallised in equilibrium with potash feldspar in a rock having the composition of 4-61. Alternatively, the potash feldspar and plagioclase may have crystallised as part of an equilibrium assemblage, but the composition of 4-61 (a specimen of border facies megacrystic granite) may represent marked contamination during emplacement and relatively rapid subsequent crystallisation. Further analytical work is clearly required in order to test these hypotheses.

The data for the specimens of hybrid granite (Table J9) also indicate disequilibrium between the average compositions of the coexisting feldspars and the total-rock compositions. However, the calculated average compositions of potash feldspar megacrysts are considered to be significantly in error. For example, the megacryst in 3-29 is complexly intergrown with plagioclase, whilst microanalyses of the megacryst in 3-27 do not include exsolved albite lamellae. On the other hand, tie-lines through the average compositions of plagioclase megacrysts and the total-rock compositions are parallel, and are consistent with tie-lines constructed for the experimental data of Seck at 650°C and 1kb

P_{H_2O}.

(iii) Discussion

X-ray diffraction and electron probe microanalytical data are consistent with an early-formed magmatic origin for the potash feldspar megacrysts in the megacrystic granites. On the basis of structural state and degree of Al,Si order, orthoclase is present in the inner parts of some potash feldspar megacrysts in the border facies megacrystic granite whereas the margins of the megacrysts are composed of microcline. The preservation of orthoclase in the inner parts of the megacrysts is considered to reflect relatively rapid cooling and crystallisation of the magma in the absence of volatiles, subsequent to the formation of orthoclase phenocrysts, from temperatures at least as high as 375°C (Steiger and Hart, 1967; Wright, 1967). This is expected to have occurred upon emplacement of the megacrystic granite into the Kanmantoo Group metasediments. On the other hand, potash feldspar megacrysts in the inner facies megacrystic granite do not contain orthoclase, presumably as the result of relatively slow cooling in the presence of abundant volatiles. An enrichment of Ba in the cores of potash feldspar megacrysts relative to their margins, and relative to groundmass potash feldspar, can be demonstrated from electron probe microanalytical data, and is considered to be further evidence in favour of an early-formed origin for the megacrysts.

Average compositions of potash feldspar megacrysts and coexisting plagioclase calculated from electron probe microanalytical data are generally consistent with crystallisation at 650°C and 1kb pressure in the synthetic An-Ab-Or system investigated by Seck (1971). However, as pointed out by Seck, the tie-lines between coexisting feldspars provide no unequivocal information on either temperature of formation or pressure, because of the opposite effect of pressure to temperature on the orientation of the tie-lines. This effect has also been discussed by Yoder, Stewart and Smith (1957). Comparison with their data suggests that the feldspars from the Encounter Bay Granites could equally well have crystallised at temperatures in the vicinity of 720°C at a pressure of 5kb.

Potash feldspar megacrysts within the hybrid granites possess similar chemical and X-ray diffraction properties to those in the host border facies megacrystic granite, and are considered to have undergone a

similar crystallisation history. This suggestion is supported by the orientation of tie-lines joining the compositions of the plagioclases and the total-rocks in Figure 32. On this basis, the simultaneous crystallisation of potash feldspar megacrysts in the megacrystic granite magma and in the essentially solid hybrid granite parent during equilibrium or near-equilibrium chemical conditions between the two rock types, as proposed from field and petrographic data, seems to be confirmed.

3.7 *THE PETROCHEMISTRY OF THE ENCOUNTER BAY GRANITES*

Chemical analyses of several specimens of most varieties of the Encounter Bay Granites (Tables G1-G10) have been plotted on Figure 33 in terms of total alkalis, total Fe and MgO. The granites define a curvilinear trend extending from the total alkalis apex towards the total Fe - MgO side of the diagram. The inner facies megacrystic granite occupies a small field part way along the trend from the total alkalis apex. The border facies megacrystic granite from Cape Willoughby occupies a small field approximately coincident with the inner facies megacrystic granite. However, the border facies megacrystic granite from the Encounter Bay area occupies an elongate field that overlaps the field of inner facies megacrystic granite, but extends towards the total Fe - MgO side of the diagram into the field occupied by Kanmantoo Group metasedimentary rocks (Table G11). The border facies megacrystic granite contains abundant metasedimentary rock fragments, and the extensive compositional field occupied by it in Figure 33 is considered to demonstrate that it has totally assimilated similar xenoliths. It is of interest that many authors (for example Oba, 1962; Butler and Ragland, 1969) ascribe trends of this type in granite suites to differentiation.

The hybrid granites, which occur as inclusions in both varieties of the megacrystic granite but are present as dyke-like bodies and large inclusions in the border facies megacrystic granite, are considered to be metasedimentary rock that has been assimilated by the granite to varying degrees. Hybrid granite$_A$ is the least modified variety of the hybrid granite and as expected, falls close to the field of metasedimentary rocks in Figure 33 along the granite trend. Hybrid granite$_B$, including the hybrid granite mapped at Cape Willoughby, has been assimilated by the megacrystic granite to a large degree and occupies a corresponding field on the trend near the inner facies megacrystic granite field. Many metasedimentary rock xenoliths within the border

facies megacrystic granite are similar in texture and lithology to contiguous Petrel Cove Formation metasediments, and as shown in Figure 33, appear to have suffered little or no chemical modification as a result of their incorporation in the granite.

The inner facies megacrystic granite contains rare hornfels and hybrid granite xenoliths, and also patches of granophyric leucogranite and inclusions of fine grained megacrystic granite. The presence of hornfels and hybrid granite xenoliths suggests that the inner facies megacrystic granite has been contaminated to some degree by metasedimentary rock material. If the contamination trend is the same as in the case of the border facies megacrystic granite, it is likely that the composition of the medium even-grained granites approximates closely the composition of the uncontaminated parent magma of the Encounter Bay Granites.

A compositional trend due to enrichment of alkalis (and consequently the formation of rocks rich in potash feldspar) is also recorded in the total-rock data for the Encounter Bay Granites. For example, the abundant potash-rich granophyric leucogranites that occur as patches in the inner facies megacrystic granite are interpreted as the result of late-stage crystallisation of residual magma in favourable sites in the host granite. In addition, the red leucogranite and the fine grained miarolitic granophyre, which exhibit granophyric textures and contain numerous small pegmatite pods, are clearly late-stage products of crystallisation of the differentiated granite magma. The numerous aplite dykes may also be placed in this category in terms of chemical composition.

Contamination of the Encounter Bay Granites by metasedimentary rock is reflected not only in the total-rock chemistry of the granites, but also in the chemistry of their constituent biotites, as discussed on pages 100 and 101 with reference to Figures 24 and 25. The total-rock composition of several granite varieties and the compositions of their constituent biotites have been plotted on Figure 34. With increasing contamination, the granites become enriched in Fe+Mg relative to alkalis whereas the Fe/(Fe+Mg) ratio of the constituent biotites decreases. The most Mg-rich biotites occur in the hybrid granites, which represent partly assimilated metasedimentary rock.

Figure 35 is a plot of K against Rb for the Encounter Bay Granites and some contiguous Kanmantoo Group metasediments. The Encounter Bay

border facies megacrystic granite has an estimated K/Rb ratio of about 180. The Cape Willoughby border facies megacrystic granite, the hybrid granites, the two fine grained granites, and most of the Kanmantoo Group metasediments also have an estimated average K/Rb ratio of about 180. Taylor (1965), and Kolbe and Taylor (1966) noted that the average K/Rb ratio for most crustal rocks was about 220, which is significantly higher than the value of 180 obtained above. Coincidence of the K/Rb ratio for contaminated varieties of the Encounter Bay Granites with that for the Kanmantoo Group metasediments is taken as further evidence that metasediments of similar composition to the Kanmantoo Group were the contaminants. This applies particularly to metasediments that are characterised by K/Rb ratios greater than 180.

K/Rb data for the Encounter Bay Granites, as well as that presented by Kolbe and Taylor (1966, Figure 9, page 12) exhibit an abrupt change of character at K concentrations of about 4%. For example, small increases in K concentration above 4% correspond to comparatively large increases in Rb concentration, in contrast to the relationship between K and Rb at K concentrations below 4%. In fact, the discontinuity is related to the maximum potash content of granitic liquids dictated by the position of the ternary minimum or eutectic in the Q-An-Ab-Or-H_2O system. However, there are no such constraints on the concentration of Rb in granitic liquids.

The medium even-grained granites and the red leucogranite are characterised by a K/Rb ratio of about 125, which is significantly lower than the average ratio for crustal rocks. The medium grained granites are considered to approximate the composition of the parent magma of the Encounter Bay Granites. According to the geochemical criteria of Taylor (1965), the low K/Rb ratio would suggest that this magma was derived through processes of marked differentiation. The significant enrichment of Rb relative to K in the parent magma is similar to that found by Kolbe and Taylor (1966) in the Snowy Mountains leucogranites in eastern Australia, and as explained above, is considered to be characteristic of granitic rocks which have a composition approaching the ternary eutectic. At an early stage of melting of sediments to form an anatectic granite, the initial melt should contain between 26% and about 35% Or, equivalent to 3.7% to 4.9% K, depending on the varying P-T conditions (Kleeman, 1965; James and Hamilton, 1969). There is no limit to the amount of Rb that can be incorporated into the early melt. In

fact, as most of the Rb in sediments is likely to be present in micas or potash feldspar, which are the first minerals to break down upon melting (Robertson and Wyllie, 1971; Wyllie, 1971), the amount of Rb in the early melt would be quite high. Similar arguments may account for the decreasing K/Rb ratio in magmas during fractional crystallisation. The bulk composition of the assumed parent magma for the Encounter Bay Granites is consistent with either postulate, and the K/Rb ratios do not help to distinguish them.

The inner facies megacrystic granite exhibits a range of K/Rb ratios from 125, which corresponds to that assumed for the parent magma, to about 150. This variation is believed to reflect minor contamination by metasedimentary rock, since the trend is towards the border facies megacrystic granite and the Kanmantoo Group metasediments. Moreover, it is consistent with the field evidence, and with the major element chemical data summarised in Figure 33.

It is of interest that the aplite dykes have a lower K/Rb ratio than the border facies megacrystic granite into which many of them were emplaced, but a significantly higher K/Rb ratio than the medium grained granites and the red leucogranite. The aplites therefore seem to be related to the border facies megacrystic granite, from which they may have been derived as a residual magma.

CIPW normative An, Ab, and Or ratios for the Encounter Bay Granites are plotted on Figure 36 in relation to the quartz-saturated two-feldspar cotectic line at 1kb P_{H_2O} projected on to the An-Ab-Or face of the Q-An-Ab-Or tetrahedron (James and Hamilton, 1969). The inner facies megacrystic granite (Table G2) occupies a small field straddling the two-feldspar boundary. On the other hand, specimens of the Encounter Bay border facies megacrystic granite (Table G1) define an elongate zone that partly overlaps the inner facies megacrystic granite, but extends well out into the plagioclase field of the diagram. As will be clear from the preceding discussion, this elongate trend records the effect of contamination. Specimens of the Cape Willoughby border facies megacrystic granite (Table G3) occupy an area which straddles the two-feldspar boundary but extends into the plagioclase field in a similar manner to the border facies megacrystic granite from the Encounter Bay area. This is again an effect of contamination, but apparently by material of different composition to that affecting the Encounter Bay border facies megacrystic granite. There is also evidence for contamin-

ation of the inner facies megacrystic granite as discussed above, and so the composition of the parent magma is best represented by the composition of the medium grained granites which fall well within the Or field in Figure 36.

Figure 36 shows that potash feldspar should occur on the liquidus for a rock of the composition assumed for the parent magma of the Encounter Bay Granites. This suggests either that the original magma carried potash feldspar crystals at the time of emplacement, or that it was capable of crystallising potash feldspar as its first phase. Contamination of the parent magma with metasedimentary rock increased the amount of plagioclase relative to potash feldspar, and so displaced the bulk composition into either the plagioclase field or the quartz field of the Q-An-Ab-Or tetrahedron. This is demonstrated by the trends outlined by the megacrystic granites in Figure 36. It is likely that the contamination induced further crystallisation, such that crystals of the two feldspars and quartz were coexisting prior to consolidation of the granite.

Observations of the field and petrographic relationships of the potash feldspar megacrysts in the Encounter Bay granites are consistent with the above interpretation. For example, textural observations suggest that the major crystallisation of plagioclase, biotite and quartz post-dated the formation of the potash feldspar megacrysts. This is supported by the data of Piwinskii and Wyllie (1970) on the experimental melting of water-saturated rocks from the Needle Point Pluton in the Wallowa Batholith, Oregon. Their results at 2kb suggest that the interpolated stability curves for biotite and quartz in granites that have a D.I. greater than 92.8 (into which group the medium grained granites representing the parent magma of the Encounter Bay Granites fall) cross the interpolated stability curve for potash feldspar, such that potash feldspar remains stable up to temperatures approaching 700°C whereas biotite and quartz dissolve in the liquid at much lower temperatures (Figure 37a). On the other hand, Robertson and Wyllie (1971) and Wyllie (1971) located the stability curve for biotite at temperatures up to 100° below the stability curves for potash feldspar and quartz during melting of granodiorite at 2kb in a water-deficient environment (Figure 37b). With greater than 1.5% total water in the system, the stability curves cross so that potash feldspar and quartz disappear at lower temperatures than biotite during progressive melting. If these

experimental data can be extrapolated to rocks of granitic composition, and can be used to interpret conditions at the time of magmatic crystallisation, the observed relatively late crystallisation of biotite in the Encounter Bay and Cape Willoughby megacrystic granites could indicate that the magma was deficient in water, and may not have contained a vapour phase at the time of crystallisation. Such conditions are intermediate between the Types II and III subsolidus assemblages of Robertson and Wyllie (1971).

The Encounter Granites, with the exception of the Cape Willoughby megacrystic granite, are generally homogeneous in terms of normative Q, Ab and Or and define a point maximum which is displaced from the isobaric minimum in the Q-Ab-Or-H_2O synthetic system (Tuttle and Bowen, 1958) towards the Q-Or side of the Q-Ab-Or ternary diagram (Figure 38). However, the ternary minimum at 1kb moves to higher temperatures and becomes displaced towards the Q-Or side of the diagram with increasing An content in the Q-An-Ab-Or-H_2O synthetic system (Winkler, 1967; James and Hamilton, 1969; Winkler and Lindemann, 1972). In fact, the composition of the Encounter Bay Granites approaches the ternary minimum at 1kb P_{H_2O} in the system containing between 3% and 5% An. The Cape Willoughby border facies megacrystic granite however, is more closely related to the minimum at 1kb P_{H_2O} in the system containing 3% An.

There is a slight but significant displacement of the granites from the projection of the cotectic line towards Q-poor compositions in Figure 38, but the explanation for this is not clear. Tuttle and Bowen (1958), and Luth, Jahns and Tuttle (1964) have shown that an increase in P_{H_2O} from 1kb to 3kb in the An-free system decreases the amount of quartz at the ternary minimum from about 37% to 32%. It is probable that a similar effect occurs in the Q-An-Ab-Or-H_2O system. Hence an extrapolation of the data of James and Hamilton (1969) to 3kb could easily decrease the Q content of the ternary minimum by about 5%. Thus the minimum for 3% An could lie at about 35%Q-30%Or-35%Ab, which is comparable with the composition of the medium grained granites. The presence of HCl in the fluid phase in water-saturated systems will shift the projection of the cotectic line towards Q-poor compositions, according to Winkler (1967) and Winkler and Lindemann (1972). If the magmas from which the Encounter Bay Granites crystallised were water-saturated at the time of crystallisation, then a displacement of the type observed

may be due to the influence of volatiles other than water (for example boron). Alternatively, the Encounter Bay Granites may have been water-deficient at the time of crystallisation. At present, there is limited information on the nature of the ternary minimum and cotectic line in water-deficient Q-An-Ab-Or-H_2O synthetic systems, and on the effect of pressure on these features. However, the composition of the Encounter Bay Granites on the Q-Ab-Or diagram (Figure 38) is displaced from the projection of the cotectic line in the water-saturated system towards a likely location of the ternary minimum in the anhydrous system (Luth, 1969).

Kleeman (1965) suggested that the origin of granitic rocks is generally indicated by their chemistry and mineralogy. He pointed out that the per-aluminous character of granites, together with the occurrence of biotite in excess of hornblende, indicates a sedimentary origin. On the other hand, meta- or sub-aluminous granites containing hornblende in excess of biotite, and soda amphiboles in some instances, indicates derivation from contaminated basic rocks. These characteristics were used by Luth, Jahns and Tuttle (1964) in their classification of granites into subsolvus and hypersolvus granites respectively. The Encounter Bay Granites are subsolvus granites, and may accordingly be of anatectic origin.

Luth, Jahns and Tuttle (1964) recorded a closer relationship between aplites and pegmatites and the ternary minimum in the Q-Ab-Or-H_2O system than between granites and the minimum, and on this basis suggested that the aplites and pegmatites were formed from water-rich residual magma. Furthermore, in view of the overlap of the compositional field of 281 "subsolvus" granites containing normative corundum and the fields of both the aplites and the pegmatites, they argued that the granites were derived from magmas with relatively high water contents through processes of crystal-liquid equilibria. All varieties of the Encounter Bay Granites, with the exception of the Cape Willoughby border facies megacrystic granite, have a homogeneous composition in terms of Q, Ab and Or (Figure 38). In particular, there is no tendency for the youngest granite varieties (red leucogranite, miarolitic granophyre or aplites) to be displaced towards the ternary minimum in the water-saturated system. There is no clear explanation for this observation, although in contrast to the water-saturated environment envisaged by Luth, Jahns and Tuttle (1964), the parent magma of the Encounter Bay Granites may have been

water-deficient.

3.8 *THE PETROCHEMISTRY OF THE ALBITISED GRANITES AND THE MEGACRYSTIC ALBITE-CHLORITE ROCK*

Chemical analyses of the albitised border facies megacrystic granite and the megacrystic albite-chlorite rock are given in Appendix G (Table G5). As discussed in earlier section, these rocks are considered to have formed by albitisation of the megacrystic granite in appropriately jointed and fractured zones. Therefore, the chemical changes involved in their formation can be assessed by recalculation of the number of cations associated with the standard unit cell (Barth, 1952), as shown in Table G12. For example, albitisation of the Rosetta Head border facies megacrystic granite to produce the megacrystic albite-chlorite rock in this locality requires a marked increase in Na, Al and Mg concentrations and a decrease in K, Si and Ca concentrations. Of particular note is the nett gain of about 7 cations, which indicates that the replacement is not isochemical. Albitisation of the Granite Island border facies megacrystic granite requires similar concentration changes and a nett gain of about 6 cations. The chemical changes accompanying the development of the albitised border facies megacrystic granite represented by specimens 7-53 and 7-55 however, are largely due to an increase in Na concentration and a decrease in K concentration. These changes balance out. Similar changes are indicated for the development of the albite leucogranite 4-8 from the red leucogranite 4-9 (Tables G7 and G12).

A source for the material responsible for the albitisation can not be suggested on the basis of the chemical data. Although field observations favour a close relationship between the granites and the material responsible for the albitisation, it is difficult to envisage a late-stage soda-rich differentiation product of the Encounter Bay Granites in view of the crystallisation sequence outlined in the previous section. In fact, the material responsible for the albitisation may have no genetic relationship to the granites. The widespread occurrence of albitisation phenomena throughout the Mount Lofty Ranges metamorphic belt (Offler, 1966; Fleming, 1971) provides considerable support for this suggestion.

3.9 *THE AGE AND Sr ISOTOPE COMPOSITION OF THE ENCOUNTER BAY GRANITES*

During a study of the accessory minerals in South Australian granites, Fander (1960) measured the age of two specimens of Encounter

Bay Granites using the Pb-α method of Larsen, Keevil and Harrison (1952) on zircon concentrates. He obtained ages of 415 ± 42m.y. and 680 ± 68m.y. for specimens of granites from Granite Island and Port Elliot respectively, but considered the 680m.y. age to be anomalous due to contamination.

Evernden and Richards (1962) published a single K-Ar biotite age of 457m.y. for an unknown variety of the Encounter Bay Granites from the Encounter Bay area, substantially supporting Fander's Pb-α age.

Dasch, Milnes and Nesbitt (1971) discussed the results of a preliminary investigation of the age and Sr isotope composition of the Encounter Bay Granites and the contiguous Kanmantoo Group metasedimentary rocks. They reported an isochron age of 487 ± 37m.y. for the granites and a similar age of 487 ± 60m.y. for the Kanmantoo Group metasediments, and suggested from these data that the emplacement of the granites was coincident with the metamorphic event recorded in the metasediments. The high initial Sr^{87}/Sr^{86} ratio for the Encounter Bay Granites (0.719) could not be distinguished from that for the Kanmantoo Group metasediments (0.722) within the analytical uncertainties, and was considered to indicate that the granites were formed by "remobilisation of associated crustal rock".

The data reported by Dasch, Milnes and Nesbitt were obtained by X-ray fluorescence determinations of total Rb and Sr, and mass spectrometer measurements of Sr isotope composition on unspiked aliquots of the same samples. The results gave a considerable scatter of points about both the granite and the metasedimentary rock isochrons. In the case of the granites, two possible explanations were considered: incomplete homogenisation of Sr at the time of crystallisation perhaps due to contamination of the magma by metasedimentary rock, or minor but real differences in age between the granite varieties sampled. In order to test these suggestions, specimens of several varieties of the Encounter Bay Granites, including some of the specimens examined by Dasch, Milnes and Nesbitt, were analysed for Rb and Sr isotope composition by isotope dilution using the techniques of chemical preparation and mass-spectrometry summarised in Appendix K. K-Ar age determinations on specimens of the Encounter Bay Granites supplemented the Rb-Sr data. The K-Ar analyses were carried out by Dr. A.W. Webb of the Australian Mineral Development Laboratories, an arrangement made possible through the kindness of Mr. B.P. Thomson of the South Australian Geological

Survey. The K-Ar data are included in a cooperative geochronology programme between the South Australian Geological Survey and the Australian Mineral Development Laboratories (Thomson, 1971, 1972).

3.9.1 *Contaminated border facies megacrystic granite*

Several specimens of the contaminated border facies megacrystic granite (7-58, 3-26, 4-55, 8-12) were selected for isotope dilution analysis on the basis of total-rock petrochemical data, including Rb and Sr concentrations (Table G1). According to these data, the specimens exhibit varying degrees of contamination by metasedimentary rock as explained on pages 114 and 115 in relation to Figures 33 and 35. In addition to the total-rock specimens, separated minerals such as potash feldspar, muscovite and biotite were analysed. The results are given in Appendix K (Table K1) and have been plotted in Figures 39 and 40. Regression analyses were carried out according to the procedure of McIntyre et al (1966). Details of the regression analyses are given in Table K2[28].

The total-rock specimens of the border facies megacrystic granite best fit a Model 3 isochron with an age of 537 ± 23m.y. and an initial Sr^{87}/Sr^{86} ratio of 0.7165 ± 0.0016. However, the total-rocks, potash feldspars and muscovite fit a Model 3 isochron with an age of 531 ± 11m.y. and an initial Sr^{87}/Sr^{86} ratio of 0.7169 ± 0.0009. The two regressions can not be separated within the analytical uncertainties,

---

[28]McIntyre et al Model 1 isochrons are characterised by a value for the Mean Square of Weighted Deviates (MSWD) which does not exceed unity. These isochrons indicate that all specimens had the same initial Sr^{87}/Sr^{86} ratio, and that all were effectively chemically closed to the diffusion of Rb and Sr at the time of crystallisation. The scatter of the points about Model 1 isochrons can be assigned to experimental error. Model 2 isochrons assume variations in the Rb^{87}/Sr^{86} ratio due to geochemical redistribution of Rb and Sr subsequent to crystallisation. A similar effect is obtained if specimens with the same initial Sr^{87}/Sr^{86} ratio have slightly different ages. Model 3 isochrons assume variations in the initial Sr^{87}/Sr^{86} ratio between the specimens.

In the regression analyses, the coefficient of variation for Rb^{87}/Sr^{86} ratios due to experimental error alone was taken as 0.5% for all specimens, and a uniform variance of 0.07×10^{-6} was assigned to Sr^{87}/Sr^{86} ratios. All errors quoted are at the 95% confidence level.

which indicates that the total-rock specimens and the minerals became closed systems to the diffusion of Rb and Sr at the time of crystallisation of the granite about 531m.y. ago. The Model 3 best fit of the isochrons suggests variations in the initial Sr^{87}/Sr^{86} ratios for each of the specimens. This is consistent with varying degrees of contamination of the total-rocks indicated by the total-rock chemical data.

The biotites separated from specimens 7-58 and 3-26 do not conform to the total-rock nor to the combined total-rock and mineral isochrons, but indicate significantly younger ages of 511m.y. and 504m.y. when regressed with their respective total-rocks. As the potash feldspars and the muscovite conform to the total-rock isochron, the variably low biotite ages are interpreted as the result of loss of radiogenic Sr.

Specimen 8-12 was collected from a boudinaged concordant megacrystic granite sheet within Petrel Cove Formation metasediments near their contact with the main mass of megacrystic granite on Wright Island (Figure 11). Near its borders, the granite sheet exhibits a well developed mica schistosity. The schistosity is a post-crystallisation feature, and is interpreted from structural evidence as S_1. Evidence for deformation subsequent to the formation of S_1 takes the form of a crenulation cleavage S_2, which overprints S_1 in the margins of the granite sheet and in the adjacent metasediments. The total-rock and the muscovite in 8-12 conform to the border facies megacrystic granite isochron. Therefore, the muscovite and the total-rock have remained closed systems to the diffusion of Rb and Sr since the granite crystallised. On the other hand, the biotite in 8-12 indicates an age of 397 ± 5m.y. when regressed with the total-rock (Figure 40). This age could reflect the loss of radiogenic Sr during the combined effects of the first and second phases of deformation, which were responsible for the development of the S_1 schistosity and S_2 crenulation cleavage in the metasediments and in the marginal granite phases. If this interpretation is correct, the second phase of deformation occurred more than 130m.y. after the crystallisation of the granite.

3.9.2 *Xenoliths within the border facies megacrystic granite*

Two specimens of metasedimentary rock xenoliths (3-10, 3-19) and two specimens of type A hybrid granite xenoliths (3-31, 3-38), all of which occur within the border facies megacrystic granite on Granite Island (Figure 21), were selected for Rb-Sr isotope dilution analysis. The metasedimentary rocks are laminated metasiltstones with well

preserved sedimentary structures including ripple-marks and small scale cross-laminations. They contain a poorly defined mica preferred orientation at a high angle to bedding. The occurrence of this preferred orientation has been taken as evidence for broad-scale folding and the incipient development of the S_1 schistosity in the Kanmantoo Group metasedimentary rocks prior to granite emplacement, since the xenoliths are lithologically similar to the contiguous metasedimentary rocks and are considered to have been derived from them. In order to obtain meaningful data for the metasedimentary rock xenoliths, Rb-Sr isotope dilution analysis of biotite separates and plagioclase concentrates from the two specimens were carried out. The isotope dilution results and the details of regression analyses are given in Tables K3 and K4.

The combined data for the metasedimentary rock xenoliths fit a Model 2 isochron with an age of 474 ± 15m.y. and an initial Sr^{87}/Sr^{86} ratio of 0.7234 ± 0.0008. However, the separate biotite - plagioclase regressions indicate slightly different ages of 479 ± 5m.y. (3-10) and 470 ± 5m.y. (3-19), which accounts for the Model 2 best fit of the combined data. The biotite age of the xenoliths is significantly lower than either the crystallisation age of the border facies megacrystic granite, or the ages obtained for biotites in the border facies megacrystic granite, and is believed to reflect loss of radiogenic Sr. Accordingly, the greater loss of radiogenic Sr from the xenolith biotites than the granite biotites may be a reflection of the very fine grain size of the xenolith biotites.

Potash feldspar separates and biotite+hornblende concentrates from the specimens of hybrid $granite_A$ xenoliths were analysed in addition to one total-rock sample (3-38). The results of isotope dilution analyses are given in Table K3, and the details of regression analyses in Table K4. The Rb-Sr data for each specimen are consistent, and when combined exhibit excess scatter about a Model 1 isochron with an age of 502 ± 6m.y. and an initial Sr^{87}/Sr^{86} ratio of 0.7150 ± 0.0007. However, the excess scatter can not be attributed either to redistribution of Rb and Sr, or to differences in the initial Sr^{87}/Sr^{86} ratios between the samples. The biotite+hornblende and plagioclase age for specimen 3-31 is 504 ± 5m.y. and the biotite and total-rock age for specimen 3-38 is 497 ± 5m.y. These ages are similar to the Rb-Sr ages of biotites in the border facies megacrystic granite. Comparison with the Rb-Sr total-rock

and total-rock - biotite data for the border facies megacrystic granite suggests that the hybrid granite biotite+hornblende concentrates have leaked radiogenic Sr, and that the age of crystallisation of the hybrid granite is older than that indicated by the biotite+hornblende data. If this interpretation is correct, then the initial Sr^{87}/Sr^{86} ratio at the time of crystallisation of the hybrid granite was about 0.7143.

3.9.3 *Kanmantoo Group metasedimentary rocks*

Dasch, Milnes and Nesbitt (1971) obtained an isochron age of 487 ± 60m.y. for eight specimens of Kanmantoo Group metasedimentary rocks collected at least 3km from the nearest granite outcrop. However, the data for these specimens showed a considerable degree of scatter about the isochron. Four of the metasedimentary rocks examined by Dasch, Milnes and Nesbitt were reanalysed using isotope dilution techniques in order to make a direct comparison between the age and Sr isotope composition of the Kanmantoo Group metasedimentary rocks and the xenoliths in the border facies megacrystic granite. It was hoped that such a comparison might provide clues to the nature and origin of the metasedimentary rock that contaminated the granite.

The Rb-Sr isotope dilution data and regression analyses for the Kanmantoo Group metasedimentary rocks are given in Table K5, and have been plotted in Figure 39. The four total-rock specimens of Kanmantoo Group metasediments exhibit excess scatter about a biotite - plagioclase isochron for the two specimens of metasedimentary rock xenoliths 3-10 and 3-19 (Figure 39). A Model 1 isochron fitted to the combined Rb-Sr data for the Kanmantoo Group metasediments and the metasedimentary rock xenoliths (MSWD=11.05) has an age of 474 ± 4m.y. and an initial Sr^{87}/Sr^{86} ratio of 0.7231 ± 0.0001, and is not significantly different from a Model 1 isochron fitted to the metasedimentary rock xenolith data alone. This suggests that the total-rock data for the Kanmantoo Group metasediments and the mineral data for the metasedimentary rock xenoliths record a metamorphic event which ended about 474m.y. ago. In fact, two nearly parallel lines are obtained on the isochron diagram (Figure 39) when the total-rock specimens are grouped in pairs. Specimens 0025 and 0029 fit an isochron with an age of 468 ± 40m.y. and an initial Sr^{87}/Sr^{86} ratio of 0.7242 ± 0.0020. Specimens 0014 and 0018 fit an isochron with an age of 460 ± 38m.y. and an initial ratio of 0.7224 ± 0.0014. Neither the ages nor the initial ratios for these two groups of specimens can be distinguished from the age and initial ratio for the metasedimentary

rock xenoliths within the analytical uncertainties. Therefore, the metasedimentary rock xenoliths are probably stoped fragments of Kanmantoo Group metasedimentary rocks as suspected from field, petrographic and mineralogical evidence. However, the Sr^{87}/Sr^{86} ratios for the Kanmantoo Group metasediments and the metasedimentary rock xenoliths at the time of crystallisation of the border facies megacrystic granite about 531m.y. ago (0.7181 to 0.7221) were significantly higher than the initial ratio for the granite (0.7165).

The specimens of hybrid $granite_A$ record a higher Rb-Sr age and a lower initial Sr^{87}/Sr^{86} ratio than the Kanmantoo Group metasedimentary rocks. As discussed above however, the biotite+hornblende concentrates from the hybrid granite indicate a lower age than the suspected crystallisation age, and so the biotite (and hornblende) may reflect the event that crystallised the Kanmantoo Group metasediments. The Sr^{87}/Sr^{86} ratio for the hybrid granite (about 0.7143) was significantly lower than the ratios for the Kanmantoo Group metasediments (between 0.7181 and 0.7221) at the time of crystallisation of the border facies megacrystic granite about 531m.y. ago. The difference in initial ratios may suggest that the hybrid granite is not related to the Kanmantoo Group metasediments. Nevertheless, the nature of the hybrid granite clearly indicates that it formed by assimilation of metasedimentary rock by granite magma. Therefore it is possible that the hybrid granite represents the final composition of unknown metasedimentary rocks, which had a Sr^{87}/Sr^{86} ratio less than that of the Kanmantoo Group metasediments, assimilated by granite magma with a low Sr^{87}/Sr^{86} ratio.

3.9.4 *Albitised border facies megacrystic granite*

Dasch, Milnes and Nesbitt (1971) reported Rb-Sr total-rock data for a specimen of albitised border facies megacrystic granite (7-55) and a specimen of megacrystic albite-chlorite rock (7-54). On the basis of the conformity of these data to the granite isochron, they suggested that both the "granite and the fluids responsible for late-stage albitisation had the same isotopic composition of strontium near the time of granite emplacement". In order to test this suggestion, further specimens of the albitised border facies megacrystic granite (7-53) and the megacrystic albite-chlorite rock (3-40), in addition to 7-55 and 7-54, were selected for Rb-Sr isotope dilution analysis during the present investigation. Biotite separates from 7-53 and 7-55, and chlorite, phlogopite and plagioclase separates and concentrates from

3-40 and 7-54 were analysed as well as the total-rocks. The results of the isotope dilution analyses are given in Table K6 and have been plotted in Figure 39. Details of the regression analyses are given in Table K7.

The total-rock data for 7-55 conform to the isochron for the border facies megacrystic granite. However, the biotite separated from 7-55 indicates an age of 510 ± 5m.y. when regressed with the total-rock. This age is similar to the ages obtained for biotites in the unaltered border facies megacrystic granite. Therefore the albitisation does not appear to have affected the Sr composition of the rock or the biotite. The total-rock data for 7-53 do not conform to the isochron for the border facies megacrystic granite, but indicate a lower Sr^{87}/Sr^{86} ratio. When regressed with the total-rock, the biotite separated from 7-53 gives an age of 494 ± 5m.y., which is lower than the biotite ages obtained for the unaltered border facies megacrystic granite. The chemical composition of the biotite in 7-53 is significantly different from the composition of biotites in the unaltered granite as the result of albitisation (see page 102). Hence the lower age is best interpreted as the result of loss of radiogenic Sr due to the chemical alteration.

The combined total-rock and mineral data for the two specimens of megacrystic albite-chlorite rock fit a Model 2 isochron with an age of 417 ± 82m.y. and an initial Sr^{87}/Sr^{86} ratio of 0.7151 ± 0.0005. However, regression of the phlogopite concentrates from each of the specimens with the respective total-rocks indicates ages of 474 ± 11m.y. (7-54) and 485 ± 6m.y. (3-40) with a common initial Sr^{87}/Sr^{86} ratio of about 0.714. On the other hand, regression of the chlorite separated from 7-54 with the total-rock and plagioclase data for both 7-54 and 3-40 indicates a significantly lower age of 306 ± 33m.y. (Model 1 fit).

The megacrystic albite-chlorite rock is the end-product of albitisation of the border facies megacrystic granite, and is composed predominantly of albite with chlorite, phlogopite and minor quartz. As described on pages 91 and 101, the phlogopite and chlorite were formed by progressive alteration of pre-existing biotite. Phlogopite clearly controls the age of the total-rock and mineral assemblages because of its high Rb^{87}/Sr^{86} ratio, but it must be regarded as a relict mineral. The fact that phlogopite - total-rock ages for the megacrystic albite-chlorite rock are significantly lower than the biotite - total-rock ages

for the border facies megacrystic granite indicates that loss of radiogenic Sr occurred during alteration of the original biotite. Further loss of radiogenic Sr consequent upon alteration of the phlogopite to chlorite is indicated by the 306m.y. age for the Model 1 regression of the chlorite, total-rock and plagioclase data for both specimens of the megacrystic albite-chlorite rock. The initial ratio for this regression (0.7154 ± 0.0005) is significantly lower than the initial ratio for the border facies megacrystic granite (0.7169 ± 0.0009).

3.9.5 *Uncontaminated granites*

Field, petrographic and petrochemical evidence indicates that several varieties of the Encounter Bay Granites have not been contaminated by metasedimentary rock. Specimens of these granite varieties, including a medium even-grained granite (4-10) which approximates the composition of the parent magma on the basis of total-rock chemical data (see page 115) the red leucogranite (4-9, 4-89), the fine grained miarolitic granophyre (4-66B) and an aplite (4-65) were selected for isotope dilution analysis on the basis of their Rb and Sr concentrations determined by routine X-ray fluorescence. Isotope dilution data for the total-rocks and several mineral separates are given in Table K8, and have been plotted on Figure 41. Details of the regression analyses are given in Table K9.

Rb-Sr data for the total-rocks fit a Model 2 isochron with an age of 522 ± 28m.y. and an initial Sr^{87}/Sr^{86} ratio of 0.7111 ± 0.0113. However, the combined data for total-rocks, feldspar concentrates and muscovite fit a Model 3 isochron with an age of 523 ± 6m.y. and an initial Sr^{87}/Sr^{86} ratio of 0.7115 ± 0.0057. The two regressions are not significantly different, which indicates that the total-rocks and the minerals became closed systems to the diffusion of Rb and Sr at the time of crystallisation of the granites about 523m.y. ago. Moreover, this age can not be distinguished from the age indicated for the crystallisation of the border facies megacrystic granite, about 531m.y. ago, within the analytical uncertainties. Similarly, the initial Sr^{87}/Sr^{86} ratio for the uncontaminated granites (0.7115 ± 0.0057) is not statistically different from the initial ratio for the border facies megacrystic granite (0.7169 ± 0.0009), although the disposition of the uncontaminated granites and their minerals on the isochron diagram (Figure 41) suggests that the initial ratios may be different. The geological evidence, on which basis the uncontaminated granites were selected for

study, is also consistent with this interpretation.

The large uncertainty in estimation of the initial ratio for the uncontaminated granites is due to the lack of control over the position of the total-rock and combined total-rock and mineral isochrons at low Rb^{87}/Sr^{86} values. Rb-Sr data for plagioclase is clearly required in order to realistically test the significance of the difference between the initial ratios of the uncontaminated granites and the border facies megacrystic granite.

The biotite separated from 4-10 does not conform to the uncontaminated granite isochron, but indicates a significantly younger age of 484 ± 4m.y. when regressed with the total-rock. As the potash feldspar in this rock falls on the uncontaminated granite isochron, the low biotite age must be regarded as the result of loss of radiogenic Sr.

A specimen of albitised red leucogranite (4-8) does not fit the uncontaminated granite isochron, but has a higher Sr^{87}/Sr^{86} ratio. Together with the albitised border facies megacrystic granite 7-53, 4-8 best fits the Rb-Sr data for the megacrystic albite-chlorite rock. This is taken as evidence that the material responsible for albitisation may have had a Sr isotope composition that was different from that of the contaminated and the uncontaminated granites, although the analytical uncertainties are presently too great to place significance upon these differences.

3.9.6 *Granitic rocks from Kangaroo Island*

Very coarse grained feldspar-quartz-muscovite-tourmaline-spessartite-beryl pegmatites occur within Kanmantoo Group metasediments at Vivonne Bay and in an area 12km south-east of Penneshaw on Kangaroo Island (Figure 8). Along the coastline north-west of Antechamber Bay, these pegmatites occur as concordant sheets within Tapanappa Formation metasediments. Rb-Sr isotope dilution analyses of total-rock specimens of the pegmatites and their constituent muscovite indicate ages of 519 ± 6m.y. (Vivonne Bay - V4) and 539 ± 7m.y. (south-east of Penneshaw - P1), as shown in Table K10. These ages are of the same order as the age of crystallisation of the Encounter Bay Granites between 523m.y. and 531m.y., and are likewise regarded as crystallisation ages of the pegmatites. The initial Sr^{87}/Sr^{86} ratios for the pegmatites are 0.7184 ± 0.0018 (V4) and 0.7014 ± 0.0124 (P1).

Rb-Sr isotope dilution analyses of a total-rock specimen of the Cape Kersaint granite and its constituent biotite indicate an age of 493

± 5m.y. and an initial Sr^{87}/Sr^{86} ratio of 0.7184 ± 0.0009 (Table K10). This is directly comparable with biotite - total-rock data for the border facies megacrystic granite in the Encounter Bay area, and points to an older total-rock age representing the age of crystallisation.

3.9.7 *K-Ar data for the Encounter Bay Granites*

K-Ar analyses of micas in the Encounter Bay Granites are given in Appendix K in the appropriate tables. K-Ar analyses of biotites separated from ten specimens of the border facies megacrystic granite from the Encounter Bay area and Cape Willoughby indicate an average age of 471m.y., with eight ages occurring in the range 472m.y. to 475m.y. Similar ages were obtained for muscovite separated from the Kangaroo Island pegmatite V4 (485m.y.) and from the miarolitic granophyre 4-66B (473m.y.), and for biotite separated from two specimens of hybrid $granite_A$ xenoliths in the border facies megacrystic granite (3-41, 478m.y.; 3-38, 466m.y.). In all cases, the K-Ar ages are significantly lower than the Rb-Sr ages for the same minerals. For example, biotite separated from the border facies megacrystic granite 3-26 has a K-Ar age of 467m.y. but a Rb-Sr age of 511m.y.; muscovite separated from the miarolitic granophyre has a K-Ar age of 473m.y. but a Rb-Sr age of 523m.y.; and muscovite separated from the pegmatite V4 has a K-Ar age of 485m.y. but a Rb-Sr age of 519m.y. On the other hand, K-Ar ages for biotites separated from the schistose granites 8-12 (417m.y.) and 8-18 (420m.y.) are comparable with the Rb-Sr age for the biotite in 8-12 (397m.y.).

Rb-Sr data for the country rock Kanmantoo Group metasediments and for metasedimentary rock xenoliths within the border facies megacrystic granite indicate an age of 474m.y. (Table K5). This age is considered to mark the end of a metamorphic event in the Encounter Bay area, and is comparable with the metamorphic age of 465m.y. obtained by Compston, Crawford and Bofinger (1966) for metasedimentary rocks elsewhere in the Mount Lofty Ranges. K-Ar ages of micas in the Encounter Bay Granites and in one specimen of the Kangaroo Island pegmatites are consistent with this metamorphic age, and may therefore reflect loss of radiogenic Ar during the metamorphism. On the other hand, biotites (but not muscovites) in the granites and the pegmatites record a small but variable loss of radiogenic Sr which may also be attributed to the metamorphism. In fact, Rb-Sr ages for biotites in the granites range from 511m.y. down to 482m.y. The retention of radiogenic Sr relative to radiogenic Ar in biotites, and the resistance of muscovite to loss of

radiogenic Sr during metamorphism is well documented (see for example Kulp, 1963; Hart, 1964; Moorbath, 1967). According to the K-Ar and Rb-Sr data for the Encounter Bay Granites and associated rocks, loss of radiogenic Sr from the biotites may have ended as early as 511m.y. and as late as 482m.y., whereas loss of radiogenic Ar from both biotite and muscovite could have ceased on the average about 471m.y. ago at the end of the metamorphism indicated by Rb-Sr data for the metasedimentary rocks.

An alternative explanation of the K-Ar data is required if a maximum of 5% of the measured ages is allowed for the possible uncertainty in the K decay constant (Aldrich and Wetherill, 1958). For example, a K-Ar age of 471m.y. might be increased to 495m.y. Under these circumstances, the K-Ar ages of micas in the border facies megacrystic granite and the Kangaroo Island pegmatite V4 more closely approach the Rb-Sr mica ages, although significant discrepancies appear between the K-Ar and Rb-Sr biotite ages in the schistose granites. This explanation requires that the loss of radiogenic Ar from the micas in the granites ended about 494m.y. ago, at approximately the same time as radiogenic Sr ceased to leak from the biotites. If this is correct, the metamorphic event indicated by Rb-Sr data for the metasedimentary rocks ended about 20m.y. after the micas became closed to leakage of radiogenic Ar.

The two models used to explain the K-Ar data in relation to the Rb-Sr data are equally valid. However, an explanation of the K-Ar data for the Encounter Bay Granites based on the former model is preferred and will be developed in the following paragraphs, firstly because it considers K-Ar ages that have been calculated from the K decay constant used by Dr. A.W. Webb in dating South Australian rocks, and secondly because the K-Ar ages so calculated agree closely with the Rb-Sr age for the end of the metamorphism in the Encounter Bay area.

3.9.8 *Discussion*

Rb-Sr isotope dilution analyses of several varieties of the Encounter Bay Granites and their constituent minerals indicate that the contaminated border facies megacrystic granite and the uncontaminated granites crystallised at about the same time between 523m.y. and 531m.y. ago in the Encounter Bay area. A similar age is given by regressions of Rb-Sr data for total-rock pegmatites and their constituent muscovites from Kangaroo Island. On the basis of field and petrographic evidence,

the border facies megacrystic granite appears to have been emplaced as a crystal-rich liquid which then crystallised fairly rapidly. Under these circumstances, the crystallisation age will approximate the age of emplacement of the border facies megacrystic granite. In view of the clear evidence for contamination of the border facies megacrystic granite by metasedimentary rock, there is a distinct possibility that the border facies megacrystic granite isochron represents a mixing line. However, the concordance in age between the uncontaminated granites and the border facies megacrystic granite indicates either that significant mixing of metasedimentary rock with granite magma did not occur, that the granite magma and the metasedimentary rock contaminant had a similar Sr isotope composition at the time of mixing, or that isotopic redistribution was completely effective. Alternatively, the analytical uncertainties may be so large that the effect of mixing has been obscured. The first possibility, that significant mixing did not occur, can be ruled out on the basis of total-rock chemical evidence. Similarly, complete isotopic redistribution can be discounted because of the disequilibrium between initial Sr^{87}/Sr^{86} ratios for the border facies megacrystic granite (0.7165) and the Sr^{87}/Sr^{86} ratios for the metasedimentary rock xenoliths (0.7181 to 0.7221), and the hybrid granite$_A$ xenoliths (about 0.7143) at the time of granite emplacement. The second and fourth possibilities are interdependent to a large degree. For example, the disposition of the data for the uncontaminated granites and the border facies megacrystic granite on the isochron diagram suggests that the uncontaminated granites have a much lower initial Sr^{87}/Sr^{86} ratio than the border facies megacrystic granite. As the chemical evidence suggests that the medium grained granite 4-10 approximates the composition of the parent magma of the Encounter Bay Granites, the uncontaminated granites (which include 4-10) are expected to reflect the initial Sr^{87}/Sr^{86} ratio of the magma parent. However, the uncertainties in the data indicate that the apparent differences between the initial Sr^{87}/Sr^{86} ratios for the uncontaminated granite and the border facies megacrystic granite are not significant. Clearly, Rb-Sr isotope dilution analyses of plagioclase concentrates are required to elucidate this problem.

The 487 ± 37m.y. age reported by Dasch, Milnes and Nesbitt (1971) for the emplacement of the Encounter Bay Granites was obtained from an attempt to fit a single Rb-Sr isochron to specimens of the border facies

megacrystic granite, the uncontaminated granites and the albitised granites. In fact, the regression was controlled to a large degree by the medium even-grained granite 4-10 and the megacrystic albite-chlorite rock 7-54. In view of the present data, both the 487 ± 37m.y. age and the initial Sr^{87}/Sr^{86} ratio (0.719) obtained for the regression have no meaning.

Rb-Sr data for the Kanmantoo Group metasedimentary rocks in the Encounter Bay area and for the metasedimentary rock xenoliths in the border facies megacrystic granite record a metamorphic event which ended about 474m.y. ago. This event may account for the variable loss of radiogenic Sr from biotites in the granites, although feldspars amd muscovite were not similarly affected. K-Ar analyses of biotites and muscovites in the granites consistently indicate an age of about 471m.y. The same age is given by K-Ar analyses of biotites in the Cape Willoughby megacrystic granite, and of muscovite from the Vivonne Bay pegmatite.

The relationships between structural and metamorphic events in the Kanmantoo Group metasediments and the emplacement of the Encounter Bay Granites are illustrated diagrammatically in Figure 17, and have been discussed in an earlier section (see page 45). The emplacement of the granites was followed by the main phase of first generation deformation at temperatures and pressures conducive to the crystallisation of andalusite. Similar metamorphic conditions persisted into the static phase post-dating the first phase of deformation, but the absence of major metamorphic crystallisation during the second phase of deformation suggests that the metamorphic grade had fallen significantly by this time. This model can therefore provide a basis for interpretation of the Rb-Sr and K-Ar data for the Encounter Bay Granites and the Kanmantoo Group metasediments. For example, the Encounter Bay Granites were emplaced between 523m.y. and 531m.y. ago, at which time the total-rocks, feldspars and muscovite became closed systems to the diffusion of Rb and Sr. Biotite probably crystallised at this time as well. However, the persistence of andalusite grade temperatures and pressures for a significant time after granite emplacement seems to have facilitated the leakage of radiogenic Sr from biotite (but not from potash feldspar or muscovite) in the granites, the loss of radiogenic Ar from biotite and muscovite in the granites and pegmatites until about 470m.y. ago, and the diffusion of Rb and Sr in the Kanmantoo Group metasediments and in the meta-

sedimentary rock xenoliths within the granites until about 474m.y. ago. Therefore the 471m.y. K-Ar mica age can be regarded as the end of the andalusite grade metamorphism in the area studied, rather than a discrete metamorphic event. If this interpretation is correct, then the andalusite grade metamorphism persisted for at least 50m.y. after emplacement of the Encounter Bay Granites.

Consistently younger Rb-Sr and K-Ar ages of between 398m.y. and 420m.y. were obtained for biotites in specimens of the schistose granites (8-12 and 8-18) that occur at the contact between the border facies megacrystic granite and the Kanmantoo Group metasedimentary rocks on Wright Island. The S_1 schistosity in these granites has been overprinted by an S_2 crenulation cleavage. Therefore the low age may reflect the combined loss of both radiogenic Sr and Ar due to both deformation phases. In contrast to the biotite, both the muscovite and the total-rock Rb-Sr data for 8-12 conform to the border facies megacrystic granite isochron. The 398m.y. to 420m.y. biotite age for the schistose granites may represent the age of the second phase of deformation in the Encounter Bay area. However, this suggestion requires that the second phase of deformation post-dates the first phase of deformation by more than 60m.y. A further study of these rocks is needed in order to ascertain the significance of the ages so far obtained.

The interpolated Sr^{87}/Sr^{86} ratios for the Kanmantoo Group metasedimentary rocks at the time of emplacement of the border facies megacrystic granite (0.7181 to 0.7221) are higher than the initial ratio for the granite (0.7165). It is therefore conceivable that the border facies megacrystic granite was derived by the contamination of a magma of low initial Sr^{87}/Sr^{86} ratio with Kanmantoo Group metasediments. This hypothesis is supported by the abundance of metasedimentary rock xenoliths in the border facies megacrystic granite. Hybrid $granite_A$ is considered to be partly assimilated metasedimentary rock of similar chemical composition to the Kanmantoo Group metasediments (see page 114) but had a Sr^{87}/Sr^{86} ratio at the time of emplacement of the border facies megacrystic granite of 0.7143. This is lower than the initial ratio for the granite, and is very much lower than the interpolated ratios for the Kanmantoo Group metasediments, and suggests that the hybrid granite does not represent partly assimilated Kanmantoo Group metasedimentary rock. In fact, the field evidence suggests that the hybrid granite parent material was incorporated into the magma parent of the Encounter

Bay Granites at an early stage in its crystallisation history, prior to emplacement into the Kanmantoo Group metasediments. Therefore it is likely that the border facies megacrystic granite experienced a complex contamination history involving Kanmantoo Group metasedimentary rocks at the present level of exposure, and metasedimentary rocks of unknown origin but of similar composition from deeper levels in the crust, perhaps nearer the site of magma generation.

The Rb-Sr data for the albitised granites and the megacrystic albite-chlorite rocks can not be interpreted unambiguously. For example, biotite - total-rock ages for two specimens of the albitised border facies megacrystic granite (7-53, 7-55) agree closely with similar ages for the unaltered megacrystic granite. Phlogopite - total-rock ages for two specimens of the megacrystic albite-chlorite rock (3-40, 7-54) are 485m.y. and 474m.y. respectively, and approach the K-Ar mica age for the granites. However, the combined total-rock, chlorite and plagioclase age for 7-54 is very much lower at 306m.y. This progressive lowering of the age from that registered by the biotites in the unaltered granites to that given by the chlorite in 7-54 can be explained by progressive loss of radiogenic Sr during the observed alteration of biotite to phlogopite and then chlorite. Under these circumstances, it is difficult to assign any significance to the ages.

3.10 *THE AGE AND Sr COMPOSITION OF OTHER PALAEOZOIC GRANITES AND ASSOCIATED ROCKS IN SOUTH-EASTERN SOUTH AUSTRALIA*

Compston, Crawford and Bofinger (1966) presented Rb-Sr data for Precambrian and Palaeozoic rocks in South Australia in an attempt to assess the duration of sedimentation in the "Adelaide Geosyncline". As part of their investigation, they reported Rb-Sr ages of metasedimentary rocks from the northern Mount Lofty Ranges as well as the ages of the Anabama Granite and of a microtonalite from Netley Hill (Figure 2). On the basis of the metasedimentary rock data, they suggested that the metamorphism in the Mount Lofty Ranges ended about 465m.y. ago. This age is not significantly different from the total-rock Rb-Sr ages obtained for Kanmantoo Group metasedimentary rocks in the Encounter Bay area, or from the K-Ar ages of micas in the Encounter Bay Granites and the Kangaroo Island pegmatites.

The combined total-rock and mineral Rb-Sr data obtained by Compston, Crawford and Bofinger (1966) for the Anabama Granite indicate a crystallisation age of 473 ± 10m.y. and an initial Sr^{87}/Sr^{86} ratio

of 0.7050 ± 0.0035 (Table K11). The crystallisation age is not significantly different from the age at which the regional metamorphism in the Mount Lofty Ranges ended. However, the combined total-rock and mineral data reported by Compston, Crawford and Bofinger for the Netley Hill microtonalite defines a crystallisation age of 436 ± 32m.y. and an initial Sr^{87}/Sr^{86} ratio of 0.7152 ± 0.0025 (Table K11). K-Ar ages of biotite and hornblende separated from the microtonalite support this lower age (Compston, Crawford and Bofinger, 1966).

White, Compston and Kleeman (1967) reported a combined total-rock, feldspar and biotite Rb-Sr age for the Palmer Granite (Figure 2) of 489 ± 15m.y. with a corresponding initial Sr^{87}/Sr^{86} ratio of 0.7086 ± 0.0010. However, a reappraisal of their data (Tables K12 and K13) in the light of experience with leakage of radiogenic Sr from biotites in the Encounter Bay Granites indicates that total-rock specimens of the Palmer Granite may have become closed systems to the diffusion of Rb and Sr as early as 512m.y. ago. As shown in Table K13 for example, the total-rocks GA-315, P5, P7 and P2 show excess scatter about a Model 1 isochron (MSWD=17.11) with an age of 514 ± 33m.y. and an initial Sr^{87}/Sr^{86} ratio of 0.7071 ± 0.0028. By excluding P5 from the regression, the remaining total-rocks closely approximate a Model 1 isochron (MSWD=3.34) with an age of 512 ± 33m.y. and an initial ratio of 0.7068 ± 0.0083. On the other hand, regression of the total-rock and feldspar data for GA-315 indicates a Model 1 isochron age of 485 ± 30m.y. and an initial ratio of 0.7090 ± 0.0025. Similarly, regression of the biotites and feldspars with their respective total-rocks indicates low ages. For example, biotite - total-rock regressions give ages of 458m.y. (GA-315 green biotite), 483m.y. (P5) and 400m.y. (GA-315 brown biotite). The low biotite and feldspar ages point to leakage of radiogenic Sr. On this basis, the 489 ± 15m.y. age estimated by White, Compston and Kleeman for the Palmer Granite is invalid because it is essentially an average of the total-rock age (512m.y.) and the P5 biotite age (483m.y.).

White, Compston and Kleeman (1967) also reported Rb-Sr data for two specimens of the Rathjen Gneiss (Figure 2; Table K12). The two-point isochron defined by these specimens indicates an age of 537 ± 25m.y. and an initial Sr^{87}/Sr^{86} ratio of 0.7133. Although it is unwise to place any significance on these data alone, it is of interest that the apparent age at which the total-rock specimens of Rathjen Gneiss closed to the diffusion of Rb and Sr agrees closely with the age of

crystallisation of the Encounter Bay Granites and the Kangaroo Island pegmatites, and is of the same order as the postulated crystallisation age of the Palmer Granite.

A Rb-Sr biotite - total-rock age of 503 ± 5m.y. and an initial Sr^{87}/Sr^{86} ratio of 0.7066 has been obtained for the Black Hill Norite, which crops out from beneath a cover of Tertiary sediments north of Mannum (Figure 2; Table K14). However, K-Ar analysis of the biotite indicates an age of 486m.y. In keeping with the observed Rb-Sr and K-Ar data for biotites in the Encounter Bay Granites and in the Palmer Granite, it is expected that the biotite in the Black Hill Norite may have registered a loss of radiogenic Sr. Under these circumstances, the crystallisation age of the norite is conceivably of the same order as the crystallisation ages of the Encounter Bay Granites and the Kangaroo Island pegmatites.

Thus the available Rb-Sr data point to a significantly older crystallisation age (between 512m.y. and 537m.y.) for the Palmer Granite and the Rathjen Gneiss than has been previously interpreted from radiometric data or suspected from field studies, although the Anabama Granite and the Netley Hill microtonalite crystallised as late as 473m.y. and 436m.y. respectively. On the other hand, K-Ar analyses of micas in the granites (and in the Black Hill Norite) and Rb-Sr analyses of metasedimentary rocks indicate that the regional metamorphism, which may be held responsible for the loss of radiogenic Sr from the biotites and feldspars in the Palmer Granite, ended in the northern Mount Lofty Ranges 465m.y. ago. Thomson (1970, 1971, 1972) has reported similar K-Ar ages for micas from many rock-types throughout the Mount Lofty Ranges. These data compare very well with the data obtained for the Encounter Bay Granites and associated rocks in the Encounter Bay area and at Cape Willoughby.

3.11 *THE ORIGIN OF THE ENCOUNTER BAY GRANITES*

On the basis of Rb-Sr data, there are three likely mechanisms for the origin of granites.

a. Liquids of granitic composition may be derived by fractional crystallisation of magmas of basic or intermediate composition generated by partial melting of mantle material.

b. Granitic liquids may be derived as in (a), but become contaminated with radiogenic Sr by assimilation of crustal rocks.

c. Granitic liquids may be derived by partial melting of crustal rocks.

The granites resulting from each of these simple models may be partly distinguished on the basis of their initial Sr^{87}/Sr^{86} ratios. For example, model (a) granites would have a low initial ratio within the range exhibited by oceanic basalts (Hurley et al, 1962; Faure and Hurley, 1963; Faure and Powell, 1972), whereas models (b) and (c) granites would have significantly higher initial ratios. However, models (b) and (c) can not be distinguished on the basis of their initial ratios.

The initial Sr^{87}/Sr^{86} ratio for the uncontaminated varieties of the Encounter Bay Granites is 0.711, and is the lowest initial ratio of varieties of the Encounter Bay Granites so far examined. As discussed in earlier sections, the initial ratio for the uncontaminated granites may be a close approximation to the Sr^{87}/Sr^{86} ratio for the parent magma. This ratio is significantly higher than the Sr^{87}/Sr^{86} ratios for oceanic basalts of mantle origin (0.701 to 0.705 at the time of granite emplacement) interpolated from the data of Faure and Powell (1972), suggesting that the uncontaminated granites (and, by inference, the parent magma of the Encounter Bay Granites) were contaminated with crustal Sr and may have originated according to one or other of models (b) and (c). A model (b) origin requires that the parent magma was homogeneously contaminated with crustal Sr prior to crystallisation and emplacement into the Kanmantoo Group metasedimentary rocks. A model (c) origin requires that the parent magma was derived by partial melting of crustal rocks that had a Sr^{87}/Sr^{86} ratio of about 0.711. Kanmantoo Group metasediments adjacent to the granites had Sr^{87}/Sr^{86} ratios of 0.718 to 0.722 at the time of emplacement of the granites and therefore can not represent the crustal rocks from which the parent magma may have been derived. However, metasediments with the appropriate initial ratio of about 0.711 may occur at depth.

The Encounter Bay Granites plot close to the cotectic line in the Q-An-Ab-Or-H_2O system (Figure 37), and thus approach the composition of either the first liquid produced by partial melting of crustal rocks, or the final product of fractionation of a magma of basic or intermediate composition. However, granite varieties having a composition close to that assumed for the parent magma plot in the potash feldspar field of the Q-An-Ab-Or-H_2O system and could not have been derived by fractionation of a magma of basic or intermediate composition (Barth,

1966; James and Hamilton, 1969) unless assimilation of potash-rich material occurred after fractionation.

If the parent magma was derived by partial melting of crustal rocks (model c), there are two limiting cases to be considered, corresponding to the partial melting of the type IV or the types II and III subsolidus assemblages of Robertson and Wyllie (1971). In the first case, the parent magma may have been produced by partial melting of crustal rocks containing excess water (type IV subsolidus assemblage). Under these circumstances, granitic liquids may be produced at temperatures as low as 630°C at a depth of 35km (10kb pressure) and will be water-saturated (Luth, Jahns and Tuttle, 1964; Kleeman, 1965; Boetcher and Wyllie, 1968). As discussed by Tuttle and Bowen (1958) and Luth (1969), a water-saturated magma can only move upwards in the crust to a lower pressure regime if sufficient amounts of superheat are postulated. Otherwise the liquid would be expected to crystallise rapidly upon rising from the site of generation due to the negative P-T slope of the solidus curve in water-saturated granite systems.

It is generally accepted however, that there is insufficient free water (greater than 1-2%) in crustal rocks in an anatectic environment to saturate a large body of granitic liquid (Tuttle and Bowen, 1958; Luth, 1969; Robertson and Wyllie, 1971; Wyllie, 1971), although there may be sufficient free water in type III subsolidus assemblages to saturate the first liquid produced upon partial melting. Alternatively, the only water available during anatexis may be derived from the breakdown of hydrous minerals, as in the case of type II subsolidus assemblages (Brown and Fyfe, 1970; Brown, 1973). Thus the second case to be considered involves water-deficient granite magmas. Brown (1973) suggested these might be generated by partial melting of type II subsolidus assemblages at depths between 25km and 30km at temperatures between 700°C and 750°C, assuming normal geothermal gradients of 20-30°C km^{-1}. Water-deficient granite liquids may be derived from type III subsolidus assemblages at similar temperatures and depths in the crust. If a reasonable amount of granite liquid was generated, it might be sufficiently mobile to migrate away from the unmelted residue. In rising upwards to lower pressure regimes, the melting point of water-deficient granitic liquids decreases until they reach a critical pressure at which the water-saturation boundary is crossed. Thereafter, the melting point of the liquid increases with decreasing pressure. If the liquid

migrated rapidly upwards from the site of generation without significant loss of heat to the surrounding rocks, the critical pressure may be reached prior to crystallisation, in which case the liquid will crystallise entirely in a water-saturated condition. On the other hand, if the upward migration was so slow that heat loss from the liquid to the surrounding rocks was able to cool the liquid sufficiently to commence crystallisation prior to reaching the critical pressure, only the final stages of crystallisation may occur under conditions of water-saturation. In either case, water-deficient magmas are potentially able to closely approach the earth's surface. Moreover, the magmas are capable of assimilating varying amounts of the rocks with which they come into contact.

If the parent magma of the Encounter Bay Granites was derived by contamination of the product of fractional crystallisation of mantle-generated magma of basic or intermediate composition (model b), it is likely to have been water-deficient, and as discussed above, could have closely approached the earth's surface prior to complete crystallisation.

The Encounter Bay Granites contained a vapour phase (and were therefore probably water-saturated) at least during the later stages of their crystallisation history. This is demonstrated by the occurrence of miarolitic cavities and abundant pod-like tourmaline-rich pegmatites in many granite varieties. Furthermore, granophyric textures and the presence of a fine grained groundmass in the border facies megacrystic granite are regarded as the result of relatively rapid crystallisation of a crystal-rich magma upon emplacement, possibly due to loss of volatiles from the margins of the intrusion. The absence of pegmatite pods or miarolitic cavities in the border facies megacrystic granite supports this suggestion. Unfortunately, none of these features indicate what proportion of the crystallisation history took place in the presence of a vapour phase.

Metamorphic assemblages containing andalusite and cordierite occur in the Kanmantoo Group metasediments adjacent to the Encounter Bay Granites in the Encounter Bay area, and as described in earlier sections (for example on pages 48 and 49), crystallised during and after the emplacement of the granites. Based on the experimental alumino-silicate equilibria and a likely paragenesis for cordierite (page 51; Figure 18), the depth of emplacement of the granites was not greater than about 14km (4kb pressure), and may have been less than 10km (3kb pressure).

The granites are out of equilibrium with their environment in terms of mineralogy and Sr isotope composition, and were clearly not formed in situ. Therefore an estimate of their depth of origin must be based on one of the following three models.

1. The parent magma may have been water-saturated, and in this case could not have been generated by partial melting of crustal rocks more than a few kilometres away from the site of emplacement for the reasons discussed above. Thus a very high geothermal gradient would be required to obtain the temperatures necessary for melting at these comparatively shallow depths. A geothermal high is indicated by the metamorphic assemblages in Kanmantoo Group metasediments adjacent to the granites. However, the metamorphism largely postdated the emplacement of the granites and therefore the geothermal high was probably not responsible for their origin.
2. The parent magma may have been derived by partial melting of water-deficient rocks at depths between 25km and 35km assuming a normal geothermal gradient of 20-30^{o}C km^{-1}. Alternatively, partial melting could occur at shallower depths with higher geothermal gradients. In either case, the magma would have been water-deficient, and may have migrated some distance to the present site of emplacement.
3. The parent magma may have been derived by crustal contamination of the product of fractional crystallisation of magma of basic or intermediate composition. The granite magma in this case would also be water-deficient, and could have migrated some distance upwards to the present site of emplacement.

It is concluded that either of models (2) or (3) provides the most likely explanation for the origin of the parent magma of the Encounter Bay Granites. Although these possibilities can not be distinguished on the basis of the available evidence, a model (2) origin is presently favoured.

SECTION 4

DISCUSSION AND CONCLUSIONS

As deduced from structural observations at the contact between the Encounter Bay Granites and the Kanmantoo Group metasedimentary rocks in the Encounter Bay area, the granites were emplaced and had crystallised prior to the onset of penetrative structural deformation of the metasedimentary rocks. Parts of the marginal phase of the granites were subsequently deformed during the two generations of folding recognised in the area, although the pluton as a whole seems to have acted as a rigid body and resisted deformation.

Observations of the structural and metamorphic fabric of the Kanmantoo Group metasedimentary rocks indicates that conditions conducive to the crystallisation of cordierite and andalusite commenced at about the time of emplacement of the Encounter Bay Granites, but continued for a significant time after the granites had crystallised. On the basis of Rb-Sr data, metamorphism of diminishing intensity appears to have continued for more than 50m.y. after emplacement of the granites.

The apparent absence of a conspicuous contact aureole adjacent to the granites is probably due to the unsuitable chemical composition of the metasedimentary rocks. In fact, Kanmantoo Group metasediments are generally of inappropriate chemical composition to develop minerals that are conspicuous indicators of metamorphic grade, and for this reason cordierite, andalusite, garnet and calc-silicate minerals occur only sparsely in these rocks. It is therefore difficult to test for a causative relationship between the emplacement of the Encounter Bay Granites and the metamorphism. However, the fact that cordierite is restricted to some pelites near the granite outcrops at Rosetta Head (Figure 7) and is pre- to syn-F_1 in age suggests that cordierite may have crystallised in metasediments of appropriate composition in the thermal aureole of the granites. On the other hand, the crystallisation of andalusite, garnet, and calc-silicate minerals occurred on a regional scale and largely post-dated the crystallisation of cordierite. These minerals are believed to have crystallised in response to a regional geothermal high which can not be directly related to the Encounter Bay Granites.

The origin of the regional geothermal high that accompanied the emplacement of the Encounter Bay Granites is not clear. It is unlikely

to have been responsible for the origin of the granites, and is equally unlikely to have been produced solely by the granites, since these are usually regarded as only local sources of thermal energy when emplaced at high levels in the crust. However, the presence of basic magmas at depth is a possible source of the geothermal high and may also have provided the high temperatures necessary for partial melting of crustal rocks to produce granite magmas. The Black Hill Norite, which crops out to the north of Mannum (Figure 2) and is about the same age as the Encounter Bay Granites on the basis of Rb-Sr data, demonstrates the presence of basic magmas within the metamorphic belt. Regional metamorphic minerals that pre-date the emplacement of the granites have not been recognised in the area investigated and therefore normal crustal temperatures probably existed at this time.

It is difficult to visualize the form of the original intrusion of Encounter Bay Granites because of poor exposure. However, the outcrops at Cape Willoughby and in the Encounter Bay area appear to be remnants of the north-western wall of an intrusion that may have extended south-eastwards beneath the present ocean (Figure 2). In all exposures of the contact between the granites and the Kanmantoo Group, the granites overlie the metasedimentary rocks at an angle between 45^{o} and 60^{o}, and are broadly concordant with bedding in the metasedimentary rocks. As discussed in an early section of the thesis, bedding planes seem to have been preferentially available as planes of weakness at this time, and may have controlled the emplacement of the Encounter Bay Granites as a whole. Under these circumstances, the pluton may be broadly sheet-like in form. The dominance of bedding as the structural inhomogeneity in Kanmantoo Group metasediments was lost after the emplacement of the granites and the F_1 phase of folding, presumably because of the combined effects of regional metamorphism and penetrative structural deformation. For example, post-F_1 basic dykes and pegmatites are always discordant.

An anatectic origin is presently favoured for the Encounter Bay Granites. The parent magma could well have been generated by partial melting of water-deficient crustal rocks at depths of less than 35km, assuming normal geothermal gradients (Brown and Fyfe, 1970; Brown, 1973). Alternatively, partial melting of crustal rocks could have been induced by high temperatures accompanying the upward movement of mantle-generated basic or intermediate magmas (see for example Cobbing and

Pitcher, 1972). Whatever the mechanism, the magma would have been water-deficient and could have migrated a significant distance upwards in the crust to the present site of emplacement, estimated to be at a depth of less than 10km. Sr^{87}/Sr^{86} ratios indicate that the parent magma (0.711) could not have been derived by partial melting of Kanmantoo Group metasediments (0.718-0.722), but was derived from crustal rocks of lower Sr^{87}/Sr^{86} ratio that probably occur at greater depth.

Subsequent to its formation, the parent magma of the Encounter Bay Granites was contaminated by crustal rocks. For example, the hybrid granites may represent metasedimentary rocks that were incorporated by the magma at an early stage of its crystallisation history. Alternatively, it is possible that the hybrid granites represent the variously assimilated refractory residue of crustal material carried upwards by the magma from the site of anatexis. Kanmantoo Group metasedimentary rocks constituted an obvious source of contamination of the margins of the intruding magma as it approached the present site of emplacement and as discussed in the previous section, the initial Sr^{87}/Sr^{86} ratio for the border facies megacrystic granite is consistent with contamination of the parent magma with Kanmantoo Group metasedimentary rocks. The magma was emplaced at the level now exposed in a mobile but crystal-rich condition. Wedging apart of bedding planes and active stoping appear to have been important emplacement mechanisms on a small scale, but there is insufficient exposure to enable an assessment of the mechanisms that may have been active during the emplacement of the pluton as a whole. The intrusion was finally constrained by the rapid crystallisation of its margins, apparently due to the relatively sudden loss of volatiles and the consequent increase in solidus temperature.

The emplacement age of the Encounter Bay Granites between 523m.y. and 531m.y. is Middle Cambrian, according to the geological time scale compiled by Harland, Smith and Wilcock (1964). The metasedimentary rocks intruded by the granites are part of the youngest formations of the type sequence of Kanmantoo Group metasedimentary rocks. The Kanmantoo Group conformably overlies fossiliferous Lower Cambrian metasediments and is regarded as Cambrian in age, although no diagnostic fossils have yet been found (Daily and Milnes, 1971a, 1972b, 1973; Figure 4 of this thesis). The fossiliferous Lower Cambrian meta-

sediments are in excess of 1,000m thick in their type section, and disconformably overlie Proterozoic Adelaide Supergroup metasediments. The Kanmantoo Group is possibly 10,000m thick in its type section, although the thickness is difficult to estimate because of repetition due to folding. Sedimentary cover on top of the Kanmantoo Group metasediments intruded by the Encounter Bay Granites may have been up to 10,000m thick, as estimated from the pressure assumed for the crystallisation of cordierite and andalusite in metasediments adjacent to the granites at about the time of their emplacement. If the age of the base of the Cambrian in this region is 570m.y. (Harland, Smith and Wilcock, 1964), then the fossiliferous Lower Cambrian metasediments, the Kanmantoo Group metasediments as presently known in the type section, and the sedimentary cover, were deposited prior to the emplacement of the granites during the Middle Cambrian, 532-531m.y. ago. This 40-50m.y. period between the base of the Cambrian and the emplacement of the Encounter Bay Granites records the deposition of up to 20,000m of sediments in the area studied, presumably in an actively subsiding basin.

The metasediments intruded by the granites must be older than 523-531m.y., and may be of Lower Cambrian age. Therefore the cover probably included sediments of Middle and Upper Cambrian age. These sediments may have correlated in part with the fossiliferous Middle Cambrian limestones and clastics intersected in bores on Yorke Peninsula (Daily, 1957, 1967, 1968; Figures 2 and 4 of this thesis). Metamorphism and regional folding of Kanmantoo Group metasediments in the area studied largely post-dated the emplacement of the Encounter Bay Granites. The onset of regional folding is assumed to have marked the end of sedimentation in the basin. Daily (private communication, 1972) suggested that sedimentation in areas of the Flinders Ranges (Figure 1) about 300km to the north continued through the Middle and Upper Cambrian and into the Lower Ordovician. This suggestion may not be at variance with the radiometric data for the Encounter Bay area. However, it should be pointed out that metamorphism outlasted the first generation folding in the Encounter Bay area, and ended about 470m.y. ago in the Lower Ordovician.

The subsequent geological history of the Encounter Bay Granites is interesting because of the fact that the granites were exposed at the

REFERENCES

Abele, C. and McGowran, B. (1959). The geology of the Cambrian south of Adelaide (Sellick Hill to Yankalilla). *Trans. R. Soc. S. Aust. 82*, 301-320.

Aldrich, L.T. and Wetherill, G.W. (1958). Geochronology by radioactive decay. *A. Rev. nucl. Sci. 8*, 257-298.

Althaus, E., Karotke, E., Nitsch, K.H. and Winkler, H.G.F. (1970). An experimental re-examination of the upper stability limit of muscovite plus quartz. *N. Jb. Miner. Mh. 7*, 289-336.

Arriens, P.A. and Compston, W. (1968). A method for isotopic ratio measurement by voltage peak switching, and its application with digital output. *J. mass Spectrom. Ion Phys. 1*, 471-481.

Ashworth, J.R. (1972). Myrmekites of exsolution and relacement origins. *Geol. Mag. 109*, 45-62.

Asthana, D.B. (1958). Structural study on granites on Encounter military sheet. S.A. Dept. Mines Rept. Bk. 47/90 (unpublished).

Atherton, M.P. (1958). The variation in garnet and chlorite composition in medium grade pelitic rocks from the Dalradian, with particular reference to the zonation in garnet. *Contr. Miner. and Petrol. 18*, 347-371.

Bailey, E.H. and Stevens, R.E. (1960). Selected staining of potassium-feldspar and plagioclase on rock slabs and thin sections. *Amer. Miner. 45*, 1020-1025.

Bailey, S.W. (1969). Refinement of an intermediate microcline structure. *Amer. Miner. 54*, 1540-1545.

Bailey, S.W. and Taylor, W.H. (1955). The structure of a triclinic potassium feldspar. *Acta Cryst. 8*, 621-632.

Baird, A.K., McIntyre, D.B., Welday, E.E. and Maldem, K.W. (1964). Chemical variations in a granitic pluton and its surrounding rocks. *Science 146*, 258-259.

Baird, A.K., McIntyre, D.B. and Welday, E.E. (1967). Geochemical and structural studies in batholithic rocks of southern California: Part II. Sampling of the Rattlesnake Pluton for chemical composition, variability, and trend analysis. *Geol. Soc. Amer. Bull. 78*, 191-222.

Balk, R. (1937). Structural behaviour of igneous rocks. *Geol. Soc. Amer. Mem. 5*, 1-177.

Balme, B.E. (1957). Upper Palaeozoic microfloras in sediments from the Lake Phillipson Bore, South Australia. *Aust. J. Sci. 20*, 61-62.

Barker, D.S. (1970). Compositions of granophyre, myrmekite and graphic granite. *Geol. Soc. Amer. Bull. 81*, 3339-3350.

Barth, T.W.F. (1952). Theoretical petrology. John Wiley and Sons, New York.

Barth, T.W.F. (1966). Aspects of the crystallisation of quartzo-feldspathic plutonic rocks. *Tsch. Miner. Pett. Mitt. 11*, 209-222.

Bateman, P.C., Clark, L.D., Huber, N.K., Moore, J.G. and Rinehart, C.D. (1963). The Sierra Nevada Batholith: a synthesis of recent work across the central part. *U.S. Geol. Survey Prof. Pap. 414D*, 1-45.

Bayly, M.B. (1965). The sampling error in modal analysis. *Amer. Miner. 50*, 196-211.

Blackburn, G., Bond, R.D. and Clarke, A.R.P. (1965). Soil development associated with stranded beach ridges in south-east South Australia. *CSIRO Soil Pub. 22*, 1-65.

Boettcher, A.L. and Wyllie, P.J. (1968). Phase relationships in the system $NaAlSiO_4$-SiO_2-H_2O to 35 kilobars pressure. *Amer. J. Sci. 267*, 875-909.

Borg, I.Y. and Smith, D.K. (1968). Calculated powder patterns for five plagioclases. *Amer. Miner. 53*, 1709-1723.

Borg, I.Y. and Smith D.K. (1969). Calculated powder patterns. Part II. Six potassium feldspars and barium feldspar. *Amer. Miner. 54,* 163-181.

Bosma, W. (1964). The spots in the spotted slates of Steige (Vosges) and Vogtland (Saxony). *Geol. Mijnb. 43,* 476-489.

Bourman, R.P. (1969). Landform studies near Victor Harbour. M.A. thesis Univ. Adelaide (unpublished).

Bourman, R.P. and Lindsay, J.M. (1973). Implications of fossiliferous Eocene marine sediments underlying part of the Waitpinga drainage basin, Fleurieu Peninsula, South Australia. *Search 4,* 77.

Bowes, D.R. (1954). The metamorphic and igneous history of Rosetta Head, South Australia. *Trans. R. Soc. S. Aust. 77,* 182-214.

Bowes, D.R. (1959). Distribution and field relations of the granitic rocks of Port Elliot, South Australia. *Trans. R. Soc. S. Aust. 82,* 7-9.

Broch, O.A. (1961). Quick identification of potash feldspar, plagioclase and quartz. *Amer. Miner. 46,* 752-753.

Brown, B.E. and Bailey, S.W. (1964). The structure of maximum microcline. *Acta Cryst. 17,* 1391-1400.

Brown, E.H. (1969). Some zoned garnets from the greenschist facies. *Amer. Miner. 54,* 1662-1677.

Brown, G.C. (1973). Evolution of granite magmas at destructive plate margins. *Nature Physical Science, 241,* 26-28.

Brown, G.C. and Fyfe, W.S. (1970). The production of granitic melts during ultrametamorphism. *Contr. Miner. and Petrol. 28,* 310-318.

Brown, G.E., Gibbs, G.V. and Ribbe, P.H. (1969). The nature and variation in length of the Al-Si-O and Al-O bonds in framework silicates. *Amer. Miner. 54,* 1044-1061.

Brown, G.E. and Gibbs, G.V. (1969). Oxygen coordination and the Si-O bond. *Amer. Miner. 54,* 1528-1539.

Browne, W.R. (1920). The igneous rocks of Encounter Bay, South Australia. *Trans. R. Soc. S. Aust. 44,* 1-57.

Butler, J.R. and Ragland, P.C. (1969). A petrochemical study of plutonic intrusions in the Piedmont, south-eastern Appalachians, U.S.A. *Contr. Miner and Petrol. 24,* 164-190.

Callegari, E. and De Pieri, R. (1967). Crystallographic observations on some chess-board albites. *Schweiz. Miner. Petrogr. Mitt. 47,* 99-110.

Campana, B. (1953). *Gawler* map sheet. Geological Atlas of South Australia, 1:63,360 series. (Geol. Surv. S. Aust.: Adelaide).

Campana, B. (1958). *In* M.F. Glaessner and L.W. Parkin (Eds.). The Geology of South Australia. *J. geol. Soc. Aust. 5,* 3-27.

Campana, B., Wilson, B. and Whittle, A.W.G. (1954). The geology of the Jervis and Yankalilla military sheets. Explanation of the geological maps. *Rep. Invest. Dep. Mines S. Aust. 3,* 1-26.

Campana, B. and Wilson, B. (1955). Tillites and related glacial topography of South Australia. *Eclog. geol. Helv. 48,* 1-30.

Chao, S.H., Hargreaves, A. and Taylor, W.H. (1940). The structure of orthoclase. *Miner. Mag. 25,* 498-512.

Chewings, C. (1894). Beitrage zur kanntnis der geologie sud und central Australiens nebt einer uebersicht des Lake Eyre beckens und seiner randgebirge. Heidelberg. Universitats - Buchdruckerci, von J. Horning. 1-41.

Chinner, G.A. (1955). The granitic gneisses of the Mount Lofty Ranges. M.Sc. thesis Univ. Adelaide (unpublished).

Claxton, C.W. (1968). Mineral layering in the Galway Granite, Connemara, Eire. *Geol. Mag. 105*, 149-159.

Coats, J.S. and Wilson, J.R. (1971). The eastern end of the Galway Granite. *Miner. Mag. 38*, 138-151.

Cobbing, E.J. and Pitcher, W.S. (1972). The coastal batholith of Central Peru. *J. geol. Soc. 128*, 421-460.

Cole, W.F., Sørum, H. and Kennard, O. (1949). The crystal structure of orthoclase and sanidinised orthoclase. *Acta Cryst. 2*, 280-287.

Coleville, A.A. and Ribbe, P.H. (1968). The crystal structure of an adularia and a refinement of the structure of orthoclase. *Amer. Miner. 53*, 25-37.

Compston, W., Lovering, J.F. and Vernon, M.J. (1965). The Rb-Sr age of the Bishopville aubrite and its constituent enstatite and feldspar. *Geochim. Cosmochim. Acta 29*, 1085-1100.

Compston, W., Crawford, A.R. and Bofinger, V.M. (1966). A radiometric estimate of the duration of sedimentation in the Adelaide Geosyncline, South Australia. *J. geol. Soc. Aust. 13*, 229-276.

Compston, W., Chappell, B.W., Arriens, P.A. and Vernon, M.J. (1969). On the feasibility of NBS70A K-feldspar as a Rb-Sr age reference sample. *Geochim. Cosmochim. Acta 33*, 753-757.

Cooper, A.F. and Lovering, J.F. (1970). Greenschist amphiboles from Haast River, New Zealand. *Contr. Miner. and Petrol. 27*, 11-24.

Cooper, J.A. and Compston, W. (1971). Rb-Sr dating within the Houghton inlier, South Australia. *J. geol. Soc. Aust. 17*, 213-219.

Crawford, A.R. and Thomson, B.P. (1959). *Encounter* map sheet, Geological Atlas of South Australia, 1:63,360 series. (Geol. Surv. S. Aust: Adelaide).

Crowell, J.C. and Frakes, L.A. (1971). Late Palaeozoic glaciation of Australia. *J. geol. Soc. Aust. 17*, 115-155.

Daily, B. (1956). The Cambrian in South Australia. *In* El sistema Cambrico su Paleogeografia Y el problema de su base. Rep. Internat. geol. Congr. 20th, Mexico, 1956, Vol. 2, 91-147.

Daily, B. (1957). Progress report on the Cambrian sequence met with in the Minlaton Stratigraphic Bore 1, Section 153, Hd. Ramsay, Yorke Peninsula, South Australia. Unpublished report to S.A. Mines Department.

Daily, B. (1963). The fossiliferous Cambrian succession on Fleurieu Peninsula, South Australia. *Rec. S. Aust. Mus. 14*, 579-601.

Daily, B. (1967). Stansbury West No. 1 and Edithburgh No. 1 Wells - subsurface stratigraphy and palaeontology of the Cambrian sequence. Unpublished report to Beach Petroleum N.L.

Daily, B. (1968). Stansbury Town No. 1 Well - subsurface stratigraphy and palaeontology of the Cambrian sequence. Unpublished report to Beach Petroleum N.L.

Daily, B. (1969). Fossiliferous Cambrian sediments and low grade metamorphics, Fleurieu Peninsula, South Australia. *In* B. Daily (Ed.), 'Geological Excursions Handbook', 49-54 ANZAAS, Section 3, 1969.

Daily, B. and Milnes, A.R. (1971a). Stratigraphic notes on Lower Cambrian fossiliferous metasediments between Campbell Creek and Tunkalilla Beach in the type section of the Kanmantoo Group, Fleurieu Peninsula, South Australia. *Trans. R. Soc. S. Aust. 95*, 199-214.

Daily, B. and Milnes, A.R. (1971b). Discovery of Late Precambrian tillites (Sturt Group) and younger metasediments (Marino Group) on Dudley Peninsula, Kangaroo Island, South Australia. *Search 2*, 431-433.

Daily, B. and Milnes, A.R. (1972a). Significance of basal Cambrian metasediments of andalusite grade, Dudley Peninsula, Kangaroo Island. *Search 3*, 89-90.

Daily, B. and Milnes, A.R. (1972b). Revision of the stratigraphic nomenclature of the Cambrian Kanmantoo Group, South Australia. *J. geol. Soc. Aust. 19*, 197-202.

Daily, B. and Milnes, A.R. (1973). Stratigraphy, structure and metamorphism of the Kanmantoo Group (Cambrian) in its type section east of Tunkalilla Beach, South Australia. *Trans. R. Soc. S. Aust.* (in press).

Dasch, E.J., Milnes, A.R. and Nesbitt, R.W. (1971). Rubidium-strontium geochronology of the Encounter Bay Granite and adjacent metasedimentary rocks, South Australia. *J. geol. Soc. Aust. 18*, 259-266.

Dawes, P.R. (1966). Genesis of rapakivi. *Nature 209*, 569-571.

Deer, W.A., Howie, R.A. and Zussman, J. (1962). Rock-forming Minerals. Vols. 1-5. Longmans.

Dietrich, R.V. (1962). K-feldspar structural states as petrogenetic indicators. *Norsk. geol. Tidsskr. 42*, 394-414.

Dodge, F.C.W., Papike, J.J. and Mays, R.E. (1968). Hornblendes from granitic rocks of the Central Sierra Nevada Batholith, California. *J. Petrol. 9*, 378-410.

Eckermann, H. von (1937). The genesis of rapakivi granites. *Geol. Fören. i Stockholm Förh. 59*, 503-524.

Elders, W.A. (1968). Mantled feldspars from the granites of Wisconsin. *J. Geol. 76*, 37-49.

Emeleus, C.H. (1963). Structural and petrographic observations on layered granites from southern Greenland. *Min. Soc. Amer. Spec. Pap. 1*, 22-29.

Emmermann, R. (1969). Genetic relations between two generations of K-feldspar in a granite pluton. *N. Jb. Miner. Abh. 111*, 289-313.

Evans, H.T., Appleman, D.E. and Handwerker, D.S. (1963). The least squares refinement of crystal unit cells with powder diffraction data by an automatic computer indexing method (abstr.). *Ann. Meet. Amer. Crystallogr. Ass., Cambridge, Mass.* Program, 42-43.

Evernden, J.F. and Richards, J.R. (1962). Potassium-argon ages in eastern Australia. *J. geol. Soc. Aust. 9*, 1-49.

Fander, H.W. (1960). Accessory minerals of South Australian granites. M.Sc. thesis Univ. Adelaide (unpublished).

Faure, G. and Powell, J.L. (1972). Strontium Isotope Geology. Springer-Verlag, New York.

Faure, G. and Hurley, P.M. (1963). The isotopic composition of strontium in oceanic and continental basalts: application to the origin of igneous rocks. *J. Petrol. 4*, 31-50.

Fawcett, J.J. and Yoder, H.S. (1966). Phase relationships of chlorites in the system MgO-Al_2O_3-SiO_2-H_2O. *Amer. Miner. 51*, 353-380.

Ferguson, R.B., Traill, R.J. and Taylor, W.H. (1958). The crystal structures of low-temperature and high-temperature albites. *Acta Cryst. 11*, 331-348.

Fershtater, G.B. (1968). Composition and some other properties of microcline phenocrysts in granitoids of Late Palaeozoic age on the east side of the Urals. *Doklady Akad. Nauk. SSR, 181*, 148-150.

Finney, J.J. and Bailey, S.W. (1964). Crystal structure of an authigenic maximum microcline. *Z. Kristallogr. 119*, 413-436.

Flanagan, F.J. (1969). U.S. Geological Survey standards - II. First compilation of data for the new U.S.G.S. rocks. *Geochim. Cosmochim. Acta, 33,* 81-120.

Fleming, P.D. (1971). Metamorphism and folding in the Mt. Lofty Ranges, South Australia, with particular reference to the Dawseley - Kanmantoo area. Ph.D. thesis Univ. Adelaide (unpublished).

Fleming, P.D. and Offler, R. (1968). Pretectonic crystallisation in the Mt. Lofty Ranges, South Australia. *Geol. Mag. 105,* 356-359.

Forbes, B.G. (1957). Stratigraphic succession east of Grey Spur, South Australia. *Trans. R. Soc. S. Aust. 80,* 59-66.

Frondel, C. (1962). Dana's system of Mineralogy. Seventh Ed. Vol. III. Silica minerals. John Wiley and Sons. New York.

Gartrell, H.W. (1903). The Port Victor granite. *Trans. R. Soc. S. Aust. 27,* 256-260.

Glaessner, M.F. and Wade, M. (1958). *In* M.F. Glaessner and L.W. Parkin (Eds.). The Geology of South Australia. *J. geol. Soc. Aust. 5,* 115-126.

Goldsmith, J.R. and Laves, F. (1954). Potassium feldspars structurally intermediate between microcline and sanidine. *Geochim. Cosmochim. Acta 6,* 100-118.

Grantham, D.R. (1928). The petrology of the Shap Granite. *Proc. Geol. Assoc. 34,* 299-331.

Greenhalgh, D. and Jeffery, P.M. (1959). A contribution to the Precambrian chronology of Australia. *Geochim. Cosmochim. Acta 16,* 39-57.

Harland, W.B., Smith, W.G. and Wilcock, B. (Eds.), (1964). The Phanerozoic time scale. *Q. Jl. geol. Soc. Lond., (Supplement) 120S,* 260-262.

Harris, W.K. and McGowran, B. (1971). Permian and reworked Devonian microfossils from the Troubridge Basin. *Quart. geol. Notes, Geol. Surv. S. Aust. 40,* 5-11.

Harry, W.T. (1952). Aluminium replacing silicon in some silicate lattices. *Miner. Mag. 29,* 142-149.

Harry, W.T. and Emeleus, C.H. (1960). Mineral layering in some granite intrusions of S.W. Greenland. *Int. Geol. Cong., XXI Sess. (Norden 1960), pt. XIV,* 172-181.

Hart, S.R. (1964). The petrology and isotopic mineral age relations of a contact zone in the Front Range, Colorado. *J. geol. 72,* 493-525.

Henstridge, D.A. (1970). The petrology and geochemistry of the upper South-East granites, South Australia. B.Sc.(Hons) thesis Univ. Adelaide (unpublished).

Hess, P.C. (1969). The metamorphic paragenesis of cordierite in pelitic rocks. *Contr. Miner. and Petrol. 24,* 191-207.

Hey, M.H. (1954). A new review of the chlorites. *Miner. Mag. 30,* 277-292.

Hibbard, M.J. (1965). Origin of some alkali feldspar phenocrysts and their bearing on petrogenesis. *Amer. J. Sci. 263,* 245-261.

Higgins, M.W. (1971). Cataclastic rocks. *U.S. Geol. Surv. Prof. Pap. 687,* 1-97.

Hirschberg, A. and Winkler, H.G.F. (1968). Stabilitätsbeziehungen zwischen chlorit, cordierit und almandin bei der metamorphose. *Contr. Miner. and Petrol. 18,* 17-42.

Hobbs, B.E. and Talbot, J.L. (1966). The analysis of strain in deformed rocks. *J. Geol. 74,* 500-513.

Holdaway, M.J. (1971). Stability of andalusite and the aluminum silicate phase diagram. *Amer. J. Sci. 271*, 97-131.

Horwitz, R.C., Thomson, B.P. and Webb, B.P. (1959). The Cambrian - Precambrian boundary in the eastern Mt. Lofty Ranges region: South Australia. *Trans. R. Soc. S. Aust. 82*, 205-218.

Horwitz, R.C. and Thomson, B.P. (1960). *Milang* map sheet, Geological Atlas of South Australia, 1:63,360 series (Geol. Surv. S. Aust.: Adelaide).

Hoscheck, G. (1969). The stability of staurolite and chloritoid and their significance in metamorphism of pelitic rocks. *Contr. Miner. and Petrol. 22*, 208-232.

Hossfeld, P.S. (1925). The Tanunda Creek Granite and its field relations. *Trans. R. Soc. S. Aust. 49*, 191-197.

Hossfeld, P.S. (1950). The Late Cainozoic history of the South-East of South Australia. *Trans. R. Soc. S. Aust. 73*, 232-279.

Howchin, W. (1898). Further discoveries of glacial remains in South Australia. *Trans. R. Soc. S. Aust. 22*, 12-17.

Howchin, W. (1899). Notes on the geology of Kangaroo Island with special reference to evidence of extinct glacial action. *Trans. R. Soc. S. Aust. 23*, 198-207.

Howchin, W. (1900). Evidences of extinct glacial action in southern Yorke's Peninsula. *Trans. R. Soc. S. Aust. 24*, 71-80.

Howchin, W. (1906). The geology of the Mount Lofty Ranges, Part II. *Trans. R. Soc. S. Aust. 30*, 227-262.

Howchin, W. (1910). The glacial (Permo-Carboniferous) moraines of Rosetta Head and King's Point, South Australia. *Trans. R. Soc. S. Aust. 34*, 1-12.

Howchin, W. (1926). The geology of the Victor Harbour, Inman Valley and Yankalilla districts, with special reference to the great Inman Valley glacier of Permo-Carboniferous age. *Trans. R. Soc. S. Aust. 50*, 89-119.

Hsu, L.C. (1968). Selected phase relationships in the system Al-Mn-Si-O-H: a model for garnet equilibria. *J. Petrol. 9*, 40-83.

Hurley, P.M., Hughes, H., Faure, G., Fairbairn, H.W. and Pinson, W.H. (1962). Radiogenic strontium-87 model of continent formation. *J. geophys. Res. 67*, 5315-5334.

Jahns, R.H. and Burnham, C.W. (1958). Experimental studies of pegmatite genesis: melting and crystallisation of granite and pegmatite. *Geol. Soc. Amer. Bull. 69*, 1592-1593.

James, R.S. and Hamilton, D.L. (1969). Phase relations in the system $NaAlSi_3O_8$-$KAlSi_3O_8$-$CaAl_2Si_2O_8$-SiO_2 at 1 kilobar water vapour pressure. *Contr. Miner. and Petrol. 21*, 111-141.

Johns, R.K. and Kruger, J.M. (1949). The Murray Bridge and Monarto Granites and associated rocks of the metamorphic aureole. *Trans. R. Soc. S. Aust. 73*, 122-136.

Jones, J.B. (1966). Order in alkali feldspars. *Nature 210*, 1352-1353.

Jones, J.B. (1968). Al-O and Si-O tetrahedral distances in alumino-silicate framework structures. *Acta Cryst. 24*, 355-358.

Jones, J.B. and Taylor, W.H. (1961). The structure of orthoclase. *Acta Cryst. 14*, 443-456.

Jones, J.B. and Taylor, W.H. (1968). Bond lengths in alkali feldspars. *Acta Cryst. 24*, 1387-1392.

Kerrick, D.M. (1968). Experiments on the upper stability of pyrophyllite at 1.8 kilobars and 3.9 kilobars water pressure. *Amer. J. Sci. 266*, 204-214.

Kerrick, D.M. (1969). K-feldspar megacrysts from a porphyritic quartz monzonite, central Sierra Nevada, California. *Amer. Miner. 54*, 839-848.

Kleeman, A.W. (1937). The nature and origin of the so-called diorite inclusions in the granite of Granite Island. *Trans. R. Soc. S. Aust. 61*, 207-220.

Kleeman, A.W. (1965). The origin of granitic magmas. *J. geol. Soc. Aust. 12*, 35-52.

Kolbe, P. and Taylor, S.R. (1966). Geochemical investigation of the granitic rocks of the Snowy Mountains area, New South Wales. *J. geol. Soc. Aust. 13*, 1-25.

Kulp, J.L. (1963). Present status of geochronometry. *Isotopics, U.S. At. Energy Comm. (Oak Ridge). 1*, 1-7.

Larsen, E.S., Keevil, N.B. and Harrison, H.C. (1952). Method for determining the age of igneous rocks using the accessory minerals. *Geol. Soc. Amer. Bull. 63*, 1045-1052.

Ludbrook, N.H. (1956). Permian foraminifera in South Australia. *Aust. J. Sci. 19*, 161-162.

Ludbrook, N.H. (1961). Stratigraphy of the Murray Basin in South Australia. *Geol. Surv. S. Aust. Bull. 36*, 1-96.

Ludbrook, N.H. (1967). Permian deposits of South Australia and their fauna. *Trans. R. Soc. S. Aust. 91*, 65-92.

Ludbrook, N.H. (1969). The Permian period. *In* L.W. Parkin (Ed.) Handbook of South Australian Geology, 117-132. (Government printer: Adelaide).

Luth, W.C. (1969). The systems $NaAlSi_3O_8$-SiO_2 and $KAlSi_3O_8$-SiO_2 to 20kb and the relationship between H_2O content, P_{H_2O} and P_{total} in granitic magmas. *Amer. J. Sci. 267*, 325-341.

Luth, W.C., Jahns, R.H. and Tuttle, O.F. (1964). The granite system at pressures of 4 to 10 kilobars. *J. geophys. Res. 69*, 759-773.

McIntyre, G.A., Brooks, C., Compston, W. and Turek, A. (1966). The statistical assessment of Rb-Sr isochrons. *J. geophys. Res. 71*, 5459-5468.

McConnell, J.D.C. (1969). Photochemical degradation of a silicate in the beam of the electron microscope. *Phil. Mag. 20*, 1195-1202.

MacKenzie, W.S. and Smith, J.V. (1961). Experimental and geological evidence for the stability of alkali feldspars. *Inst. Invest. Geol. "Lucas Mallada" Cursillos y Conferencias 8*, 53-63.

MacKenzie, W.S. and Smith, J.V. (1962). Single crystal X-ray studies of crypto- and micro-perthites. *Norsk. geol. Tiddskr. 42*, 72-103.

Madigan, C.T. (1925). The geology of the Fleurieu Peninsula. Part I - The coast from Sellick's Hill to Victor Harbour. *Trans. R. Soc. S. Aust. 44*, 198-212.

Marmo, V., Hytönen, K. and Vorma, A. (1963). On the occurrence of potash feldspars of inferior triclinicity within the Precambrian rocks in Finland. *C.R. Soc. Geol. Finlande 35*, 51-78. *Bull. Comm. geol. Finlande 212.*

Mawson, D. (1926). A brief resume of the present knowledge relating to the igneous rocks of South Australia. *Rept. Aust. Assn. Adv. Science 18*, 230-274.

Mawson, D. and Parkin, L.W. (1943). Some granitic rocks of south-eastern South Australia. *Trans. R. Soc. S. Aust. 67*, 233-243.

Mawson, D. and Dallwitz, W.B. (1944). Palaeozoic igneous rocks of lower south-eastern South Australia. *Trans. R. Soc. S. Aust. 68*, 191-204.

Mawson, D. and Segnit, E.R. (1945a). Porphyritic potash-soda microgranites of Mt. Monster. *Trans. R. Soc. S. Aust. 69*, 217-222.

Mawson, D. and Segnit, E.R. (1945b). Granites of the Tintinara district. *Trans. R. Soc. S. Aust. 69*, 263-276.

Mawson, D. and Sprigg, R.C. (1950). Sub-division of the Adelaide System. *Aust. J. Sci. 13*, 69-72.

Miguel, A. San (1969). The aplite-pegmatite association and its petrogenetic interpretation. *Lithos 2*, 25-37.

Mills, K.J. (1963). The geology of the Mt. Crawford granite gneiss and associated metasediments. *Trans. R. Soc. S. Aust. 87*, 167-183.

Milnes, A.R. (1967). A petrological study of the Encounter Bay Granites. B.Sc.(Hons). thesis Univ. Adelaide (unpublished).

Milnes, A.R. (1969). A guide to the petrology and field relationships of the Encounter Bay Granites. *In* B. Daily (Ed.), Geological Excursions Handbook, 57-60, ANZAAS, Section 3, 1969.

Milnes, A.R. and Bourman, R.P. (1972). A Late Palaeozoic glaciated granite surface at Port Elliot, South Australia. *Trans. R. Soc. S. Aust. 96*, 149-155.

Mirams, R.C. (1961). Field relationships of the Anabama Granite. *Trans. R. Soc. S. Aust. 85*, 121-131.

Miyashiro, A. (1961). Evolution of metamorphic belts. *J. Petrol. 2*, 277-311.

Moorbath, S. (1967). Recent advances in the application and interpretation of radiometric age data. *Earth-Sci. Rev. 3*, 111-133.

Moulden, J.C. (1895). Petrographical observations on some South Australian rocks. *Trans. R. Soc. S. Aust. 19*, 70-78.

Müller, G. and Schneider, A. (1971). Chemistry and genesis of garnets in metamorphic rocks. *Contr. Miner. and Petrol. 31*, 178-200.

Newton, R.C. (1966a). Kyanite-sillimanite equilibrium at 750°C. *Science 151*, 1222-1225.

Newton, R.C. (1966b). Kyanite-andalusite equilibrium from 700° to 800°C. *Science 153*, 170-172.

Nilssen, B. and Smithson, S.B. (1965). Studies of the Precambrian Herefoss Granite. I. K-feldspar obliquity. *Norsk. geol. Tiddskr. 4*, 367-396.

Norrish, K. and Chappell, B.W. (1967). X-ray fluorescence spectrography. *In* J. Zussman (Ed.), Physical Methods in Determinative Mineralogy, Chapt. 4. Academic Press.

Norrish, K. and Hutton, J.T. (1969). An accurate X-ray spectrographic method for the analysis of a wide range of geological samples. *Geochim. Cosmochim. Acta 33*, 431-453.

Ôba, N. (1962). Petrochemical studies of the Kyûshû Outer Zone Granites, Japan. *J. geol. Soc. Japan 68*, 162-171.

O'Driscoll, E.P.D. (1960). The hydrology of the Murray Basin Province in South Australia. *Geol. Surv. S. Aust. Bull. 35*, 1-148.

Oertel, A.C. (1971). The calculation of results in electron-probe microanalysis. *C.S.I.R.O. Division of Soils, Technical Paper 9.*

Offler, R. (1966). The structure and metamorphism of the Pewsey Vale area, north-east of Williamstown, S.A. Ph.D. thesis Univ. Adelaide (unpublished).

Offler, R. and Fleming, P.D. (1968). A synthesis of folding and metamorphism in the Mt. Lofty Ranges, South Australia. *J. geol. Soc. Aust. 15*, 245-266.

Orville, P.M. (1967). Unit-cell parameters of the microcline - low albite and sanidine - high albite solid solution series. *Amer. Miner. 52*, 55-86.

Parslow, G.R. (1968). The physical and structural features of the Cairnsmore of Fleet granite and its aureole. *Scott. J. geol. 4*, 91-108.

Parslow, G.R. (1971). Variations in mineralogy and major elements in the Cairnsmore of Fleet granite, S.W. Scotland. *Lithos 4*, 43-55.

Peng, C.C.J. (1970). Intergranular albite in some granites and syenites of Hong Kong. *Amer. Miner. 55*, 270-282.

Phillips, E.R. (1968). Mafic hybrid rocks from the New England Batholith, New South Wales. *Geol. Mag. 105*, 160-165.

Pitcher, W.S. and Read, H.H. (1958). The main Donegal Granite. *Q. Jl. geol. Soc. Lond. 102*, 389-446.

Piwinskii, A.J. and Wyllie, P.J. (1970). Experimental studies of igneous rock series: felsic body suite from the Needle Point Pluton, Wallowa Batholith, Oregon. *J. geol. 78*, 52-76.

Plas, L. Van der and Tobi, A.C. (1965). A chart for judging the reliability of point counting results. *Amer. J. Sci. 263*, 87-90.

Powell, D. and Treagus, J.E. (1970). Rotational fabrics in metamorphic minerals. *Miner. Mag. 37*, 801-814.

Ragland, P.C. (1970). Composition and structural state of the potassic phase in perthites as related to petrogenesis of a granitic pluton. *Lithos 3*, 167-189.

Ramberg, H. (1962). Intergranular precipitation of albite formed by unmixing of alkali feldspar. *N. Jb. Miner. Abh. 98*, 14-34.

Rao, S.V.L.N. (1960). X-ray study of potash feldspar of the contact metamorphic zones at Gjellerasen, Oslo. *Norsk. geol. Tiddskr. 40*, 1-12.

Ribbe, P.H. and Gibbs, G.V. (1969). Statistical analysis and discussion of mean Al/Si-O bond distances and the aluminum content of tetrahedra in feldspars. *Amer. Miner. 54*, 85-94.

Ribbe, P.H., Megaw, H.D. and Taylor, W.H. (1969). The albite structures. *Acta Cryst. 25*, 1503-1518.

Richardson, S.W. (1968). Staurolite stability in part of the system Fe-Al-Si-O-H. *J. Petrol. 9*, 467-488.

Rivalenti, G. and Sighinolfi, G.P. (1971). The influence of the local pressure gradient and of the metamorphic grade on the composition of pegmatites in metamorphic terrains. *Contr. Miner. and Petrol. 34*, 80-83.

Robertson, J.K. and Wyllie, P.J. (1971). Rock-water systems, with special reference to the water-deficient region. *Amer. J. Sci. 271*, 252-277.

Sando, M. (1957). The granitic and metamorphic rocks of the Reedy Creek area, Mannum, South Australia. M.Sc. thesis Univ. Adelaide (unpublished).

Savolahti, A. (1956). The Ahvenisto Massif in Finland. *Bull. Comm. geol. Finlande 174*, 1-96.

Savolahti, A. (1962). The rapakivi granite problem and the rules of idiomorphism in minerals. *C.R. Soc. Geol. Finlande 37*, 33-111. *Bull. Comm. geol. Finlande 204*.

Schermerhorn, L.J.G. (1956). The granites of Trancoso (Portugal): a study in microclinisation. *Amer. J. Sci. 254*, 329-348.

Seck, H.A. (1971). Koexistierende alkali-feldspate und plagioklase im system $NaAlSi_3O_8$-$KAlSi_3O_8$-$CaAl_2Si_2O_8$-H_2O bei temperaturen von 650° bis 900°. *N. Jb. Miner. Abh. 115*, 315-345.

Siefert, F. (1970). Low temperature compatability relations of cordierite in haplopelites of the system K_2O-MgO-Al_2O_3-SiO_2-H_2O. *J. Petrol. 11*, 73-99.

Siefert, F. and Schreyer, W. (1970). Lower temperature stability limit of Mg cordierite in the range 1-7kb water pressure: a redetermination. *Contr. Miner. and Petrol. 27*, 225-238.

Shelley, D. (1964). On myrmekite. *Amer. Miner. 49*, 41-52.

Shelley, D. (1966). Significance of granophyric and myrmekitic textures in the Lundy Granites. *Miner. Mag. 35*, 678-693.

Simonen, A. and Vorma, A. (1969). Amphibole and biotite from rapakivi. *Bull. Comm. geol. Finlande 238*, 1-28.

Slade, P.G. (1962). A study of the alkali feldspars from a granite-xenolith contact at Victor Harbour. B.Sc.(Hons). thesis Univ. Adelaide (unpublished).

Smith, J.V. (1956). The powder patterns and lattice parameters of plagioclase feldspars. I. The soda-rich plagioclases. *Miner. Mag. 31*, 47-68.

Smith, J.V. (1970). Physical properties of order-disorder structures with especial reference to feldspar minerals. *Lithos 3*, 145-160.

Smith, J.V. and MacKenzie, W.S. (1955). The alkali feldspars. II. A simple X-ray technique for the study of alkali feldspars. *Amer. Miner. 40*, 733-747.

Smith, J.V. and MacKenzie, W.S. (1961). Atomic, chemical and physical factors that control the stability of alkali feldspars. Inst. Invest. Geol. "*Lucas Mallada*" *Cursillos y Conferencias 8*, 39-52.

Smith, J.V. and Bailey, S.W. (1963). Second review of Al-O and Si-O tetrahedral distances. *Acta Cryst. 16*, 801-811.

Smithson, S.B. (1962). Symmetry relations in alkali feldspars of some amphibolite facies rocks from the southern Norwegian Precambrian. *Norsk. geol. Tiddskr. 42*, 386-399.

Sprigg, R.C. (1952). Sedimentation in the Adelaide Geosyncline and the formation of the continental terrace. *In* M.F. Glaessner and A.E. Rudd (Eds.), Sir Douglas Mawson Anniv. Vol., 153-159. Univ. Adelaide.

Sprigg, R.C. (1954). KINGSCOTE map sheet, Geological Atlas of South Australia, 1:250,000 series (Geol. Surv. S. Aust.: Adelaide).

Sprigg, R.C. and Campana, B. (1953). The age and facies of the Kanmantoo Group, eastern Mt. Lofty Ranges and Kangaroo Island, S.A. *Aust. J. Sci. 16*, 12-14.

Sprigg, R.C., Whittle, A.W.G. and Campana, B. (1951). *Adelaide* map sheet, Geological Atlas of South Australia, 1:63,360 series (Geol. Surv. S. Aust.: Adelaide).

Sprigg, R.C. and Wilson, B. (1954). *Echunga* map sheet, Geological Atlas of South Australia, 1:63,360 series (Geol. Surv. S. Aust.: Adelaide).

Spry, A. (1963). The chronological analysis of crystallisation and deformation of some Tasmanian Precambrian rocks. *J. geol. Soc. Aust. 11*, 33-48.

Spry, A. (1969). Metamorphic Textures. Pergamon Press, Oxford.
Starkey, J. (1959). Chess board albite from New Brunswick, Canada. *Geol. Mag. 96*, 141-145.
Steiger, R.H. and Hart, S.R. (1967). The microcline - orthoclase transition within a contact aureole. *Amer. Miner. 52*, 87-116.
Stewart, D.B. and Ribbe, P.H. (1969). Structural explanation for variations in cell parameters of alkali feldspar with Al/Si ordering. *Amer. J. Sci. 267*, 444-462.
Streckeisen, A.L. (1967). Classification and nomenclature of igneous rocks. *N. Jb. Miner. Abh. 107*, 144-240.
Stuart, W.J. (1970). The Cainozoic stratigraphy of the south-eastern coastal area of Yorke Peninsula, South Australia. *Trans. R. Soc. S. Aust. 94*, 151-178.
Stuart, W.J. and Sanden, A.T. von (1972). Palaeozoic history of the St. Vincent Gulf Region, South Australia. *APEA* Jour. 1972, 9-16.
Sturt, B.A. (1962). The composition of garnets from pelitic schists in relation to the grade of regional metamorphism. *J. Petrol. 3*, 181-191.
Suwa, K. (1966). Maximum microcline in Aswan granitic rocks, Egypt. *J. Earth Sci. Nagoya Univ. 14*, 116-136.
Sweatman, T.R. and Long, J.V.P. (1969). Quantitative electron probe microanalysis of rock-forming minerals. *J. Petrol. 10*, 332-379.
Talbot, J.L. (1963). Retrograde metamorphism of the Houghton Complex, South Australia. *Trans. R. Soc. S. Aust. 87*, 185-196.
Talbot, J.L. and Hobbs, B.E. (1968). The relationship of metamorphic differentiation to other structural features at three localities. *J. Geol. 76*, 581-587.
Talbot, J.L. and Hobbs, B.E. (1969). Reconstruction of tectonically deformed sedimentary structures. *Geol. Rundschau* 59, 213-222.
Taylor, S.R. (1965). The application of trace element data to problems in petrology. *Physics and Chemistry of the Earth, 6*.
Terzaghi, R.D. (1940). The rapakivi of Head Harbour, Maine. *Amer. Miner. 25*, 111-122.
Thomas, H.H. and Smith, W.C. (1932). Xenoliths of igneous origin in the Trégastel -Ploumanac'h Granite, Côtes du Nord, France. *Q. Jl. geol. Soc. Lond. 88*, 274-296.
Thomson, B.P. (1966). The lower boundary of the Adelaide System and older basement relationships in South Australia. *J. geol. Soc. Aust. 13*, 203-228.
Thomson, B.P. (1969). The Kanmantoo Group and Early Palaeozoic Tectonics. *In* L.W. Parkin (Ed.) Handbook of South Australian Geology, 97-108. (Government Printer: Adelaide).
Thomson, B.P. (1970). A review of the Precambrian and Lower Palaeozoic tectonics of South Australia. *Trans. R. Soc. S. Aust. 94*, 193-221.
Thomson, B.P. (1971). *In* Ann. Rept. Director Mines Govt. Geologist, S.A. Dept. Mines, 1970-71.
Thomson, B.P. (1972). *In* Ann. Rept. Director Mines Govt. Geologist, S.A. Dept. Mines, 1971-72.
Thomson, B.P. and Horwitz, R.C. (1962). BARKER map sheet, Geological Atlas of South Australia, 1:250,000 series (Geol. Surv. S. Aust.: Adelaide).
Tilley, C.E. (1919a). The occurrence and origin of certain quartz-tourmaline nodules in the granite of Cape Willoughby. *Trans. R. Soc. S. Aust. 43*, 156-165.

Tilley, C.E. (1919b). The petrology of the granitic mass of Cape Willoughby, Kangaroo Island. - Part I. *Trans. R. Soc. S. Aust. 43*, 316-341.

Tilling, R.I. (1968). Zonal distribution of variations in structural state of alkali feldspar within the Rader Creek Pluton, Boulder Batholith, Montana. *J. Petrol. 9*, 331-357.

Turner, F.J. and Verhoogen, J. (1962). Igneous and Metamorphic Petrology. (2nd Edn.). McGraw-Hill, New York.

Tuttle, O.F. and Bowen, N.L. (1958). Origin of granite in the light of experimental studies in the system $NaAlSi_3O_8$-$KAlSi_3O_8$-SiO_2-H_2O. *Geol. Soc. Amer. Mem. 74*, 1-153.

Vance, J.A. (1969). On synneusis. *Contr. Miner. and Petrol. 24*, 7-29.

Voll, G. (1960). New work on petrofabrics. *Liverpool and Manchester Geol. Jour. 2*, 536-544.

Vorma, A. (1971). Alkali feldspars of the Wiborgite rapakivi Massif in south-eastern Finland. *Bull. Comm. geol. Finlande 246*, 1-72.

Volborth, A. (1962). Rapakivi-type granites in the Precambrian complex of Gold Butte, Clark County, Nevada. *Geol. Soc. Amer. Bull. 73*, 813-832.

Wahl, W. (1925). Die gesteine des Wiborger rapakivigebietes. *Fennia 45*, No. 20.

Waters, A.C. and Krauskopf, K. (1941). Protoclastic border of the Coleville Batholith. *Geol. Soc. Amer. Bull. 52*, 1355-1418.

Wellman, P. (1971). The age and palaeomagnetism of the Australian Cainozoic volcanic rocks. Ph.D. thesis Aust. National Univ. (unpublished).

Wells, A.K. and Woolridge, S.W. (1931). The rock groups of Jersey, with special reference to intrusive phenomena. *Proc. Geol. Assoc. 42*, 178-215.

Wells, B.E. (1956). Geology of the Casterton district. *Proc. R. Soc. Victoria 68*, 85-110.

White, A.J.R. (1966). Petrology and structure of the Rathjen Granitic Gneiss of the Palmer region, South Australia. *J. geol. Soc. Aust. 13*, 471-490.

White, A.J.R., Compston, W. and Kleeman, A.W. (1967). The Palmer Granite - a study of a granite within a regional metamorphic environment. *J. Petrol. 8*, 29-50.

Winkler, H.G.F. (1967). Petrogenesis of Metamorphic Rocks. (2nd Edn.). Springer-Verlag, New York.

Winkler, H.G.F. (1970). Abolition of Metamorphic facies, introduction of the four divisions of metamorphic stage, and of a classification based on isograds in common rocks. *N. Jb. Miner. Mh. 5*, 189-248.

Winkler, H.G.F. and Lindemann, W. (1972). The system Qz-Or-An-H_2O within the granitic system Qz-Or-Ab-An-H_2O. Application to granitic magma formation. *N. Jb. Miner. Mh. 2*, 49-61.

Wones, D.R. and Eugster, H.P. (1965). Stability of biotite: experiment, theory and application. *Amer. Miner. 50*, 1228-1272.

Wright, T.L. (1964). The alkali feldspars of the Tatoosh Pluton in Mount Rainier National Park. *Amer. Miner. 49*, 715-735.

Wright, T.L. (1967). The microcline-orthoclase transformation in the contact aureole of the Eldora Stock, Colorado. *Amer. Miner. 52*, 87-116.

Wright, T.L. (1968). X-ray and optical study of alkali feldspar: II. An X-ray method for determining the composition and structural state from measurement of 2θ values for three reflections. *Amer. Miner. 53*, 88-104.

Wright, T.L. and Stewart, D.B. (1968). X-ray and optical study of alkali feldspar: I. Determination of composition and structural state from refined unit-cell parameters, 2V. *Amer. Miner. 53*, 38-87.

Wyllie, P.J. (1971). Experimental limits for melting in the earth's crust and upper mantle. *In* J.G. Heacock (Ed.) The Structure and Physical Properties of the Earth's Crust 279-301. *Geophysical Monograph Series 14* (Amer. Geophys. Union).

Yoder, H.S., Stewart, D.B. and Smith, J.R. (1957). Ternary feldspars. *Carnegie Inst. Wash. Yr. Bk. 56*, 206-214.

Zwart, H.J. (1962). On the determination of polymetamorphic mineral associations, and its application to the Bosost area, (Central Pyrenees). *Geol. Rundschau 52*, 38-65.

APPENDICES

APPENDIX A

The results of several aspects of the investigation of the Encounter Bay Granites and their environment have been published or are in press. Reprints (or pre-prints) of these papers, as listed below in order of date of publication, are included in this Appendix.*

1. Daily, B. and Milnes, A.R. (1971). Stratigraphic notes on the Lower Cambrian fossiliferous metasediments between Campbell Creek and Tunkalilla Beach in the type section of the Kanmantoo Group, Fleurieu Peninsula, South Australia. Trans. R. Soc. S. Aust. 95, 199-214.
2. Daily, B. and Milnes, A.R. (1971). Discovery of Late Precambrian tillites (Sturt Group) and younger metasediments (Marino Group) on Dudley Peninsula, Kangaroo Island. Search 2, 431-433.
3. Dasch, E.J., Milnes, A.R. and Nesbitt, R.W. (1971). Rubidium-strontium geochronology of the Encounter Bay Granite and adjacent metasedimentary rocks, South Australia. J. geol. Soc. Aust. 18, 259-266.
4. Daily, B. and Milnes, A.R. (1972). Significance of Basal Cambrian metasediments of andalusite grade, Dudley Peninsula, Kangaroo Island. Search 3, 89-90.
5. Milnes, A.R. and Bourman, R.P. (1972). A Late Palaeozoic glaciated granite surface at Port Elliot, South Australia. Trans. R. Soc. S. Aust. 96, 149-155.
6. Daily, B. and Milnes, A.R. (1972). Revision of the stratigraphic nomenclature of the Cambrian Kanmantoo Group, South Australia. J. geol. Soc. Aust. 19, 197-202.
7. Daily, B. and Milnes, A.R. (1973, in press). Stratigraphy, structure and metamorphism of the Kanmantoo Group (Cambrian) in its type section east of Tunkalilla Beach, South Australia. Trans. R. Soc. S. Aust.
8. Daily, B., Jago, J.B. and Milnes, A.R. (1973, in press). Precambrian blocks and arcuate trends in South Australia and Tasmania. Nature Physical Science.

*See back pocket.

APPENDIX B

Electron probe microanalysis of amphibole in S_2 fracture-cleavage in Middleton Sandstone in Middleton quarry

	Average of 6 spot analyses
	SiO_2 51.3
	Al_2O_3 4.4
	TiO_2 0.15
	MnO 0.15
Total Fe as	FeO 8.9
	MgO 17.3
	CaO 12.5
	Na_2O 0.81
	TOTAL 95.5

Structural formula calculated on the basis of 23 oxygen atoms:

Si	7.45
Al	0.55
Tetrahedral	8.00
Al	0.21
Ti	0.02
Fe as Fe^{+2}	1.09
Mg	3.76
Mn	0.02
Y	5.10
Ca	1.95
Na	0.23
X	2.18

The analysis is quoted to within the calculated counting errors.

The analytical conditions were as follows:

Accelerating voltage - 20Kv
Beam current - 50nA
Beam fully focussed
Flow proportional counters
Counting time - 10 seconds (peak and one background position)
Standards used - Olivine (Fe, Si, Mg)
Mn metal
Rutile (Ti)
Bytownite (Ca, Al)
Jadeite (Na)

According to Deer, Howie and Zussman (1962), hornblende can be distinguished from actinolite on the basis of the number of Al ions allocated to tetrahedral positions in the structural formula: hornblende contains greater than 0.5 tetrahedral Al ions per formula unit. The amphibole analysed here is therefore hornblende.

The Cambridge Instruments "Geoscan" electron microprobe used for this and all other analyses in this thesis incorporates a servo-control system which moves each of the two spectrometers to four pre-set angular positions, thus allowing the rapid determination of up to eight elements in a selected spot. Background counts may be taken at pre-

selected angles up to $5^{o}2\theta$ from each peak position, also using the servo-control mechanism. The results of each spot analysis are printed as peak (and corresponding background) counts per second on a teletype with paper-tape facility. The raw data are converted to absolute element or oxide concentrations according to the method of Sweatman and Long (1969) using the procedure of Oertel (1971). The paper-tape reading program MICANCOR (written by H. Rosser, C.S.I.R.O. Division of Soils) provides direct entry of the raw data into a CDC 3200 computer and incorporates the correction program of Oertel (1971).

Electron probe microanalyses must be quoted to within counting error since the analytical precision can not be any better than this. In general, the analytical precision is expected to be worse than counting error because of drifts in count rate due to decomposition of many minerals (including hydrous minerals and alkali-rich minerals such as feldspars and jadeite) under the influence of the electron beam in the evacuated specimen chamber (McConnell, 1969; Sweatman and Long, 1969), and because of serious sampling errors on a micron scale. Uncertainty in many of the parameters used in correction of the raw data may account for significant errors in the accuracy of electron probe microanalyses, but these errors are difficult to assess.

APPENDIX C

Electron microprobe examination of the striped layering in Petrel Cove Formation metasediments adjacent to the Encounter Bay Granites at Rosetta Head

A polished-thin section of a metasiltstone containing two stripes was prepared for electron microprobe examination. The stripes are light coloured layers deficient in biotite relative to the remainder of the rock. Each stripe is bordered by a biotite-rich zone, and contains a distinct but thin central-fracture filled with quartz and biotite. Electron probe microanalyses[1] of biotite and plagioclase[2] in the stripes and in the host metasiltstone were carried out in order to test for differences in the composition of these minerals (Table C1). In addition, changes in the rock composition were determined at 150 micron intervals across the boundary between a stripe and the host metasiltstone. At each spot, the analysis was made with the focussed electron beam rapidly scanning an area 100 microns square. The area scanned generally included parts of several mineral grains because of the fine grain size of the rock, and so each of the analyses (Table C2) is considered to at least approximate the composition of the rock in that area.

The biotite and plagioclase analyses given in Table C1 indicate that there is no apparent difference in the chemical composition of these minerals in the stripe and in the host metasiltstone.

On the other hand, the "rock" analyses given in Table C2 (and

---

[1]Analytical conditions:

Accelerating voltage - 20Kv
Beam Current - 50nA (Beam focussed)
Flow proportional counters
Counting time - 10 seconds (peak and one background position)
Standards used - Biotite (Fe, Ti, K, Si, Al, Mg)
Bytownite (Ca)
Jadeite (Na)
Corrections to the raw data were applied according to the method of Sweatman and Long (1969) using the procedure of Oertel (1971).

The analyses given in Tables C1 and C2 are quoted to within calculated counting error.

[2]Plagioclase is untwinned, but is readily distinguished from quartz in the microanalyser because of a distinctive blue luminescence emitted upon electron bombardment

summarised in Figure C1) indicate a decrease in the concentration of Na_2O, CaO, FeO and Al_2O_3, but an increase in the concentration of SiO_2 in the stripe relative to the host metasiltstone. These differences point to a deficiency of biotite and plagioclase and an enrichment of quartz in the stripe relative to the host metasiltstone.

The data presented here are consistent with recrystallisation following the rearrangement of mineral components in the local environment of the stripes. For example, the occurrence of biotite-rich borders along the stripes and the concentration of andalusite poikiloblasts adjacent to stripes in andalusite schists points to the preferential migration of Fe, Mg, K and Al out of the striped layers and into the adjacent metasediment. There is no evidence for the accumulation of Na and Ca in the adjacent metasediment in the specimen examined, and it seems likely that these elements may have been lost from the local system. However, Si appears to have been introduced into the stripe. All stripes exhibit a thin central fracture which is commonly filled with quartz and/or biotite. Migration of elements out of the zone adjacent to the fracture, which is believed to be of tensional origin on the basis of field evidence, may well have been facilitated by the percolation of water-rich fluids along the fracture. The occurrence of thin quartz-rich pegmatite veins parallel to the striped layering in several parts of the Petrel Cove Formation supports this suggestion. Recrystallisation of the metasediments immediately adjacent to the stripes accompanied the alteration, and occurred at temperatures conducive to the formation of andalusite poikiloblasts. The composition of the plagioclase (about An_{38}) in both the stripe and the host metasiltstone is consistent with metamorphic conditions of andalusite grade.

TABLE C1

Comparison of the mineral chemistry of biotite and plagioclase in stripe and host metasiltstone (specimen V3- coll. Prof. J.L. Talbot)

1. Electron probe microanalyses of biotite and plagioclase crystals in the host metasiltstone

		Biot 1	Biot 2	Biot 3	Plag 1	Plag 2	Plag 3	Plag 4
	SiO_2	36.3	35.8	36.4	59.7	59.1	59.3	58.7
	Al_2O_3	20.2	20.1	20.0	26.4	26.3	26.3	26.5
	TiO_2	1.53	1.51	1.51	0.00	0.02	0.03	0.00
Total Fe as	FeO	18.7	18.0	18.6	0.03	0.06	0.15	0.01
	MgO	10.7	10.8	10.8	0.04	0.03	0.04	0.04
	CaO	0.01	0.01	0.00	7.7	7.9	7.8	8.4
	Na_2O	0.34	0.46	0.42	7.3	7.1	7.1	6.9
	K_2O	8.7	8.8	8.8	0.04	0.05	0.06	0.04
	TOTAL	96.5	95.5	96.5	101.2	100.6	100.8	100.6
					An 36.7	38.0	37.6	40.1
					Ab 63.0	61.7	62.0	59.6
					Or 0.3	0.3	0.4	0.3

2. Electron probe microanalyses of biotite crystals in the biotite-rich zone bordering the stripe

		Biot 1	Biot 2	Biot 3	Biot 4
	SiO_2	36.2	35.6	36.5	35.9
	Al_2O_3	20.1	19.8	19.8	19.9
	TiO_2	1.52	1.51	1.50	1.49
Total Fe as	FeO	18.3	18.5	17.9	18.9
	MgO	10.8	10.9	11.1	10.9
	CaO	0.01	0.00	0.02	0.00
	Na_2O	0.31	0.29	0.12	0.27
	K_2O	8.9	8.5	9.0	8.7
	TOTAL	96.1	95.1	95.9	96.1

3. Electron probe microanalyses of mica and plagioclase crystals in the stripe

		Biot 1	Biot 2	Musc.	Plag 1	Plag 2	Plag 3	Plag 4
	SiO_2	36.5	36.2	48.0	59.9	59.0	58.8	59.0
	Al_2O_3	20.1	19.9	37.8	26.4	25.8	25.9	25.8
	TiO_2	1.41	1.48	0.44	0.00	0.00	0.00	0.00
Total Fe as	FeO	18.4	17.8	0.74	0.05	0.01	0.10	0.01
	MgO	10.6	10.7	0.60	0.03	0.01	0.04	0.02
	CaO	0.03	0.05	0.02	7.8	8.0	8.1	8.0
	Na_2O	0.32	0.31	1.12	7.3	7.3	7.0	7.2
	K_2O	8.9	8.7	8.8	0.06	0.04	0.05	0.05
	TOTAL	96.3	95.1	97.5	101.5	100.2	100.0	100.1
					An 37.0	37.6	38.9	37.9
					Ab 62.7	62.1	60.8	61.8
					Or 0.3	0.3	0.3	0.3

Analyst: A.R. Milnes

TABLE C2

Electron probe microanalyses of 100 micron squares at 150 micron intervals across boundary between stripe and host metasiltstone (specimen V3- coll. Prof. J.L. Talbot)

		1	2	3	4	5	6	7
	SiO_2	73.3	77.7	76.5	66.7	74.8	79.4	64.6
	Al_2O_3	12.6	12.5	12.6	17.2	13.8	11.1	19.3
	TiO_2	0.34	0.23	0.55	0.97	0.22	0.28	0.37
Total Fe as	FeO	4.61	2.72	2.68	4.06	2.93	2.45	3.35
	MgO	2.85	1.22	1.30	1.94	1.50	1.51	1.91
	CaO	2.21	2.84	1.85	3.55	2.18	1.57	2.34
	Na_2O	2.30	2.55	1.91	3.70	2.51	1.51	2.60
	K_2O	2.44	1.52	2.27	2.08	2.43	2.32	3.43
	TOTAL	100.7	101.3	99.7	100.2	100.4	100.1	97.9

		8	9	10	11	*12	*13	*14
	SiO_2	74.2	79.0	84.0	66.8	52.6	41.8	48.1
	Al_2O_3	15.3	9.41	8.31	14.3	16.3	18.4	19.8
	TiO_2	0.23	0.38	0.19	0.64	0.99	1.35	0.96
Total Fe as	FeO	2.03	4.49	2.29	7.7	12.5	16.2	11.3
	MgO	1.04	2.45	1.15	4.60	7.0	9.5	6.7
	CaO	2.13	1.59	1.60	1.52	0.74	0.03	1.74
	Na_2O	2.31	1.50	1.59	1.68	1.18	0.41	1.68
	K_2O	2.61	2.44	1.50	3.92	5.99	7.96	6.07
	TOTAL	99.9	101.3	100.6	101.2	97.3	95.7	96.3

		*15	#16	#17	#18	#19	#20	#21
	SiO_2	65.2	77.6	74.4	76.0	84.8	88.9	77.6
	Al_2O_3	13.4	12.9	16.8	15.1	7.89	6.74	12.5
	TiO_2	0.52	0.23	0.13	0.14	0.33	0.08	0.19
Total Fe as	FeO	5.91	2.22	0.93	0.80	2.81	0.65	2.02
	MgO	3.29	1.07	0.61	0.46	1.24	0.38	1.05
	CaO	2.27	2.41	2.71	1.94	1.51	1.41	2.12
	Na_2O	1.85	2.33	2.98	2.19	1.46	1.72	2.17
	K_2O	3.39	1.65	2.09	2.19	1.44	0.58	1.28
	TOTAL	95.8	100.4	100.7	98.8	101.5	100.5	98.9

		#22	#23	#24	#25	*26	*27	*28
	SiO_2	77.2	88.2	74.2	70.2	71.3	50.0	42.1
	Al_2O_3	13.9	7.85	13.4	16.2	12.1	18.2	20.9
	TiO_2	0.39	0.07	0.27	2.41	0.46	0.85	1.06
Total Fe as	FeO	0.71	0.27	2.67	3.43	5.14	11.3	14.0
	MgO	0.41	0.18	1.66	1.26	2.62	6.0	8.3
	CaO	1.55	1.46	2.40	1.96	1.80	1.88	1.19
	Na_2O	1.69	1.34	2.33	2.20	1.98	1.88	1.54
	K_2O	2.04	0.88	2.03	2.35	2.62	5.25	7.19
	TOTAL	97.9	100.3	99.0	100.0	98.0	95.4	96.3

TABLE C2 (Cont'd)

Electron probe microanalyses of 100 micron squares at 150 micron intervals across boundary between stripe and host metasiltstone (specimen V3- coll. Prof. J.L. Talbot)

		*29	30	31
	SiO_2	65.8	78.8	72.3
	Al_2O_3	14.0	9.74	13.9
	TiO_2	0.77	0.40	0.33
Total Fe as	FeO	8.2	2.87	3.45
	MgO	5.47	1.58	1.63
	CaO	1.12	2.12	3.03
	Na_2O	1.32	2.01	2.98
	K_2O	4.29	1.55	1.58
	TOTAL	101.0	99.1	99.2

*Biotite-rich border zones
#Striped layer

Analyst: A.R. Milnes

FIGURE C1

Diagram showing the changes in SiO_2, Al_2O_3, Na_2O, FeO and CaO concentration in an electron microprobe traverse across a single striped layer with biotite-rich margins in Petrel Cove Formation metasiltstone V3. The distance between adjacent analyses (numbered 1 to 31) was 150 microns. Each analysis included the determination of all five oxides, and was made with the focussed electron beam scanning an area 100 microns square on the specimen surface.

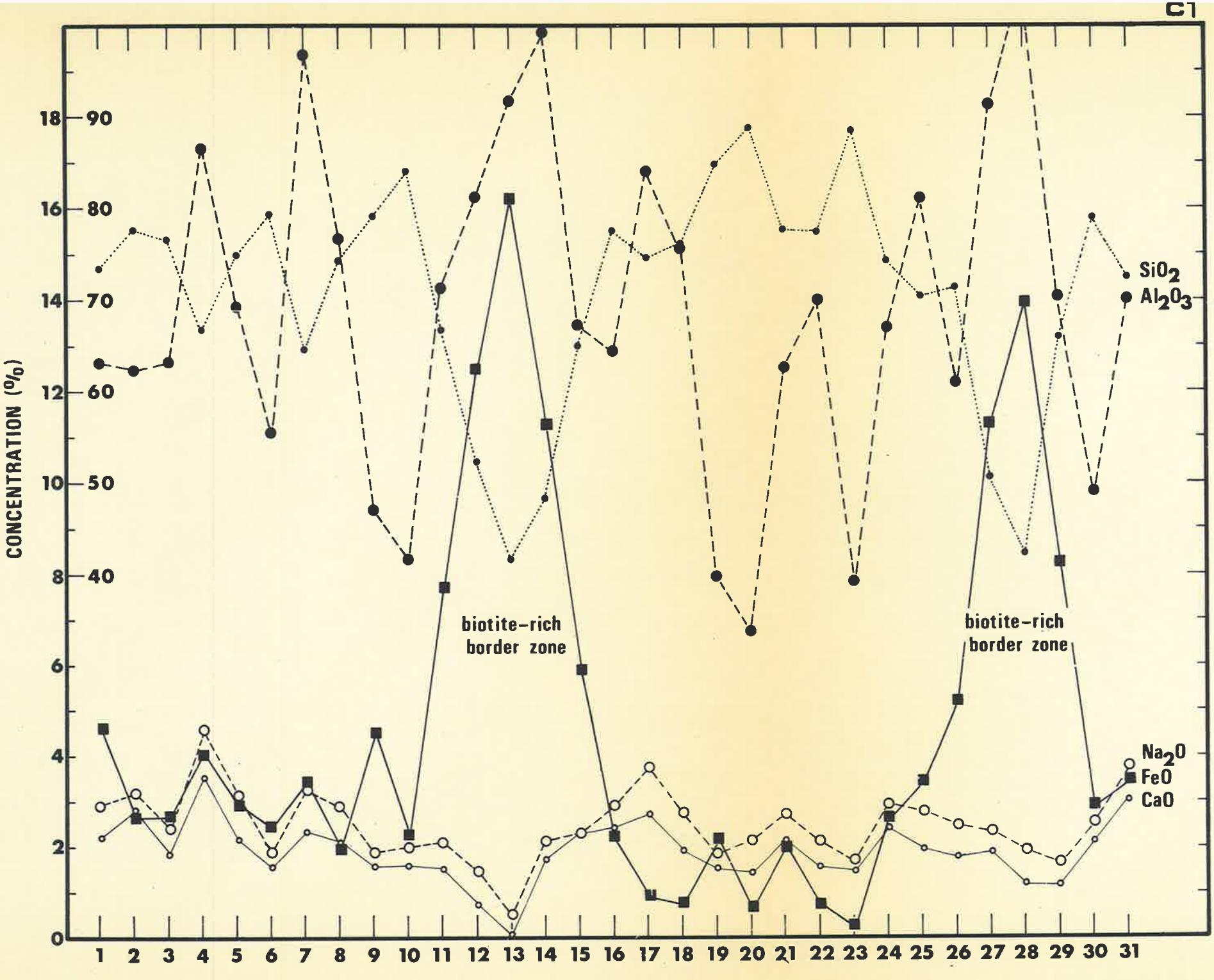
C1
CONCENTRATION (%)
18
16
14
12
10
8
6
4
2
0
90
80
70
60
50
40
1 2 3 4 5 6 7 8 9 10 11 12 13 14 15 16 17 18 19 20 21 22 23 24 25 26 27 28 29 30 31
biotite-rich
border zone
biotite-rich
border zone
SiO2
Al2O3
Na2O
FeO
CaO

APPENDIX D

Identification of altered poikiloblasts in Kanmantoo Group metasedimentary rocks

Many andalusite-cordierite schists in the Petrel Cove Formation in the type section of the Kanmantoo Group contain altered poikiloblasts composed of microcrystalline yellow-brown coloured material that is almost isotropic. Electron probe microanalyses[1] of the altered poikiloblasts in a polished-thin section of specimen SC-106 (andalusite schist) for the elements detected during reconnaissance spectrometer scans are given in Table D1. The analyses are variable due to the difficulty of locating the focussed electron beam on areas free of inclusions. Nevertheless, they are sufficiently consistent to indicate that the alteration product is probably a hydrated alumino-silicate. X-ray powder diffraction photographs of the altered poikiloblasts carefully cut from the specimen using a dentist's drill with small diamond-tipped circular saw attachment indicate that the alteration product is kaolinite.

As described in the main text of the thesis, poikiloblasts composed of the material identified here as kaolinite are considered to be altered cordierite poikiloblasts. Many authors have optically identified the fine grained alteration products of cordierite as pinite, which is a general term used to denote very fine grained chlorite and sericite (Deer, Howie and Zussman, 1962). Although the identification of these alteration products by optical means is tenuous, some authors have confirmed their optical identification by X-ray powder diffraction techniques (see for example Bosma, 1964). The identification of kaolinite as an alteration product of cordierite has not previously been recorded. There is however, considerable scope for further electron microprobe studies of the fine grained alteration products of cordierite, both in Petrel Cove Formation metasediments and in rocks from other areas.

Altered post-S_1 poikiloblasts in a spotted phyllite (SC-47) in

---

[1]Analytical conditions:
Accelerating voltage - 20Kv
Beam current - 50nA (Beam focussed)
Flow proportional counters
Counting time - 10 seconds (peak and one background position)
Corrections to the raw data were applied according to the method of Sweatman and Long (1969) using the procedure of Oertel (1971).

the Tapanappa Formation at Tunkalilla Beach in the type section of the Kanmantoo Group are composed of a microcrystalline material which has low to intermediate birefringence and a distinctive wavy extinction. The poikiloblasts are considered to be altered andalusite, as explained in the main text. Electron probe microanalyses of the altered poikiloblasts are given in Table D1. The analyses do not include K. However, the high concentrations of Si and Al and the low concentrations of other elements are consistent with the alteration product being muscovite. On the basis of its optical characteristics, in particular its microcrystalline habit and wavy extinction, the alteration product is herein identified as illite.

Muscovite is commonly reported as an alteration product of andalusite (Deer, Howie and Zussman, 1962). In many andalusite schists in the Petrel Cove Formation in the type section of the Kanmantoo Group, the andalusite has altered to fine grained muscovite (sericite) which is readily identified on the basis of its optical characteristics. The alteration of andalusite in these rocks to illite is a less common but more distinctive phenomenon.

TABLE D1

Electron probe microanalyses of altered poikiloblasts in specimen SC-106

		1	2	3	4	5
	SiO_2	40.1	44.5	43.3	39.6	43.3
	Al_2O_3	36.6	41.7	41.1	34.8	39.3
Total Fe as	FeO	5.60	1.06	0.37	2.98	2.46
	MgO	1.15	0.96	0.90	4.11	2.22
	TOTAL	83.5	88.2	85.7	81.5	87.3

Standard used: Biotite (Fe, Si, Al, Mg)

Electron probe microanalyses of altered poikiloblasts in specimen SC-47

		1	2	3
	SiO_2	47.0	49.8	48.8
	Al_2O_3	34.6	33.5	34.2
	TiO_2	0.02	0.02	0.04
	MnO	0.03	0.03	0.04
Total Fe as	FeO	1.85	2.40	1.93
	MgO	0.77	1.43	0.88
	CaO	0.29	0.40	0.44
	Na_2O	0.16	0.16	0.19
	TOTAL	84.7	87.7	86.5

Standards used: Garnet (Fe, Ca, Si, Al)
Olivine (Mg)
Mn metal
Rutile (Ti)
Jadeite (Na)

Analyst: A.R. Milnes

Analyses are quoted to within calculated counting error

APPENDIX E

The mineral chemistry of some calc-silicates and metasiltstones from the type section of the Kanmantoo Group, with special reference to garnets

Total-rock, garnet, chlorite and hornblende chemical analyses[1] for three specimens of calc-silicates from the Carrickalinga Head Formation (Figure 5) are given in Tables E1-E3. On the basis of the total-rock chemical analyses and textural observations, the calc-silicates are considered to have originally been impure dolomitic siltstones. The calc-silicate mineralogy supports this postulate. As described in the main text of the thesis, the metamorphic fabric of the calc-silicates is believed to have been the result of post-F_1 crystallisation.

Chlorite in the calc-silicates can be identified as ripidolite on the basis of the structural formulae (Hey, 1954; Deer, Howie and Zussman, 1962). Hornblende in the calc-silicates contains on the average 1.71 atoms of Al replacing Si in tetrahedral coordination.

Garnets in the calc-silicates SC-1 and SC-2 record a depletion of spessartite component and a corresponding enrichment of grossularite component in their rims (Tables E1 and E2). The garnet in calc-silicate SC-3 records a depletion of spessartite and grossularite, and a corresponding enrichment of almandine and pyrope in its rims (Table E3). In contrast, garnets in two metasiltstones (SC-4 and 446) record depletions of grossularite with enrichments of almandine and to a lesser extent pyrope in their rims (Tables E4 and E5). These data are summarised graphically in Figure E1.

Brown (1969) suggested that depletion of spessartite in garnet

---

[1]Total-rock chemical analyses were carried out by X-ray fluorescence according to the method of Norrish and Hutton (1969). Mineral analyses were carried out on a Cambridge Instruments "Geoscan" electron probe microanalyser using the following conditions:

Accelerating voltage - 20Kv
Beam current - 50nA
Beam fully focussed
Flow proportional counters
Counting time - 10 seconds (peak and one background position)
Standards used - Garnet (Fe, Mn, Ca, Si, Al, Mg)
Rutile (Ti)
Jadeite (Na)
Corrections to the raw data were made according to the method of Sweatman and Long (1969) using the procedure of Oertel (1971)

The analyses in the accompanying Tables are quoted to within counting error.

rims may result either from depletion of Mn from the equilibrium system during crystallisation, or from a change in metamorphic grade. In general, a depletion of spessartite (or grossularite) accompanied by an enrichment of almandine in garnet rims is attributed to an increase in metamorphic grade (Sturt, 1962; Atherton, 1968; Brown, 1969). However, this postulate has been challenged by Muller and Schneider (1971), whose data suggests that changes in Mn content are dependent in a complex manner on temperature, pressure and oxygen fugacity.

Calc-silicates SC-1, SC-2 and SC-3 contain sufficient mineral phases to suggest that their garnets were unlikely to have compositional freedom at constant metamorphic grade. Therefore it seems likely that the depletion of spessartite in the rims of the garnets in these rocks resulted from a change in metamorphic grade, and hence a change in the garnet-forming reactions. The fact that garnets in SC-1 and SC-2 exhibit enrichments of grossularite in their rims whereas garnets in SC-3 contain almandine enriched rims is puzzling, but may indicate that the garnet-forming reactions in each case were different. The metasiltstone SC-4 contains too few mineral phases to have controlled the compositional invariance of the garnets at constant metamorphic grade, and so the depletion of spessartite in the garnet rims is probably the result of Mn depletion of the system during garnet growth. As these specimens were collected from the same locality, it is unlikely that they were affected by different metamorphic conditions. Therefore, an explanation of the zoning in terms of Mn depletion of the systems induced by a change in metamorphic grade (of unknown magnitude or direction) seems to be the most acceptable in terms of the available data.

The garnet in the metasiltstone 446 exhibits an enrichment of almandine and to a lesser extent spessartite, and a depletion of grossularite in its rims, and so contrasts with the compositional zoning in the garnets described above. However, this specimen was collected from the Petrel Cove Formation in the immediate vicinity of the Encounter Bay Granites at Rosetta Head, about 40km east of the calc-silicates and the metasiltstone SC-4. As it is unlikely that the metamorphic conditions were exactly comparable in the two areas, especially in view of the proximity of the Encounter Bay Granites to 446, the nature of the zoning in the garnets can not be directly compared. Analysis of garnets and associated minerals in the intervening parts of the type section are clearly required.

TABLE E1

The total-rock and mineral chemistry of calc-silicate SC-1 from the Carrickalinga Head Formation

	TR	GARNET		GARNET		CHL*	HBL**
		core	rim	core	rim		
SiO_2	61.7	37.1	37.0	36.4	37.2	24.3	41.7
Al_2O_3	14.3	21.1	21.4	21.4	21.6	21.5	15.4
TiO_2	0.71	-	-	-	-	0.15	0.44
MnO	0.41	11.2	9.86	11.4	8.47	0.47	0.75
Total Fe as Fe_2O_3	5.64	-	-	-	-	-	-
Total Fe as FeO	-	21.2	20.7	21.4	20.3	22.0	15.7
MgO	2.60	1.32	1.30	1.36	1.47	16.4	8.6
CaO	9.19	7.69	9.11	7.66	10.9	0.10	12.4
Na_2O	1.00	-	-	-	-	0.19	1.45
K_2O	0.37	-	-	-	-	-	-
P_2O_5	0.20	-	-	-	-	-	-
Ignition loss	2.98	-	-	-	-	-	-
TOTAL	99.1	99.6	99.4	99.6	99.9	85.1	96.4
Sr ppm	270						
Rb ppm	50						
Structural formulae							
Si		5.98	5.95	5.89	5.92	5.22	6.29
Al		0.02	0.05	0.11	0.08	2.78	1.71
Tetrahedral		6.00	6.00	6.00	6.00	8.00	8.00
Al		3.99	4.01	3.96	3.98	2.65	1.02
Ti		-	-	-	-	0.02	0.05
Estimated Fe^{+3}		0.02	0.01	0.12	0.07	-	-
Fe^{+2}		2.83	2.78	2.78	2.64	3.96	1.98
Mg		0.32	0.31	0.33	0.35	5.26	1.93
Mn		1.53	1.34	1.57	1.14	0.09	0.10
Y		4.01	4.02	4.08	4.05	-	5.09
Ca		1.33	1.57	1.33	1.87	0.02	2.00
Na		-	-	-	-	0.08	0.21
X		6.00	6.00	6.00	6.00	-	2.21
X+Y						12.08	
Proportions of garnet end-members							
Almandine		46.9	46.2	45.4	43.4		
Spessartite		25.4	22.3	25.6	18.8		
Pyrope		5.3	5.2	5.4	5.8		
Grandrite		22.4	26.3	23.6	32.0		
(Andradite)		0.4	0.2	1.9	1.2		

* Chlorite - average of 3 spot analyses (ripidolite)

** Hornblende - average of 4 spot analyses

Structural formulae calculations:
garnet - basis of 24 oxygen atoms
chlorite - basis of 28 oxygen atoms
hornblende - basis of 23 oxygen atoms

Total-rock X-ray fluorescence analysis by I.C. Madsen
Electron microprobe analyses of minerals by A.R. Milnes

TABLE E2

The total-rock and mineral chemistry of calc-silicate SC-2 from the Carrickalinga Head Formation

	TR	GARNET		GARNET		CHL*	HBL**
		core	rim	core	rim		
SiO_2	65.0	36.4	36.3	36.8	36.5	23.9	41.7
Al_2O_3	14.1	21.2	21.1	21.2	21.5	21.7	15.1
TiO_2	0.74	0.10	0.21	0.14	0.09	0.10	0.32
MnO	0.31	12.5	8.85	12.0	8.67	0.29	0.53
Total Fe as Fe_2O_3	6.94	-	-	-	-	-	-
Total Fe as FeO	-	19.9	21.6	23.3	24.0	22.7	15.0
MgO	3.17	1.21	1.25	1.62	1.78	15.8	8.8
CaO	4.37	8.05	10.0	5.11	7.04	0.01	12.1
Na_2O	1.00	0.01	0.04	0.04	0.02	0.02	1.25
K_2O	0.42	-	-	-	-	-	-
P_2O_5	0.21	-	-	-	-	-	-
Ignition loss	3.44	-	-	-	-	-	-
TOTAL	99.7	99.4	99.4	100.2	99.6	84.5	94.8
Sr ppm	108						
Rb ppm	14						
Structural formulae							
Si		5.90	5.86	5.94	5.89	5.18	6.35
Al		0.10	0.14	0.06	0.11	2.82	1.65
Tetrahedral		6.00	6.00	6.00	6.00	8.00	8.00
Al		3.95	3.90	3.97	3.98	2.73	1.07
Ti		0.01	0.02	0.02	0.01	0.02	0.04
Estimated Fe^{+3}		0.10	0.18	0.04	0.07	-	-
Fe^{+2}		2.59	2.75	3.09	3.17	4.12	1.91
Mg		0.29	0.30	0.39	0.43	5.11	2.00
Mn		1.72	1.21	1.63	1.19	0.05	0.07
Y		4.06	4.10	4.03	4.06	-	5.08
Ca		1.40	1.74	0.88	1.22	tr	1.98
Na		tr	tr	tr	tr	0.01	0.18
X		6.00	6.00	6.00	6.00	-	2.17
X+Y						12.03	
Proportions of garnet end-members							
Almandine		42.4	44.4	51.1	52.1		
Spessartite		28.2	19.6	27.0	19.5		
Pyrope		4.8	4.9	6.4	7.1		
Grandrite		24.7	31.2	15.5	21.3		
(Andradite)		1.8	3.2	1.0	1.3		

* Chlorite - average of 4 spot analyses (ripidolite)
** Hornblende - average of 5 spot analyses

Structural formula calculations: see Table E1

Total-rock X-ray fluorescence analysis by I.C. Madsen
Electron microprobe analyses of minerals by A.R. Milnes

TABLE E3

The total-rock and mineral chemistry of calc-silicate SC-3 from the Carrickalinga Head Formation

	TR	GARNET		GARNET		CHL*	HBL**
		core	rim	core	rim		
SiO_2	66.0	36.3	36.9	36.3	36.7	24.2	41.1
Al_2O_3	13.5	21.0	21.4	21.2	21.5	21.9	16.0
TiO_2	0.66	0.27	0.15	0.32	0.23	0.14	0.44
MnO	0.34	14.2	9.05	16.3	10.2	0.44	0.91
Total Fe as Fe_2O_3	5.92	-	-	-	-	-	-
Total Fe as FeO	-	19.0	26.0	18.5	22.4	23.1	17.0
MgO	2.50	1.09	2.09	1.01	1.75	15.8	7.6
CaO	6.62	9.08	5.86	7.92	8.24	0.07	12.2
Na_2O	1.70	0.00	0.12	0.05	0.09	0.09	1.50
K_2O	0.27	-	-	-	-	-	-
P_2O_5	0.13	-	-	-	-	-	-
Ignition loss	1.57	-	-	-	-	-	-
TOTAL	99.2	100.9	101.6	101.6	101.1	85.7	96.8
Sr ppm	235						
Rb ppm	14						
Structural formulae							
Si		5.83	5.88	5.81	5.85	5.18	6.22
Al		0.17	0.12	0.19	0.15	2.82	1.78
Tetrahedral		6.00	6.00	6.00	6.00	8.00	8.00
Al		3.81	3.89	3.82	3.89	2.72	1.08
Ti		0.03	0.02	0.04	0.03	0.02	0.05
Estimated Fe^{+3}		0.30	0.18	0.29	0.18	-	-
Fe^{+2}		2.25	3.28	2.19	2.80	4.14	2.15
Mg		0.26	0.50	0.24	0.42	5.04	1.70
Mn		1.92	1.22	2.21	1.37	0.08	0.12
Y		4.15	4.10	4.14	4.10	-	5.10
Ca		1.56	1.00	1.36	1.41	0.02	1.98
Na		0.00	tr	tr	tr	0.04	0.22
X		6.00	6.00	6.00	6.00	-	2.20
X+Y						12.05	
Proportions of garnet end-members							
Almandine		35.6	52.9	34.6	45.2		
Spessartite		30.4	19.7	35.0	22.1		
Pyrope		4.1	8.0	3.8	6.7		
Grandrite		29.9	19.4	26.6	26.0		
(Andradite)		5.2	3.3	5.1	3.3		

* Chlorite - average of 5 spot analyses (ripidolite)
** Hornblende - average of 7 spot analyses

Structural formula calculations: see Table E1

Total-rock X-ray fluorescence analysis by I.C. Madsen
Electron microprobe analyses of minerals by A.R. Milnes

TABLE E4

Electron probe microanalyses of garnet in metasiltstone SC-4 from the Carrickalinga Head Formation

		GARNET		GARNET		GARNET	
		core	rim	core	rim	core	rim
	SiO_2	36.4	36.7	36.6	36.3	36.6	36.7
	Al_2O_3	21.3	21.6	21.5	21.6	21.4	21.8
	TiO_2	0.21	0.08	0.22	0.08	0.15	0.09
	MnO	10.9	10.4	10.7	10.0	11.4	9.01
Total Fe as	FeO	21.5	23.5	21.1	23.9	21.5	24.4
	MgO	1.52	1.69	1.48	1.66	1.49	1.81
	CaO	7.43	6.55	8.12	6.33	7.25	6.24
	Na_2O	0.02	0.00	0.04	0.03	0.09	0.04
	TOTAL	99.3	100.5	99.8	99.9	99.9	100.1
Structural formulae							
	Si	5.89	5.88	5.89	5.86	5.91	5.90
	Al	0.11	0.12	0.11	0.14	0.09	0.10
Tetrahedral		6.00	6.00	6.00	6.00	6.00	6.00
	Al	3.96	3.97	3.96	3.97	3.96	4.02
	Ti	0.03	0.01	0.03	0.01	0.02	0.01
Estimated	Fe^{+3}	0.07	0.09	0.05	0.10	0.07	0.00
	Fe^{+2}	2.84	3.06	2.78	3.13	2.83	3.27
	Mg	0.37	0.40	0.35	0.40	0.36	0.43
	Mn	1.50	1.41	1.46	1.38	1.56	1.22
	Y	4.05	4.07	4.05	4.07	4.05	4.10
	Ca	1.29	1.12	1.40	1.10	1.25	1.07
	Na	tr	0.00	tr	tr	tr	tr
	X	6.00	6.00	6.00	6.00	6.00	6.00
Proportions of end-members							
Almandine		46.6	50.2	45.8	51.2	46.6	53.8
Spessartite		24.6	23.2	24.1	22.5	25.6	20.2
Pyrope		6.0	6.6	5.8	6.5	5.9	7.1
Grandrite		22.7	20.0	23.4	19.7	22.0	18.9
(Andradite)		1.6	1.6	1.3	1.7	1.4	1.3

Structural formulae calculated on the basis of 24 oxygen atoms

Analyst: A.R. Milnes

TABLE E5

Electron probe microanalyses of garnet in metasiltstone 446 from the Petrel Cove Formation

		GARNET		GARNET	
		core	rim	core	rim
	SiO	36.3	36.5	36.3	36.7
	Al O	21.6	21.7	21.5	21.3
	TiO	0.07	0.03	0.02	0.02
	MnO	7.51	7.69	7.33	7.91
Total Fe as	FeO	27.3	27.7	27.2	27.7
	MgO	1.79	2.48	1.88	2.36
	CaO	5.04	3.51	5.34	3.55
	Na O	0.05	0.10	0.10	0.06
	TOTAL	99.7	99.7	99.7	99.6
Structural formulae					
	Si	5.88	5.89	5.88	5.94
	Al	0.12	0.11	0.12	0.06
Tetrahedral		6.00	6.00	6.00	6.00
	Al	4.00	4.03	3.99	4.01
Estimated	Fe^{+}	0.04	0.00	0.07	0.02
	Fe^{+}	3.66	3.74	3.61	3.73
	Mg	0.43	0.60	0.45	0.57
	Mn	1.03	1.05	1.01	1.08
	Y	4.05	4.03	4.06	4.03
	Ca	0.88	0.61	0.93	0.62
	Na				
	X	6.00	6.00	6.00	6.00
Proportions of end-members					
Almandine		60.5	62.3	59.6	62.0
Spessartite		17.0	17.5	16.6	18.0
Pyrope		7.1	9.9	7.5	9.5
Grandrite		15.3	10.2	16.4	10.6
(Andradite)		0.9	0.2	1.1	0.3

Structural formulae calculated on the basis of 24 oxygen atoms

Analyst: A.R. Milnes

Graphical representation of zoning in garnet porphyroblasts in Kanmantoo Group metasediments from the type section. Calculated from data in tables **E1-E5.**

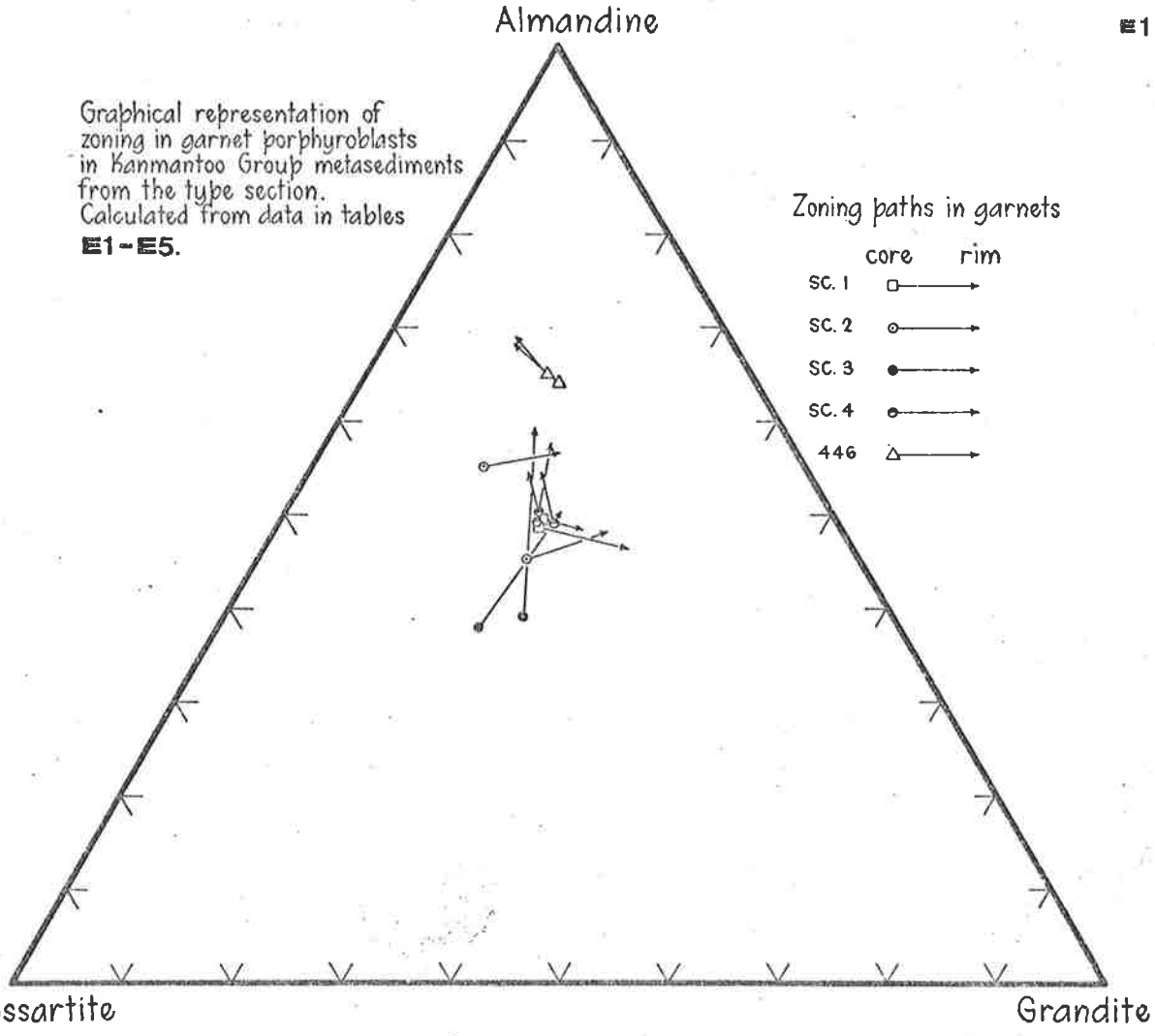

APPENDIX F

Techniques of macro-modal analysis of varieties of the Encounter Bay Granites

Stained slabs were prepared for macro-modal analysis of the major varieties of the Encounter Bay Granites because of their medium to coarse grain size. The slabs were cut serially from 5-10kgm samples of the granites. The large sample size was required in order that the sample might be representative of the granite in the locality from which it was collected. Successive faces of the slabs were partly polished, and then stained with sodium cobalti-nitrite after etching with hydrofluoric acid (Bailey and Stevens, 1960; Broch, 1961).

The megacrystic granites contain fine to medium grained groundmass crystals of potash feldspar, plagioclase, quartz and biotite, as well as coarse grained megacrysts of potash feldspar, plagioclase and quartz. The average grain diameters of these minerals intersected in linear traverses across the stained slabs are generally less than 5mm in the megacrystic granites, and are always less than 5mm in the medium grained granites (see discussion of the "mean intercept i" by Bayly, 1965). Following the discussion of van der Plas and Tobi (1965), a counting interval of 5mm was selected in order to achieve a balance between the number of non-correlated counts required for a low counting error, and the area to be counted for a low sampling error.

Each slab was attached to a glass plate on to which a 5mm grid had been drawn. A binocular microscope was then used to count sufficient points to achieve a counting error of about 2% (see van der Plas and Tobi, 1965, page 88) for potash feldspar, which forms between 20% and 40% of the specimens examined, by identifying the crystals that occurred at the intersection of the grid lines. The results of these analyses are given in Tables F1-F3. The analyses are considered to be representative of the granite specimens. For example, replicate analyses of one specimen of border facies megacrystic granite indicate a coefficient of variation of the modal composition of all minerals of less than 2%.

TABLE F1

Macro-modal analyses of specimens of the border facies megacrystic granite from the Encounter Bay area

	4-61	4-64	4-100	4-101	3-26	3-28	3-30
Potash feldspar	32.9	40.2	32.4	32.6	37.5	22.8	29.0
Plagioclase	27.0	21.6	23.1	22.7	29.0	26.9	25.9
Quartz	25.8	30.0	33.0	31.4	25.6	32.2	27.8
Biotite	14.3	8.2	11.5	13.3	7.9	18.1	17.3
No. points counted	1719	1817	2021	684	1437	1579	1257
Equivalent area (cm^2)	430	454	505	171	359	395	314
2-sigma counting error for potash feldspar	2.3	2.3	2.1	3.5	2.5	2.0	2.7

	3-33	3-35	3-41	3-42	8-14	8-15	7-52
Potash feldspar	24.4	30.1	31.5	27.0	31.5	33.3	29.2
Plagioclase	26.4	23.6	21.6	24.2	24.2	23.2	25.4
Quartz	33.2	31.3	32.2	31.1	29.5	28.3	27.9
Biotite	16.0	15.0	14.7	17.7	14.8	15.2	17.5
No. points counted	1871	2409	1160	592	1996	2260	1930
Equivalent area (cm^2)	468	602	290	148	499	565	483
2-sigma counting error for potash feldspar	2.0	1.8	2.8	3.7	2.1	2.0	2.1

	7-57	7-58	9-6	9-11	9-13	*7-56
Potash feldspar	27.1	20.2	28.4	34.1	26.1	27.7
Plagioclase	27.4	28.7	27.0	24.8	29.3	15.1
Quartz	28.3	33.0	27.8	26.2	28.2	43.5
Biotite	17.2	18.1	16.8	15.0	16.4	13.7
No. points counted	2962	2399	2746	1824	1497	1936
Equivalent area (cm^2)	741	600	687	456	374	484
2-sigma counting error for potash feldspar	1.7	1.7	1.7	2.2	2.2	2.0

Prefices on specimen numbers have the following locality key:

4- Port Elliot (Figure 19)
3- Granite Island (Figure 21)
8- Wright Island (Figure 11)
7- Rosetta Head (Figure 12)
9- West Island (Figure 22)

*Fine to medium grained granite sheet within Petrel Cove Formation metasediments adjacent to contact with the main mass of border facies megacrystic granite at Rosetta Head

TABLE F2

Macro-modal analyses of specimens of inner facies megacrystic granite

	4-78	4-79	4-80	4-81	4-86	4-87
Potash feldspar	38.9	37.1	38.9	40.4	35.7	35.9
Plagioclase	18.1	18.9	19.5	16.5	20.1	21.5
Quartz	35.2	34.1	34.7	34.2	31.7	32.0
Biotite	7.8	9.9	6.9	8.9	12.5	10.6
No. points counted	2078	1922	3012	1706	1869	2454
Equivalent area (cm^2)	520	481	753	427	467	614
2-sigma counting error for potash feldspar	2.2	2.2	1.8	2.3	2.2	1.9

	4-88	4-92	4-93	4-95	4-98	4-99
Potash feldspar	38.8	42.1	34.7	36.0	42.0	36.4
Plagioclase	19.9	18.0	21.8	19.7	17.8	17.8
Quartz	31.6	32.2	34.1	36.5	31.4	36.5
Biotite	9.7	7.7	9.4	7.8	8.8	9.3
No. points counted	2635	2777	2305	2987	741	1684
Equivalent area (cm^2)	659	694	576	747	185	421
2-sigma counting error for potash feldspar	1.9	1.9	2.0	1.8	3.6	2.4

All specimens collected from Port Elliot (Figure 19)

TABLE F3

Macro-modal analyses of medium even-grained granites from the Encounter Bay area

	4-10	4-15	4-53	4-59	4-103	*4-89
Potash feldspar	39.4	43.4	44.8	45.0	42.2	44.4
Plagioclase	20.4	18.0	21.1	16.7	18.3	18.4
Quartz	36.1	33.9	29.8	34.3	34.7	31.4
Biotite	4.1	4.7	4.3	4.0	4.8	5.8
No. points counted	1890	1609	802	1687	1882	756
Equivalent area (cm^2)	473	402	201	422	471	189
2-sigma counting error for potash feldspar	2.2	2.6	3.5	2.6	2.3	3.8

All specimens collected from Port Elliot (Figure 19)

*Collected from transition zone between red leucogranite and medium even-grained granite represented by 4-10

APPENDIX G

Methods of sample preparation, and the techniques of chemical analysis of specimens of the Encounter Bay Granites and associated rocks

Significant sampling errors may arise during the collection of specimens of coarse grained granitic and other rocks for chemical analysis because the specimens may be too small to be representative of the rock mass from which they were collected. This problem is likely to be accentuated in the case of coarse grained megacrystic granites in which large feldspars, quartz and other crystals may occur sporadically throughout the groundmass of the rock. Baird et al (1964) and Baird, McIntyre and Welday (1967) found that diamond drill cores 30cm long and 2cm in diameter overcame this problem in the case of coarse grained granites from the Rattlesnake Mountain Pluton in California. In the present investigation, the megacrystic granites and other rocks such as the albitised megacrystic granites and the hybrid granites were potentially subject to the most serious sampling errors. In order to minimise these errors, large samples of fresh rock weighing up to 10kgm were collected in the field. However, samples of the finer grained granites did not exceed 4kgm in weight and may have been as small as 2kgm, whereas samples of Kanmantoo Group metasedimentary rocks were not greater than about 1kgm.

Each of the samples collected in the field was cut into 1-2cm thick slabs in the laboratory using a 46cm diameter diamond-tipped circular saw. Several slabs were set aside for macro-modal analysis. The remainder were stripped of weathered edges, carefully scrubbed in running water, allowed to dry, and were then crushed without loss to pebble-sized fragments in a screw-press with stainless steel plates. Up to 3.8kgm of each sample was crushed in this manner. Subsequent steps in sample preparation are illustrated in the accompanying diagram. In the case of specimens of Kanmantoo Group metasedimentary rocks and of the fine grained varieties of the Encounter Bay Granites however, the weight of slabs crushed may have been as low as 500-1000gms, and therefore the first and second stages of sample splitting were omitted.

The total-rock specimens prepared as described in the preceding paragraph were analysed for the elements reported in the following Tables by X-ray fluorescence spectrography. Fused glass discs composed of rock powder mixed with lithium borate and lanthanum oxide, and pressed mounts of rock powder, were analysed according to the techniques

described by Norrish and Chappell (1967) and Norrish and Hutton (1969). The glass discs were analysed for Si, Al, Ti, Mn, Fe, Mg, Ca, K and P against an artificial counting standard of accurately known composition kindly supplied by Dr. K. Norrish of C.S.I.R.O. Division of Soils. Standard U.S.G.S. rocks (Flanagan, 1969) were analysed with the unknown samples as a check on the techniques. Analyses for Na were carried out on pressed powder mounts using a sodium glass disc that had been carefully calibrated against the available U.S.G.S. standard rocks and feldspars as a standard. Analyses for Rb and Sr were also carried out on pressed powder mounts using the U.S.G.S. feldspar NBS70a as a standard (see Compston et al, 1969). Loss on ignition was determined by heating a 0.5-1.0gm sample in an electric furnace at 1000°C to constant weight.

The analyses were carried out on a Phillips PW1540 X-ray spectrograph coupled to a 3Kw PW1140 generator.

The analytical results are given, together with CIPW norms, in the following Tables, and are reported to within calculated counting error. In the CIPW norm calculations, 25% of the total Fe present in the samples was assumed to be Fe_2O_3 and the remainder was assigned to FeO. This assumption is consistent with the Fe_2O_3 and FeO values reported for similar rocks in previously published wet chemical analyses also given in the Tables.

Diagrammetric representation of method of sample preparation

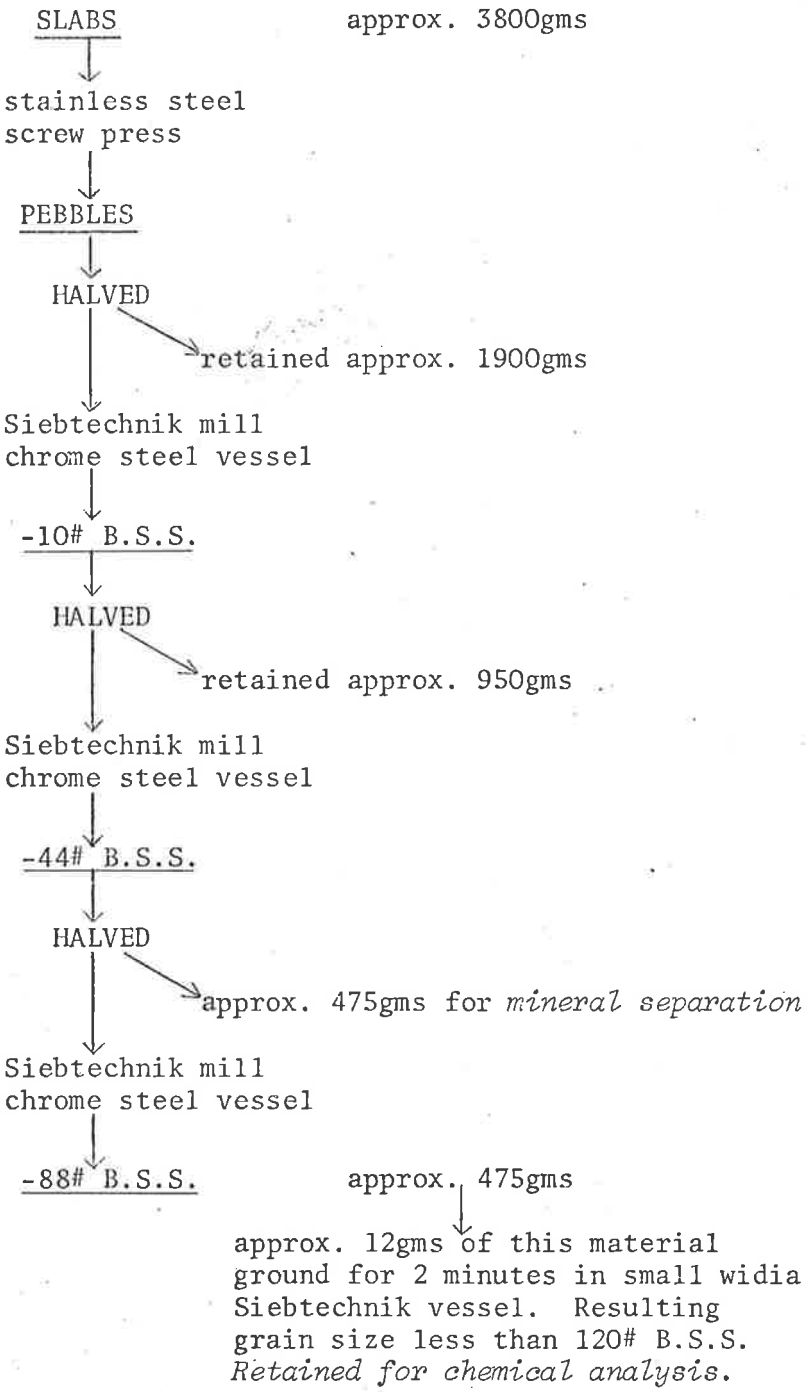

TABLE G1

Chemical analyses of specimens of the border facies megacrystic granite from the Encounter Bay area

		4-55	4-61	4-64	4-102	3-26	3-28	3-30
	SiO_2	76.3	72.9	73.3	71.5	72.8	72.1	71.4
	Al_2O_3	12.3	13.3	12.5	13.6	12.8	13.3	13.5
	TiO_2	0.17	0.38	0.32	0.33	0.33	0.44	0.47
	MnO	0.02	0.04	0.05	0.07	0.05	0.08	0.10
Total Fe as	Fe_2O_3	1.39	2.36	2.34	3.40	2.18	3.08	3.30
	FeO	-	-	-	-	-	-	-
	MgO	0.4	1.3	0.8	0.7	1.3	1.2	1.2
	CaO	1.24	1.26	0.89	1.15	1.47	1.74	1.74
	Na_2O	3.1	4.8	2.9	3.1	2.6	2.8	2.6
	K_2O	3.59	2.17	5.49	5.79	4.64	4.65	4.90
	P_2O_5	0.08	0.07	0.07	0.08	0.00	0.10	0.03
	H_2O^+	-	-	-	-	-	-	-
	H_2O^-	-	-	-	-	-	-	-
Ignition loss		0.68	0.72	0.68	0.75	0.73	0.55	0.52
	TOTAL	99.3	99.3	99.3	100.5	98.9	100.0	99.8
	Sr ppm	74	117	54	62	100	110	114
	Rb ppm	258	96	388	442	184	221	227
	K/Rb	115.5	187.6	117.5	108.7	209.3	174.7	179.2
CIPW norm								
	Q	40.7	31.2	31.6	26.7	33.8	31.8	30.3
	C	1.2	0.9	0.4	0.4	0.7	0.8	0.8
	Or	21.2	12.8	32.5	34.2	27.4	27.5	29.0
	Ab	26.6	40.7	24.6	26.2	22.3	23.4	22.3
	An	5.6	5.8	4.0	5.2	7.3	8.0	8.4
	Hy En	1.0	3.3	1.9	1.8	3.3	3.0	3.6
	Fs	1.2	1.9	2.0	3.1	1.8	2.6	2.8
	Mt	0.5	0.9	0.8	1.2	0.8	1.1	1.2
	Il	0.3	0.7	0.6	0.6	0.6	0.8	0.9
	Ap	0.2	0.2	0.2	0.2	-	0.2	0.1
	D.I.	88.5	84.8	88.6	87.0	83.5	82.7	81.5
Norm. An%		17.5	12.5	13.9	16.5	24.6	25.5	27.5

TABLE G1 (Cont'd)

Chemical analyses of specimens of the border facies megacrystic granite from the Encounter Bay area

		3-32	3-33	3-35	3-36	A	8-12	8-14
	SiO_2	72.8	70.0	72.0	71.3	68.20	79.4	70.2
	Al_2O_3	12.5	13.6	13.3	13.3	15.99	10.6	13.1
	TiO_2	0.43	0.52	0.52	0.60	0.58	0.31	0.52
	MnO	0.06	0.09	0.09	0.09	0.04	0.06	0.06
Total Fe as	Fe_2O_3	2.90	3.58	3.31	3.80	0.89*	2.79	3.45
	FeO	-	-	-	-	2.58	-	-
	MgO	1.1	1.5	1.4	1.6	0.80	1.0	1.2
	CaO	0.98	1.89	1.47	1.82	2.61	1.73	1.51
	Na_2O	2.6	2.7	2.5	2.6	2.85	2.4	2.6
	K_2O	5.30	4.54	5.55	5.01	4.60	1.54	5.44
	P_2O_5	0.09	0.11	0.13	0.13	0.14	0.08	0.12
	H_2O^+	-	-	-	-	0.64	-	-
	H_2O^-	-	-	-	-	0.21	-	-
Ignition loss		0.91	0.82	0.58	0.49	-	0.62	0.46
	TOTAL	99.7	99.4	100.9	100.7	100.13	100.5	98.7
	Sr ppm	80	113	113	120	-	123	88
	Rb ppm	356	214	249	230	-	78	265
	K/Rb	123.6	176.1	185.0	180.8	-	163.9	170.4
CIPW norm								
	Q	32.7	29.4	30.1	29.7	26.2	53.5	28.2
	C	0.9	1.1	0.8	0.6	1.9	2.0	0.5
	Or	31.3	26.8	32.8	29.6	27.2	9.1	32.2
	Ab	22.3	23.1	21.2	21.8	24.1	20.1	22.1
	An	4.3	8.7	6.4	8.2	12.0	8.1	6.7
	Hy En	2.7	3.7	3.6	4.0	2.0	2.5	3.0
	Fs	2.4	3.0	2.7	3.1	3.1	2.5	2.8
	Mt	1.1	1.3	1.2	1.4	1.3	1.0	1.3
	Il	0.8	1.0	1.0	1.1	1.1	0.6	1.0
	Ap	0.2	0.3	0.3	0.3	0.3	0.2	0.3
	D.I.	86.4	79.3	84.0	81.2	77.5	82.8	82.4
Norm. An%		16.1	27.3	23.4	27.3	33.3	28.6	23.3

TABLE G1 (Cont'd)

Chemical analyses of specimens of the border facies megacrystic granite from the Encounter Bay area

		8-15	8-16	7-52	7-56	7-57	7-58	B
	SiO_2	71.5	74.6	70.9	69.1	70.3	70.5	71.45
	Al_2O_3	13.0	12.6	13.4	13.7	14.0	13.8	13.78
	TiO_2	0.55	0.44	0.45	0.66	0.57	0.60	0.54
	MnO	0.06	0.06	0.06	0.06	0.06	0.06	0.01
Total Fe as	Fe_2O_3	3.34	3.22	3.35	4.80	3.64	3.65	0.08*
	FeO	-	-	-	-	-	-	2.79
	MgO	1.1	1.1	1.5	2.0	1.4	1.4	1.11
	CaO	1.49	1.07	1.56	1.79	1.70	1.54	1.86
	Na_2O	2.4	2.8	2.6	2.3	2.5	2.9	2.74
	K_2O	5.31	2.64	5.28	4.48	5.08	4.24	4.35
	P_2O_5	0.14	0.08	0.09	0.09	0.13	0.13	0.14
	H_2O^+	-	-	-	-	-	-	0.48
	H_2O^-	-	-	-	-	-	-	0.11
Ignition loss		0.53	0.99	0.52	0.58	0.60	0.91	-
	TOTAL	99.4	99.6	99.7	99.6	100.0	99.7	99.44
	Sr ppm	97	127	119	123	125	146	-
	Rb ppm	246	127	226	230	228	192	-
	K/Rb	179.2	172.6	193.9	161.7	185.0	183.3	-
CIPW norm								
	Q	31.2	43.4	29.2	30.3	29.4	30.9	31.7
	C	0.9	3.4	0.8	2.1	1.6	2.0	1.5
	Or	31.4	15.6	31.2	26.5	30.0	25.1	25.7
	Ab	20.7	23.6	21.7	19.3	21.3	24.8	23.2
	An	6.5	4.8	7.2	8.3	7.6	6.8	8.3
	Hy En	2.8	2.7	3.7	4.9	3.6	3.4	2.8
	Fs	2.6	2.7	2.8	4.0	2.9	2.9	4.2
	Mt	1.2	1.2	1.2	1.7	1.3	1.3	0.1
	Il	1.0	0.8	0.8	1.3	1.1	1.1	1.0
	Ap	0.3	0.2	0.2	0.2	0.3	0.3	0.3
	D.I.	83.3	82.6	82.1	76.1	80.8	80.8	80.6
Norm. An%		23.9	16.9	24.8	30.1	26.2	21.5	26.4

TABLE G1 (Cont'd)

Chemical analyses of specimens of the border facies megacrystic granite from the Encounter Bay area

		9-6	9-11	C
	SiO_2	70.7	74.0	71.44
	Al_2O_3	13.4	12.4	15.09
	TiO_2	0.57	0.43	0.53
	MnO	0.06	0.06	0.02
Total Fe as	Fe_2O_3	3.53	2.84	0.86*
	FeO	-	-	2.35
	MgO	1.2	1.4	0.80
	CaO	1.71	1.49	1.18
	Na_2O	2.7	2.4	2.1
	K_2O	5.12	4.77	4.46
	P_2O_5	0.13	0.09	0.22
	H_2O^+	-	-	0.24
	H_2O^-	-	-	0.04
Ignition loss		0.51	0.53	-
	TOTAL	99.6	100.4	99.33
	Sr ppm	103	91	-
	Rb ppm	236	226	-
	K/Rb	180.1	175.2	-
CIPW norm				
	Q	29.2	35.5	37.9
	C	0.7	0.8	5.2
	Or	30.3	28.2	26.4
	Ab	22.5	20.6	17.7
	An	7.6	6.8	4.4
	Hy En	3.1	3.5	2.0
	Fs	2.8	2.3	2.8
	Mt	1.3	1.0	1.3
	Il	1.1	0.8	1.0
	Ap	0.3	0.2	0.5
	D.I.	82.0	84.3	81.9
	Norm. An%	25.3	24.9	20.0

Specimen numbers have the following locality key:

4- Port Elliot (Figure 19)
3- Granite Island (Figure 21)
8- Wright Island (Figure 11)
7- Rosetta Head (Figure 12)
9- West Island (Figure 22)

These specimens were analysed using X-ray fluorescence techniques.

Analyst: A.R. Milnes

Specimen A - Granite Island. Analyst: W.R. Browne (Browne, 1920)
Specimen B - Rosetta Head. Analyst: D.R. Bowes (Bowes, 1954)
Specimen C - West Island. Analyst: W.S. Chapman (Mawson, 1926)

*Fe_2O_3

TABLE G2

Chemical analyses of specimens of the Cape Willoughby megacrystic granite

		W1	W3	W9	W15B	W20	W22	W24
	SiO_2	72.8	72.6	74.4	74.5	75.1	73.2	73.8
	Al_2O_3	13.1	12.9	13.1	12.6	12.4	12.4	12.9
	TiO_2	0.41	0.47	0.33	0.32	0.34	0.44	0.38
	MnO	0.06	0.07	0.03	0.05	0.03	0.06	0.06
Total Fe as	Fe_2O_3	2.72	2.74	2.36	2.13	2.51	3.11	2.33
	FeO	-	-	-	-	-	-	-
	MgO	1.0	1.2	0.6	0.5	0.9	0.9	1.0
	CaO	1.31	1.25	1.31	0.66	1.24	1.42	1.15
	Na_2O	3.4	3.5	3.8	3.3	3.2	3.6	3.6
	K_2O	4.48	4.63	4.08	5.17	4.24	3.94	4.74
	P_2O_5	0.06	0.11	0.08	0.05	0.07	0.09	0.07
	H_2O^+	-	-	-	-	-	-	-
	H_2O^-	-	-	-	-	-	-	-
Ignition loss		0.53	0.57	0.48	0.64	0.51	0.41	0.63
	TOTAL	99.9	100.0	100.6	99.9	100.5	99.6	100.7
	Sr ppm	122	154	154	104	105	116	148
	Rb ppm	193	193	150	221	183	196	198
	Kb/Rb	192.7	199.1	225.8	194.2	192.3	169.5	198.7
CIPW norm								
	Q	39.9	29.4	32.3	32.6	35.6	32.0	29.9
	C	0.5	0.1	0.2	0.4	0.4	0.0	0.0
	Or	26.5	27.4	24.1	30.6	25.1	23.3	28.0
	Ab	28.4	29.5	32.2	28.0	26.9	30.2	30.8
	An	6.1	5.5	6.0	2.9	5.7	6.2	4.8
	Di Wo	0.0	0.0	0.0	0.0	0.0	0.1	0.2
	En	0.0	0.0	0.0	0.0	0.0	0.0	0.1
	Fs	0.0	0.0	0.0	0.0	0.0	0.1	0.1
	Hy En	2.5	3.1	1.5	1.4	2.2	2.3	2.4
	Fs	2.3	2.2	1.9	1.8	2.1	2.6	1.8
	Mt	1.0	1.0	0.9	0.8	0.9	1.1	0.8
	Il	0.8	0.9	0.6	0.6	0.7	0.8	0.7
	Ap	0.1	0.3	0.2	0.1	0.2	0.2	0.2
	D.I.	85.8	86.2	88.6	91.1	87.6	85.5	88.8
Norm. An%		17.7	15.7	15.7	9.5	17.5	17.1	13.5

TABLE G2 (Cont'd)

Chemical analyses of specimens of the Cape Willoughby megacrystic granite

		W32	W36A
	SiO_2	73.8	74.4
	Al_2O_3	13.1	12.5
	TiO_2	0.35	0.36
	MnO	0.04	0.05
Total Fe as	Fe_2O_3	2.06	2.35
	FeO	-	-
	MgO	0.7	0.9
	CaO	1.33	0.90
	Na_2O	3.6	3.1
	K_2O	4.65	4.75
	P_2O_5	0.06	0.05
	H_2O^+	-	-
	H_2O^-	-	-
Ignition loss		0.62	0.55
	TOTAL	100.3	99.9
	Sr ppm	164	156
	Rb ppm	184	204
	K/Rb	209.8	193.3
CIPW norm			
	Q	30.9	33.9
	C	0.0	0.7
	Or	27.5	28.1
	Ab	30.0	26.6
	An	6.0	4.1
	Di Wo	0.1	0.0
	En	0.1	0.0
	Fs	0.1	0.0
	Hy En	1.7	2.3
	Fs	1.6	1.9
	Mt	0.8	0.9
	Il	0.7	0.7
	Ap	0.1	0.1
	D.I.	88.4	88.5
	Norm. An%	16.6	13.5

All specimens were analysed using X-ray fluorescence techniques.

Analyst: A.R. Milnes

TABLE G3

Chemical analyses of specimens of the inner facies megacrystic granite

		4-78	4-79	4-80	4-81	4-86	4-87	4-88
	SiO_2	73.5	72.9	74.5	74.7	73.9	73.8	73.1
	Al_2O_3	12.5	12.4	12.3	12.8	13.0	12.9	12.6
	TiO_2	0.34	0.37	0.28	0.38	0.37	0.40	0.36
	MnO	0.04	0.05	0.04	0.04	0.05	0.05	0.05
Total Fe as	Fe_2O_3	2.27	2.44	2.03	2.45	2.70	2.77	2.38
	FeO	-	-	-	-	-	-	-
	MgO	0.9	0.8	0.8	0.7	1.1	0.9	1.0
	CaO	0.90	1.00	0.93	0.87	0.91	1.17	0.94
	Na_2O	2.6	2.6	2.7	2.8	2.5	2.6	2.7
	K_2O	5.56	5.05	5.66	5.34	5.54	5.42	5.61
	P_2O_5	0.07	0.07	0.05	0.10	0.06	0.09	0.08
	H_2O^+	-	-	-	-	-	-	-
	H_2O^-	-	-	-	-	-	-	-
Ignition loss		0.54	1.00	0.53	0.67	0.63	0.76	0.51
	TOTAL	99.2	98.7	99.8	100.9	100.8	100.9	99.3
	Sr ppm	57	57	55	65	66	65	64
	Rb ppm	353	325	377	321	354	349	344
	K/Rb	130.7	129.0	124.6	138.1	129.9	128.9	135.4
CIPW norm								
	Q	33.2	34.4	33.4	34.4	33.5	33.3	31.4
	C	0.7	1.0	0.2	1.1	1.4	0.9	0.5
	Or	32.9	29.8	33.5	31.6	32.7	32.0	33.2
	Ab	22.1	22.0	22.9	23.8	21.3	22.1	23.2
	An	4.0	4.5	4.3	3.7	4.1	5.2	4.1
	Hy En	2.2	2.0	1.9	1.8	2.8	2.1	2.6
	Fs	1.9	2.0	1.7	2.0	2.3	2.3	2.0
	Mt	0.8	0.9	0.7	0.9	1.0	1.0	0.9
	Il	0.7	0.7	0.5	0.7	0.7	0.8	0.7
	Ap	0.2	0.2	0.1	0.2	0.1	0.2	0.2
	D.I.	88.1	86.2	89.7	89.7	87.6	87.4	87.8
Norm. An%		15.4	17.0	15.8	13.4	16.2	19.1	15.2

TABLE G3 (Cont'd)

Chemical analyses of specimens of the inner facies megacrystic granite

		4-92	4-93	4-95	4-97
	SiO_2	74.3	75.5	74.3	72.4
	Al_2O_3	12.3	11.9	12.2	12.6
	TiO_2	0.26	0.36	0.35	0.42
	MnO	0.04	0.05	0.05	0.05
Total Fe as	Fe_2O_3	2.18	2.56	2.35	2.93
	FeO	-	-	-	-
	MgO	0.7	0.9	0.7	0.8
	CaO	0.87	1.05	0.96	1.07
	Na_2O	2.6	2.8	2.8	2.7
	K_2O	5.79	4.97	5.13	5.32
	P_2O_5	0.07	0.16	0.06	0.08
	H_2O^+	-	-	-	-
	H_2O^-	-	-	-	-
Ignition loss		0.56	0.54	0.54	0.23
	TOTAL	99.7	100.8	99.4	98.6
	Sr ppm	55	58	60	75
	Rb ppm	352	288	288	311
	K/Rb	136.5	143.2	147.9	142.0
CIPW norm					
	Q	33.1	36.4	34.5	32.2
	C	0.3	0.5	0.4	0.7
	Or	34.2	29.4	30.3	31.4
	Ab	22.3	23.3	23.8	22.5
	An	3.9	4.2	4.4	4.8
	Hy En	1.8	2.2	1.7	2.1
	Fs	1.9	2.2	2.0	2.4
	Mt	0.8	0.9	0.9	1.1
	Il	0.5	0.7	0.7	0.8
	Ap	0.2	0.4	0.1	0.2
	D.I.	89.7	89.1	88.6	86.1
Norm. An%		14.7	15.2	15.5	17.5

All specimens were collected from Port Elliot (Figure 19)
Specimens were analysed using X-ray fluorescence techniques.

Analyst: A.R. Milnes

TABLE G4

Chemical analyses of inclusions within the megacrystic granites in the Encounter Bay area

	Metasedimentary rock		Biotite-rich material	Granophyric leucogranites		
	A	B	9-8	4-41	4-95A	9-9
SiO_2	72.90	63.55	51.5	76.4	77.2	74.3
Al_2O_3	13.74	16.55	13.2	12.4	12.8	13.3
TiO_2	0.56	0.86	2.69	0.09	0.09	0.10
MnO	-	0.09	0.19	0.05	0.03	0.03
Total Fe as Fe_2O_3	0.04*	0.97*	16.7	0.97	0.58	0.48
FeO	3.29	4.67	-	-	-	-
MgO	1.85	3.12	6.1	0.2	0.4	0.2
CaO	2.12	3.11	1.42	0.32	0.29	0.42
Na_2O	3.02	3.33	0.6	3.5	3.8	2.5
K_2O	1.99	3.24	6.54	5.93	5.33	7.86
P_2O_5	0.15	0.19	0.74	0.07	0.13	0.15
H_2O^+	0.46	0.50	-	-	-	-
H_2O^-	0.11	0.10	-	-	-	-
Ignition loss	-	-	0.90	0.48	0.44	0.49
TOTAL	100.23	100.28	100.6	100.4	101.3	99.8
Sr ppm	-	-	35	49	40	105
Rb ppm	-	-	620	327	277	263
K/Rb	-	-	87.6	150.5	165.7	248.1
CIPW norm						
Q	38.5	18.0	3.9	32.2	32.9	28.6
C	3.1	2.3	4.2	0.0	0.3	0.2
Or	11.8	19.2	38.7	35.1	32.7	46.5
Ab	25.6	28.2	5.4	29.8	32.1	21.4
An	9.5	14.3	2.2	0.4	0.6	1.1
Di Wo	0.0	0.0	0.0	0.3	0.0	0.0
En	0.0	0.0	0.0	0.1	0.0	0.0
Fs	0.0	0.0	0.0	0.2	0.0	0.0
Hy En	4.6	7.8	15.1	0.4	1.0	0.5
Fs	5.1	6.5	19.4	0.7	0.5	0.4
Mt	0.1	1.4	2.4	0.4	0.2	0.2
Il	1.1	1.6	5.1	0.2	0.2	0.2
Ap	0.4	0.4	1.7	0.2	0.3	0.4
D.I.	75.8	65.4	48.0	97.1	97.7	96.4
Norm. An%	27.2	33.5	29.0	1.3	1.8	4.9

TABLE G4 (Cont'd)

Chemical analyses of inclusions within the megacrystic granites in the Encounter Bay area

		Fine grained megacrystic granites		Schist-like material
		4-36	4-97A	4-84
	SiO_2	74.6	74.4	46.5
	Al_2O_3	12.8	13.0	27.8
	TiO_2	0.45	0.49	0.20
	MnO	0.04	0.05	0.12
Total Fe as	Fe_2O_3	1.93	2.12	9.27
	FeO	-	-	-
	MgO	0.5	0.6	3.9
	CaO	0.31	0.37	0.42
	Na_2O	3.18	3.40	0.52
	K_2O	5.46	5.31	7.04
	P_2O_5	0.11	0.11	0.33
	H_2O^+	-	-	-
	H_2O^-	-	-	-
Ignition loss		0.91	1.00	4.85
	TOTAL	100.3	100.9	100.9
	Sr ppm	59	81	111
	Rb ppm	327	318	373
	K/Rb	138.6	138.6	156.7
CIPW norm				
	Q	33.5	32.2	
	C	1.3	1.2	
	Or	32.3	31.3	
	Ab	26.9	28.8	
	An	0.8	1.1	
	Di Wo	0.0	0.0	
	En	0.0	0.0	
	Fs	0.0	0.0	
	Hy En	1.3	1.5	
	Fs	1.3	1.5	
	Mt	0.7	0.8	
	Il	0.9	0.9	
	Ap	0.3	0.3	
	D.I.	92.6	92.4	
Norm. An%		3.0	3.7	

Specimen numbers have the following locality key:
4- Port Elliot (Figure 19)
9- West Island (Figure 22)
These specimens were analysed using X-ray diffraction techniques.
Analyst: A.R. Milnes

Specimens A and B - Granite Island. Analyst: A.W. Kleeman (Kleeman, 1937)

*Fe_2O_3

TABLE G5

Chemical analyses of specimens of albitised megacrystic granite and the megacrystic albite-chlorite rock from the Encounter Bay area

	albitised megacrystic granite		megacrystic albite-chlorite rock				
	7-53	7-55	3-40	7-54	A	B	C
SiO_2	70.6	76.0	65.4	61.9	56.24	59.00	58.63
Al_2O_3	13.5	11.7	17.5	19.5	19.75	19.41	20.10
TiO_2	0.63	0.39	0.74	0.75	0.98	0.72	0.73
MnO	0.06	0.02	0.04	0.01	0.01	0.04	0.04
Total Fe as Fe_2O_3	3.64	2.96	1.77	0.94	0.76*	0.34*	1.01*
FeO	-	-	-	-	1.63	3.59	2.08
MgO	2.8	1.0	3.2	3.3	7.00	6.44	6.15
CaO	0.58	1.52	0.57	0.63	0.75	1.00	1.09
Na_2O	4.1	3.2	8.7	10.1	8.62	6.42	6.95
K_2O	2.40	1.66	0.63	0.20	0.40	0.09	0.16
P_2O_5	0.10	0.12	0.16	0.21	0.19	0.18	0.20
H_2O^+	-	-	-	-	2.90	2.47	2.34
H_2O^-	-	-	-	-	0.09	0.09	0.06
Ignition loss	1.17	0.89	1.56	1.99	-	-	-
TOTAL	99.6	99.5	100.3	98.6	99.32	99.45	99.54
Sr ppm	76	129	91	118	-	-	-
Rb ppm	93	107	13	2	-	-	-
K/Rb	214.2	128.8	402.3	871.6	-	-	-
CIPW norm							
Q	31.4	45.4	6.7	0.0	0.0	7.7	5.8
C	3.4	2.1	1.9	2.1	4.2	7.4	7.0
Or	14.2	9.8	3.7	1.2	2.4	0.5	1.0
Ab	34.4	27.2	73.4	83.8	68.8	54.3	58.8
An	2.2	6.8	1.8	1.8	2.5	3.8	4.1
Hy En	6.9	2.5	7.9	0.0	0.0	16.0	15.3
Fs	2.8	2.5	0.7	0.0	0.0	5.2	1.9
Ol Fo	0.0	0.0	0.0	5.7	12.2	0.0	0.0
Fa	0.0	0.0	0.0	0.0	0.6	0.0	0.0
Mt	1.3	1.1	0.6	0.0	1.1	0.5	1.5
Il	1.2	0.7	1.4	1.3	1.9	1.4	1.4
Ap	0.2	0.3	0.4	0.5	0.4	0.4	0.5
D.I.	79.9	82.4	83.8	85.8	73.5	62.6	65.6
Norm. An%	6.1	19.9	2.4	2.1	3.5	6.5	6.5

TABLE G5 (Cont'd)

Chemical analyses of specimens of albitised megacrystic granite and the megacrystic albite-chlorite rock from the Encounter Bay area

	megacrystic albite-chlorite rock	
	D	E
SiO_2	59.49	64.60
Al_2O_3	21.16	21.37
TiO_2	-	1.04
MnO	-	-
Fe_2O_3	0.17	0.31
FeO	7.00	0.67
MgO	1.89	1.15
CaO	0.82	0.41
Na_2O	5.66	9.94
K_2O	0.84	0.16
P_2O_5	-	0.22
H_2O^+	2.98	0.85
H_2O^-	0.18	0.15
TOTAL	100.19	100.87
CIPW norm		
Q	13.0	4.0
C	9.5	3.5
Or	5.0	1.0
Ab	47.9	84.1
An	4.1	1.0
Hy En	4.7	2.9
Fs	12.7	0.0
Mt	0.3	0.0
Il	0.0	1.4
Hm	0.0	0.3
Ru	0.0	0.3
Ap	0.0	0.4
D.I.	65.9	89.1
Norm. An%	7.8	1.2

Specimen numbers have the following locality key:

7- Rosetta Head (Figure 12)

3- Granite Island (Figure 21)

These specimens were analysed using X-ray fluorescence techniques.
Analyst: A.R. Milnes

Specimens A, B and C - Rosetta Head. Analyst: D.R. Bowes (Bowes, 1954)
Specimen D - Rosetta Head. Analyst: B.F. Goode (Mawson, 1926)
Specimen E - Rosetta Head. Analyst: W.R. Browne (Browne, 1920)

*Fe_2O_3

TABLE G6

Chemical analyses of specimens of fine and medium even-grained granites from the Encounter Bay area

		medium grained granites						fine grained granites	
		4-10	4-15	4-59	4-75	4-103	A	4-52	9-2
	SiO_2	74.9	76.5	77.4	75.4	77.2	75.48	67.1	70.3
	Al_2O_3	12.2	11.7	11.6	11.8	11.5	12.99	14.2	13.7
	TiO_2	0.18	0.13	0.11	0.18	0.14	0.12	0.67	0.78
	MnO	0.04	0.03	0.04	0.04	0.03	-	0.07	0.07
Total Fe as	Fe_2O_3	1.52	1.01	1.06	1.67	1.04	0.25*	3.90	3.59
	FeO	-	-	-	-	-	0.85	-	-
	MgO	0.3	0.5	0.4	0.3	0.2	0.13	1.6	1.1
	CaO	0.64	0.48	0.46	0.52	0.68	0.74	2.85	1.80
	Na_2O	2.9	3.0	2.8	2.9	3.1	2.31	3.1	3.1
	K_2O	5.65	5.55	5.33	5.46	5.35	6.06	4.47	4.16
	P_2O_5	0.04	0.05	0.08	0.03	0.04	-	0.12	0.21
	H_2O^+	-	-	-	-	-	0.60	-	-
	H_2O^-	-	-	-	-	-	0.17	-	-
Ignition loss		0.63	0.46	0.46	0.61	0.35	-	0.80	0.80
	TOTAL	99.0	99.4	99.7	98.9	99.6	99.70	98.9	99.6
	Sr ppm	30	34	21	-	34	-	118	43
	Rb ppm	392	373	338	354	341	-	202	198
	K/Rb	119.6	123.5	130.9	128.0	130.0	-	183.7	174.4
CIPW norm									
	Q	34.4	35.8	39.1	35.5	37.2	36.5	23.0	30.2
	C	0.3	tr	0.6	0.2	0.0	1.3	0.0	1.3
	Or	33.4	32.8	31.5	32.3	31.6	35.8	26.4	24.6
	Ab	24.1	25.3	23.4	24.6	25.8	19.6	26.1	26.3
	An	2.9	2.1	1.8	2.4	1.8	3.7	11.8	7.6
	Di Wo	0.0	0.0	0.0	0.0	0.5	0.0	0.7	0.0
	En	0.0	0.0	0.0	0.0	0.2	0.0	0.4	0.0
	Fs	0.0	0.0	0.0	0.0	0.3	0.0	0.3	0.0
	Hy En	0.8	1.2	1.1	0.7	0.4	0.3	3.6	2.8
	Fs	1.4	0.9	1.0	1.5	0.6	1.2	2.8	2.5
	Mt	0.6	0.4	0.4	0.6	0.4	0.4	1.4	1.3
	Il	0.3	0.3	0.2	0.3	0.3	0.4	1.3	1.5
	Ap	0.1	0.1	0.2	0.1	0.1	0.0	0.3	0.5
	D.I.	91.9	93.9	94.0	92.4	94.6	91.9	75.4	81.1
Norm. An%		10.8	7.5	7.0	8.8	6.6	15.8	31.1	22.3

Specimen numbers have the following locality key:
4- Port Elliot (Figure 19)
9- West Island (Figure 22)

These specimens were analysed using X-ray fluorescence techniques. Analyst: A.R. Milnes

Specimen A - Port Elliot. Analyst: W.R. Browne (Browne, 1920)

*Fe_2O_3

TABLE G7

Chemical analyses of specimens of the red leucogranite and its albitised equivalent from Port Elliot

		red leucogranite			albitised red leucogranite
		4-9	4-89	A	4-8
	SiO_2	76.4	77.9	76.65	78.4
	Al_2O_3	12.6	11.6	12.98	12.0
	TiO_2	0.09	0.09	0.11	0.09
	MnO	0.04	0.04	-	0.03
Total Fe as	Fe_2O_3	0.55	0.49	0.25*	0.33
	FeO	-	-	0.32	-
	MgO	0.2	0.3	0.00	0.2
	CaO	0.28	0.29	0.40	0.26
	Na_2O	2.7	2.8	2.64	8.4
	K_2O	7.00	5.87	6.18	0.24
	P_2O_5	0.03	0.03	-	tr
	H_2O^+	-	-	0.29	-
	H_2O^-	-	-	0.17	-
Ignition loss		0.14	0.60	-	0.42
	TOTAL	100.0	100.0	99.95	100.4
	Sr ppm	26	28	-	57
	Rb ppm	451	407	-	4
	K/Rb	128.8	119.7	-	498.1
CIPW norm					
	Q	32.6	38.2	36.7	33.8
	C	0.1	0.2	1.2	0.0
	Or	41.4	34.7	36.5	1.4
	Ab	23.2	23.4	22.3	60.6
	An	1.2	1.2	2.0	0.0
	Ac	0.0	0.0	0.0	0.2
	NS	0.0	0.0	0.0	2.3
	Di Wo	0.0	0.0	0.0	0.5
	En	0.0	0.0	0.0	0.3
	Fs	0.0	0.0	0.0	0.2
	Hy En	0.5	0.7	0.0	0.2
	Fs	0.5	0.4	0.2	0.1
	Mt	0.2	0.2	0.4	0.0
	Il	0.2	0.2	0.2	0.2
	Ap	0.1	0.1	0.0	0.0
	D.I.	97.2	96.3	95.6	95.9
Norm. An%		4.9	5.0	8.2	0.0

Numbered specimens were analysed using X-ray fluorescence techniques.
Analyst: A.R. Milnes

Specimen A - analysed by W.R. Browne (Browne, 1920)

*Fe_2O_3

TABLE G8

Chemical analyses of specimens of the fine grained miarolitic granophyre from Port Elliot

		4-66B	4-67B
	SiO_2	74.9	75.2
	Al_2O_3	13.2	13.9
	TiO_2	0.10	0.15
	MnO	0.03	0.03
Total Fe as	Fe_2O_3	0.95	1.52
	MgO	0.2	0.3
	CaO	0.10	0.16
	Na_2O	2.4	1.5
	K_2O	6.19	4.50
	P_2O_5	0.03	0.02
Ignition loss		1.05	2.18
	TOTAL	99.2	99.5
	Sr ppm	49	28
	Rb ppm	504	505
	K/Rb	102.0	74.0
CIPW norm			
	Q	36.3	47.8
	C	2.4	6.3
	Or	36.6	26.6
	Ab	20.5	12.6
	An	0.3	0.7
	Hy En	0.6	0.8
	Fs	0.9	1.4
	Mt	0.4	0.6
	Il	0.2	0.3
	Ap	0.1	0.1
	D.I.	93.4	87.1
	Norm. An%	1.4	5.0

Both specimens were analysed using X-ray fluorescence techniques.
Analyst: A.R. Milnes

TABLE G9

Chemical analyses of specimens of the hybrid granites

		Type A hybrid granite					Type B hybrid granite		
		3-29#	3-37	3-38#	A	B#	3-27	3-34	3-39
	SiO_2	66.4	76.4	66.1	68.60	67.10	79.3	69.3	69.4
	Al_2O_3	14.2	11.5	14.4	14.30	14.32	9.8	13.3	13.6
	TiO_2	0.88	0.15	0.96	0.59	0.89	0.31	0.69	0.68
	MnO	0.08	0.04	0.11	-	0.06	0.06	0.07	0.10
Total Fe as	Fe_2O_3	4.68	1.37	4.99	0.79*	1.51*	2.23	4.35	4.50
	FeO	-	-	-	4.70	2.84	-	-	-
	MgO	1.9	0.4	2.1	1.24	1.50	0.9	1.6	1.7
	CaO	3.35	0.45	3.72	2.88	3.26	0.60	1.86	2.01
	Na_2O	3.0	3.1	3.1	3.40	3.05	1.6	2.7	2.6
	K_2O	4.37	5.14	4.20	2.28	4.23	4.63	4.67	4.52
	P_2O_5	0.15	0.03	0.17	tr	0.17	0.05	0.10	0.18
	H_2O^+	-	-	-	0.87	0.56	-	-	-
	H_2O^-	-	-	-	0.24	0.04	-	-	-
Ignition loss		0.79	0.53	0.70	-	-	0.56	0.60	0.69
	TOTAL	99.8	99.1	100.6	99.89	99.53	100.0	99.2	100.0
	Sr ppm	121	32	126	-	-	96	129	135
	Rb ppm	176	320	158	-	-	183	218	211
	K/Rb	206.1	133.3	220.7	-	-	210.0	177.8	177.8
CIPW norm									
	Q	21.6	36.9	20.6	28.9	23.7	49.1	28.1	29.1
	C	0.0	0.2	0.0	1.0	0.0	1.2	0.7	1.3
	Or	25.8	30.4	24.8	13.5	25.0	27.4	27.6	26.7
	Ab	25.6	25.8	26.3	28.8	25.8	13.4	22.6	21.7
	An	12.2	2.0	12.9	14.3	12.9	2.7	8.6	8.8
	Di Wo	1.4	0.0	1.8	0.0	0.9	0.0	0.0	0.0
	En	0.8	0.0	1.0	0.0	0.5	0.0	0.0	0.0
	Fs	0.6	0.0	0.8	0.0	0.4	0.0	0.0	0.0
	Hy En	3.9	1.1	4.1	3.1	3.2	2.2	4.1	4.3
	Fs	2.9	1.2	3.0	7.0	2.3	1.9	3.5	3.7
	Mt	1.7	0.5	1.8	1.2	2.2	0.8	1.6	1.6
	Il	1.7	0.3	1.8	1.1	1.7	0.6	1.3	1.3
	Ap	0.4	0.1	0.4	0.0	0.4	0.1	0.2	0.4
	D.I.	73.0	93.1	71.7	71.1	74.5	89.8	78.3	77.5
Norm. An%		32.3	7.3	32.9	33.2	33.3	16.5	27.5	28.9

TABLE G9 (Cont'd)

Chemical analyses of specimens of the hybrid granites

		Type B hybrid granite						
		C	D	9-7	W19D	W38	W39	W41
	SiO_2	69.56	69.06	72.2	73.2	74.6	72.5	71.8
	Al_2O_3	13.98	14.28	13.6	12.4	12.8	12.8	12.7
	TiO_2	0.79	0.70	0.45	0.44	0.35	0.49	0.51
	MnO	0.05	0.05	0.05	0.06	0.05	0.06	0.05
Total Fe as	Fe_2O_3	0.60*	0.71*	2.51	2.95	2.11	3.76	3.31
	FeO	3.75	3.23	-	-	-	-	-
	MgO	1.76	1.46	0.9	1.0	0.6	1.0	1.1
	CaO	1.92	2.11	0.99	1.03	1.06	0.98	1.24
	Na_2O	2.65	2.69	2.7	3.2	3.3	2.7	2.8
	K_2O	4.27	4.59	5.77	4.58	4.64	5.00	5.29
	P_2O_5	0.07	0.13	0.04	0.10	0.06	0.09	0.11
	H_2O^+	0.66	0.46	-	-	-	-	-
	H_2O^-	0.10	0.11	-	-	-	-	-
Ignition loss		-	-	0.57	0.56	0.45	0.77	0.57
	TOTAL	100.16	99.58	99.8	99.5	100.0	100.2	99.5
	Sr ppm	-	-	97	104	114	110	-
	Rb ppm	-	-	241	203	177	271	259
	K/Rb	-	-	198.7	187.3	217.6	153.2	169.5
CIPW norm								
	Q	28.9	27.6	30.0	32.3	33.7	33.0	30.0
	C	1.7	1.4	1.2	0.5	0.5	1.5	0.3
	Or	25.2	27.1	34.1	27.1	27.4	29.6	31.3
	Ab	22.4	22.8	23.0	27.4	28.3	22.6	23.8
	An	9.1	9.6	4.7	4.5	4.9	4.3	5.4
	Hy En	4.4	3.6	2.3	2.5	1.5	2.6	2.8
	Fs	5.2	4.3	1.9	2.4	1.7	3.2	2.7
	Mt	0.9	1.0	0.9	1.1	0.8	1.4	1.2
	Il	1.5	1.3	0.9	0.8	0.7	0.9	1.0
	Ap	0.2	0.3	0.1	0.2	0.1	0.2	0.3
	D.I.	76.6	77.5	87.1	86.8	89.4	85.1	85.0
Norm.	An%	28.8	29.7	16.8	14.0	14.7	15.9	18.6

Specimen numbers have the following locality key:

3- Granite Island (Figure 21)
9- West Island (Figure 22)
W Cape Willoughby (Figure 13)

These specimens were analysed using X-ray fluorescence techniques.
Analyst: A.R. Milnes

Specimen A - Granite Island. Analyst: C.E. Tilley (Browne, 1920)
Specimens B, C and D - Granite Island. Analyst: A.W. Kleeman (Kleeman, 1937)

#variety of Type A hybrid granite containing hornblende
*Fe_2O_3

TABLE G10

Chemical analyses of specimens of aplite dykes from Port Elliot

		4-60*	4-65
	SiO_2	77.2	77.8
	Al_2O_3	12.8	11.7
	TiO_2	0.13	0.06
	MnO	0.03	0.05
Total Fe as	Fe_2O_3	0.74	0.51
	MgO	0.5	0.2
	CaO	0.30	0.31
	Na_2O	3.3	3.2
	K_2O	6.22	5.15
	P_2O_5	0.06	0.03
Ignition loss		0.67	0.62
	TOTAL	101.9	99.6
	Sr ppm	40	45
	Rb ppm	338	293
	K/Rb	152.8	145.9
CIPW norm			
	Q	32.6	38.5
	C	0.2	0.4
	Or	36.8	30.4
	Ab	28.0	26.9
	An	1.1	1.3
	Hy En	1.3	0.5
	Fs	0.6	0.5
	Mt	0.3	0.2
	Il	0.3	0.1
	Ap	0.1	0.1
	D.I.	97.4	95.8
	Norm. An%	3.8	4.8

Both specimens were analysed using X-ray fluorescence techniques.
Analyst: A.R. Milnes

*contains significant tourmaline

TABLE G11

Chemical analyses of specimens of Kanmantoo Group metasedimentary rocks from the Encounter Bay area

		0010[m]	0011[m]	0014[m]	0015[m]	0018[m]	0023[b]	0025[b]
	SiO_2	76.1	66.0	63.7	76.1	70.3	60.6	58.4
	Al_2O_3	11.9	14.7	15.8	11.2	12.9	17.3	18.4
	TiO_2	0.56	0.95	0.88	0.39	0.70	0.80	0.82
	MnO	0.03	0.08	0.06	0.04	0.12	0.14	0.11
Total Fe as	Fe_2O_3	0.93	5.74	6.54	2.17	5.05	7.80	7.84
	FeO	-	-	-	-	-	-	-
	MgO	1.4	3.2	3.4	1.3	2.4	3.9	3.9
	CaO	3.52	2.76	1.24	3.47	2.37	1.02	0.92
	Na_2O	5.6	3.3	2.2	3.4	2.6	0.8	1.2
	K_2O	0.14	2.70	4.22	1.06	2.62	5.56	6.03
	P_2O_5	0.15	0.17	0.16	0.10	0.18	0.18	0.15
	H_2O^+	-	-	-	-	-	-	-
	H_2O^-	-	-	-	-	-	-	-
Ignition loss		0.40	0.70	1.23	0.77	0.75	2.23	2.19
	TOTAL	100.7	100.3	99.4	100.0	100.0	100.3	100.0
	Sr ppm	465	295	147	348	211	87	131
	Rb ppm	2	177	226	68	115	225	242
	K/Rb	-	126.6	155.0	129.4	189.1	205.1	206.8
CIPW norm								
	Q	36.1	24.2	25.2	43.5	34.9	24.0	18.0
	C	0.0	1.8	5.8	0.0	1.9	8.6	8.6
	Or	0.8	16.0	24.9	6.3	15.5	32.9	35.6
	Ab	47.0	27.9	18.3	28.4	22.3	6.8	9.8
	An	7.3	12.6	5.1	12.5	10.6	3.9	3.6
	Di Wo	3.9	0.0	0.0	1.7	0.0	0.0	0.0
	En	3.3	0.0	0.0	1.1	0.0	0.0	0.0
	Fs	0.1	0.0	0.0	0.5	0.0	0.0	0.0
	Hy En	0.1	7.9	8.5	2.3	6.0	9.7	9.7
	Fs	0.0	4.5	5.4	1.1	4.3	7.0	7.0
	Mt	0.3	2.1	2.4	0.8	1.8	2.8	2.8
	Il	1.1	1.8	1.7	0.7	1.3	1.5	1.6
	Ap	0.4	0.4	0.4	0.2	0.4	0.4	0.4
Norm. An%		13.4	31.1	21.8	30.6	32.2	36.5	26.7

TABLE G11 (Cont'd)

Chemical analyses of specimens of Kanmantoo Group metasedimentary rocks from the Encounter Bay area

		0029[b]	A[p]	B[p]	C[p]	D[p]	365[m]
	SiO_2	57.5	68.92	68.76	58.82	58.75	74.7
	Al_2O_3	17.5	12.65	13.79	18.34	20.48	11.7
	TiO_2	0.82	0.88	0.74	0.96	0.70	0.50
	MnO	0.12	0.02	0.07	0.05	0.03	0.04
Total Fe as	Fe_2O_3	7.82	1.60*	0.66*	0.96*	0.63*	3.73
	FeO	-	5.07	4.60	5.93	3.97	-
	MgO	4.4	2.52	2.65	4.00	5.93	1.6
	CaO	3.38	2.06	2.81	3.53	0.70	1.53
	Na_2O	2.6	2.80	2.54	3.39	3.33	2.2
	K_2O	3.79	2.10	2.29	3.28	1.97	2.45
	P_2O_5	0.13	0.17	0.21	0.19	0.60	0.23
	H_2O^+	-	0.96	0.53	0.27	1.43	-
	H_2O^-	-	0.04	0.04	0.10	0.15	-
Ignition loss		1.01	-	-	-	-	1.29
	TOTAL	99.1	99.79	99.69	99.82	98.67	100.0
	Sr ppm	235	-	-	-	-	182
	Rb ppm	190	-	-	-	-	124
	K/Rb	165.6	-	-	-	-	163.7
CIPW norm							
	Q	11.2	32.8	32.7	9.6		46.2
	C	3.3	1.5	2.5	3.3		3.2
	Or	22.4	12.4	13.5	19.4		14.5
	Ab	22.1	23.7	21.5	28.7		18.5
	An	15.9	11.8	12.6	16.3		6.1
	Di Wo	0.0	0.0	0.0	0.0		0.0
	En	0.0	0.0	0.0	0.0		0.0
	Fs	0.0	0.0	0.0	0.0		0.0
	Hy En	10.9	6.3	6.6	10.0		4.0
	Fs	7.0	6.6	6.8	8.6		3.1
	Mt	2.8	2.3	1.0	1.4		1.4
	Il	1.6	1.7	1.4	1.8		1.0
	Ap	0.3	0.4	0.5	0.4		0.5
Norm. An%		41.9	33.2	36.9	36.2		24.8

Numbered specimens were analysed using X-ray fluorescence techniques.
Analyst: A.R. Milnes (except for 365 which was analysed by I.C. Madsen)

m - Middleton Sandstone
p - Petrel Cove Formation
b - Balquhidder Formation

Specimens A, B, C, and D were analysed by D.R. Bowes (Bowes, 1954)

*Fe_2O_3

TABLE G12

Numbers of cations associated with the standard unit cell (160 oxygen atoms) of varieties of the Encounter Bay Granites and their albitised equivalents

		border facies megacrystic granite				albitised equivalent			
		7-52	7-57	7-58	Av	7-53	7-55	Av	change
	Si	63.1	62.4	62.6	62.7	62.6	66.0	64.3	+1.6
	Al	14.0	14.7	14.5	14.4	14.1	12.0	13.1	-1.3
	Ti	0.3	0.4	0.4	0.4	0.4	0.2	0.3	-0.1
	Mn	tr	tr	tr	tr	tr	tr	tr	-
Fe as	Fe^{+3}	2.2	2.4	2.4	2.3	2.4	1.9	2.2	-0.1
	Mg	1.9	1.9	1.8	1.9	3.7	1.3	2.5	+0.6
	Ca	1.5	1.6	1.5	1.5	0.6	1.4	1.0	-0.5
	Na	4.4	4.3	5.0	4.6	7.0	5.4	6.2	+1.6
	K	6.0	5.8	4.8	5.5	2.7	1.8	2.3	-3.2
	P	0.1	0.1	0.1	0.1	0.1	0.1	0.1	0.0
								nett change	-1.4

		megacrystic albite-chlorite rock							
		7-54	A	B	C	D	E	Av	change
	Si	56.2	52.3	53.8	53.5	54.4	57.3	54.6	-8.1
	Al	20.9	21.7	20.8	21.6	22.8	21.3	21.5	+7.1
	Ti	0.5	0.7	0.5	0.5	-	0.7	0.5	+0.1
	Mn	tr	tr	tr	tr	-	-	tr	-
Fe as	Fe^{+3}	0.6	1.8	3.0	2.3	5.5	0.7	2.3	0.0
	Mg	4.4	9.7	8.7	8.4	2.6	1.5	5.9	+4.0
	Ca	0.6	0.7	1.0	1.1	0.8	0.4	0.8	-0.5
	Na	17.7	15.5	11.3	12.3	10.0	17.1	14.0	+9.4
	K	0.2	0.5	0.1	0.2	1.0	0.2	0.4	-5.1
	P	0.2	0.1	0.1	0.2	-	0.2	0.1	0.0
								nett change	+6.7

		border facies megacrystic granite			megacrystic albite-chlorite rock	
		3-26	3-28	Av	3-40	change
	Si	64.6	63.6	64.1	58.3	-5.8
	Al	13.4	13.8	13.6	18.4	+4.8
	Ti	0.2	0.3	0.3	0.5	+0.2
	Mn	tr	0.1	tr	tr	-
Fe as	Fe^{+3}	1.5	2.0	1.8	1.2	-0.6
	Mg	1.7	1.6	1.7	4.2	+2.5
	Ca	1.4	1.6	1.5	0.5	-1.0
	Na	4.5	4.7	4.6	15.0	+10.4
	K	5.3	5.2	5.3	0.7	-4.6
	P	tr	0.1	tr	0.1	-

TABLE G12 (Cont'd)

Numbers of cations associated with the standard unit cell (160 oxygen atoms) of varieties of the Encounter Bay Granites and their albitised equivalents

	red leucogranite 4-9	albitised equivalent 4-8	change
Si	66.6	66.9	+0.3
Al	12.9	12.1	-0.8
Ti	0.1	0.1	0.0
Mn	tr	tr	-
Fe as Fe^{+3}	0.4	0.2	-0.2
Mg	0.3	0.3	0.0
Ca	0.3	0.2	-0.1
Na	4.6	13.8	+9.2
K	7.8	0.3	-7.5
P	tr	tr	-
		nett change	+0.9

Specimen numbers have the following locality key:

7- Rosetta Head (Figure 12)
3- Granite Island (Figure 21)
4- Port Elliot (Figure 19)

TABLE G13

Chemical analyses of specimens of Kangaroo Island pegmatites and granites

		P-1	V-4	SBR-8	R-1
	SiO_2	68.3	73.9	71.9	73.1
	Al_2O_3	18.5	15.1	12.5	12.5
	TiO_2	0.04	0.08	0.72	0.41
	MnO	0.16	0.01	0.07	0.04
Total Fe as	Fe_2O_3	1.55	0.91	4.85	2.97
	MgO	0.2	0.5	1.5	0.7
	CaO	0.11	0.34	1.91	1.53
	Na_2O	2.3	3.2	2.3	3.3
	K_2O	7.14	5.17	3.31	4.83
	P_2O_5	0.52	0.12	0.09	0.09
Ignition loss		1.34	0.90	0.81	0.62
	TOTAL	100.2	100.2	100.0	100.1
	Sr ppm	33	79	159	-
	Rb ppm	929	257	172	-
	K/Rb	63.8	167.0	159.8	-
CIPW norm					
	Q		34.3	37.7	30.6
	C		4.0	1.8	0.0
	Or		30.6	19.6	28.5
	Ab		26.7	19.8	28.0
	An		0.9	8.9	5.0
	Di Wo		0.0	0.0	0.9
	En		0.0	0.0	0.4
	Fs		0.0	0.0	0.5
	Hy En		1.2	3.8	1.4
	Fs		0.8	4.0	2.0
	Mt		0.3	1.8	1.1
	Il		0.2	1.4	0.8
	Ap		0.3	0.2	0.2
	D.I.		91.6	77.0	87.2
	Norm. An%		3.3	31.0	15.0

All specimens were analysed using X-ray fluorescence techniques.
Analyst: I.C. Madsen

P-1 pegmatite about 12km south-east of Penneshaw (Figure 8)
V-4 pegmatite from coastline at Vivonne Bay (Figure 2)
SBR-8 Cape Kersaint granite collected from banks of StunSailBoom River (Figure 2)
R-1 Remarkable Rocks granite, about 6km east of Cape du Couedic (Figure 2)

APPENDIX H

X-ray fluorescence and electron microprobe analyses of micas, chlorite and hornblende in varieties of the Encounter Bay Granites

X-ray fluorescence analyses of mica separates were carried out according to the method of Norrish and Hutton (1969). Electron probe microanalyses of several mica, chlorite or hornblende crystals in polished-thin sections of several granite varieties were made under the following conditions:

Accelerating voltage - 20Kv
Beam current - 50nA
Beam fully focussed
Flow proportional counters
Counting time - 10 seconds (peak and one background position)
Standards used - Biotite (Fe, K, Si, Al, Mg)
Rutile (Ti)
Barytes (Ba)
Jadeite (Na)
Corrections to the raw data were made according to the method of Sweatman and Long (1969) using the procedure of Oertel (1971)

The analyses given in the following Tables are quoted to within calculated counting error. Electron probe microanalyses are the average of two or more spot analyses of different crystals.

Specimen numbers have the same locality key as given in Appendix G. (ie. 4- Port Elliot, 3- Granite Island, 7- Rosetta Head, 8- Wright Island, 9- West Island).

TABLE H1

Chemical analyses of micas in specimens of the border facies megacrystic granite

	4-55 biotite*	4-61 biotite^{A}	4-61 biotite^{B}	4-63 biotite^{B}	4-63 musc.^{B}	4-63 biotite^{C}
SiO_2	34.5	36.3	35.6	35.8	45.6	35.8
Al_2O_3	16.1	16.4	16.5	16.7	31.1	16.9
TiO_2	3.03	2.59	2.51	2.44	0.46	2.37
MnO	0.25	-	-	-	-	-
Total Fe as Fe_2O_3	27.7	-	-	-	-	-
Total Fe as FeO	-	25.1	25.4	20.9	4.55	20.1
MgO	6.95	7.77	7.92	8.25	1.19	8.96
CaO	0.44	-	-	-	-	-
Na_2O	-	0.10	0.07	0.19	0.23	0.12
K_2O	9.11	9.87	9.91	9.90	9.63	9.54
BaO	-	0.24	0.18	0.03	0.03	0.11
P_2O_5	0.14	-	-	-	-	-
Ignition loss	2.02	-	-	-	-	-
TOTAL	100.2	98.4	98.1	94.2	92.8	93.9
Structural formula calculated on the basis of 22 oxygen atoms						
Si	5.43	5.52	5.47	5.58	6.31	5.57
Al	2.57	2.48	2.53	2.42	1.69	2.43
Tetrahedral	8.00	8.00	8.00	8.00	8.00	8.00
Al	0.41	0.47	0.44	0.66	3.40	0.67
Ti	0.35	0.29	0.28	0.28	0.05	0.27
Mn	0.03	-	-	-	-	-
Total Fe as Fe^{+2}	3.27	3.20	3.25	2.73	0.53	2.62
Mg	1.63	1.76	1.81	1.92	0.25	2.08
P	0.02	-	-	-	-	-
Octahedral	5.71	5.72	5.78	5.59	4.23	5.64
Ca	0.07	-	-	-	-	-
Na	-	0.03	0.02	0.06	0.06	0.04
K	1.83	1.92	1.93	1.97	1.70	1.89
Ba	-	0.01	0.01	trace	trace	0.01
Interstitial	1.90	1.96	1.96	2.03	1.76	1.94
$Fe^{+2}/(Fe^{+2}+Mg)$	0.67	0.64	0.64	0.59	-	0.56

TABLE H1 (Cont'd)

Chemical analyses of micas in specimens of the border facies megacrystic granite

	3-26 biotite*	3-32 biotite*	3-33 biotite*	8-12 biotite*	8-12 musc.*	7-52 biotite[B]
SiO_2	35.4	36.9	35.9	35.3	49.5	37.0
Al_2O_3	16.4	16.9	17.0	19.6	34.8	17.1
TiO_2	3.05	3.03	3.08	1.90	0.39	2.63
MnO	0.26	0.26	0.26	0.28	0.06	-
Total Fe as Fe_2O_3	24.5	21.3	25.2	23.3	1.14	-
Total Fe as FeO	-	-	-	-	-	22.9
MgO	8.62	10.3	9.00	8.51	0.57	8.24
CaO	0.34	0.14	0.15	0.07	0.15	-
Na_2O	-	-	-	-	-	0.12
K_2O	9.20	9.80	9.84	9.11	9.39	9.49
BaO	-	-	-	-	-	0.08
P_2O_5	0.22	0.11	0.08	0.10	0.05	-
Ignition loss	2.15	1.52	1.37	1.60	4.46	-
TOTAL	100.1	100.3	101.9	99.8	100.5	97.6
Structural formula calculated on the basis of 22 oxygen atoms						
Si	5.47	5.55	5.43	5.38	6.41	5.59
Al	2.53	2.45	2.57	2.62	1.59	2.41
Tetrahedral	8.00	8.00	8.00	8.00	8.00	8.00
Al	0.45	0.54	0.46	0.89	3.71	0.63
Ti	0.35	0.33	0.34	0.21	0.04	0.29
Mn	0.03	0.03	0.03	0.04	0.13	-
Total Fe as Fe^{+2}	2.84	2.41	2.86	2.67	0.11	2.89
Mg	1.99	2.32	2.03	1.93	0.11	1.85
P	0.03	0.01	0.01	0.01	0.01	-
Octahedral	5.70	5.64	5.73	5.75	4.11	5.66
Ca	0.06	0.02	0.02	0.01	0.02	-
Na	-	-	-	-	-	0.04
K	1.81	1.88	1.90	1.77	1.55	1.83
Ba	-	-	-	-	-	0.01
Interstitial	1.87	1.90	1.92	1.78	1.57	1.88
$Fe^{+2}/(Fe^{+2}+Mg)$	0.59	0.51	0.58	0.58	-	0.61

TABLE H1 (Cont'd)

Chemical analyses of micas in specimens of the border facies megacrystic granite

	7-52 biotite[C]	7-56 biotite[C]	9-11 biotite[A]	9-11 musc.[A]	9-11 biotite[B]
SiO_2	37.5	34.8	36.1	47.2	36.0
Al_2O_3	17.1	17.8	17.2	31.7	17.6
TiO_2	2.63	2.62	3.06	1.60	2.92
MnO	-	-	-	-	-
Total Fe as Fe_2O_3	-	-	-	-	-
Total Fe as FeO	22.8	20.2	23.4	3.07	22.8
MgO	8.26	7.67	7.75	1.19	7.77
CaO	-	-	-	-	-
Na_2O	0.09	0.10	0.14	0.30	0.11
K_2O	9.66	9.31	9.88	10.6	9.70
BaO	0.18	0.09	0.15	0.05	0.07
P_2O_5	-	-	-	-	-
Ignition loss	-	-	-	-	-
TOTAL	98.2	92.6	97.7	95.7	97.0
Structural formula calculated on the basis of 22 oxygen atoms					
Si	5.62	5.50	5.49	6.32	5.49
Al	2.38	2.50	2.51	1.68	2.51
Tetrahedral	8.00	8.00	8.00	8.00	8.00
Al	0.64	0.81	0.57	.3.33	0.65
Ti	0.29	0.30	0.34	0.16	0.33
Mn	-	-	-	-	-
Total Fe as Fe^{+2}	2.86	2.67	2.97	0.34	2.90
Mg	1.85	1.81	1.76	0.24	1.76
P	-	-	-	-	-
Octahedral	5.64	5.59	5.64	4.07	5.64
Ca	-	-	-	-	-
Na	0.03	0.03	0.04	0.08	0.03
K	1.85	1.88	1.92	1.82	1.89
Ba	0.01	0.01	0.01	trace	trace
Interstitial	1.89	1.92	1.97	1.90	1.92
$Fe^+ / (Fe^+ + Mg)$	0.61	0.60	0.63	-	0.62

*X-ray fluorescence analysis

A,B,C electron microprobe analysis:

A - inclusions in potash feldspar megacrysts
B - groundmass biotite
C - biotite in xenolith

Analyst: A.R. Milnes

TABLE H2

Chemical analyses of biotites in specimens of the inner facies megacrystic granite

	4-79 biotite*	4-79 biotite^{A}	4-79 biotite^{B}	4-93 biotite^{A}	4-93 biotite^{B}
SiO_2	35.1	35.7	35.4	37.1	37.6
Al_2O_3	16.4	16.3	15.9	16.0	16.3
TiO_2	2.94	2.74	2.59	2.27	2.43
MnO	0.23	-	-	-	-
Total Fe as Fe_2O_3	26.8	-	-	-	-
Total Fe as FeO	-	24.5	25.2	24.6	24.8
MgO	7.61	7.58	7.70	7.95	7.68
CaO	0.31	-	-	-	-
Na_2O	-	0.08	0.05	0.05	0.05
K_2O	9.36	9.94	9.57	9.06	9.47
BaO	-	0.25	0.13	0.13	0.17
P_2O_5	0.18	-	-	-	-
Ignition loss	1.33	-	-	-	-
TOTAL	100.3	97.9	96.5	97.2	98.5
Structural formulae calculated on the basis of 22 oxygen atoms					
Si	5.44	5.51	5.51	5.67	5.67
Al	2.56	2.49	2.49	2.33	2.33
Tetrahedral	8.00	8.00	8.00	8.00	8.00
Al	0.44	0.48	0.42	0.54	0.56
Ti	0.33	0.31	0.30	0.25	0.27
Mn	0.03	-	-	-	-
Total Fe as Fe^{+2}	3.13	3.16	3.28	3.14	3.13
Mg	1.76	1.74	1.79	1.81	1.73
P	0.02	-	-	-	-
Octahedral	5.71	5.69	5.79	5.75	5.69
Ca	0.05	-	-	-	-
Na	-	0.02	0.02	0.02	0.15
K	1.85	1.96	1.90	1.76	1.82
Ba	-	0.02	0.01	0.01	0.01
Interstitial	1.90	2.00	1.92	1.79	1.85
$Fe^{+2}/(Fe^{+2}+Mg)$	0.64	0.64	0.65	0.64	0.64

*X-ray fluorescence analysis

^{A,B,C}electron microprobe analysis as in Table H1

Analyst: A.R. Milnes

TABLE H3

Chemical analyses of micas and chlorite in xenoliths within the border facies megacrystic granite, and of biotite in a Petrel Cove Formation metasiltstone

	3-10 biotite	3-19 biotite	9-8 biotite*	4-84 biotite	4-84 musc.	4-84 chlorite	V3 biotite
SiO_2	35.9	35.9	36.0	35.4	47.6	23.7	36.0
Al_2O_3	17.3	18.0	16.6	18.2	35.2	21.8	20.0
TiO_2	2.35	1.99	3.18	1.37	0.02	0.02	1.52
MnO	-	-	0.22	-	-	-	-
Total Fe as Fe_2O_3	-	-	23.82	-	-	-	-
Total Fe as FeO	17.5	17.5	-	21.1	2.23	24.1	18.3
MgO	10.4	10.5	8.04	9.86	0.85	13.6	10.8
CaO	-	-	0.05	0.05	0.00	0.00	0.01
Na_2O	0.08	0.16	-	0.19	0.92	0.04	0.38
K_2O	9.55	9.07	9.57	9.38	10.1	0.01	8.70
BaO	0.13	0.13	-	-	-	-	-
P_2O_5	-	-	0.04	-	-	-	-
Ignition loss	-	-	1.60	-	-	-	-
TOTAL	93.2	93.3	99.1	95.6	96.9	83.3	95.7
Structural formulae calculated on the basis of 22 oxygen atoms and 28 oxygen atoms for micas and chlorite respectively							
Si	5.55	5.53	5.56	5.42	6.24	5.25	5.39
Al	2.45	2.47	2.44	2.58	1.76	2.75	2.61
Tetrahedral	8.00	8.00	8.00	8.00	8.00	8.00	8.00
Al	0.71	0.80	0.59	0.71	3.67	2.94	0.92
Ti	0.27	0.23	0.36	0.15	trace	trace	0.17
Mn	-	-	0.03	-	-	-	-
Total Fe as Fe^{+2}	2.27	2.25	2.77	2.71	0.24	4.49	2.29
Mg	2.40	2.41	1.85	2.25	0.17	4.46	2.41
P	-	-	0.01	-	-	-	-
Octahedral	5.65	5.69	5.61	5.82	4.08	-	5.79
Ca	-	-	0.01	0.01	trace	trace	trace
Na	0.02	0.05	-	0.06	0.23	0.02	0.11
K	1.88	1.78	1.89	1.83	1.69	trace	1.66
Ba	0.01	0.01	-	-	-	-	-
Interstitial	1.91	1.84	1.89	1.90	1.92	-	1.78
$Fe^{+2}/(Fe^{+2}+Mg)$	0.49	0.48	0.60	0.55	-	0.50	0.49

*X-ray fluorescence analysis
Others are electron microprobe analyses

Analyst: A.R. Milnes

TABLE H4

Chemical analyses of micas and chlorite in specimens of albitised megacrystic granite

	4-26 biotite[B]	7-53 biotite*	7-55 biotite*	7-55 musc.*	7-55 biotite[B]	8-13 biotite*	8-13 chlorit
SiO_2	36.2	36.6	35.4	47.5	35.4	37.2	28.6
Al_2O_3	16.9	18.0	16.9	32.2	17.6	19.0	22.9
TiO_2	2.35	2.78	3.27	0.60	2.42	1.63	0.71
MnO	-	0.20	0.25	0.05	-	0.12	0.15
Total Fe as Fe_2O_3	-	17.0	24.8	2.95	-	13.3	18.0
Total Fe as FeO	18.5	-	-	-	20.3	-	-
MgO	10.1	13.2	8.05	1.14	8.22	13.8	19.8
CaO	-	0.10	0.15	0.16	-	0.21	0.21
Na_2O	0.09	-	-	-	0.12	-	-
K_2O	9.56	9.97	9.60	11.2	9.52	9.36	0.59
BaO	0.08	-	-	-	0.23	-	-
P_2O_5	-	0.11	0.08	0.03	-	0.28	0.25
Ignition loss	-	2.31	1.80	4.51	-	4.15	8.45
TOTAL	93.8	100.3	100.3	100.3	93.8	99.1	99.7
Structural formulae calculated on the basis of 22 oxygen atoms and 28 oxygen atoms for micas and chlorite respectively							
Si	5.60	5.43	5.45	6.37	5.53	5.54	5.60
Al	2.40	2.57	2.55	1.63	2.47	2.46	2.40
Tetrahedral	8.00	8.00	8.00	8.00	8.00	8.00	8.00
Al	0.67	0.57	0.53	3.45	0.76	0.86	2.88
Ti	0.27	0.30	0.37	0.06	0.28	0.18	0.10
Mn	-	0.03	0.03	0.01	-	0.02	0.03
Total Fe as Fe^{+2}	2.40	1.90	2.87	0.30	2.65	1.49	2.65
Mg	2.31	2.92	1.85	0.23	1.91	3.06	5.79
P	-	0.01	0.01	trace	-	0.04	0.04
Octahedral	5.65	5.73	5.66	4.05	5.60	5.65	-
Ca	-	0.02	0.03	0.02	-	0.03	0.04
Na	0.03	-	-	-	0.04	-	-
K	1.89	1.89	1.89	1.91	1.89	1.78	0.15
Ba	0.01	-	-	-	0.01	-	-
Interstitial	1.93	1.90	1.92	1.93	1.95	1.81	-
$Fe^{+2}/(Fe^{+2}+Mg)$	0.51	0.39	0.61	-	0.58	0.33	0.31

*X-ray fluorescence analyses

[B]electron microprobe analyses of groundmass biotite

Analyst: A.R. Milnes

TABLE H5

Chemical analyses of phlogopite and chlorite in a specimen of the megacrystic albite-chlorite rock

	7-54 phlogopite	7-54 chlorite*	7-54 chlorite
SiO_2	41.4	28.8	28.4
Al_2O_3	18.8	24.4	24.4
TiO_2	0.69	1.21	0.05
MnO	-	0.08	-
Total Fe as Fe_2O_3	-	7.60	-
Total Fe as FeO	5.14	-	6.63
MgO	20.6	27.1	27.8
CaO	-	0.14	-
Na_2O	0.24	-	0.00
K_2O	10.2	0.15	0.00
BaO	0.06	-	0.00
P_2O_5	-	0.03	-
Ignition loss	-	9.99	-
TOTAL	97.2	99.5	87.3
Structural formulae calculated on the basis of 22 oxygen atoms and 28 oxygen atoms for phlogopite and chlorite respectively			
Si	5.73	5.41	5.41
Al	2.27	2.59	2.59
Tetrahedral	8.00	8.00	8.00
Al	0.81	2.81	2.90
Ti	0.07	0.17	0.01
Mn	-	0.01	-
Total Fe as Fe^{+2}	0.60	1.08	1.06
Mg	4.25	7.60	7.88
P	-	0.01	-
Octahedral	5.73	-	-
Ca	-	0.03	-
Na	0.06	-	trace
K	1.80	0.04	trace
Ba	trace	-	trace
Interstitial	1.86	-	-
$Fe^{+2}/(Fe^{+2}+Mg)$	0.12	0.12	0.12

*X-ray fluorescence analyses
Others are electron microprobe analyses

Analyst: A.R. Milnes

TABLE H6

Chemical analyses of biotite in specimens of fine and medium even-grained granites

	4-10 biotite	4-13[1] biotite	4-52 biotite	4-73 biotite*	4-59 biotite	4-103 biotite
SiO_2	35.7	38.2	34.6	37.1	35.2	34.8
Al_2O_3	16.1	18.0	16.5	18.3	16.0	16.2
TiO_2	2.38	1.68	2.24	2.00	2.30	2.35
MnO	-	-	-	0.12	-	-
Total Fe as Fe_2O_3	-	-	-	20.7	-	-
Total Fe as FeO	24.2	11.4	22.9	-	22.7	24.1
MgO	6.57	15.4	6.6	10.1	6.88	6.45
CaO	-	-	-	0.10	-	-
Na_2O	0.08	0.14	0.17	-	0.07	0.36
K_2O	9.56	9.58	9.18	9.38	9.17	9.27
BaO	0.14	0.04	0.05	-	0.07	0.03
P_2O_5	-	-	-	0.10	-	-
Ignition loss	-	-	-	2.08	-	-
TOTAL	94.7	94.4	92.2	100.0	92.4	93.6
Structural formulae calculated on the basis of 22 oxygen atoms						
Si	5.63	5.63	5.57	5.57	5.65	5.56
Al	2.37	2.37	2.43	2.43	2.35	2.44
Tetrahedral	8.00	8.00	8.00	8.00	8.00	8.00
Al	0.61	0.74	0.70	0.81	0.66	0.61
Ti	0.27	0.18	0.26	0.22	0.27	0.28
Mn	-	-	-	0.15	-	-
Total Fe as Fe^{+2}	3.19	1.40	3.08	2.34	3.04	3.22
Mg	1.54	3.39	1.59	2.25	1.64	1.54
P	-	-	-	0.01	-	-
Octahedral	5.61	5.71	5.63	5.68	5.62	5.65
Ca	-	-	-	0.02	-	-
Na	0.02	0.04	0.05	-	0.02	0.11
K	1.92	1.80	1.89	1.80	1.88	1.89
Ba	0.01	trace	trace	-	trace	trace
Interstitial	1.96	1.84	1.94	1.82	1.90	2.00
$Fe^{+2}/(Fe^{+2}+Mg)$	0.67	0.29	0.66	0.51	0.65	0.68

[1]4-13 is the albitised equivalent of 4-10

*X-ray fluorescence analysis
Others are electron microprobe analyses

Analyst: A.R. Milnes

TABLE H7

Chemical analyses of muscovite in specimens of the fine grained miarolitic granophyre

	4-66B muscovite*	4-67B muscovite*
SiO_2	46.3	45.8
Al_2O_3	33.5	33.8
TiO_2	0.26	0.23
MnO	0.06	0.06
Total Fe as Fe_2O_3	3.83	3.36
MgO	0.64	0.56
CaO	0.10	0.07
K_2O	10.9	10.8
P_2O_5	0.03	0.03
Ignition loss	3.53	4.56
TOTAL	99.2	99.3
Structural formulae calculated on the basis of 22 oxygen atoms		
Si	6.24	6.21
Al	1.76	1.79
Tetrahedral	8.00	8.00
Al	3.56	3.62
Ti	0.03	0.02
Mn	0.01	0.01
Total Fe as Fe^{+2}	0.39	0.34
Mg	0.13	0.11
P	trace	trace
Octahedral	4.12	4.10
Ca	0.01	0.01
K	1.87	1.87
Interstitial	1.88	1.88

*X-ray fluorescence analyses

Analyst: A.R. Milnes

TABLE H8

Chemical analyses of coexisting biotite and hornblende in specimens of type A hybrid granite

	3-31 biotite[B]	3-31 hbl.[B]	3-29 biotite[B]	3-29 hbl.[B]	3-29 hornblende megacryst		
SiO_2	36.3	44.3	36.8	44.2	48.9	44.9	52.5
Al_2O_3	14.8	8.53	14.7	8.69	4.76	7.87	2.86
TiO_2	1.85	1.27	1.60	1.14	0.32	1.17	0.10
Total Fe as FeO	22.6	22.3	20.4	19.4	16.0	18.7	13.5
MgO	10.5	8.74	11.9	9.67	12.8	10.2	15.0
CaO	-	11.4	-	12.1	12.6	12.4	13.0
Na_2O	0.10	1.33	0.10	1.28	0.78	1.29	0.47
K_2O	9.64	1.19	9.88	1.08	0.48	1.03	0.24
BaO	0.15	-	0.13	-	-	-	-
TOTAL	95.9	99.1	95.5	97.6	96.6	97.6	97.7
Structural formulae calculated on the basis of 22 oxygen atoms and 23 oxygen atoms for biotite and hornblende respectively							
Si	5.61	6.73	5.66	6.74	7.37	6.81	7.62
Al	2.39	1.27	2.34	1.26	0.63	1.19	0.38
Tetrahedral	8.00	8.00	8.00	8.00	8.00	8.00	8.00
Al	0.31	0.25	0.31	0.30	0.20	0.22	0.11
Ti	0.21	0.14	0.18	0.13	0.04	0.13	0.01
Total Fe as Fe^{+2}	2.92	2.83	2.62	2.47	1.97	2.37	1.64
Mg	2.43	1.98	2.73	2.20	2.82	2.32	3.25
Octahedral (Y)	5.87	5.20	5.84	5.10	5.03	5.04	5.01
Ca	-	1.85	-	1.97	2.00	2.02	2.02
Na	0.03	0.39	0.03	0.38	0.22	0.38	0.13
K	1.90	0.23	1.94	0.21	0.09	0.20	0.04
Ba	0.01	-	0.01	-	-	-	
Interstitial (X)	1.94	2.47	1.98	2.56	2.31	2.60	2.19
$Fe^{+2}/(Fe^{+2}+Mg)$	0.55	0.59	0.49	0.53	0.41	0.51	0.34

Note: all are electron microprobe analyses

[B] analyses of groundmass biotite and hornblende

Analyst: A.R. Milnes

TABLE H9

Chemical analyses of biotite in a specimen of type B hybrid granite

	3-27 biotite[A]	3-27 chlorite[A]	3-27 biotite[B]	3-27 biotite[C]
SiO_2	35.6	25.4	36.3	36.2
Al_2O_3	16.7	20.0	16.6	16.5
TiO_2	2.76	0.08	3.08	2.90
Total Fe as FeO	23.2	28.5	21.8	21.8
MgO	8.86	14.1	9.26	9.56
Na_2O	0.09	0.03	0.07	0.09
K_2O	9.26	0.05	9.79	9.83
BaO	0.15	0.06	0.22	0.18
TOTAL	96.6	88.2	97.1	97.1
Structural formula calculated on the basis of 22 oxygen atoms				
Si	5.46		5.51	5.50
Al	2.54		2.49	2.50
Tetrahedral	8.00		8.00	8.00
Al	0.48		0.49	0.45
Ti	0.31		0.34	0.32
Total Fe as Fe^{+2}	2.97		2.77	2.78
Mg	2.02		2.09	2.17
Octahedral	5.78		5.69	5.72
Na	0.03		0.02	0.03
K	1.81		1.90	1.91
Ba	0.01		0.01	0.01
Interstitial	1.85		1.93	1.95
$Fe^{+2}/(Fe^{+2}+Mg)$	0.60		0.57	0.56

[A,B,C] electron microprobe analyses as in Table H1

Analyst: A.R. Milnes

APPENDIX I

Measurement of the degree of Al,Si order in alkali feldspars based on data for "standard" alkali feldspars, and the detection of "anomalous" alkali feldspars

In view of the data now available in the literature, it seems desirable that alkali feldspars encountered during routine petrological investigations be described in terms of Al,Si order, rather than their monoclinic or triclinic geometry as determined from parameters such as extinction angle or X-ray triclinicity, although Wright and Stewart (1968, page 40) have doubts as to the desirability of such a classification. In pursuing such a classification, it is important to distinguish between *local* and *distant* Al,Si order (Smith and MacKenzie, 1961). The degree of Al,Si order calculated from T-O bond length measurements from X-ray crystallographic data represents *distant* order averaged over an entire single crystal; on the other hand, according to Smith (1970), cell dimensions, refractive indices and other physical properties depend primarily on *local* order. Thus, Smith considers that a simple relationship between physical properties and the degree of order determined from X-ray crystallographic data can only exist when local and distant order are correlated.

Jones (1966) suggested that the ratio c*/b* be used as a measure of the degree of Al,Si order in alkali feldspars. The ratio can be measured directly from diffraction charts of monoclinic feldspars (where $c^*/b^* = 2.d_{040}/d_{002}$), or obtained for both monoclinic and triclinic feldspars by using all low angle reflections resolved on diffraction charts to calculate c* and b*. Stewart and Ribbe (1969) used the parameters $\Delta(b.c)$ and $\Delta(\alpha^*.\gamma^*)$ for the estimation of Al,Si order in alkali feldspars, based on the relative positions of the "standard" feldspars on the b - c graph of Wright and Stewart (1968). In order to examine unknown specimens however, these methods require computer refinement of powder diffraction data, or single crystal data. The ratio $2\theta.\bar{2}04/060$ is linearly related to c*/b* (Figure I1) and can be used as a measure of the degree of Al,Si order. Furthermore, $2\theta.\bar{2}04/060$ has the advantage that it can be measured directly from X-ray diffraction charts of both monoclinic and triclinic alkali feldspars.

Data for "standard" alkali feldspars, including those alkali feldspars for which X-ray crystallographic structure analyses exist and a range of alkali-exchanged feldspars described in the recent

literature, have been compiled in Table I1. The parameters c*/b* and $20.\bar{2}04/060$ were computed from the published unit cell dimensions of the "standard" feldspars. The relationships between c*/b* and $20.\bar{2}04/060$ and the degree of distant Al,Si order (as calculated from T-O bond length data[1]) were studied graphically.

Figure I1 is a graph of $20.\bar{2}04/060$ against c*/b* for the "standard" potash and soda feldspars listed in Table I1. A parallel linear relationship between the two parameters for both sets of feldspars is well defined. However, there are exceptions to this relationship. In the case of the soda feldspars, the exceptions include the high albite examined structurally by Ferguson, Traill and Taylor (1958) and Ribbe, Megaw and Taylor (1969)[2], and S63-30, Na-exchanged P50-90 and Na-exchanged Spencer B (Wright and Stewart, 1968). These anomalous feldspars, especially Ferguson, Traill and Taylor's high albite, are significantly displaced from the normal soda feldspars. Exceptional potash feldspars include K-exchanged S63-30 and K-exchanged albite III (Wright and Stewart, 1968), and Pellotsalo (Brown and Bailey, 1964). These feldspars define a linear distribution which is parallel to but significantly displaced from the normal potash feldspar distribution. Tie-lines joining the potash-rich feldspars to their soda-rich equivalents in Figure I1 represent alkali-exchange paths which, for the anomalous feldspars, do not end on the normal feldspar lines. However,

---

[1]The relationship between average T-O bond lengths and the Al content of tetrahedral sites in alumino-silicates is linear according to Smith and Bailey (1963), Jones (1968), Stewart and Ribbe (1969) and Ribbe and Gibbs (1969). However, Jones and Taylor (1968), Brown, Gibbs and Ribbe (1969) and Brown and Gibbs (1969) are amongst many authors who have shown that T-O bond distances in framework silicates are dependent on T-O-T angles as well as on the nature of the T cations. These findings support the suggestion of Jones (private communication, 1969) that the relationship between T-O bond lengths and tetrahedral Al is perhaps best represented by a polynomial curve rather than a straight line. For the present investigation, the linear relationship of Jones (1968), namely

$$Al/(Al+Si) = 6.3481(T-O) - 10.1780,$$

was used to predict the Al ocupation of tetrahedral sites in the "standard" alkali feldspars from published bond length data.

[2]The high albite of Orville (1967) is not displaced from the normal soda feldspar curve

reference to Table I1 indicates that these discrepancies can not be explained as an effect of systematic compositional differences between the normal and the anomalous feldspars.

Figure I2a is a graph of c*/b* against degree of Al,Si order for "standard" feldspars for which T-O bond length data have been obtained, and is a revision of the graph devised by Jones (1966). The data for Figure I2a are given in Table I2. If c*/b* is plotted against the natural log of the degree of Al,Si order, the complex distribution in Figure I2a can be reduced to a linear distribution (Figure I2b). Jones (1966) suggested that the soda feldspars are displaced from the potash feldspar line, and may define a distribution of their own. Statistically however, the soda feldspars can not be separated from the potash feldspars.

As Pellotsalo is normal in terms of c*/b* and degree of distant Al,Si order, its displacement from the normal potash feldspar distribution in Figure I1 can be attributed to an abnormally high value of $2\theta.\bar{2}04/060$ in relation to c*/b*. The displacement of K-exchanged albite III and K-exchanged S63-30 from the normal potash feldspar distribution (and possibly the displacement of S63-30, Ferguson, Traill and Taylor's high albite, Na-exchanged P50-90 and Na-exchanged Spencer B from the normal soda feldspar distribution) can be similarly explained.

Figure I3 is a graph of $2\theta.\bar{2}04/060$ against distant Al,Si order for the "standard" alkali feldspars listed in Table I3. Where possible, the distant Al,Si order was calculated from T-O bond length data (see Table I2), but in the absence of such data the degree of order was estimated from c*/b* with reference to Figure I2b.

As shown in Figures I3 and I4, the normal and the anomalous potash feldspars define parallel distributions between $\bar{2}04/060$ and the degree of Al,Si order. St. Gotthard adularia (data from Jones, private communication, 1969) and Spencer C (data from Coleville and Ribbe, 1968) are significantly displaced from the normal potash feldspar distribution (Figures I3 and I4). This can only be the effect of a higher degree of Al,Si order than appropriate for the value of $\bar{2}04/060$, if reference is made to Figure I1. A study of this type of anomaly was not undertaken during the present investigation. On the other hand, the displacement of Pellotsalo, K-exchanged albite III and K-exchanged S63-30 from the normal potash feldspar distribution is due to higher values of $\bar{2}04/060$

than appropriate for a particular value of Al,Si order. More specifically, for a given value of $2\theta.\bar{2}04/060$ the degree of Al,Si order is about 25% higher for anomalous than for normal potash feldspars.

Low and high albite are significantly displaced from both the normal and the anomalous potash feldspars in Figure I3. However, it should be noted that high albite (data from Ferguson, Traill and Taylor, 1958) has an abnormally high $\bar{2}04/060$ value (Figure I1), and contrasts with the high albite studied by Orville (1967).

It is clear from these graphs that potash feldspars and soda feldspars can each be divided into two groups on the basis of the parameter $2\theta.\bar{2}04/060$. The anomalous potash feldspars are a minority compared with the normal potash feldspars, and are characterised by predictably high values of $\bar{2}04/060$. The anomalous soda feldspars are also characterised by predictably high values of $\bar{2}04/060$, but there are not enough soda feldspars for which T-O bond length data have been determined to permit further comment.

The cause of the abnormality of certain potash feldspars is not clear, although the $\bar{2}04$ term is sensitive to it. Brown and Bailey (1963) did not recognise evidence for the anomalous nature of Pellotsalo microcline. Similarly, Finney and Bailey (1964) found no evidence for a discrepancy between Pontiskalk and Pellotsalo microclines during their investigation of optical properties and cell parameters in relation to Al,Si order, and in fact made comment to the contrary. However, a graph of c versus c* for the "standard" potash feldspars (Figure I5) reveals that the anomalous potash feldspars are characterised by a significantly different but parallel relationship to the normal potash feldspars. In fact, the anomalous potash feldspars appear to have a c cell edge that is smaller than expected.

Wright and Stewart (1968) and Wright (1968) described this type of anomalous alkali feldspar, which they recognised on the basis of $a_{(\text{observed})} - a_{(\text{estimated from b and c})} > 0.02\text{Å}$ or $2\theta.\bar{2}01_{(\text{estimated from } \bar{2}04 \text{ and } 060)} - 2\theta.\bar{2}01_{(\text{observed})} > 0.01°$. Reference to the graphs of b versus c, and $\bar{2}04$ versus 060 of these authors indicates that the anomalous feldspars are characterised either by a small c cell edge or by a high $2\theta.\bar{2}04$ value. It is of interest that Wright and Stewart (1968, page 71) referred to a "surprisingly large number of natural alkali feldspars" that are anomalous in this regard, but they were not

able to explain the anomaly.

It is clear from this discussion that the parameter $2\theta.\bar{2}04/060$ is a sensitive indicator of the degree of Al,Si order in both normal and anomalous alkali feldspars, providing that the anomalous alkali feldspars can be recognised by some independent means, for example according to the method described by Wright (1968). Alternatively, anomalous alkali feldspars can be distinguished on the basis of c*/b* and $\bar{2}04/060$ with reference to Figure I1, or from the relationship between c and c* with reference to Figure I5. In the case of the Encounter Bay Granites, the $\bar{2}04$ - 060 graph of Wright (1968) was used to illustrate the apparent structural states of the alkali feldspars examined, and to distinguish between normal and anomalous specimens.

Technique of sample extraction and preparation

Potash felspar grain fragments, as small as possible, were sampled sequentially across potash feldspar megacrysts in slabs of both varieties of the megacrystic granite using a dentist's drill with accessory diamond-tipped circular saw. Groundmass potash feldspar was similarly sampled. The individual fragments varied in weight from 2mgm to 7mgm, and were invariably heterogeneous, in that they contained fine grained quartz and/or plagioclase inclusions, exsolved albitic plagioclase, or more than one potash feldspar phase. Nevertheless, the method provided data that could not be obtained from bulk potash feldspar separates, although the nature of the diffraction pattern of the bulk separate, especially in the region between 29° and 31°2θ, may indicate the presence of more than one potash feldspar polymorph in the rock (see for example Vorma, 1971).

Sufficient silicon (about 1/10 of the sample weight) was added as internal standard to each sample, which was then finely ground. The powdered mix was smeared on to a narrow quartz plate[3] and scanned at least twice in a Philips X-ray diffractometer using Ni-filtered Cu radiation. Suitable peak intensities were obtained with a 1° divergence slit, 0.2mm receiving slit, and a 1° scatter slit, generator settings

---

[3]Due to the small sample size, it was necessary to limit the area of quartz plate on to which the sample was smeared. A quartz plate 1cm wide was used. Calculations indicate that the width of smear sample covered by the X-ray beam using a 1° divergence slit was less than 1cm during more than 70% of the scan interval.

of 40kV and 20mA, and a channel setting of 50% on the pulse height analyser.

In most samples, the $\bar{2}01$, 131, $1\bar{3}1$, 060 and $\bar{2}04$ reflections were measured to within less than $\pm$ 0.02°2θ. However, $\bar{2}01$ reflections could not be measured in those grain fragments containing quartz inclusions. In addition, the scan region 29° to 31°2θ was often complicated by the presence of more than one potash feldspar phase, or by the presence of a near monoclinic potash feldspar phase such that measurement of the 131 and $1\bar{3}1$ reflections was not attempted. In such cases, characterisation of the sample, to a first approximation, was based on the positions of the 060 and $\bar{2}04$ reflections. Indexing of the patterns was carried out with the aid of the calculated feldspar patterns of Borg and Smith (1968,1969). In the case of selected grain fragment samples, all resolved low angle reflections up to and including $\bar{2}04$ were measured, and the results were used for computer refinement of the unit cell dimensions, using the programme of Evans, Appleman and Handwerker (1963). In the diffraction patterns of some samples, it was possible to measure up to 13 plagioclase reflections, and so determine the nature of this coexisting phase. In some samples containing less plagioclase, it was possible to identify the plagioclase from the position of the 060 and $\bar{2}04$ reflections.

(Acknowledgements: Mr. K.M. Cellier, CSIRO Division of Mathematical Statistics, kindly examined the Figures given in this appendix and applied statistical tests of significance to the displacement of the anomalous feldspars from the normal feldspar curves. Dr. A.C. Oertel, CSIRO Division of Soils, wrote the computer program used to fit linear and polynomial expressions to the graphical data.)

TABLE I1

Composition and X-ray diffraction data for "standard" alkali feldspars.

	Or	c*/b*	$1\bar{3}1$-131	060a[1]	204a[1]	$\bar{2}04$/060
I-Hugo microcline	88	1.9949	0.762	41.815	50.534	1.2086
I-Hugo albite K-exch	99	1.9944	0.796	41.806	50.519	1.2085
I-131-62	99.5	1.9943	0.776	41.809	50.511	1.2082
2-Pontiskalk	99.8	1.9948	0.797	41.813	50.541	1.2088
3-Pellotsalo	-95	1.9947	0.777	41.800	50.561	1.2096
4-Spencer U	94	1.9999	0.269	41.789	50.599	1.2109
5-Spencer U	94	1.9989	0.245	41.798	50.586	1.2103
6-Spencer B	89	2.0024	-	41.750	50.628	1.2127
5-Spencer B	89	2.0024	-	41.750	50.629	1.2127
5-Low albite III K-exch	100	2.0020	-	41.719	50.653	1.2142
5-SH 1070	96	2.0069	-	41.694	50.678	1.2155
5-Benson Or	95	2.0082	-	41.660	50.683	1.2167
5-Benson NaCl K-exch	97	2.0094	-	41.649	50.686	1.2170
5-P50-56 K-exch	86	2.0093	-	41.656	50.710	1.2174
5-S62-34 K-exch	100	2.0128	-	41.601	50.746	1.2199
5-Puye K-exch	95	2.0171	-	41.590	50.816	1.2219
5-P50-90 K-exch	98	2.0147	-	41.575	50.775	1.2213
5-SynSanShaw	100	2.0202	-	41.590	50.902	1.2239
5-S63-30 K-exch	98	2.0181	-	41.543	50.851	1.2241
7-St. Gotthard		2.0119	-			1.2192
8-Spencer C		2.0104	-	41.662	50.733	1.2178
6-Spencer C		2.0107	-	41.663	50.744	1.2180
9-Sanidinised Spencer C		2.0204	-	41.549	50.874	1.2245
I-Hugo albite	1.7	1.9960	1.095	42.518	51.148	1.2030
I-128-62	1	1.9975	1.088	42.512	51.152	1.2033
5-Spencer U Na-exch	-0	1.9995	1.614	42.434	51.122	1.2052
5-Spencer B Na-exch	-6	2.0055	1.557	42.203	51.074	1.2102
5-Low albite III	-0	2.0083	1.567	42.367	51.302	1.2109
5-SH 1070 Na-exch	4	2.0108	1.760	42.254	51.218	1.2122
5-Benson Or Na-exch	7	2.0130	1.760	42.223	51.210	1.2129
5-P50-56 Na-exch	8.4	2.0125	1.656	42.204	51.212	1.2135
5-S62-34	0	2.0170	1.779	42.277	51.394	1.2157
5-P50-90 Na-exch	12	2.0187	1.590	42.073	51.272	1.2187
5-Puye Na-exch	2	2.0189	1.937	42.233	51.418	1.2175
5-SynSanShaw Na-exch	0	2.0220	2.013	42.206	51.436	1.2187
I-High albite	0	2.0190	1.935	42.230	51.436	1.2180
5-S63-30	0	2.0214	1.979	42.200	51.500	1.2204
10-Low albite	1.0	1.9965	1.119	42.498	51.164	1.2039
10-High albite	1.6	2.0218	1.929	42.157	51.488	1.2216

Numbers prefixing the samples listed in this Table indicate the following sources of data:

I- Orville (1967)
2- Finney and Bailey (1964)
3- Brown and Bailey (1963)
4- Bailey and Taylor (1955); Bailey (1969)
5- Wright and Stewart (1968)
6- Coleville and Ribbe (1968)
7- Jones (private communication, 1969)
8- Cole, Sørum and Kennard (1949); Jones and Taylor (1961)
9- Cole, Sørum and Kennard (1949)
10- Ferguson, Traill and Taylor (1958); Ribbe, Megaw and Taylor (1969)

TABLE I2

T-O bond length data, and calculated Al,Si order for "standard" alkali feldspars for which X-ray structure analyses have been completed.

		$T_1(o)$	$T_1(m)$	$T_2(o)$	$T_2(m)$	S	% order	c*/b*	$\bar{2}04/060$
3-Pellotsalo									
T-O bond (Å)		1.741	1.614	1.611	1.612				
Al/(*Al*+Si) calc.	A	0.874	0.067	0.049	0.055	1.045	80.2	1.9947	1.2096
	B	0.895	0.059	0.039	0.047	1.040	83.3		
2-Pontiskalk									
T-O bond (Å)		1.735	1.613	1.619	1.609				
Al/(*Al*+Si) calc.	A	0.836	0.061	0.100	0.036	1.033	75.9	1.9948	1.2088
	B	0.855	0.053	0.092	0.026	1.026	78.9		
4-Spencer U									
T-O bond (Å)		1.700	1.645	1.614	1.611				
Al/(*Al*+Si) calc.	A	0.614	0.265	0.068	0.049	0.996	50.8	1.9999	1.2109
	B	0.625	0.263	0.059	0.039	0.986	52.7		
6-Spencer B									
T-O bond (Å)		1.664		1.622					
Al/(*Al*+Si) calc.	A	0.385		0.119		1.008	35.5	2.0024	1.2127
	B	0.388		0.112		1.000	36.8		
8-Spencer C									
T-O bond (Å)		1.653		1.633					
Al/(*Al*+Si) calc.	A	0.315		0.188		1.006	16.9	2.0104	1.2178
	B	0.316		0.184		1.000	17.6		
6-Spencer C									
T-O bond (Å)		1.656		1.628					
Al/(*Al*+Si) calc.	A	0.334		0.157		0.982	23.6	2.0107	1.2180
	B	0.336		0.151		0.974			
7-St. Gotthard									
T-O bond (Å)		1.653		1.631					
Al/(*Al*+Si) calc.	A	0.315		0.176		0.982	18.5	2.0119	1.2192
	B	0.316		0.171		0.974	19.3		
9-Sanidinised Spencer C									
T-O bond (Å)		1.645		1.640					
Al/(*Al*+Si) calc.	A	0.265		0.233		0.996	4.3	2.0204	1.2245
	B	0.263		0.230		0.986	4.4		
10-Low albite									
T-O bond (Å)		1.746	1.610	1.615	1.612				
Al/(*Al*+Si) calc.	A	0.906	0.042	0.074	0.055	1.077	82.3	1.9965	1.2039
	B	0.928	0.033	0.066	0.046	1.073	85.5		
10-High albite									
T-O bond (Å)		1.648	1.644	1.639	1.643				
Al/(*Al*+Si) calc.	A	0.284	0.258	0.227	0.252	1.021	4.5	2.0218	1.2216
	B	0.283	0.257	0.224	0.250	1.014	4.4		

Sources of data indicated by numbers prefixing samples as in Table I1

A Tetrahedral *Al*/(*Al*+Si) calculated from T-O bond lengths using linear feldspar equation of Jones (1968)

B Tetrahedral *Al*/(*Al*+Si) calculated from T-O bond lengths using linear feldspar equation of Ribbe and Gibbs (1969)

S is the distant order function defined as $\Sigma_{i=1}^{i=4}|0.25-S_i|/1.50$ where S_i is the distant order *Al*/(*Al*+Si) in the four different feldspar tetrahedral sites (Smith and MacKenzie, 1961)

TABLE I3

c*/b*, 20.$\bar{2}$04/060 and degree of Al,Si order for "standard" alkali feldspars.

	c*/b*	% order A	% order B	$\bar{2}$04/060
I-Hugo microcline	1.9949		81.6	1.2086
I-Hugo albite K-exch	1.9944		86.3	1.2085
I-131-62	1.9943		87.3	1.2082
2-Pontiskalk	1.9948	75.9		1.2088
3-Pellotsalo	1.9947	80.2		1.2096
4-Spencer U	1.9999	50.8		1.2109
5-Spencer U	1.9989		52.3	1.2103
6-Spencer B	2.0024	35.5		1.2127
5-Spencer B	2.0024		35.5	1.2127
5-Low albite III K-exch	2.0020		37.1	1.2142
5-SH 1070	2.0069		21.5	1.2155
5-Benson Or	2.0082		18.6	1.2167
5-Benson NaCl K-exch	2.0094		16.3	1.2170
5-P50-56 K-exch	2.0093		16.5	1.2174
5-S62-34	2.0128		11.2	1.2199
5-Puye K-exch	2.0171		6.9	1.2219
5-P50-90 K-exch	2.0147		9.0	1.2213
5-SynSanShaw	2.0202		4.9	1.2239
5-S63-30 K-exch	2.0181		6.2	1.2241
7-St. Gotthard	2.0119	18.5		1.2192
8-Spencer C	2.0104	16.9		1.2178
6-Spencer C	2.0107	23.6		1.2180
9-Sanidinised Spencer C	2.0204	4.3		1.2245
10-Low albite	1.9965	82.3		1.2039
10-High albite	2.0218	4.5		1.2216

Sources of data indicated by numbers prefixing samples as in Table I1

% order A - calculated from T-O bond lengths using linear equation of Jones (1968)

% order B - estimated from Figure I2b, using linear relationship between c*/b* and ln(% Al,Si order)

TABLE I4

Direct (c) and reciprocal (c*) c-cell dimensions for "standard" potash feldspars

	c	c*
I-Hugo microcline	7.2199	0.15404
I-Hugo albite K-exch.	7.2219	0.15397
I-131-62	7.2230	0.15398
2-Pontiskalk	7.2188	0.15402
3-Pellotsalo	7.215	0.15399
4-Spencer U	7.2112	0.15433
5-Spencer U	7.213	0.15428
6-Spencer B	7.207	0.15439
5-Spencer B	7.207	0.15439
5-Low albite III K-exch.	7.204	0.15425
5-SH1070	7.201	0.15435
5-Benson Or	7.200	0.15451
5-Benson NaCl K-exch.	7.200	0.15457
5-P50-56 K-exch.	7.197	0.15458
5-S62-34	7.192	0.15466
5-Puye K-exch.	7.183	0.15494
5-P50-90 K-exch.	7.188	0.15471
5-SynSanShaw	7.172	0.15519
5-S63-30 K-exch.	7.178	0.15485
8-Spencer C	7.193	0.15469
6-Spencer C	7.192	0.15471
9-Sanidinised Spencer C	7.175	0.15506

Sources of data indicated by numbers prefixing samples as in Table I1.

TABLE I5

Potash feldspars from specimens of the border facies megacrystic granite

	$\bar{2}01\alpha^1$	$1\bar{3}1\bar{\alpha}$	$131\bar{\alpha}$	$1\bar{3}1$-131	$060\alpha^1$	$\bar{2}04\alpha^1$	$\bar{2}04/060$	Anomalous Normal	% order*
Specimen 4-61 slab A									
1	quartz	29.585	30.170	0.585	41.794	50.602	1.2108	A	66.0
2	quartz	smeared		-	41.763	50.650	1.2128	A	46.3
3	quartz	smeared		-	41.746	50.617	1.2125	N	39.0
4	20.983	near monoclinic		-	41.732	50.619	1.2130	N	35.6
5	specimen too small								
6	20.997	near monoclinic		-	41.755	50.596	1.2117	N	45.0
7	quartz	smeared		-	41.783	50.553	1.2099	N	62.1
8	quartz	29.512	30.199	0.687	41.822	50.546	1.2086	N	78.4
9	20.992	29.547	30.165	0.618	41.775	50.581	1.2108	N	52.9
10	21.028	29.599	30.173	0.574	41.768	50.591	1.2113	N	48.3
11	21.011	29.551	30.154	0.603	41.795	50.580	1.2102	N	58.9
12	quartz	smeared		-	41.804	50.518	1.2085	N	79.8
13	21.006	29.509	30.181	0.672	41.802	50.563	1.2096	N	65.5
14	21.025	29.527	30.201	0.674	41.819	50.546	1.2087	N	77.0
15	21.034	29.549	30.216	0.667	41.814	50.564	1.2093	N	69.2
Specimen 4-61 slab B									
1	quartz	29.632	30.077	0.445	41.787	50.597	1.2109	N	51.9
2	21.000	29.613	30.107	0.494	41.746	50.584	1.2117	N	45.0
3	20.998	29.635	30.110	0.475	41.759	50.590	1.2115	N	46.6
4	quartz	29.554	30.117	0.563	41.768	50.608	1.2117	N	45.0
5	quartz	smeared		-	41.766	50.591	1.2113	N	48.3
6	quartz	near monoclinic		-	41.762	50.625	1.2122	N	41.1
7	21.031	smeared		-	41.736	50.614	1.2127	N	37.6
8	21.027	smeared		-	41.737	50.598	1.2123	N	40.4
9	quartz	29.705	30.060	0.355	41.761	50.623	1.2122	N	41.1
10	quartz	29.554	30.157	0.603	41.786	50.537	1.2094	N	64.7
11	20.978	smeared		-	41.785	50.599	1.2109	N	51.9
12	21.011	near monoclinic		-	41.758	50.602	1.2118	N	44.2
13	21.028	near monoclinic		-	41.741	50.606	1.2124	N	39.7
14	21.004	near monoclinic		-	41.759	50.592	1.2115	N	46.6
15	quartz	smeared		-	41.775	50.597	1.2112	N	49.2
16	quartz	29.633	30.108	0.475	41.779	50.631	1.2119	A	54.3
17	20.955	29.578	30.127	0.549	41.775	50.648	1.2124	A	49.7
18	21.028	29.587	30.113	0.526	41.780	50.594	1.2110	N	51.0
19	20.978	29.603	30.110	0.507	41.789	50.647	1.2120	A	53.4
20	21.025	29.654	30.116	0.462	41.777	50.578	1.2107	N	53.8
21	21.004	29.557	30.170	0.613	41.814	50.583	1.2097	N	64.4
22	20.992	29.563	30.129	0.566	41.765	50.574	1.2109	N	51.9
23	quartz	29.554	30.173	0.619	41.788	50.567	1.2101	N	59.9
24	quartz	29.558	30.189	0.631	41.781	50.535	1.2095	N	66.7

TABLE I5 (Cont'd)

Potash feldspars from specimens of the border facies megacrystic granite

	$\bar{2}01\alpha^1$	$1\bar{3}1\bar{\alpha}$	$131\bar{\alpha}$	$1\bar{3}1$-131	$060\alpha^1$	$\bar{2}04\alpha^1$	$\bar{2}04/060$	Anomalous Normal	% order*
Specimen 4-55									
1	quartz	smeared		-	41.771	50.644	1.2124	A	49.7
2	21.030	smeared		-	41.762	50.603	1.2117	N	45.0
3	20.987	29.609	30.051	0.442	41.775	50.623	1.2118	A	55.3
4	21.018	29.668	30.080	0.412	41.774	50.651	1.2125	A	48.8
5	21.024	smeared		-	41.752	50.621	1.2124	N	39.7
6	quartz near monoclinic			-	41.738	50.652	1.2137	N	31.4
7	20.993	smeared		-	41.757	50.630	1.2125	N	39.0
8	specimen too small								
9	specimen too small								
10	21.063	29.581	30.167	0.586	41.788	50.581	1.2104	N	56.8
11	21.007	29.538	30.190	0.652	41.800	50.609	1.2108	N	52.9
12	21.015	29.602	30.133	0.531	41.792	50.599	1.2107	N	53.8
13	21.005	29.562	30.171	0.609	41.811	50.597	1.2102	N	58.9
14	21.064	29.573	30.201	0.628	41.807	50.554	1.2092	N	70.4
15	21.009	tricl.+monoc.		-	41.803	50.604	1.2107	N	53.8
16	quartz	29.565	30.124	0.559	41.762	50.573	1.2108	N	52.9
17	21.027	29.578	30.159	0.581	41.792	50.611	1.2110	N	51.0
18	21.025	29.575	30.172	0.597	41.794	50.621	1.2112	A	61.5
19	21.033	29.560	30.193	0.633	41.797	50.591	1.2104	N	56.8
20	21.069	29.551	30.195	0.644	41.798	50.522	1.2094	N	67.9
21	21.017	29.493	30.176	0.683	41.792	50.577	1.2103	N	57.8
Specimen 9-11									
1	21.026	29.485	30.189	0.704	41.791	50.552	1.2096	N	65.5
2	21.001	29.544	30.212	0.668	41.805	50.560	1.2094	N	67.9
3	21.022	29.558	30.175	0.617	41.788	50.587	1.2106	N	54.8
4	21.004	29.576	30.179	0.621	41.807	50.611	1.2106	A	68.4
5	21.053	29.580	30.179	0.599	41.793	50.602	1.2108	A	66.0
6	21.022	29.532	30.139	0.607	41.778	50.543	1.2098	N	63.2
7	21.016	29.603	30.219	0.616	41.816	50.616	1.2104	A	70.9
8	21.084	29.587	30.201	0.614	41.808	50.564	1.2094	N	67.9
9	21.041	29.542	30.134	0.592	41.807	50.606	1.2105	N	55.8
10	21.045	29.563	30.197	0.634	41.809	50.579	1.2098	N	63.2
11	21.030	29.536	30.172	0.636	41.789	50.580	1.2104	N	56.8
12	20.994	29.528	30.109	0.581	41.796	50.634	1.2115	A	58.3
13	21.045	29.542	30.188	0.646	41.812	50.601	1.2102	N	58.9
14	21.032	29.524	30.329	0.715	41.875	50.616	1.2088	A	94.1
15	21.027	near monoclinic		-	41.762	50.573	1.2110	N	51.0
16	quartz	near monoclinic		-	41.732	50.565	1.2117	N	45.0
17	21.022	29.709	30.103	0.394	41.765	50.626	1.2122	N	41.1
18	21.045	tricl.+monoc.		-	41.758	50.629	1.2125	N	39.0
19	21.014	tricl.+monoc.		-	41.747	50.623	1.2126	N	38.3
20	21.042	tricl.+monoc.		-	41.746	50.607	1.2123	N	40.4
21	21.039	near monoclinic		-	41.750	50.641	1.2130	N	35.6
22	specimen too small								
23	21.003	near monoclinic		-	41.760	50.666	1.2133	A	42.4

*% order estimated from $\bar{2}04/060$ with reference to Figures I3 and I4

Prefices on specimen numbers have the following locality key:

4- Port Elliot

9- West Island

TABLE I6

Potash feldspars from specimens of the inner facies megacrystic granite

	$\bar{2}01\alpha^1$	$131\bar{\alpha}$	$1\bar{3}1\bar{\alpha}$	$1\bar{3}1$-131	$060\alpha^1$	$\bar{2}04\alpha^1$	$\bar{2}04/060$	Anomalous Normal	% order*
Specimen 4-79									
1	21.032	29.483	30.224	0.741	41.810	50.535	1.2087	N	77.0
2	20.985	29.495	30.209	0.714	41.837	50.582	1.2090	A	90.8
3	21.020	29.527	30.186	0.659	41.785	50.551	1.2098	N	63.2
4	21.001	29.502	30.181	0.679	41.817	50.592	1.2098	A	78.8
5	21.059	smeared		-	41.789	50.590	1.2106	N	54.8
6	21.027	29.571	30.170	0.599	41.801	50.573	1.2099	N	62.1
7	21.020	29.556	30.186	0.630	41.820	50.587	1.2096	N	65.5
8	quartz	29.547	30.167	0.620	41.801	50.567	1.2097	N	64.4
9	21.045	29.542	30.183	0.641	41.785	50.579	1.2105	N	55.8
10	21.023	29.496	30.256	0.760	41.798	50.536	1.2091	N	71.7
11	quartz	29.496	30.185	0.689	41.811	50.597	1.2101	A	74.7
12	20.999	29.534	30.169	0.635	41.809	50.588	1.2100	N	61.0
13	21.050	tricl.+monoc.		-	41.797	50.592	1.2104	N	56.8
14	20.968	29.507	30.220	0.713	41.809	50.558	1.2093	N	69.2
15	21.045	29.502	30.214	0.712	41.798	50.554	1.2095	N	66.7
16	21.083	29.554	30.267	0.713	41.875	50.620	1.2088	A	94.1
17	21.007	29.563	30.154	0.591	41.785	50.603	1.2110	N	51.0
18	20.991	29.576	30.148	0.572	41.780	50.596	1.2110	N	51.0
19	20.990	29.506	30.183	0.677	41.793	50.570	1.2100	N	61.0
20	quartz	29.515	30.205	0.690	41.799	50.545	1.2092	N	70.4
21	21.038	29.552	30.190	0.638	41.793	50.587	1.2104	N	56.8
22	20.987	29.574	30.164	0.590	41.820	50.592	1.2098	A	78.8
Specimen 4-81									
1	21.006	29.574	30.139	0.565	41.788	50.624	1.2114	A	59.3
2	21.019	29.590	30.147	0.557	41.787	50.620	1.2114	A	59.3
3	21.043	29.606	30.170	0.564	41.784	50.608	1.2112	N	49.2
4	21.038	29.676	30.130	0.427	41.769	50.625	1.2120	N	42.6
5	21.022	29.627	30.133	0.506	41.788	50.575	1.2103	N	57.8
6	20.986	29.602	30.104	0.502	41.760	50.589	1.2114	N	47.5
7	20.978	29.576	30.136	0.560	41.811	50.643	1.2112	A	61.5
8	20.992	29.646	30.118	0.472	41.749	50.595	1.2119	N	43.4
9	21.003	29.613	30.112	0.499	41.782	50.617	1.2115	N	46.6
10	21.035	29.637	30.131	0.494	41.762	50.581	1.2112	N	49.2
11	21.003	29.580	30.105	0.525	41.784	50.600	1.2110	N	51.0
12	20.978	29.571	30.138	0.567	41.783	50.641	1.2120	A	53.4
13	21.001	29.588	30.154	0.566	41.768	50.578	1.2109	N	51.9
14	21.009	29.635	30.104	0.469	41.779	50.608	1.2113	N	48.3

*% order estimated from $\bar{2}04/060$ with reference to Figures I3 and I4

The specimens of inner facies megacrystic granite were collected from Port Elliot

TABLE I7

Potash feldspars from a specimen of type B hybrid granite

	$\bar{2}01\alpha^1$	$131\bar{\alpha}$	$1\bar{3}1\bar{\alpha}$	$1\bar{3}1$-131	$060\alpha^1$	$204\alpha^1$	$\bar{2}04/060$	Anomalous Normal	% order*
Specimen 3-27									
1	quartz	29.609	30.115	0.506	41.780	50.591	1.2109	N	51.9
2	21.039	29.599	30.156	0.557	41.802	50.587	1.2102	N	58.9
3	21.056	29.655	30.151	0.496	41.759	50.591	1.2115	N	46.6
4	21.062	29.666	30.167	0.501	41.764	50.591	1.2114	N	47.5
5	21.063	29.598	30.137	0.539	41.784	50.538	1.2095	N	66.7
6	21.040	29.553	30.124	0.571	41.780	50.583	1.2107	N	53.8
7	21.040	29.552	30.174	0.622	41.789	50.574	1.2102	N	58.9
8	21.039	near monoclinic		-	41.745	50.644	1.2137	N	31.4
9	21.007	near monoclinic		-	41.778	50.671	1.2128	A	46.3
10	21.029	near monoclinic		-	41.740	50.640	1.2132	N	34.4
11	20.986	near monoclinic		-	41.764	50.655	1.2129	A	45.5
12	20.998	smeared		-	41.748	50.632	1.2128	N	36.9
13	21.049	smeared		-	41.712	50.581	1.2126	N	38.3
14	21.028	smeared		-	41.746	50.619	1.2125	N	39.0
15	21.023	smeared		-	41.746	50.589	1.2118	N	44.2
16	21.026	near monoclinic		-	41.761	50.635	1.2125	N	39.0
17	21.064	29.694	30.125	0.431	41.776	50.652	1.2125	A	48.8

FIGURE I1

Graph of $2\theta.\bar{2}04/060$ versus c*/b* for "standard" soda and potash feldspars (Table I1).

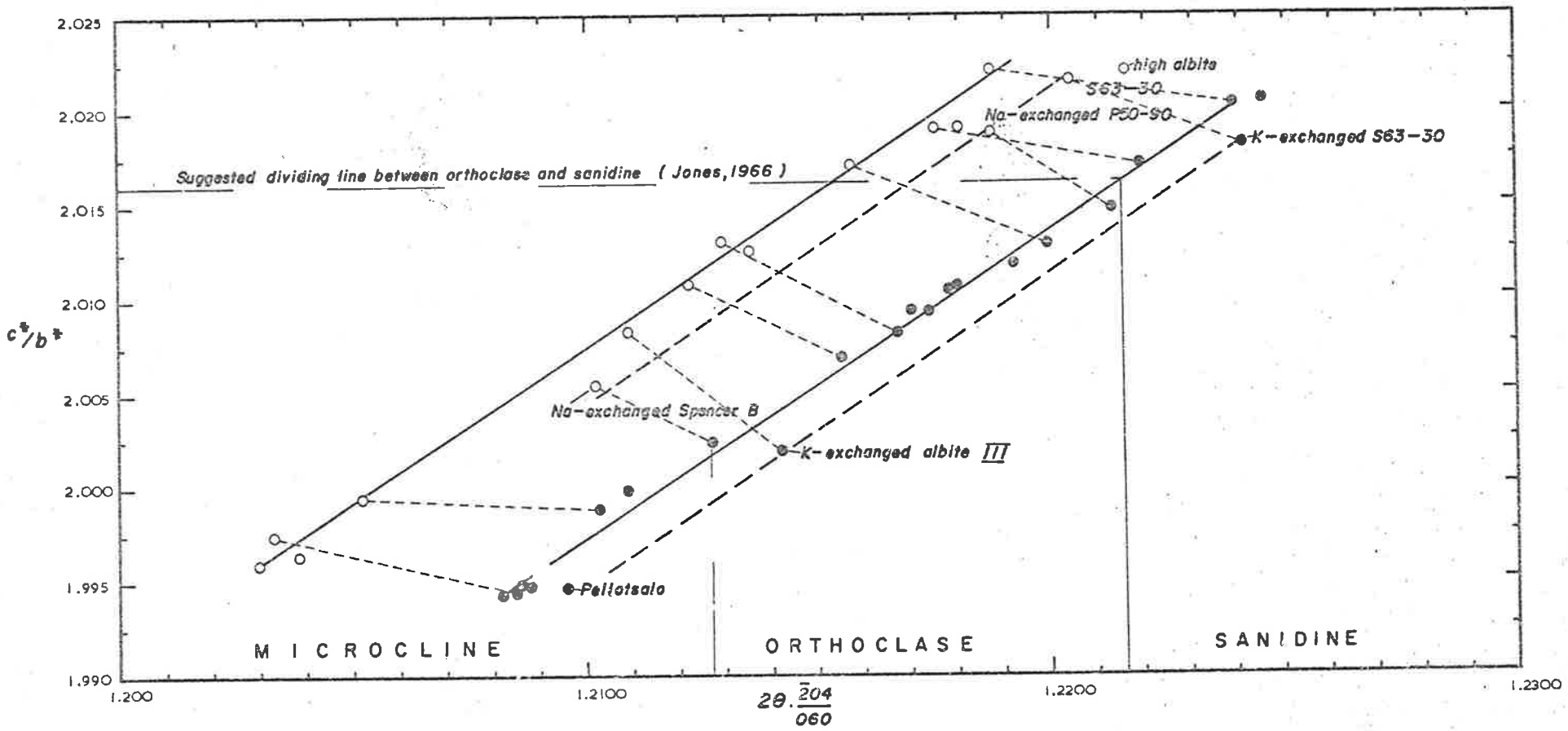
2.025
2.020
2.015
2.010
2.005
2.000
1.995
1.990
c*/b*
high albite
S63-30
Na-exchanged P50-90
K-exchanged S63-30
Suggested dividing line between orthoclase and sanidine (Jones, 1966)
Na-exchanged Spencer B
K-exchanged albite III
Pellotsalo
MICROCLINE
ORTHOCLASE
SANIDINE
1.200
1.2100
1.2200
1.2300
2θ. 204/060

FIGURE I2

a. Graph of c*/b* versus degree of Al,Si order in "standard" alkali feldspars for which X-ray crystal structure analyses have been completed (revised from Jones, 1966).

b. Graph of c*/b* versus natural logarithm of degree of Al,Si order in "standard" alkali feldspars for which X-ray crystal structure analyses have been completed.

T2a

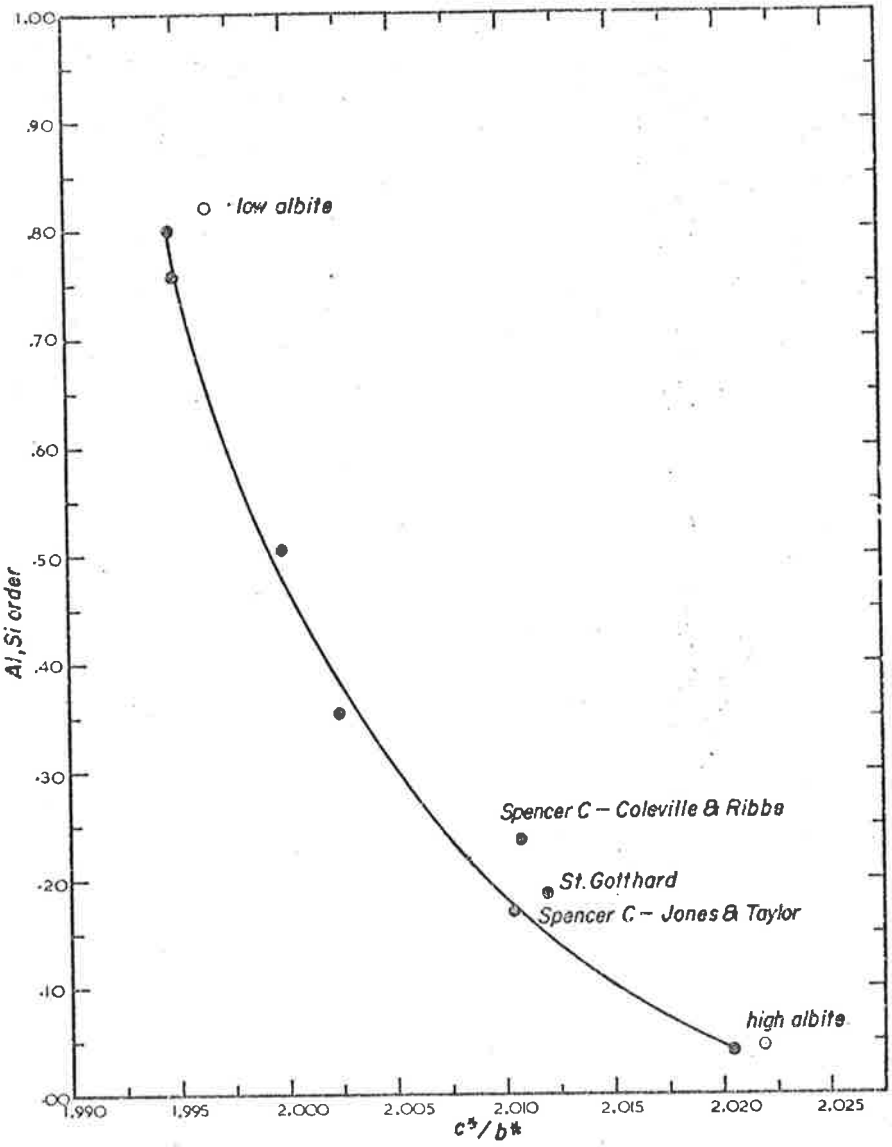
1.00
.90
.80
.70
.60
.50
.40
.30
.20
.10
.00
Al, Si order
low albite
Spencer C – Coleville & Ribbe
St. Gotthard
Spencer C – Jones & Taylor
high albite
1.990
1.995
2.000
2.005
2.010
2.015
2.020
2.025
c*/b*

T2b

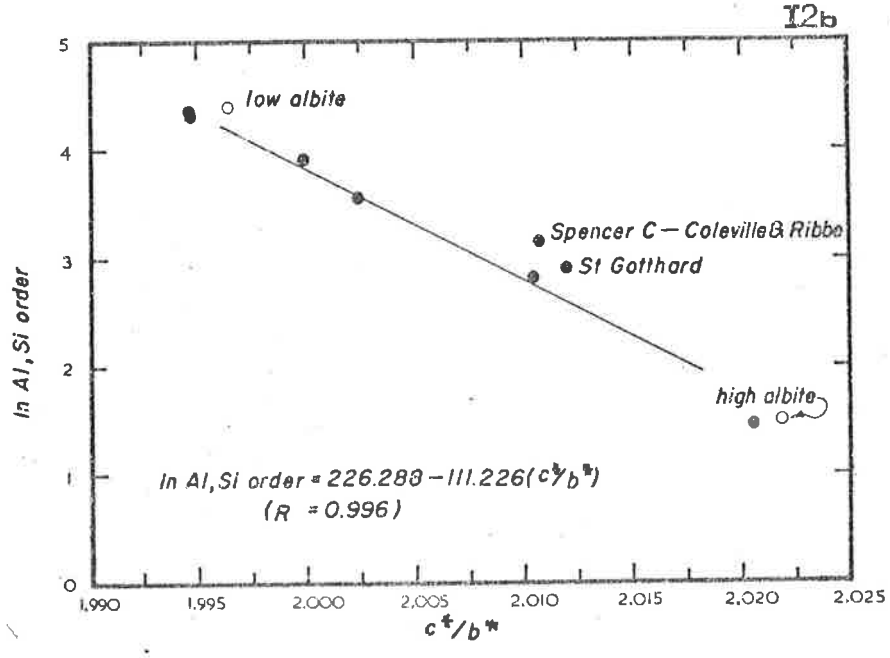
5
4
3
2
1
0
ln Al, Si order
low albite
Spencer C – Coleville & Ribbe
St Gotthard
high albite
ln Al, Si order = 226.288 – 111.226(c*/b*)
(R = 0.996)
1.990
1.995
2.000
2.005
2.010
2.015
2.020
2.025
c*/b*

FIGURE I3

Graph of $2\theta.\bar{2}04/060$ versus degree of Al,Si order for "standard" soda and potash feldspars.

FIGURE I4

Graph of $2\theta.\bar{2}04/060$ versus natural logarithm of degree of Al,Si order for "standard" potash feldspars.

I3

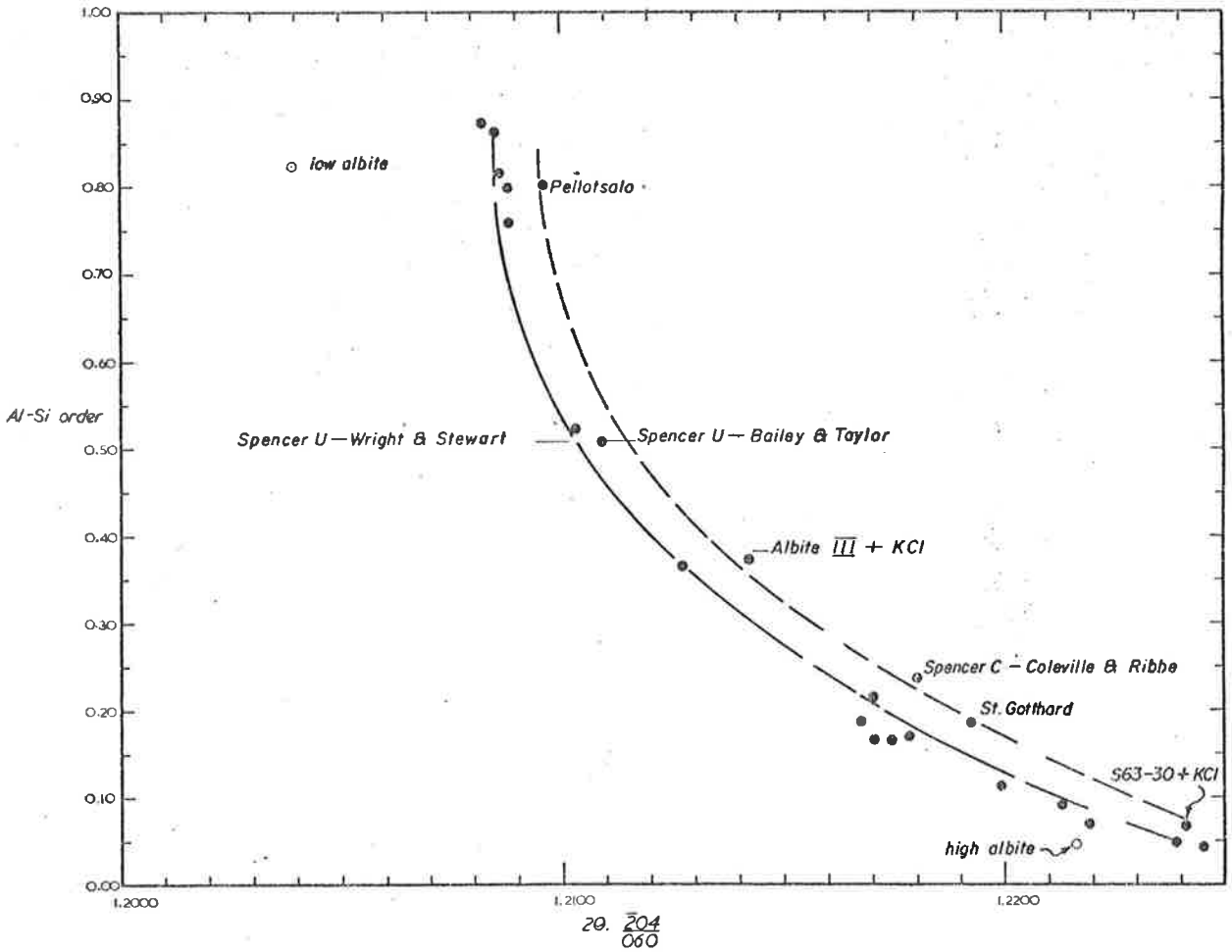
1.00
0.90
0.80
0.70
0.60
0.50
0.40
0.30
0.20
0.10
0.00
Al-Si order
o low albite
Pellotsalo
Spencer U — Wright & Stewart
Spencer U — Bailey & Taylor
Albite III + KCl
Spencer C — Coleville & Ribbe
St. Gotthard
S63-30 + KCl
high albite
1.2000
1.2100
1.2200
2θ. 204/060

I4

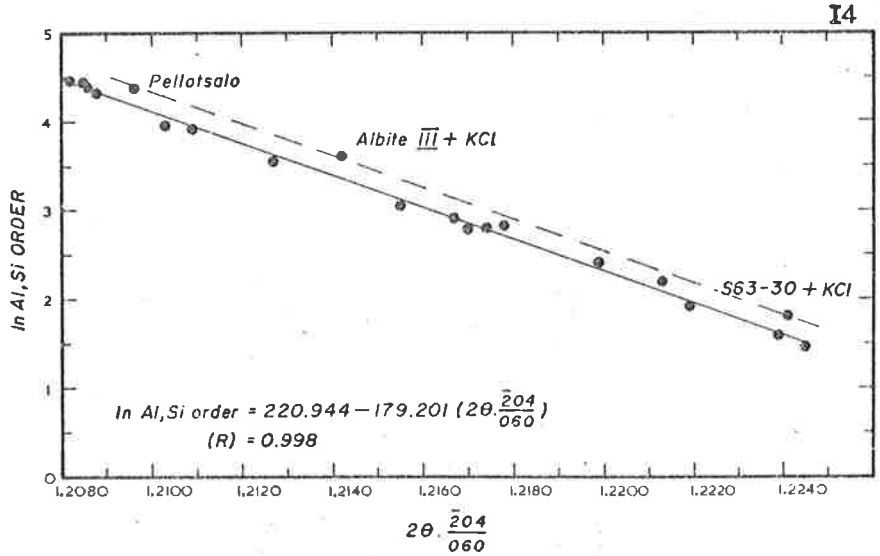
5
4
3
2
1
0
ln Al,Si ORDER
Pellotsalo
Albite III + KCl
S63-30 + KCl
ln Al,Si order = 220.944 − 179.201 (2θ. 204/060)
(R) = 0.998
1.2080
1.2100
1.2120
1.2140
1.2160
1.2180
1.2200
1.2220
1.2240
2θ. 204/060

FIGURE I5

Graph of c* (reciprocal) versus c (direct) cell dimensions for "standard" potash feldspars.

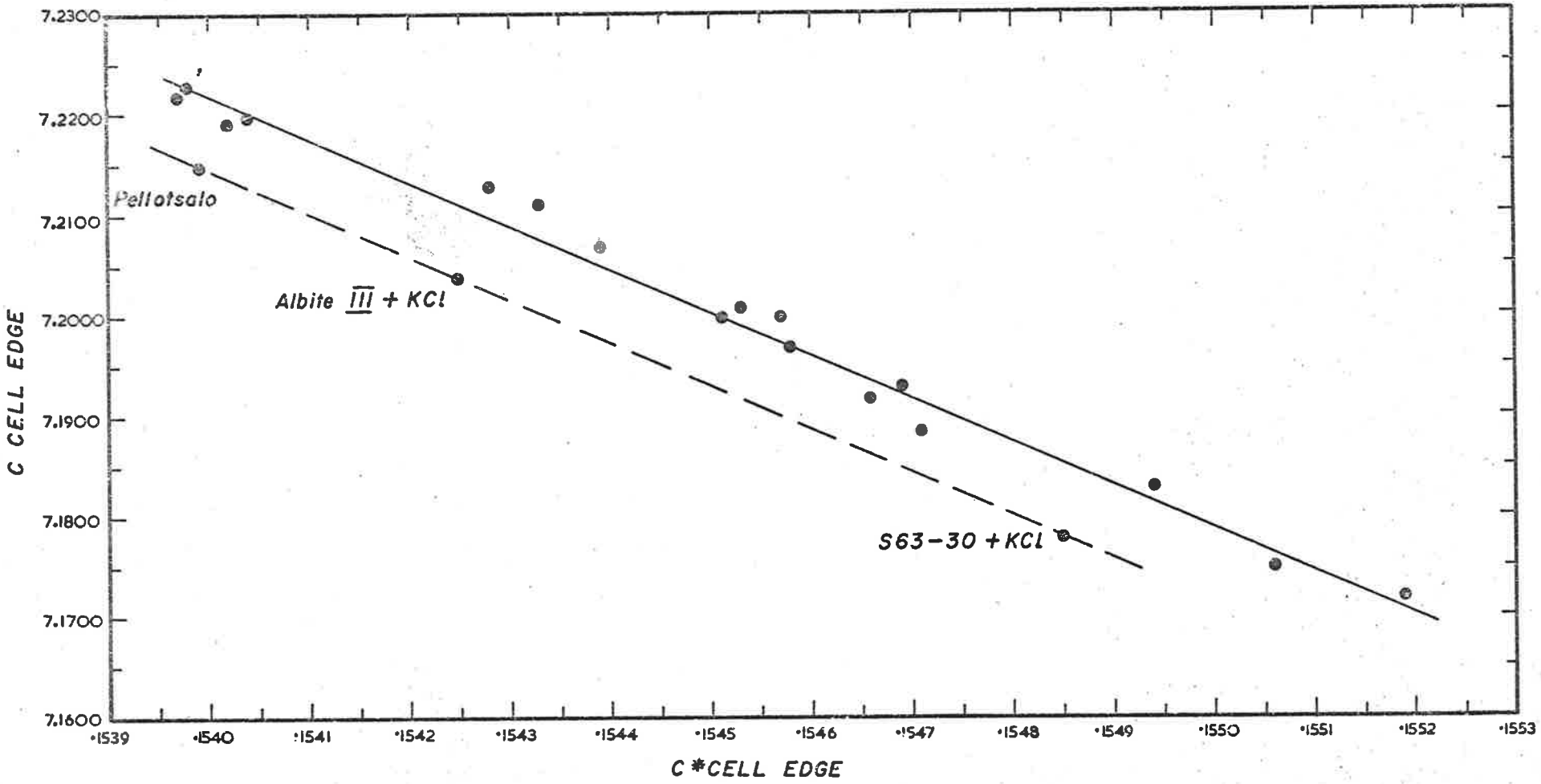
7.2300
7.2200
7.2100
7.2000
7.1900
7.1800
7.1700
7.1600
C CELL EDGE
Pellotsalo
Albite III + KCl
S63-30 + KCl
·1539
·1540
·1541
·1542
·1543
·1544
·1545
·1546
·1547
·1548
·1549
·1550
·1551
·1552
·1553
C*CELL EDGE

APPENDIX J

Electron microprobe analyses of coexisting feldspars in the Encounter Bay Granites

The electron microprobe analyses were carried out under the following conditions:

Accelerating voltage - 20Kv
Beam current - 50nA
Beam fully focussed
Flow proportional counters
Counting time - 10 seconds (peak and one background position)
Standards used - Orthoclase (K)
Bytownite (Ca)
Barytes (Ba)
Celestite (Sr)
Corundum (Al)
Quartz (Si)
Jadeite (Na)
Fe metal
Corrections to the raw data were made according to the method of Sweatman and Long (1969) using the procedure of Oertel (1971)

The analyses given in the following Tables are quoted to within calculated counting error.

TABLE J1

Electron microprobe analyses of coexisting feldspars in the inner facies megacrystic granite. Specimen 4-79.

Traverse across potash feldspar megacryst

		0 edge 1	0.34mm	0.98mm	1.75mm	2.71mm	3.49mm	3.81mm	4.28mm	4.77mm	5.16mm
	SiO_2	67.4	64.9	67.3	66.3	65.7	65.9	63.9	65.8	65.2	65.1
	Al_2O_3	20.0	18.7	19.8	19.2	19.2	18.5	18.7	19.1	18.9	18.7
Total Fe as	FeO	0.08	0.08	0.07	0.22	0.08	0.12	0.09	0.06	0.05	0.07
	CaO	0.79	0.04	0.36	0.15	0.11	0.10	0.04	0.08	0.05	0.10
	Na_2O	10.6	0.52	7.2	4.27	3.10	0.52	0.59	2.48	0.86	0.57
	K_2O	0.66	15.6	6.3	9.9	12.3	15.4	15.2	13.1	14.9	15.4
	BaO	0.05	0.15	0.07	0.20	0.33	0.26	0.34	0.27	0.35	0.26
	SrO	0.28	0.27	0.32	0.30	0.36	0.24	0.32	0.33	0.30	0.29
	TOTAL	99.9	100.3	101.4	100.5	101.2	101.0	99.2	101.2	100.6	100.5
Molecular percentages of end-members											
	An	3.8	0.2	1.7	0.8	0.5	0.5	0.5	0.4	0.3	0.5
	Or	3.8	94.7	35.9	59.6	71.5	94.2	93.4	76.9	91.1	93.7
	Ab	92.3	4.8	62.3	39.2	27.4	4.8	5.5	22.2	8.0	5.3
	Cn	0.1	0.3	0.1	0.3	0.6	0.5	0.6	0.5	0.7	0.5

TABLE J1 (Cont'd)

Electron microprobe analyses of coexisting feldspars in the inner facies megacrystic granite. Specimen 4-79.

	5.54mm	6.09mm	6.91mm	6.98mm	7.80mm	8.56mm	9.09mm	9.80mm	9.80mm[A]	10.61mm
SiO_2	65.0	64.2	64.9	63.5	65.2	65.3	66.0	65.7	65.4	65.6
Al_2O_3	18.9	18.8	18.9	18.5	18.8	18.7	19.1	18.7	18.6	18.8
Total Fe as FeO	0.03	0.08	0.03	0.12	0.08	0.06	0.04	0.08	0.09	0.06
CaO	0.06	0.03	0.04	0.07	0.03	0.03	0.09	0.02	0.08	0.02
Na_2O	1.06	0.70	0.86	3.96	0.67	0.84	1.80	0.71	2.71	0.99
K_2O	14.5	14.7	14.6	11.1	14.9	14.4	13.5	14.9	11.8	14.3
BaO	0.21	0.71	0.28	0.31	0.42	0.46	0.42	0.33	0.38	0.50
SrO	0.33	0.32	0.29	0.28	0.33	0.32	0.32	0.31	0.27	0.28
TOTAL	100.1	99.5	99.9	97.8	100.4	100.1	101.3	100.8	99.3	100.6
Molecular percentages of end-members										
An	0.3	0.2	0.2	0.3	0.1	0.1	0.5	0.1	0.4	0.1
Or	89.4	91.8	91.1	64.2	92.7	90.9	82.1	92.6	73.4	89.5
Ab	9.9	6.6	8.2	34.9	6.4	8.0	16.6	6.7	25.5	9.4
Cn	0.4	1.4	0.5	0.6	0.8	0.9	0.8	0.6	0.7	0.9

TABLE J1 (Cont'd)

Electron microprobe analyses of coexisting feldspars in the inner facies megacrystic granite. Specimen 4-79.

	11.19mm	11.33mm	11.47mm pl. edge	11.85mm pl. core	12.08mm pl. edge	12.41mm	13.28mm	14.26mm	14.96mm edge 2
SiO_2	65.9	65.7	69.2	66.3	67.1	65.5	65.6	65.0	64.3
Al_2O_3	18.7	18.7	20.5	21.1	20.6	19.0	18.8	18.6	19.0
Total Fe as FeO	0.07	0.09	0.03	0.50	0.03	0.06	0.06	0.06	0.09
CaO	0.03	0.08	0.63	3.29	1.56	0.04	0.16	0.03	0.03
Na_2O	0.87	0.47	11.8	7.1	10.7	1.08	0.93	0.44	0.80
K_2O	14.6	15.2	0.11	0.85	0.19	14.1	14.7	15.5	14.7
BaO	0.24	0.22	0.20	0.28	0.04	0.74	0.31	0.12	0.09
SrO	0.31	0.28	0.23	0.23	0.24	0.21	0.28	0.30	0.30
TOTAL	100.7	100.7	102.7	99.7	100.5	100.7	100.8	100.1	99.3
Molecular percentages of end-members									
An	0.2	0.4	2.8	19.1	7.4	0.2	0.8	0.2	0.2
Or	91.1	94.7	0.6	5.9	1.1	88.1	89.9	95.5	92.1
Ab	8.3	4.5	96.2	74.5	91.5	10.3	8.6	4.1	7.6
Cn	0.4	0.4	0.3	0.6	0.1	1.4	0.6	0.2	0.2

[A]repeat analysis, beam shifted up to 20 microns

Analyst: A.R. Milnes

pl = plagioclase

TABLE J2

Electron microprobe analyses of coexisting feldspars in the inner facies megacrystic granite. Specimen 4-93.

Traverse across potash feldspar megacryst

		0 edge 1	0.67mm	1.17mm	1.17mm[A]	1.47mm	1.82mm	2.33mm	3.29mm	4.37mm	5.31mm
	SiO_2	64.0	63.9	65.4	64.4	70.1	62.6	63.3	63.8	63.9	63.9
	Al_2O_3	18.3	18.6	21.6	20.1	19.2	21.5	19.2	19.4	19.7	19.4
Total Fe as	FeO	0.11	0.05	0.23	0.13	0.00	0.00	0.08	0.02	0.03	0.04
	CaO	0.08	0.05	1.95	0.57	1.17	2.45	0.09	0.03	0.05	0.04
	Na_2O	0.38	0.57	11.0	5.3	10.9	10.4	0.56	0.65	0.95	0.69
	K_2O	16.0	16.2	0.85	10.5	0.03	0.08	15.4	15.7	14.8	15.4
	BaO	0.13	0.10	0.05	0.05	0.07	0.03	0.08	0.23	0.71	0.69
	SrO	0.40	0.32	0.24	0.28	0.38	0.03	0.29	0.26	0.29	0.37
	TOTAL	99.4	99.8	101.3	101.3	101.9	97.4	99.0	100.1	100.4	100.5
Molecular proportions of end-members											
	An	0.4	0.2	8.6	2.5	5.6	11.5	0.5	0.2	0.3	0.2
	Or	95.9	94.5	4.4	55.3	0.2	0.4	94.2	93.5	89.7	92.2
	Ab	3.5	5.1	86.9	42.1	94.1	88.0	5.2	5.9	8.7	6.3
	Cn	0.2	0.2	0.1	0.1	0.1	0.1	0.1	0.4	1.3	1.3

TABLE J2 (Cont'd)

Electron microprobe analyses of coexisting feldspars in the inner facies megacrystic granite. Specimen 4-93.

		7.36mm	7.96mm	8.41mm	9.12mm	10.05mm	11.14mm edge 2	Groundmass potash	Groundmass feldspar
	SiO_2	64.1	63.7	63.1	64.0	63.0	61.9	63.7	63.5
	Al_2O_3	19.6	19.3	19.6	19.7	19.4	19.0	19.6	19.4
Total Fe as	FeO	0.02	0.05	0.04	0.04	0.01	0.03	0.04	0.02
	CaO	0.08	0.05	0.03	0.05	0.03	0.11	0.12	0.05
	Na_2O	3.95	0.36	0.73	0.71	0.65	0.97	0.66	0.74
	K_2O	11.6	15.5	14.9	14.9	15.2	14.4	15.0	14.9
	BaO	0.43	0.12	0.35	0.57	0.52	0.21	0.07	0.05
	SrO	0.26	0.25	0.26	0.40	0.31	0.34	0.29	0.30
	TOTAL	100.0	99.3	99.0	100.4	99.7	97.0	99.5	99.0
Molecular percentages of end-members									
	An	0.4	0.3	0.1	0.2	0.2	0.6	0.6	0.3
	Or	65.2	96.1	92.3	92.0	92.8	89.8	93.0	92.7
	Ab	33.7	3.4	6.9	6.7	6.0	9.2	6.2	7.0
	Cn	0.7	0.2	0.7	1.1	1.0	0.4	0.1	0.1

TABLE J2 (Cont'd)

Electron microprobe analyses of coexisting feldspars in the inner facies megacrystic granite. Specimen 4-93.

Traverse across plagioclase megacryst

	0 Core	0.68mm	1.37mm	1.94mm	2.71mm	3.50mm edge
SiO	56.9	58.4	55.2	59.0	66.1	66.8
Al O	26.6	27.1	29.3	26.7	21.9	21.8
Total Fe as FeO	0.15	0.07	0.09	0.02	0.04	0.3
CaO	7.4	7.4	9.8	7.3	1.69	0.84
Na O	7.3	8.0	6.5	7.8	11.4	11.8
K O	0.14	0.14	0.11	0.08	0.06	0.10
BaO	0.01	0.01	0.03	0.02	0.02	0.00
SrO	0.20	0.25	0.32	0.24	0.31	0.22
TOTAL	98.7	101.4	101.4	101.2	101.5	101.6
Molecular percentages of end-members						
An	35.6	33.3	45.2	34.1	7.5	3.8
Or	0.8	0.8	0.6	0.4	0.3	0.5
Ab	63.6	65.9	54.2	65.4	92.1	95.7
Cn	trace	trace	trace	trace	trace	0.0

Analyst: A.R. Milnes

TABLE J3

Electron microprobe analyses of coexisting feldspars in the border facies megacrystic granite. Specimen 3-26.

Traverse across potash feldspar megacryst

		0 Plag.	0.66mm Plag.	0.73mm edge 1	1.26mm	1.80mm	2.60mm	3.29mm	4.02mm	4.62mm	5.41mm	5.83mm	8.12mm	8.70mm	9.10mm edge 2
	SiO_2	62.9	63.6	64.1	64.7	64.7	64.4	65.3	64.5	65.4	64.9	65.2	65.5	65.0	67.7
	Al_2O_3	22.9	22.5	18.2	18.3	18.5	18.3	18.4	18.5	18.4	18.3	18.4	18.3	18.6	16.4
Total Fe as	FeO	0.16	0.00	0.02	0.02	0.03	0.01	0.02	0.01	0.02	0.00	0.02	0.02	0.02	0.02
	CaO	4.13	3.83	0.06	0.06	0.02	0.01	0.01	0.01	0.01	0.02	0.00	0.02	0.12	0.11
	Na_2O	9.2	9.3	0.43	1.09	0.77	0.47	0.69	0.39	0.99	0.47	0.45	0.96	2.21	0.59
	K_2O	0.09	0.09	15.9	14.4	15.8	16.4	15.9	16.9	15.9	16.8	16.5	16.2	15.0	14.3
	BaO	0.00	0.02	0.41	0.53	0.87	0.54	0.52	0.36	0.48	0.28	0.30	0.19	0.30	0.24
	SrO	0.26	0.30	0.34	0.31	0.37	0.32	0.34	0.32	0.33	0.31	0.30	0.31	0.38	0.35
	TOTAL	99.6	99.7	99.5	99.4	101.1	100.5	100.8	101.0	101.5	101.1	101.2	101.5	101.6	99.7
Molecular percentages of end-members															
	An	19.8	18.4	0.3	0.3	0.1	trace	0.1	trace	trace	0.1	0.0	0.1	0.5	0.6
	Or	0.5	0.5	95.0	88.5	91.6	94.9	95.9	96.0	90.5	95.4	95.5	91.3	80.9	93.1
	Ab	79.7	81.1	3.9	10.2	6.8	4.1	3.1	3.4	8.6	4.1	4.0	8.2	18.1	5.8
	Cn	0.0	trace	0.8	1.0	1.5	1.0	1.0	0.6	0.8	0.5	0.5	0.3	0.5	0.5

TABLE J3 (Cont'd)

Electron microprobe analyses of coexisting feldspars in the border facies megacrystic granite. Specimen 3-26.

Plagioclase rimming potash feldspar megacryst

		edge 1	core	edge 2
	SiO_2	61.1	59.5	62.8
	Al_2O_3	24.8	25.2	23.6
Total Fe as	FeO	0.09	0.00	0.01
	CaO	5.6	6.5	4.43
	Na_2O	8.0	7.5	8.8
	K_2O	0.18	0.27	0.14
	BaO	0.01	0.00	0.00
	SrO	0.22	0.28	0.32
	TOTAL	100.0	99.2	100.1
Molecular percentages of end-members				
	An	27.6	31.8	21.5
	Or	1.1	1.6	0.8
	Ab	71.3	66.6	77.7
	Cn	trace	0.00	0.00

Analyst: A.R. Milnes

TABLE J4

Electron microprobe analyses of coexisting feldspars in the border facies megacrystic granite. Specimen 4-61.

Traverse across potash feldspar megacryst

		0 edge 1	0.50mm	1.09mm	1.57mm	1.65mm	2.51mm	2.77mm	2.84mm	4.03mm	4.75mm	5.53mm	6.05mm
	SiO_2	65.7	64.7	66.0	64.6	64.3	64.6	65.4	64.4	65.0	67.3	65.1	65.5
	Al_2O_3	18.6	18.3	19.3	18.4	18.3	24.0	18.5	18.1	18.5	20.8	18.6	18.3
Total Fe as	FeO	0.13	0.08	0.03	0.00	0.00	0.08	0.01	0.03	0.00	0.00	0.00	0.03
	CaO	0.20	0.02	0.61	0.02	0.04	1.98	0.02	0.05	0.01	1.75	0.02	0.04
	Na_2O	3.93	0.81	8.3	0.48	0.57	8.8	0.89	1.39	0.90	10.7	0.74	0.77
	K_2O	10.8	14.4	5.7	15.2	15.3	0.20	15.1	14.6	15.3	0.16	15.1	15.0
	BaO	0.21	0.44	0.33	0.47	0.58	0.00	0.55	0.61	0.61	0.00	0.56	0.32
	SrO	0.27	0.35	0.25	0.36	0.26	0.22	0.29	0.31	0.29	0.26	0.35	0.24
	TOTAL	99.8	99.1	100.6	99.5	99.4	99.7	100.8	99.8	100.6	101.0	100.5	100.2
Molecular percentages of end-members													
	An	1.0	0.1	2.7	0.1	0.2	10.9	0.1	0.2	trace	8.2	0.1	0.2
	Or	63.5	91.2	30.0	94.5	93.4	1.3	90.8	86.2	90.7	0.9	92.0	92.0
	Ab	35.1	7.8	66.8	4.5	5.3	87.8	8.1	12.5	8.1	90.9	6.9	7.2
	Cn	0.4	0.9	0.5	0.9	1.1	0.0	1.0	1.1	1.1	0.0	1.0	0.6

TABLE J4 (Cont'd)

Electron microprobe analyses of coexisting feldspars in the border facies megacrystic granite. Specimen 4-61.

		6.46mm	6.59mm Plag.	6.96mm Plag.	7.32mm Plag.	7.80mm Plag.	7.86mm Plag.	8.47mm	10.91mm	11.76mm edge 2	Groundmass potash	Groundmass Feldspar	
	SiO_2	65.6	59.4	59.7	59.0	64.2	68.1	64.8	65.1	65.3	64.9	66.1	65.4
	Al_2O_3	18.6	25.8	25.3	26.2	22.7	19.8	18.0	18.0	18.1	18.4	18.5	18.3
Total Fe as	FeO	0.00	0.00	0.04	0.00	0.00	0.00	0.05	0.06	0.02	0.02	0.04	0.01
	CaO	0.02	7.2	7.2	8.0	4.26	1.01	0.06	0.01	0.02	0.22	0.15	0.00
	Na_2O	0.49	7.8	7.6	6.8	9.6	10.3	1.06	0.41	0.66	0.85	2.04	0.83
	K_2O	15.2	0.13	0.13	0.09	0.12	2.25	14.1	15.4	15.8	14.5	12.3	15.1
	BaO	0.50	0.03	0.00	0.00	0.00	0.11	0.41	0.12	0.06	0.04	0.11	0.04
	SrO	0.32	0.22	0.26	0.26	0.22	0.33	0.29	0.30	0.27	0.26	0.31	0.30
	TOTAL	100.7	100.6	100.2	100.4	101.1	101.9	98.8	99.4	100.2	99.2	99.6	100.0
Molecular percentages of end-members													
	An	0.1	33.5	34.1	39.2	19.6	4.5	0.3	0.1	0.1	1.2	0.8	0.00
	Or	94.3	0.7	0.7	0.5	0.7	12.0	88.8	95.8	93.8	90.7	79.0	92.2
	Ab	4.6	65.7	65.1	60.3	79.7	83.3	10.1	3.9	6.0	8.1	19.9	7.7
	Cn	1.0	0.1	0.00	0.0	0.0	0.2	0.8	0.2	0.1	0.1	0.2	0.1

Analyst: A.R. Milnes

TABLE J5

Electron microprobe analyses of coexisting feldspars in the border facies megacrystic granite. Specimen 7-52.

Traverse across potash feldspar megacryst

		0 edge 1	0.82mm	1.36mm	2.01mm	2.67mm	3.30mm	4.21mm	4.31mm	5.08mm	6.14mm	7.26mm	8.15mm
	SiO_2	65.0	65.6	64.7	65.3	65.0	65.0	64.5	64.5	65.2	65.2	65.0	65.1
	Al_2O_3	18.2	17.9	18.3	18.1	18.2	18.2	18.4	18.1	18.2	18.2	18.1	18.2
Total Fe as	FeO	0.05	0.03	0.05	0.01	0.05	0.03	0.08	0.06	0.05	0.02	0.02	0.03
	CaO	0.06	0.04	0.08	0.02	0.02	0.03	0.02	0.02	0.03	0.02	0.05	0.14
	Na_2O	0.79	0.98	1.25	0.62	0.73	0.76	0.49	1.03	1.00	0.77	0.52	0.43
	K_2O	13.7	14.4	14.1	14.7	14.6	14.6	15.0	14.5	14.7	15.0	15.2	15.2
	BaO	0.20	0.25	0.23	0.28	0.25	0.21	0.28	0.28	0.41	0.31	0.41	0.30
	SrO	0.33	0.36	0.32	0.32	0.36	0.37	0.37	0.35	0.34	0.31	0.34	0.29
	TOTAL	98.3	99.6	99.0	99.4	99.2	99.2	99.1	98.8	99.9	99.8	99.6	99.7
Molecular percentages of end-members													
	An	0.3	0.2	0.4	0.1	0.1	0.2	0.1	0.1	0.2	0.1	0.3	0.7
	Or	91.3	90.0	87.4	93.4	92.4	92.1	94.7	89.7	89.8	92.1	94.1	94.6
	Ab	8.0	9.3	11.8	6.0	7.0	7.3	4.7	9.7	9.3	7.2	4.9	4.1
	Cn	0.4	0.5	0.4	0.5	0.5	0.4	0.5	0.5	0.8	0.6	0.8	0.6

TABLE J5 (Cont'd)

Electron microprobe analyses of coexisting feldspars in the border facies megacrystic granite. Specimen 7-52.

	8.77mm	9.74mm	10.58mm	11.26mm edge 2	Plagioclase grains in hornfels xenolith core 1	rim 1	core 2	rim 2	core 3	rim 3
SiO_2	65.1	65.0	65.3	65.3	60.3	60.8	60.2	62.0	61.3	60.6
Al_2O_3	18.2	18.4	18.4	17.9	24.1	24.6	24.5	23.2	24.2	24.6
FeO	0.03	0.03	0.03	0.01	0.03	0.04	0.00	0.03	0.01	0.03
CaO	0.01	0.01	0.02	0.03	5.9	4.45	6.1	5.1	6.1	5.1
Na_2O	0.87	0.93	0.87	0.86	8.4	8.4	8.0	8.9	8.4	8.6
K_2O	14.7	14.7	15.3	14.9	0.13	0.21	0.14	0.15	0.13	0.16
BaO	0.39	0.30	0.14	0.12	0.00	0.0	0.00	0.02	0.01	0.02
SrO	0.30	0.36	0.32	0.32	0.20	0.27	0.21	0.25	0.26	0.19
TOTAL	99.6	99.7	100.4	99.4	99.0	98.8	99.2	99.7	100.4	99.3
Molecular percentages of end-members										
An	0.1	0.1	0.1	0.2	27.7	22.4	29.4	23.8	28.4	24.4
Or	91.0	90.7	91.7	91.6	0.7	1.3	0.8	0.8	0.7	0.9
Ab	8.2	8.7	7.9	8.0	71.6	76.4	69.8	75.3	70.8	74.6
Cn	0.7	0.6	0.3	0.2	0.00	0.00	0.0	trace	trace	trace

Analyst: A.R. Milnes

TABLE J6

Electron microprobe analyses of coexisting feldspars in the border facies megacrystic granite. Specimen 9-11.

Traverse across potash feldspar megacryst

		0 edge 1	0.54mm	0.83mm	1.49mm	2.50mm	3.38mm	4.47mm	5.42mm	6.36mm	7.43mm	8.56mm	9.44mm	10.31mm	11.51mm	11.78mm edge 2
	SiO_2	65.1	62.1	65.5	65.7	65.7	64.9	64.0	63.6	65.8	65.8	65.1	65.4	65.5	65.6	65.5
	Al_2O_3	18.9	20.9	18.9	19.01	18.9	18.9	19.1	19.9	18.8	19.0	19.2	19.1	19.1	19.0	19.3
Total Fe as	FeO	0.06	0.05	0.07	0.05	0.06	0.07	0.05	0.05	0.03	0.04	0.06	0.03	0.08	0.07	0.67
	CaO	0.08	0.04	0.05	0.07	0.04	0.04	0.06	0.04	0.03	0.04	0.08	0.03	0.08	0.04	0.11
	Na_2O	0.86	1.02	0.97	1.12	1.02	0.70	0.79	0.62	0.91	0.91	4.45	0.87	4.87	0.84	3.25
	K_2O	15.9	15.1	15.9	15.6	15.6	16.2	15.8	16.4	16.2	16.2	11.5	16.3	10.2	15.8	10.3
	BaO	0.14	0.17	0.16	0.30	0.19	0.34	0.18	0.25	0.25	0.27	0.22	0.35	0.32	0.26	0.09
	SrO	0.28	0.27	0.31	0.30	0.33	0.28	0.29	0.29	0.32	0.32	0.30	0.29	0.32	0.31	0.27
	TOTAL	101.3	99.7	101.9	102.2	101.8	101.4	100.3	101.2	102.3	102.6	100.9	102.4	100.5	101.9	99.5
Molecular percentages of end-members																
	An	0.4	0.2	0.2	0.3	0.2	0.2	0.3	0.2	0.1	0.2	0.4	0.1	0.4	0.2	0.6
	Or	91.8	90.2	91.0	89.4	90.5	93.1	92.4	94.0	91.6	91.5	62.5	91.8	57.4	91.9	67.1
	Ab	7.5	9.3	8.4	9.8	9.0	6.1	7.0	5.4	7.8	7.8	36.8	7.4	41.7	7.4	32.2
	Cn	0.2	0.3	0.3	0.5	0.3	0.6	0.3	0.4	0.4	0.5	0.4	0.6	0.6	0.5	0.2

Analyst: A.R. Milnes

TABLE J7

Electron microprobe analyses of coexisting feldspars in type A hybrid granite. Specimen 3-29.

Traverse Across potash feldspar megacryst

	0 edge 1	0.99mm	1.77mm	3.29mm	4.09mm	5.47mm	6.40mm	7.74mm	9.21mm	10.36mm	11.76mm	12.87mm	14.69mm
SiO_2	61.9	58.9	61.7	63.4	62.2	64.0	63.7	64.6	61.4	60.1	63.9	62.4	61.4
Al_2O_3	23.7	23.7	24.1	19.1	23.6	18.2	18.4	19.3	24.0	24.4	18.4	22.5	23.8
Total Fe as FeO	0.51	0.08	0.08	0.12	0.06	0.17	0.10	0.10	0.04	0.06	0.07	0.08	0.04
CaO	4.9	4.4	5.6	0.04	4.9	0.07	0.10	0.03	5.4	6.4	0.03	3.85	4.64
Na_2O	6.6	8.1	8.2	0.48	8.6	0.87	0.65	0.60	8.1	7.7	0.74	9.0	8.4
K_2O	1.76	0.14	0.17	15.5	0.12	15.4	15.2	15.5	0.12	0.12	14.9	0.18	0.13
BaO	0.28	0.02	0.00	0.22	0.02	0.42	0.29	0.28	0.00	0.01	0.27	0.07	0.02
SrO	0.25	0.27	0.19	0.30	0.26	0.35	0.31	0.34	0.22	0.27	0.24	0.18	0.22
TOTAL	99.9	99.6	100.0	99.2	99.8	99.5	98.8	100.8	99.3	99.1	98.6	98.3	98.7
Molecular proportions of end-members													
An	25.7	22.9	27.1	0.2	23.8	0.3	0.5	0.2	26.7	31.3	0.2	18.9	23.2
Or	11.0	0.9	1.0	94.9	0.7	91.1	92.9	93.8	0.7	0.7	92.4	1.1	0.8
Ab	62.7	76.2	71.9	4.5	75.5	7.8	6.0	5.5	72.6	68.0	7.0	79.9	76.0
Cn	0.5	trace	0.00	0.4	trace	0.8	0.5	0.5	0.0	trace	0.5	0.1	trace

TABLE J7 (Cont'd)

Electron microprobe analyses of coexisting feldspars in type A hybrid granite. Specimen 3-29.

		14.69mm	16.05mm	16.68mm edge 2	Traverse across plagioclase megacryst core									
	SiO_2	61.4	62.7	63.6	57.0	56.8	58.2	58.1	57.2	58.0	57.7	57.6	57.3	59.6
	Al_2O_3	23.8	22.7	22.1	26.8	26.9	25.7	26.0	26.5	25.9	26.2	26.0	26.6	25.1
Total Fe as	FeO	0.04	0.12	0.06	0.14	0.07	0.10	0.06	0.13	0.07	0.09	0.17	0.07	0.08
	CaO	4.64	3.72	3.85	8.4	8.3	7.2	7.4	7.7	7.9	8.0	7.7	8.2	6.2
	Na_2O	8.4	9.0	9.4	6.3	6.4	6.9	6.8	6.6	6.6	6.9	6.9	6.3	7.4
	K_2O	0.13	0.19	0.12	0.14	0.13	0.47	0.24	0.17	0.16	0.13	0.18	0.11	0.11
	BaO	0.02	0.02	0.02	0.05	0.01	0.05	0.02	0.04	0.02	0.03	0.02	0.06	0.01
	SrO	0.22	0.22	0.29	0.16	0.23	0.23	0.21	0.21	0.23	0.21	0.17	0.23	0.24
	TOTAL	98.7	98.7	99.4	99.0	98.8	98.9	98.8	98.6	98.9	99.3	98.7	97.9	98.7
Molecular proportions of end-members														
	An	23.2	18.4	18.4	42.0	41.4	35.5	37.0	38.8	39.4	38.7	37.7	41.5	31.4
	Or	0.8	1.1	0.7	0.8	0.8	2.8	1.4	1.0	1.0	0.7	1.1	0.7	0.7
	Ab	76.0	80.5	80.9	57.0	57.8	61.6	61.5	60.1	59.6	60.5	61.2	57.7	67.9
	Cn	trace	trace	trace	0.1	trace	0.1	0.1	0.1	trace	0.1	trace	0.1	trace

Analyst: A.R. Milnes

TABLE J8

Electron microprobe analyses of coexisting feldspars in the type B hybrid granite. Specimen 3-27.

Traverse across potash feldspar megacryst

		0 edge 1	1.16mm	2.45mm	3.77mm	4.98mm	6.06mm	7.44mm	8.49mm	9.71mm edge 2	Plagioclase grain core	Plagioclase grain rim
	SiO_2	65.4	65.4	65.0	65.3	65.2	65.8	65.3	65.5	65.0	57.08	58.9
	Al_2O_3	18.7	18.9	18.6	18.8	18.9	18.8	18.8	18.9	19.0	27.35	26.2
Total Fe as	FeO	0.06	0.02	0.07	0.05	0.05	0.08	0.04	0.04	0.08	0.02	0.00
	CaO	0.03	0.03	0.05	0.02	0.03	0.03	0.02	0.02	0.02	10.0	7.8
	Na_2O	0.89	1.01	0.96	0.95	0.75	0.92	0.73	6.58	0.82	6.0	7.5
	K_2O	14.7	14.4	14.4	14.8	14.7	14.5	14.9	15.2	15.4	0.08	0.13
	BaO	0.39	0.61	0.55	0.29	0.39	0.38	0.45	0.35	0.34	0.01	0.05
	SrO	0.31	0.35	0.31	0.30	0.29	0.37	0.33	0.31	0.31	0.28	0.25
	TOTAL	100.5	100.7	99.9	100.5	100.3	100.9	100.6	100.9	101.0	100.8	100.8
Molecular percentages of end-members												
	An	0.2	0.2	0.3	0.1	0.2	0.2	0.1	0.1	0.1	47.7	36.2
	Or	90.8	89.2	89.6	90.5	92.0	90.4	92.2	93.8	91.8	0.5	0.7
	Ab	8.4	9.5	9.1	8.8	7.1	8.7	6.9	5.4	7.4	51.8	63.0
	Cn	0.7	1.2	1.1	0.5	0.7	0.7	0.9	0.7	0.6	trace	0.1

TABLE J8 (Cont'd)

Electron microprobe analyses of coexisting feldspars in the type B hybrid granite. Specimen 3-27.

Traverse across plagioclase megacryst 1

		0 edge 1	0.40mm	0.97mm	1.61mm	2.08mm	2.87mm	3.68mm	4.33mm	4.96mm edge 2
	SiO_2	59.8	60.4	56.9	60.4	59.4	58.2	58.0	60.5	63.1
	Al_2O_3	24.5	25.1	27.2	25.4	25.2	25.0	26.9	25.5	23.4
Total Fe as	FeO	0.09	0.06	0.00	0.02	0.06	0.14	0.09	0.02	0.03
	CaO	5.5	6.3	8.6	6.7	6.9	6.9	7.9	6.6	4.3
	Na_2O	7.4	8.0	6.1	7.9	7.2	6.7	6.9	7.3	9.2
	K_2O	0.72	0.22	0.10	0.19	0.93	0.67	0.25	0.31	0.13
	BaO	0.13	0.03	0.02	0.03	0.04	0.02	0.02	0.03	0.01
	SrO	0.20	0.19	0.19	0.22	0.21	0.28	0.25	0.26	0.24
	TOTAL	98.3	100.3	99.1	100.9	99.9	97.9	100.3	100.5	100.4
Molecular percentages of end-members										
	An	27.8	29.9	43.5	31.6	32.8	34.8	38.2	32.7	20.4
	Or	4.3	1.2	0.6	1.1	5.3	4.0	1.4	1.8	0.7
	Ab	67.6	68.8	55.8	67.3	61.9	61.1	60.3	65.4	78.9
	Cn	0.2	0.1	trace	0.1	0.1	trace	trace	0.1	trace

TABLE J8 (Cont'd)

Electron microprobe analyses of coexisting feldspars in the type B hybrid granite. Specimen 3-27.

Traverse across plagioclase megacryst 2

	edge 1							edge of section
SiO_2	60.7	59.3	60.5	58.9	58.9	58.4	59.1	58.5
Al_2O_3	25.0	23.5	24.8	26.4	26.8	26.3	26.3	27.0
Total Fe as FeO	0.01	1.82	0.13	0.03	0.10	0.07	0.06	0.01
CaO	5.7	4.7	7.0	7.9	8.2	8.0	7.6	8.3
Na_2O	8.4	3.8	6.4	7.0	7.0	7.2	6.5	6.7
K_2O	0.11	5.9	0.84	0.44	0.22	0.24	1.12	0.17
BaO	0.03	0.31	0.06	0.06	0.04	0.06	0.07	0.03
SrO	0.23	0.29	0.21	0.22	0.27	0.26	0.28	0.24
TOTAL	100.2	99.6	99.9	101.0	101.5	100.5	101.0	101.0
Molecular percentages of end-members								
An	27.1	25.1	35.7	37.4	38.8	37.5	36.7	40.2
Or	0.6	37.5	5.1	2.5	1.2	1.3	6.4	1.0
Ab	72.2	36.7	59.1	60.0	59.9	61.1	56.8	58.7
Cn	0.1	0.6	0.1	0.1	0.1	0.1	0.1	0.1

Analyst: A.R. Milnes

TABLE J9

Average compositions of coexisting feldspars in Encounter Bay Granites calculated from data in Tables J1 to J8.

	An	Or	Ab	Cn
Specimen 4-79. Inner facies megacrystic granite.				
K-feldspar megacryst excluding plagioclase inclusion	0.4	84.8	14.2	0.6
Plagioclase inclusion in k-feldspar megacryst	9.8	2.5	87.4	0.3
Specimen 4-93. Inner facies megacrystic granite.				
K-feldspar megacryst	1.9	71.6	26.0	0.5
Groundmass potash feldspar	0.5	92.9	6.6	0.1
Plagioclase megacryst	26.6	0.6	72.8	trace
Specimen 3-26. Border facies megacrystic granite.				
K-feldspar megacryst excluding plagioclase border	0.2	92.4	6.7	0.8
Plagioclase border around k-feldspar megacryst	23.8	0.9	75.3	trace
Specimen 4-61. Border facies megacrystic granite.				
K-feldspar megacryst excluding plagioclase inclusion	1.8	71.2	26.4	0.6
Plagioclase inclusion in k-feldspar megacryst	31.6	0.7	67.7	0.0
Groundmass k-feldspar	0.7	87.3	11.9	0.1
Specimen 7-52. Border facies megacrystic granite.				
K-feldspar megacryst	0.2	91.7	7.6	0.5
Plagioclase in hornfels xenolith	26.0	0.9	73.1	trace
Specimen 9-11. Border facies megacrystic granite.				
K-feldspar megacryst	0.3	85.7	13.6	0.4
Specimen 3-29. Type A hybrid granite.				
K-feldspar + plagioclase megacryst	15.9	32.3	51.7	0.4
Plagioclase megacryst	38.3	1.1	60.5	0.1
Specimen 3-27. Type B hybrid granite.				
K-feldspar megacryst	0.2	91.1	7.9	0.8
Plagioclase megacryst 1	32.4	2.3	65.2	0.1
Plagioclase megacryst 2	36.2	2.6	61.1	0.1
Plagioclase grain	42.0	0.6	57.4	0.1
Average plagioclase	36.9	1.9	61.2	0.1

APPENDIX K

Rb-Sr isotope dilution analyses of the Encounter Bay Granites

The techniques of chemical preparation of specimens and mass-spectrometry used during the present investigation are largely those described by Compston, Lovering and Vernon (1965) and Arriens and Compston (1968).

Rb analyses were carried out on a 15cm 90°-sector Metropolitan Vickers MS2 mass spectrometer. Sr analyses were carried out on a 30cm 60°-sector Nuclide mass spectrometer. Both machines use the triple filament ionisation technique. Rb isotope ratios were measured on the MS2 by rapid peak-switching controlled by push-button selector switches to pre-set values for the magnet current. A chart recorder (for display purposes), a voltage-to-frequency converter, a counter, and a digital recorder were coupled to a Carey electrometer. The Rb^{85} and Rb^{87} beam voltages were measured for two seconds, while a fixed delay of five seconds was allowed for switching. Two sets, each comprising at least ten counts at each mass station, were taken for each side filament of the triple filament source. The results for each specimen, together with static and dynamic zero values, were reduced to concentrations of total Rb and Rb^{87} using the programme MASSSPEC written by Dr. P.A. Arriens (Arriens and Compston, 1968).

The Nuclide was operated by magnet current switching, but was controlled by a Hall probe field-sensing device (compare with the method described by Arriens and Compston, 1968). A digitised output similar to that employed for the MS2 was obtained. Sr isotope ratios were measured in the following order:

88/86 - 86/84 - 88/86 - 85(Rb) - 87/86 - 85(Rb) - 88/86

The beam voltages for each isotope were measured for two seconds, while a fixed delay of six seconds was allowed for switching. About ten measurements of each isotope ratio were taken during each specimen run. Static and dynamic zero values were taken at the beginning and end of each run. Measurements of the Rb^{85} abundance in each Sr run were used to assess the amount of Rb^{87} present (from the constant ratio Rb^{85}/Rb^{87}= 2.600), and hence to determine the correction to be applied to the Sr^{87}/Sr^{86} ratio. These data were reduced to concentrations of total Sr, common Sr (masses 88, 86 and 84) and Sr^{87}/Sr^{86} ratio using the programme MASSSPEC (Arriens and Compston, 1968).

The constants used in the data reduction and subsequent Rb-Sr age calculations are as follows:

$Rb_{half\text{-}life} = 1.39 \times 10^{-11} y^{-1}$

$Rb^{85}/Rb^{87} = 2.600$

$Sr^{88}/Sr^{86} = 8.3752$

$Sr^{86}/Sr^{84} = 17.6830$

K-Ar isotope dilution analyses of the Encounter Bay Granites

The techniques used for K-Ar age determination by Dr. A.W. Webb are summarised in Progress Report No. 3 - "The geochronology of the granitic rocks of southeast South Australia" (unpublished, 1971) from Australian Mineral Development Laboratories to the South Australian Geological Survey. Biotite or muscovite were separated from the rocks of interest. Separate aliquots of the 60 to 120 BS mesh grain size were taken from each mica concentrate for K and Ar analysis. K was determined in duplicate on a Jarrell-Ash direct reading emission spectrometer. Radiogenic Ar was determined by isotope dilution. The constants used in the analyses and subsequent age calculations are as follows:

$K^{40} = 0.0119$ atom percent

$\lambda\beta = 4.72 \times 10^{-10} y^{-1}$

$\lambda_e = 0.584 \times 10^{-10} y^{-1}$

The overall precision of the K-Ar ages was quoted as ± 1.5%.

TABLE K1

Rb-Sr isotope dilution data for specimens of the contaminated border facies megacrystic granite

Specimen	Rb (ppm)	Sr (ppm)	Rb^{87}/Sr^{86}	Sr^{87}/Sr^{86}
8-12 total-rock	76.33	118.5	1.86	0.7312
8-12 muscovite	231.0	58.23	11.56	0.8021
8-12 biotite	630.2	11.00	181.9	1.7275
7-58 total-rock	194.9	141.2	4.00	0.7459
7-58 total-rock repeat	195.3	140.9	4.02	0.7453
7-58 total-rock repeat	195.3	141.0	4.01	0.7452
7-58 potash feldspar	291.8	212.2	3.98	0.7468
7-58 biotite	897.8	5.08	787.0	6.2471
3-26 total-rock	190.7	106.9	5.18	0.7553
3-26 total-rock repeat	190.7	107.3	5.16	0.7560
3-26 potash feldspar	352.7	152.7	6.71	0.7665
3-26 biotite	963.8	7.03	547.4	4.6227
4-55 total-rock	258.3	78.46	9.58	0.7885

Analyst: A.R. Milnes

TABLE K2

Regression analyses for the contaminated border facies megacrystic granite

Regression	No. specimens	MSWD for Model 1	Age (m.y.)	Initial Sr^{87}/Sr^{86}	Isochron model
1. Total-rocks	5	3.66	537 ± 23	0.7165 ± 0.0016	3
2. Total-rocks, potash feldspars, muscovite	8	2.50	531 ± 11	0.7169 ± 0.0009	3
3. Specimen 3-26. Total-rock, biotite	2	-	511 ± 5	0.7188 ± 0.0013	Assume Model 1
4. Specimen 7-58. Total-rock, biotite	2	-	504 ± 5	0.7173 ± 0.0011	Assume Model 1
5. Specimen 8-12. Total-rock, biotite	2	-	397 ± 5	0.7209 ± 0.0007	Assume Model 1

K-Ar ages for biotite in specimens of the contaminated border facies megacrystic granite

Specimen	Age (m.y.)	Specimen	Age (m.y.)
Encounter Bay area		Cape Willoughby	
4-55	473	W34C	472
4-61	474	W22	474
3-26	467	W36A	475
8-14	472	W20	473
9-11	472		
7-56	460		
8-12	417		
8-18	420		

TABLE K3

Rb-Sr isotope dilution data for specimens of xenoliths within the border facies megacrystic granite

Specimen	Rb (ppm)	Sr (ppm)	Rb^{87}/Sr^{86}	Sr^{87}/Sr^{86}
Metasediment xenolith 3-10				
biotite	615.3	8.27	250.1	2.3933
plagioclase concentrate	28.88	268.3	0.31	0.7254
Metasediment xenolith 3-19				
biotite	585.3	12.30	150.8	1.7119
plagioclase concentrate	25.53	198.1	0.37	0.7260
Hybrid granite 3-31				
biotite+hornblende conc.	878.6	9.11	344.8	3.1414
potash feldspar	300.3	154.0	5.66	0.7552
Hybrid granite 3-38				
total-rock	160.3	126.9	3.66	0.7414
biotite+hornblende conc.	716.9	9.99	241.3	2.3904
potash feldspar	232.4	169.3	3.98	0.7414

Analyst: A.R. Milnes

TABLE K4

Regression analyses for metasediment and hybrid granite$_A$ xenoliths

Regression	No. specimens	MSWD for Model 1	Age (m.y.)	Initial Sr^{87}/Sr^{86}	Isochron model
1. Metasediment xenoliths. biotites, plagioclase concs.	4	3.53	474 ± 15	0.7234 ± 0.0008	2
2. Metasediment xenoliths 3-10. biotite, plagioclase conc.	2	-	479 ± 5	0.7233 ± 0.0006	Assume Model 1
3. Metasediment xenoliths 3-19. biotite, plagioclase conc.	2	-	470 ± 5	0.7236 ± 0.0006	Assume Model 1
4. Hybrid granite$_A$ xenoliths. minerals and 3-38 total-rock	5	12.42	502 ± 6	0.7150 ± 0.0007	1
5. Hybrid granite$_A$ xenolith 3-31. biotite+hornblende conc., potash feldspar	2	-	504 ± 5	0.7154 ± 0.0014	Assume Model 1
6. Hybrid granite$_A$ xenolith 3-38. total-rock, potash feldspar, biotite+hornblende conc.	3	28.05	498 ± 33	0.7145 ± 0.0144	3
7. Hybrid granite$_A$ xenolith 3-38. biotite+hornblende conc., total-rock	2	-	497 ± 5	0.7160 ± 0.0011	Assume Model 1

K-Ar ages of biotite in specimens of hybrid granite$_A$

Specimen	Age (m.y.)
3-31	478
3-38	466

TABLE K5

Rb-Sr isotope dilution data for specimens of Kanmantoo Group metasedimentary rocks

Specimen	Rb (ppm)	Sr (ppm)	Rb^{87}/Sr^{86}	Sr^{87}/Sr^{86}
0025 total-rock	243.2	137.9	5.12	0.7576
0029 total-rock	193.2	237.2	2.36	0.7396
0014 total-rock	221.7	149.8	4.29	0.7499
0018 total-rock	118.8	223.0	1.56	0.7324

Analyst: A.R. Milnes

Regression analyses for the Kanmantoo Group metasedimentary rocks

Regression	No. specimens	MSWD for Model 1	Age (m.y.)	Initial Sr^{87}/Sr^{86}	Isochron model
1. Combined total-rock and mineral data for Kanmantoo Group metasediments and metasedimentary rock xenoliths	8	11.05	474 ± 4	0.7231 ± 0.0003	1
2. 0025, 0029 total-rocks	2	-	468 ± 40	0.7242 ± 0.0020	Assume Model 1
3. 0014, 0018 total-rocks	2	-	460 ± 38	0.7224 ± 0.0014	Assume Model 1

TABLE K6

Rb-Sr isotope dilution data for specimens of albitised granites

Specimen	Rb (ppm)	Sr (ppm)	Rb^{87}/Sr^{86}	Sr^{87}/Sr^{86}
Albitised border facies megacrystic granite 7-53				
total-rock	95.60	76.52	3.62	0.7410
biotite	430.6	5.87	247.3	2.4205
Albitised border facies megacrystic granite 7-55				
total-rock	111.8	135.3	2.39	0.7341
biotite	883.6	5.16	754.6	6.0889
Megacrystic albite-chlorite rock 7-54				
total-rock	6.27	125.3	0.14	0.7158
plagioclase	2.47	137.5	0.05	0.7156
chlorite	5.70	7.21	2.29	0.7251
phlogopite concentrate	47.85	10.84	12.86	0.7998
Megacrystic albite-chlorite rock 3-40				
total-rock	12.42	38.03	0.94	0.7195
plagioclase	9.20	100.1	0.27	0.7167
phlogopite	258.5	13.52	57.35	1.1013
chlorite concentrate	95.96	9.62	29.37	0.9085

Analyst: A.R. Milnes

TABLE K7

Regression analyses for the albitised border facies megacrystic granite and the megacrystic albite-chlorite rock

Regression	No. specimens	MSWD for Model 1	Age (m.y.)	Initial Sr /Sr	Isochron model
1. Albitised border facies megacrystic granite 7-53. biotite, total-rock	2	-	494 ± 5	0.7161 ± 0.0011	Assume Model 1
2. Albitised border facies megacrystic granite 7-55. biotite, total-rock	2	-	510 ± 5	0.7171 ± 0.0009	Assume Model 1
3. Megacrystic albite-chlorite rock. Combined total-rock and minerals, 7-54 and 3-40	8	47.16	417 ± 82	0.7154 ± 0.0005	2
4. Megacrystic albite-chlorite rock. Plagioclases, total-rocks, 7-54 chlorite	5	0.35	306 ± 33	0.7154 ± 0.0005	1
5. Megacrystic albite-chlorite rock 7-54. Total-rock, phlogopite concentrate	2	-	474 ± 11	0.7149 ± 0.0006	Assume Model 1
6. Megacrystic albite-chlorite rock 3-40. total-rock, phlogopite	2	-	485 ± 6	0.7131 ± 0.0007	Assume Model 1

TABLE K8

Rb-Sr isotope dilution data for specimens of uncontaminated granites

Specimen	Rb (ppm)	Sr (ppm)	Rb^{87}/Sr^{86}	Sr^{87}/Sr^{86}
Aplite 4-65				
total-rock	299.9	48.03	18.27	0.8433
Miarolitic granophyre 4-66B				
total-rock	499.0	52.78	27.85	0.9147
potash feldspar	865.8	77.41	33.09	0.9597
muscovite	1416	10.11	569.2	4.8665
Medium grained granite 4-10				
total-rock	399.6	32.59	36.33	0.9754
potash feldspar	769.7	39.42	58.72	1.1317
biotite	2036	9.67	1017	7.573
Red leucogranite 4-89				
total-rock	390.6	29.29	39.63	1.0042
Red leucogranite 4-9				
total-rock	443.7	24.02	55.44	1.1123
total-rock repeat	449.0	24.16	55.76	1.1106
potash feldspar	779.8	30.27	78.65	1.2924
plagioclase concentrate	284.1	26.80	31.30	0.9414
Albitised red leucogranite 4-8				
total-rock	7.72	58.54	0.38	0.7175

Analyst: A.R. Milnes

TABLE K9

Regression analyses for the uncontaminated granites

Regression	No. specimens	MSWD for Model 1	Age (m.y.)	Initial Sr^{87}/Sr^{86}	Isochron model
1. Total-rocks	5	7.06	522 ± 28	0.7111 ± 0.0113	2
2. Total-rocks, potash feldspars, plagioclase conc., muscovite	10	9.47	523 ± 6	0.7115 ± 0.0057	3
3. Total-rocks, potash feldspars, plagioclase conc.	9	10.80	524 ± 18	0.7113 ± 0.0083	2
4. Miarolitic granophyre 4-66B. total-rock, muscovite	2	-	523 ± 6	0.7114 ± 0.0049	Assume Model 1
5. Medium even-grained granite 4-10. total-rock, biotite	2	-	482 ± 5	0.7310 ± 0.0056	Assume Model 1

K-Ar age of muscovite in miarolitic granophyre 4-66B is 473m.y.

TABLE K10

Rb-Sr isotope dilution data for Kangaroo Island granites and pegmatites

Specimen	Rb (ppm)	Sr (ppm)	Rb^{87}/Sr^{86}	Sr^{87}/Sr^{86}
Vivonne Bay pegmatite V4				
total-rock	226.6	83.76	7.86	0.7753
muscovite	576.4	11.56	160.4	1.8795
Penneshaw pegmatite P1				
total-rock	818.6	37.03	66.95	1.2058
total-rock repeat	818.6	36.98	67.02	1.2058
muscovite	1669	13.28	495.1	4.4296
Cape Kersaint granite SBR8				
total-rock	161.4	167.1	2.80	0.7377
biotite	688.5	6.76	367.1	3.2424

Analyst: A.R. Milnes

Regression analyses for Kangaroo Island granites and pegmatites

Regression	No. specimens	MSWD for Model 1	Age (m.y.)	Initial Sr^{87}/Sr^{86}	Isochron model
1. Vivonne Bay pegmatite V4. total-rock, muscovite	2	-	519 ± 6	0.7184 ± 0.0018	Assume Model 1
2. Penneshaw pegmatite P1. total-rock, muscovite	2	-	539 ± 7	0.7014 ± 0.0124	Assume Model 1
3. Cape Kersaint granite SBR8. total-rock, biotite	2	-	493 ± 5	0.7184 ± 0.0009	Assume Model 1

K-Ar ages of micas from Kangaroo Island granites and pegmatites

V4 muscovite 485m.y. Biotite from Remarkable Rocks granite 442m.y.

TABLE K11

Rb-Sr isotope dilution data of Compston, Crawford and Bofinger (1966) for the Anabama Granite and for a microtonalite from Netley Hill

Specimen	Rb (ppm)	Sr (ppm)	Rb^{87}/Sr^{86}	Sr^{87}/Sr^{86}
Anabama Granite GA-357				
total-rock	139.8	140.0	2.874	0.7251
plagioclase	15.5	125.3	0.357	0.7079
plagioclase repeat	16.2	128.1	0.364	0.7071
microcline	437.5	121.9	10.33	0.7715
biotite	889.8	10.2	250.6	2.358
Netley Hill microtonalite GA-355				
total-rock	266.2	479.5	1.598	0.7246
plagioclase	125.4	920.0	0.392	0.7178
biotite	515.9	67.3	22.08	0.8495

Regression analyses for the Anabama Granite and the Netley Hill microtonalite

Regression	No. specimens	MSWD for Model 1	Age (m.y.)	Initial Sr^{87}/Sr^{86}	Isochron model
1. GA-357 combined total-rock and minerals	4	13.02	473 ± 10	0.7050 ± 0.0035	3
2. GA-357 total-rock, biotite	2	-	473 ± 5	0.7062 ± 0.0009	Assume Model 1
3. GA-355 combined total-rock and minerals	3	2.01	436 ± 32	0.7152 ± 0.0025	1
4. GA-355 total-rock, biotite	2	-	437 ± 9	0.7149 ± 0.0008	Assume Model 1

TABLE K12

Rb-Sr isotope dilution data (White, Compston and Kleeman, 1967) for the Palmer Granite and the Rathjen Gneiss

Specimen	Rb (ppm)	Sr (ppm)	Rb^{87}/Sr^{86}	Sr^{87}/Sr^{86}
Palmer Granite				
GA-315				
total-rock	179	80.3	6.45	0.7536
total-rock repeat	175	77.9	6.49	0.7531
potash feldspar	412	106.0	11.22	0.7849
potash feldspar repeat	415	107.7	11.14	0.7859
plagioclase	12.0	63.0	0.55	0.714
plagioclase repeat u/s Sr run	-	-	-	0.7122
green biotite	1286	2.69	1378	9.529
brown biotite	1226	6.50	544.6	3.745
brown biotite repeat	1236	6.50	549.1	3.790
P5				
total-rock	144	70	5.93	0.7513
potash feldspar	465	97	13.82	0.7946
biotite	1191	1.81	1893	13.499
biotite	1181	2.50	1369	9.883
P7				
total-rock	151	52	8.35	0.7660
potash feldspar (1)	447	64	21.48	0.8464
potash feldspar (2)	463	70.1	19.29	0.8357
potash feldspar (2) repeat	459	69.5	19.30	0.8373
P2				
total-rock	138	103	3.86	0.7342
Rathjen Gneiss				
P15				
total-rock	109	144	2.16	0.7295
PR12				
total-rock	141	109	3.68	0.7409

TABLE K13

Regression analyses for the Palmer Granite and the Rathjen Gneiss

Regression	No. specimens	MSWD for Model 1	Age (m.y.)	Initial Sr^{87}/Sr^{86}	Isochron model
Palmer Granite					
1. Total-rocks	4	17.11	514 ± 33	0.7071 ± 0.0028	1
2. Total-rocks excluding P5	3	3.34	512 ± 97	0.7068 ± 0.0083	1
3. GA-315 total-rock, potash feldspar, plagioclase	3	0.70	485 ± 30	0.7090 ± 0.0025	1
4. GA-315 total-rock, green biotite	2	-	459 ± 5	0.7120 ± 0.0014	Assume Model 1
5. GA-315 total-rock, brown biotite	2	-	400 ± 4	0.7173 ± 0.0013	Assume Model 1
6. P5 total-rock, biotite	2	-	483 ± 5	0.7114 ± 0.0013	Assume Model 1
Rathjen Gneiss					
P15 and PR12 total-rocks	2	-	537 ± 71	0.7113 ± 0.0028	Assume Model 1

TABLE K14

Rb-Sr isotope dilution analyses for the Black Hill Norite (Analyst: A.R. Milnes)

Specimen	Rb (ppm)	Sr (ppm)	Rb^{87}/Sr^{86}	Sr^{87}/Sr^{86}
Black Hill Norite				
total-rock	82.91	609.6	0.39	0.7093
biotite	934.4	212.9	12.78	0.7963

Regression analysis for the Black Hill Norite

Regression	No. specimens	MSWD for Model 1	Age (m.y.)	Initial Sr^{87}/Sr^{86}	Isochron model
Black Hill Norite total-rock, biotite	2	-	503 ± 12	0.7066 ± 0.0006	Assume Model 1

K-Ar analysis of the biotite indicates an age of 486m.y.